2016

Modeling The Spatiotemporal Dynamics Of Cells In The Lung

Joshua Jeremy Pothen
University of Vermont

MODELING THE SPATIOTEMPORAL DYNAMICS OF CELLS IN THE LUNG

A Dissertation Presented

by

Joshua Jeremy Pothen

to

The Faculty of the Graduate College

of

The University of Vermont

In Partial Fulfillment of the Requirements
for the Degree of Doctor of Philosophy
Specializing in Bioengineering

May, 2016

Defense Date: Mar 17, 2016
Dissertation Examination Committee:

Jason Bates, Ph.D., Advisor
Maggie Eppstein, Ph.D., Chairperson
Matthew Poynter, Ph.D.
Daniel Weiss, M.D., Ph.D.
Cynthia J. Forehand, Ph.D., Dean of the Graduate College

ABSTRACT

Multiple research problems related to the lung involve a need to take into account the spatiotemporal dynamics of the underlying component cells. Two such problems involve better understanding the nature of the allergic inflammatory response to explore what might cause chronic inflammatory diseases such as asthma, and determining the rules underlying stem cells used to engraft decellularized lung scaffolds in the hopes of growing new lungs for transplantation. For both problems, we model the systems computationally using agent-based modeling, a tool that enables us to capture these spatiotemporal dynamics by modeling any biological system as a collection of agents (cells) interacting with each other and within their environment. This allows to test the most important pieces of biological systems together rather than in isolation, and thus rapidly derive biological insights from resulting complex behavior that could not have been predicted beforehand, which we can then use to guide wet lab experimentation.

For the allergic response, we hypothesized that stimulation of the allergic response with antigen results in a response with formal similarity to a muscle twitch or an action potential, with an inflammatory phase followed by a resolution phase that returns the system to baseline. We prepared an agent-based model (ABM) of the allergic inflammatory response and determined that antigen stimulation indeed results in a twitch-like response. To determine what might cause chronic inflammatory diseases where the twitch presumably cannot resolve back to baseline, we then tested multiple potential defects to the model. We observed that while most of these potential changes lessen the magnitude of the response but do not affect its overall behavior, extending the lifespan of activated pro-inflammatory cells such as neutrophils and eosinophil results in a prolonged inflammatory response that does not resolve to baseline. Finally, we performed a series of experiments involving continual antigen stimulation in mice, determining that there is evidence in the cytokine, cellular and physiologic (mechanical) response consistent with our hypothesis of a finite twitch and an associated refractory period.

For stem cells, we made a 3-D ABM of a decellularized scaffold section seeded with a generic stem cell type. We then programmed in different sets of rules that could conceivably underlie the cell's behavior, and observed the change in engraftment patterns in the scaffold over selected timepoints. We compared the change in those patterns against the change in experimental scaffold images seeded with C10 epithelial cells and mesenchymal stem cells, two cell types whose behaviors are not well understood, in order to determine which rulesets more closely match each cell type. Our model indicates that C10s are more likely to survive on regions of higher substrate while MSCs are more likely to proliferate on regions of higher substrate.

CITATIONS

Material from this dissertation has been published in the following form:

Pothen, J.J., Poynter, M.E., Bates, J.H.. (2013). The Inflammatory Twitch as a General Strategy for Controlling the Host Response. Journal of Immunology, 190(7):3510-6.

Pothen, J.J., Poynter, M.E., Bates, J.H.. (2015). A Computational Model of Unresolved Allergic Inflammation in Chronic Asthma. American Journal of Physiology Lung Cellular and Molecular Physiology, 308(4):L384-90.

AND/OR

Material from this dissertation has been submitted for publication to Tissue Engineering on February 10, 2016 in the following form:

Pothen, J.J., Rajendran, V., Wagner, D., Weiss, D.J., Smith, B.J., Ma, B., Bates, J.H.. A Computational Model of Cellular Engraftment on Lung Scaffolds. Tissue Engineering.

AND/OR

Material from this dissertation has been accepted for publication in American Journal of Physiology – Lung Cellular and Molecular Physiology on February 29, 2016 in the following form:

Pothen, J.J., Poynter, M.E., Lundblad, L.K., Bates, J.H.. Dissecting the inflammatory twitch in allergically inflamed mice. American Journal of Physiology Lung Cellular and Molecular Physiology.

ACKNOWLEDGEMENTS

To Jason Bates: It is an honor to be a disciple of someone both kind and prolific. To my committee—Dan Weiss, Maggie Eppstein and Matt Poynter: you have each been crucial in my medical-graduate growth, nurturing my abilities while pushing me to grow. I will always love the University of Vermont College of Medicine, particularly MD/PhD program director Dr. Steven Lidofsky and the Vermont Lung Center, for enabling me to pursue a computationally-oriented dual degree.

Thanks also to the many connected to our lab whose assistance has been critical to our work. Among them: Bradford Smith, Baoshun Ma, David Chapman and Kate Hamlington Smith, for teaching me how to perform and present research well and for assisting me when I needed it. Erika Martinez Nieves, instrumental in assembling the first version of the computational allergic response models. Lennart Lundblad, for insight into the setup for our mouse studies. Nirav Daphtary and Minara Aliyeva, for their assistance with mouse care, sacrifice and analysis. Jen Ather and Laura Hoyt, whose assistance was crucial to generating our mouse cytokine analysis. Darcy Wagner and Dino Sokocevic, whose work and insights were critical to our stem cell work. Vignesh Rajendran, who designed the image analysis software tool that revealed patterns in our stem cell data.

The journey to my PhD has also involved encouragement and support from many outside of my lab. A few: Dr. Marc Asher at the University of Kansas Medical Center, for inspiring me to pursue this path when I was in a high school student. Dr. Jean Lee, who

allowed me to follow and learn from her PhD journey at UVM. Dr. Alan Rubin, my medical teacher and friend who always encourages me to get back up when I think I can go no further. I am also deeply endebted to the evangelical Christian community in Vermont, among them John and Diane Byrnes of the Lafountain Ministry House; Alex and Tamara Cameron, Eric Taylor, Tim and Christa Loescher and the many others at St. Timothy Anglican Mission; Terri Seward, Deb Couture and the board and staff of CareNet Pregnancy Center; and Dr. Rachel DiSanto, Dr. Ted James, Erin Keller, Elizabeth Landell, and the other doctors and students in UVM's Christian Medical and Dental Association chapter. Their kindness saved my life in a very real way.

To my family, thank you for your love and support throughout the years.

My final and ultimate thanks are to the Holy Trinity, Le Bon Dieu, who inexplicably loves me and has been saving my life for longer than I know. Without Him, all of this would be meaningless. With Him, it somehow has more meaning than I can imagine. Thank you. Thank you. Thank you.

TABLE OF CONTENTS

LIST OF TABLES

Table Page

LIST OF FIGURES

CHAPTER 1: INTRODUCTION

A variety of seemingly dissimilar research problems related to the lung have, at their core, a need to take into account the underlying dynamics of the involved cells over both space and time.

One such problem deals with the failure in generating ovalbumin (OVA) mouse models of chronic asthma. Many individuals have severe, continual asthma attacks that can be fatal, which according to current theory is most often due to an allergic response triggered by the presence of inhaled antigen. Researchers have attempted to create animal models of chronic asthma by sensitizing and subsequently challenging mice repeatedly with OVA protein as an allergen. Unlike what occurs in chronic asthma, however, the mice eventually stop responding to OVA and return to baseline—a phenomenon known as tolerance. However, if they are challenged again after a month, the mice now undergo a vigorous allergic response. This leads us to suggest a novel hypothesis for the allergic inflammatory response in the lung, which we term the inflammatory twitch. It states that the normal allergic response is a sequence of events that leads to both inflammation and its subsequent resolution, with the implication that chronic inflammatory conditions such as asthma involve a defect that prevents resolution to baseline. This raises the questions of whether the behaviors of the cells involved in the normal allergic response could result in a twitch-like response, and if so, what abnormalities in the response would result in a non-resolving twitch.

Studying issues of lung function leads naturally to questions about how the lung is formed in the first place. We focus on the research problem of how to generate new lungs

from old lungs that have been stripped of their cellular material, leaving behind a protein scaffold that can be subsequently seeded with stem cells in the hopes of growing a new organ. This could eventually enable growth of a new organ specific to an individual's immune system using their own stem cells. However, current efforts in this direction have been mostly exploratory, with little to no formal understanding of the rules of behavior for the utilized cells.

To make headway on both these research questions requires a firm understanding of the spatiotemporal dynamics of the cells and environments. In the case of the allergic response, we must determine the most important behaviors of the cells involved, as well as how they affect and are affected by their local environment. For stem cells, we must critically test hypotheses regarding how the cells could engraft and proliferate on the scaffold and how the cells and the scaffold could interact and affect each other. In both instances, it would be difficult, if not impossible, to take all these interactions into account to make mental predictions of the response over a long period of time. Furthermore, addressing all these issues experimentally would be challenging and require a great deal of time and effort.

However, computational modeling enables us to rapidly vet potential hypotheses regarding the behavior of all the components of biological systems, and can thus serve as a useful adjunct to experimental work to guide our understanding of these systems. Computational modeling is widely used throughout science for understanding complex phenomena and for predictive purposes, and is gaining increasing acceptance in medicine. In this dissertation we examine the use of a specific form of computational

modeling known as agent-based modeling to address questions related to the spatiotemporal dynamics of cells in the lungs. Agent-based models have been widely used for several decades and have recently gained greater interest due to increased available computational power that enables more rapid simulation.

In Chapter 2, we present a comprehensive literature review of computational modeling, with an emphasis on agent-based modeling and its potential usefulness in the biomedical realm.

In Chapter 3, we present an agent-based model of the allergic inflammatory response to determine if twitch-like behavior can emerge from the major cell-cell and cell-environment interactions, which was published in the Journal of Immunology (Pothen, J.J., Poynter, M.E., Bates, J.H.. (2013). The Inflammatory Twitch as a General Strategy for Controlling the Host Response. Journal of Immunology, 190(7):3510-6.).

Chapter 4 shows how we use this model to test a range of potential defects to the twitch mechanism to determine which (if any) prevent its resolution to baseline, which was published in the American Journal of Physiology Lung Cellular and Molecular Physiology (Pothen, J.J., Poynter, M.E., Bates, J.H.. (2015). A Computational Model of Unresolved Allergic Inflammation in Chronic Asthma. American Journal of Physiology Lung Cellular and Molecular Physiology, 308(4):L384-90).

In Chapter 5, we then critically test the twitch hypothesis's implications of the twitch duration and the refractory period in OVA mouse models (submitted for publication: Pothen, J.J., Poynter, M.E., Lundblad, L.K., Bates, J.H.. Dissecting the inflammatory

twitch in allergically inflamed mice. American Journal of Physiology Lung Cellular and Molecular Physiology.).

In Chapter 6, we use agent-based modeling to model the behavior of stem cells on decellularized lung scaffolds in order to determine the potential rules underlying the cellular behaviors (submitted for publication: Pothen, J.J., Rajendran, V., Wagner, D., Weiss, D.J., Smith, B.J., Ma, B., Bates, J.H.. A Computational Model of Cellular Engraftment on Lung Scaffolds. Tissue Engineering.)

Chapter 7 closes with a summary of the major findings and future directions for the work featured in this dissertation.

CHAPTER 2: REVIEW OF BIOMEDICAL COMPUTATIONAL MODELS

2.1 Introduction

Investigation into clinical issues often begins with *in vitro* laboratory work, followed by *in vivo* investigation in established animal models and eventual clinical testing [1]. However, initial inquiries in the laboratory often require extensive amounts of both time and costly experimental resources. A more rapid, effective means of vetting proposed hypotheses to determine the most promising to pursue at the experimental stage could thus greatly accelerate the advancement of biomedical knowledge.

To this end, we endorse computational modeling as an alternate, complementary means of studying biological systems. While it cannot replace experimental inquiry due to the complexities of *in vivo* biological systems, computational modeling can serve a useful adjunct, particularly at the initial stages of investigation. *In silico* models provide a rapid, cost-effective way to test the feasibility of potential hypotheses regarding a biological system, thereby facilitating experimental pursuit of hypotheses with increased likelihood of success. These models represent our understanding of the most important features of a biological system. If the model fails to behave like the system under study, then it indicates that there is at least one other important feature missing in the model, and thus from our understanding. The model can then serve as a virtual laboratory for the investigation of what these missing factors might be.

2.2 Forms Of Computational Models

Here we highlight some of the more common forms of computational modeling encountered in biological studies.

One means of computationally representing a biological system is via a system of mathematical equations, often ordinary or partial differential equations (ODEs or PDEs, respectively). Such models have been used, for example, to model the normal and diabetic response in the glucose-insulin regulatory system [2-8], the MAPK/ERK pathway implicated in many forms of cancer [9-11], the β-adrenergic and NO/cGMP/PKG pathways in cardiac cells [12-13], the hemodynamic response to occlusion of blood vessels [14-15], and the number of cells in each stage of the differentiation process for adipose cells [16] and hematopoietic stem cells [17-20].

Differential equations are by their nature continuous, and assume that the variables involved are continuous in nature. Therefore they cannot capture discrete events, such as variables that undergo a discontinuous transition between different values such as from zero to non-zero (which may serve as a transition from an off state to an on state), or discrete agents in the model that alter their behavior over the course of the simulation. These equations often involve multiple parameters that must be determined by fitting the equations to an existing dataset. Thus to effectively utilize this form of modeling also requires some foreknowledge of the quantitative behavior of the phenomenon being studied, which can be problematic in cases where continual experimental measurement of the phenomenon is difficult or impossible to perform. Furthermore, ODE equations capture change in a system with respect to a single variable,

often time. PDEs can determine the change in a system with respect to multiple variables, such as both time and space, but are more difficult to solve.

However, systems of differential equations can be discretized, as in a form of modeling known as finite element modeling, which is often used to represent systems in which spatial details are important. Here a geometric surface of interest is broken down into simpler individual elements, each of which has mathematical equations governing its behavior. Combining these elements computationally thus enables prediction of the entire structure's behavior. Some examples of biomedical research questions studied using FEM include repair of bone fractures [21-22]; mechanical behavior of normal and abnormal aortic valves [23-35], along with those valves following surgical interventions in the aorta [36-44]; the change in forces and movement of the bone, ligament, muscle and cartilage components of the knee joint in response to normal movement [45-58] and in response to osteoarthritis [59-63], the flow of lymph fluid across lymphatic valves [64-65], and the effects of deep brain stimulation therapy on electrical activity in various brain structures [66-69]. In all of these, FEM is an intuitive modeling form because of the emphasis on the geometry and known mechanical or physical behavior.

Another discretized mode of modeling is the cellular automaton (CA) [70]. Here, a system is modeled as a grid of stationary "cells", each of which has a state. Each cell's state during a timepoint in the simulation is determined by the state of that cell and others, often neighboring cells. Thus it is intuitive that CA modeling can simulate the growth or spread of a pattern throughout an environment. There are many published CA

models that study, for example, the behavior of tumor cells such as their growth and apoptosis [71-80], genetic evolution [81-87], and their eventual metastasis throughout an environment [87-89]. Other examples of CA models include the spread of HIV-1 throughout lymphoid tissue [90], simulation of pressure in uterine cells during pregnancy contractions [91] and electrical wave propagation in both cardiac [92] and intestinal cells [93-95]. In these models, the cells involved are often stationary. It is possible to model motile elements such as cells that traverse the environment in CAs, though it is less intuitive relative to other methods.

2.3 Overview Of Agent-Based Modeling

For the remainder of this review, we concern ourselves with agent-based modeling. While there are other ways of defining an agent-based model (ABM), we use the definition in which an ABM is a discretized model in which a group of agents interact over space and time within an environment according to user-set rules [96-98]. This environment can be modeled either continuous (real space) or discrete (e.g. a 16 x 16 tile grid), and can be tailored to represent a variety of 2-D or 3-D structures. Agents, as indicated by their name, are distinct from the environment and can affect both the environment and other agents over the timecourse of the simulation. They can represent a variety of objects, such as molecules, cells, tissues, or organs. Each agent has a local neighborhood defining the subset of the environment and agents that it can interact with at a particular instant in time. To determine the state of the agents at a particular timepoint, the rules are applied to each agent in the model at the previous instant in time.

The flexibility in the design of ABM's enables us to easily represent and investigate the spatiotemporal dynamics of a variety of biological systems at many scales. Modeling multiple pieces of a biological system simultaneously allows for cross-talk between different types of interactions such as cell-cell or cell-environment (as defined by the model rules). Even when these interactions are simple, they can lead to emergent behavior—phenomena with complex behavior that could not have been easily predicted beforehand. This is particularly advantageous, as it means that the precise quantitative behavior of the system does not need to be known beforehand but arises naturally out of the interactions inherent in the model.

It should be noted that ABMs can have formal similarity to other forms of modeling. For instance, a CA model can be thought of as a type of ABM. However, ABMs are perhaps the most intuitive form of computational modeling for any biological system. This enables easier comprehension of the model's formal construction across multiple research disciplines.

Interestingly, many of the earliest ABM's were developed in the realm of social science. In 1971, Thomas Schelling proposed a model of segregation in which agents within a two-dimensional environment can move and dynamically self-segregate based on rules determining each agent's preferences regarding neighbors and space [99]. Since then, ABM's have been utilized by many social science fields, including psychology, economics, law and anthropology [100]. Questions addressed by many of these models include decision-making as it pertains to individuals, groups and markets [101-115],

dissemination of ideas and resources across groups and societies [116-136], the use and change in land and urban areas [106-108, 137-157], the formation and dynamics of social networks in groups and societies [158-178], and understanding and predicting the outbreak of sociopolitical change and conflict within a region [179-196].

2.4 Agent-Based Models In Biomedical Research

In the field of biology, ABM's have been used to model such phenomena as animal behavior [197-217], the epidemiology and transmission dynamics of infectious diseases [218-237], and the pathogenesis, growth and metastasis of tumors [238-255]. To illustrate the numerous possibilities for ABM's to elucidate human disease, we discuss seven recently published biomedical ABM's. These include models of breast cancer, the immune system, melanoma, pressure ulcer formation, embryonic vasculogenesis, muscle atrophy and lung inflammation. Together, these models demonstrate the breadth and depth of systems that can be rapidly investigated using this form of computational modeling.

In the subsequent sections, we discuss the biomedical question each ABM was designed to answer and explain the authors' reasoning for utilizing a computational approach. We provide a brief overview of the key features of each model, with an emphasis on how the agents, environments and rules were chosen and calibrated. We then show and discuss results generated from the model, with an emphasis on emergent phenomena and insights into the biological systems that can be used to generate hypotheses for future wet lab experimentation.

2.4.1. Breast Cancer

The first model we examine is an ABM of the pathogenesis of breast cancer in ductal epithelium [256]. This model examines how different combinations of genetic events accumulate over time, resulting in sequences of events that can transform normal mammary cells into tumors that do or do not express estrogen receptors. The classification of tumors into ER+ and ER- types, respectively, is a classical method for studying breast tumors and determines appropriate medication regimens.

The impetus for creating a computational model to explore the pathogenesis was the inherent difficulty in utilizing a detailed experimental investigation. Longitudinal study of the breast epithelium's transformation into the early tumor is difficult if not impossible, as the timescale over which the mutations accumulate and result in cancer is both long and highly variable. The mutations associated with breast cancer are also rare, making it difficult to identify how combinations of these genetic changes affect the normal function of the epithelium prior to detection of the tumor, by which point the tumor has already grown to a considerable size. The complex nature of the cellular environment further complicates this analysis, as it contains both activating pathways that lead to tumor formation, along with inactivating pathways and means of compensating for molecular changes.

This led the researchers to develop an ABM where the environment is a 2-dimensional section of bilayered mammary epithelium, indicative of a mammary duct that has been cut open and laid flat. The agents are the cell types selected by the

researchers as the most importance to maintenance of the ductal epithelium: luminal and myoepithelial cells, stem and progenitor cells, and fibroblasts. While the model is presented in extensive detail in the paper, we summarize its major features here. Myoepthelial cells and their progenitor cells have a neighborhood defined by the

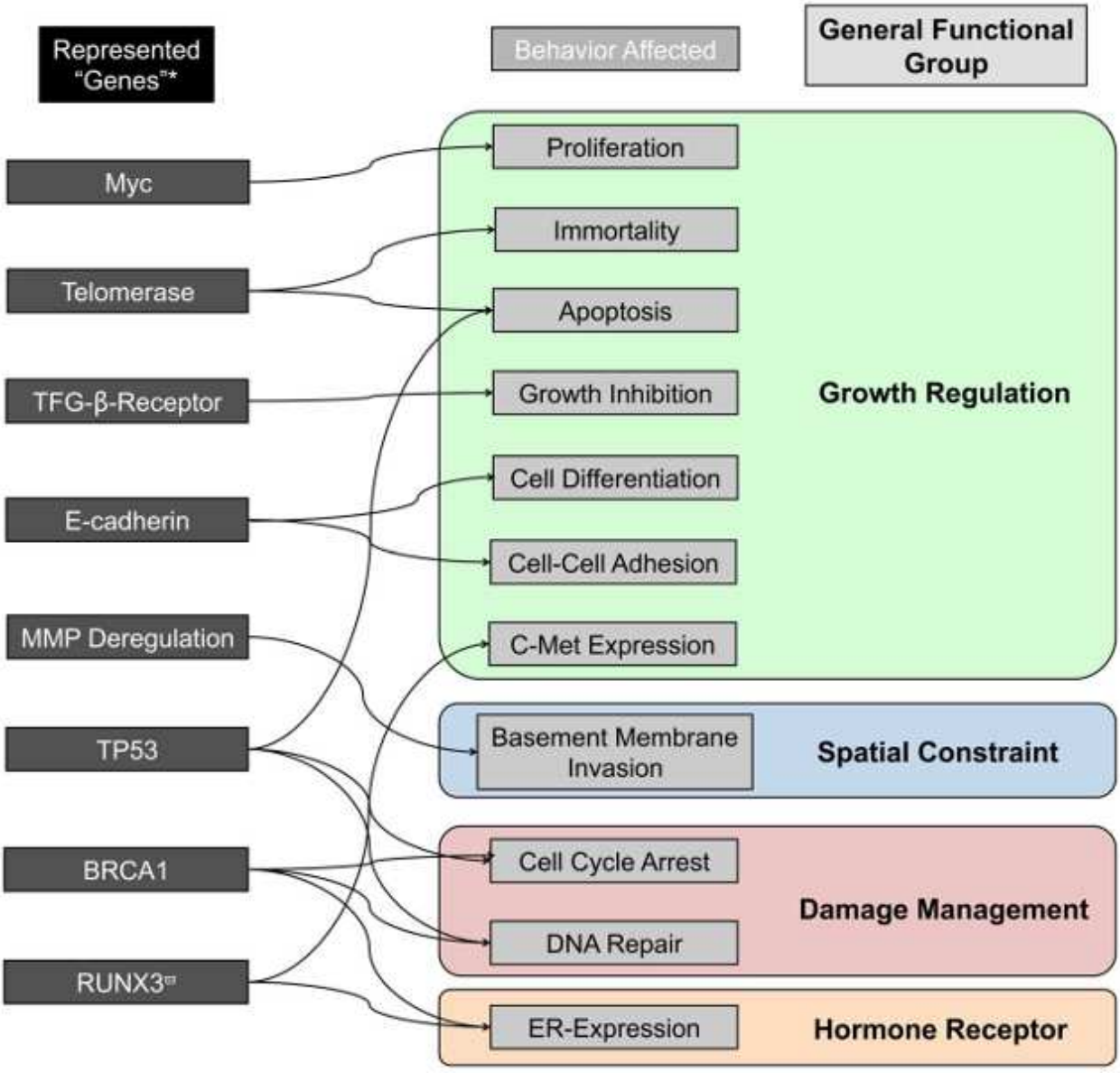

Figure 1: Set of genes and the rules underlying their direct effects on cellular behavior and the environment in the ductal epithelial ABM. Modified from [254]

surrounding patches, i.e. if they are in the center tile of a 3x3 tile grid, their neighbors are the eight surrounding tiles. Other cells tend to consider the grid patch they are currently on or the patch directly ahead. Each cell is represented as having both DNA and cellular receptors, and thus has variables representing receptors, signaling molecules (e.g. hormones), genes, gene transcription factors and DNA lesions. Furthermore, the cells have DNA repair mechanisms that can fix damage to the genes. The cells in the model undergo division and apoptosis, and can pass on subsequently damaged or mutated DNA to cells, allowing mutations to accumulate over time. While cells have two copies of each gene, one functional copy of the gene enables the cell to maintain that gene's function. The rules for this model, summarized briefly in Figure 1, dictate the effects of the

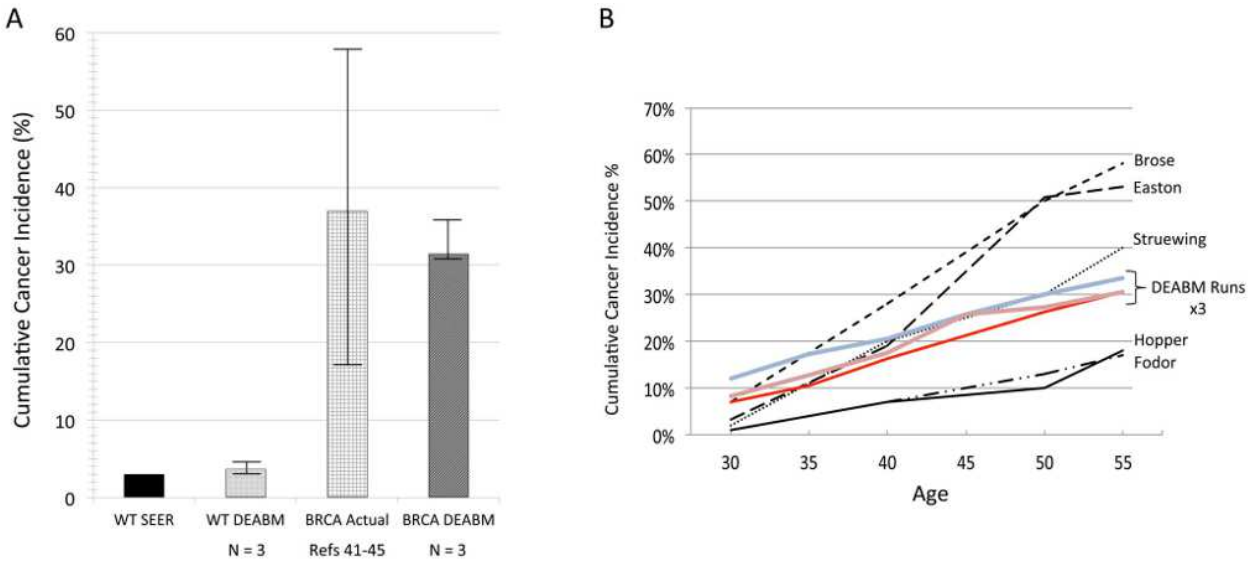

Figure 2: (A) Cumulative cancer incidences, reported as percentages of all individuals, from SEER 2010 review data and the ductal epithelial ABM, for individuals with and without BRCA1-mutations (simulated as in the ABM as a loss-of-function). For the computational model, these percentages were reported after 15000 steps or ~40 simulated years, with the average result of 3 subgroups, each with 500 simulations. (B) Longitudinal cancer incidences between ages 30 and 55 as reported in 3 separate runs of the ABM (with 500 simulations for each run) and from previously published studies (with each one labeled by author name). Modified from [254]

expressed genes on the cell, such as expression of hormone receptors, damage management, space constraints and growth regulation of the cell. The model was calibrated so that 1 time step is the equivalent of 1 day, and then run for the equivalent of 15,000 days (about 40 years).

The ABM enabled the researchers to determine factors missing from their understanding of tumorigenesis. Given the impossibility of accounting for every gene related to the mammary duct, the model initially contained a minimal set of 7 genes known to be critical in tumor development. However, this version of the model only yielded ER- tumors, which they determined was a result of ER+ cells being unable to divide. They then searched for a gene that could modulate ER+ cell proliferation, which led them to the gene RUNX3. Once this was included in the gene set, the ABM yielded outputs for the cumulative cancer index for both BRCA and non-BRCA mutated tumors (Figure 2) that were consistent with previously reported experimental measures, both for tumors with a mutated, nonfunctional BRCA gene and for tumors where this gene was unperturbed. The percentage of ER+ tumors for both BRCA and non-BRCA mutated tumors were also consistent with percentages previously reported in longitudinal studies, as seen in Figure 3.

As RUNX3 had not previously been considered a potential player in ER+ tumorigenesis, the researchers investigated this gene using data from two databases of cancer transcriptomes, and confirmed that loss of RUNX3 was correlated to ER+ status in formation of ER+ tumors. The ABM simulations indicate that loss of RUNX3 results in

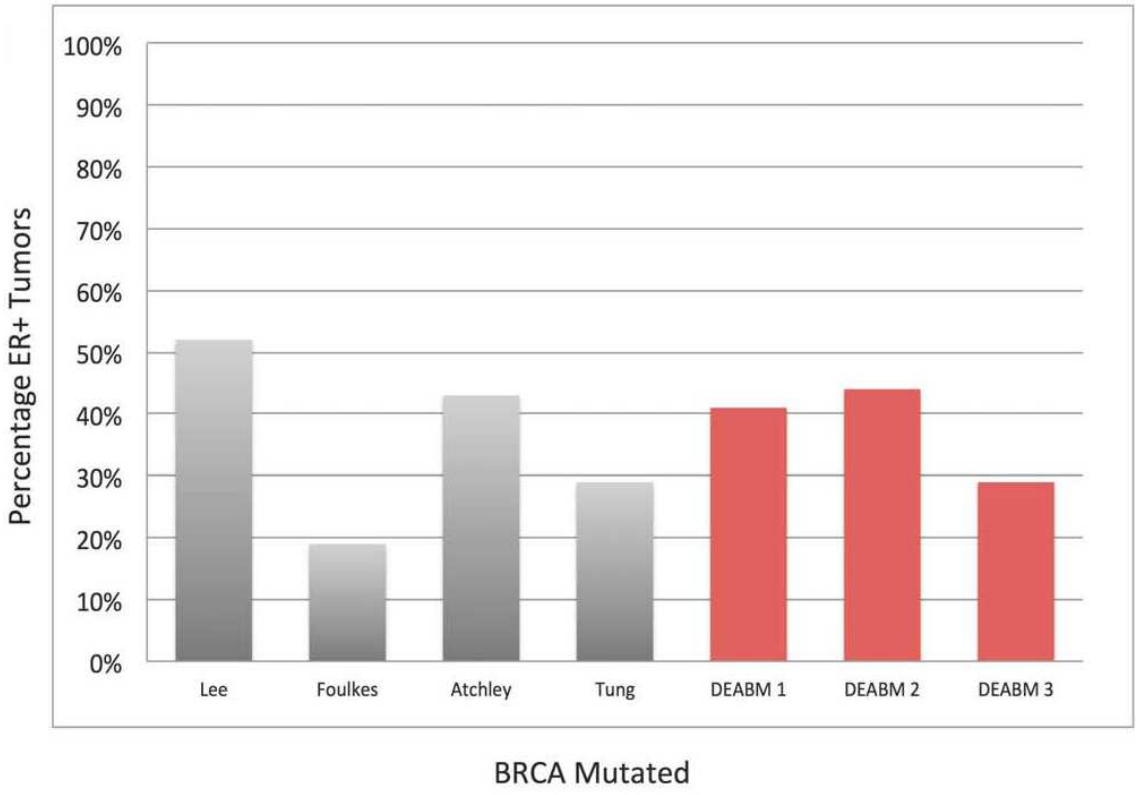

Figure 3: Percentage of ER+ tumors with a BRCA mutation, from literature studies (shaded in gray, labeled by author name) and from 3 separate runs of the ductal epithelial ABM (shaded in red, each with 500 simulations). Modified from [254]

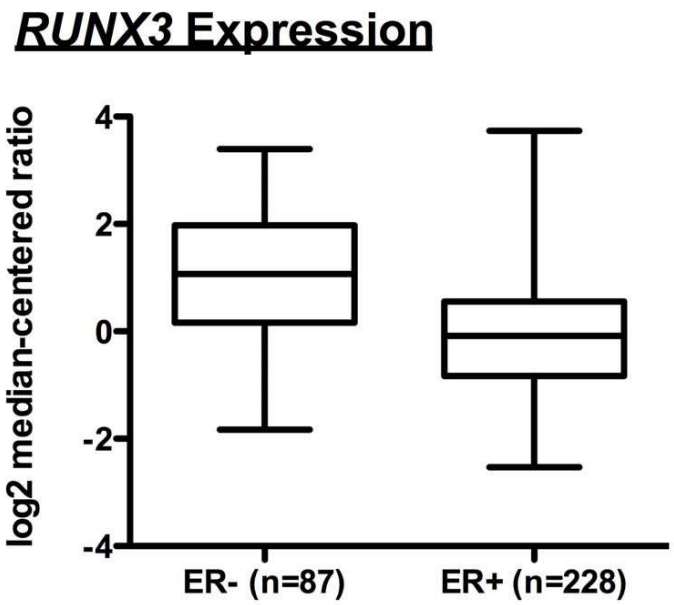

Figure 4: RUNX3 expression for ER- and ER+ individuals utilizing data from the Cancer Genome Atlas and Oncomine, expressed as log2 median-centered ratios. Modified from [254]

breast tumors (Figure 4). This raised the question as to how RUNX3's loss affects the ER+ luminal cell expression of c-Met, and allows ER+ cells to receive proliferative stimuli via HGF signaling. Thus the ABM provided a novel hypothesis about a critical gene involved in ER+ tumorigenesis and its role in tumor formation, which can now be tested experimentally.

2.4.2. Human Immune System

We now turn our attention to a 3-dimensional ABM that studies the decentralized processes in the human immune response to viral infection [257]. This response incorporates humoral and cell-mediated immunities in both lung and lymph node regions of the human body.

The model was developed due to the difficulty in utilizing a purely experimental approach to study immune processes in multiple regions of the body, specifically cellular movement and interactions throughout the entire timecourse of the response. Even in isolated regions the immune processes are inherently complex, involving so many cells and signals that measuring all the interactions at each moment in time would require great effort. Furthermore, responses such as the host immunity to pathogens are known to be complex emergent phenomena, and thus unable to be predicted mentally due to the sheer number of components and the associated behaviors.

This led the researchers to create a multiscale 3D ABM of the immune system as seen in the lung and a regional lymph node, incorporating modeling at the sub-cellular,

cell, tissue and organ scales. The individual agents are epithelial cells, viruses and the immune cells involved in the humoral and/or cell-mediated responses (namely macrophages, dendritic cells, B cells, T cells and antibodies), as shown in Figure 5. In the model, each agent has an attraction sphere centered around it, enabling two agents to interact if one of them enters the attraction sphere of the other. This defines the neighborhood over which agents can interact. Figure 6 shows the set of interactions in the model and how they change the states of the cellular agents. The lung region of the model is created as an environment of 200 epithelial cells that are initially placed in the model, after which they can reproduce and arrange themselves depending on their interactions. The lung also contains immature dendritic cells that, upon activation with viral particles, can migrate to the lymph node region of the model, which contains B and T cells. These can both become specific to the virus in order to help clear it from the model, as well as undergo proliferation or apoptosis. Cell migration between the two regions is modeled by having the lung and lymph node environments exchange the total number of agents within them along with the current environmental state at each timepoint. The agents in these compartments then use the latter information to update their behavior accordingly. The ABM was run for 20 simulations with each simulation taking 6000 time steps, calibrated to be the equivalent of 30 days.

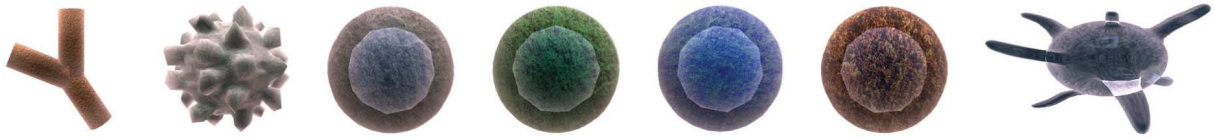

Figure 5: List of agents utilized in the immune system ABM (not drawn to scale): a) antibody, b) virus, c) epithelial cell, d) B cell, e) T cell, f) macrophage and g) dendritic cell. Modified from [255]

Using this model, the researchers could visualize the spread of infection with virus (in this case, influenza A) through the lung and lymph nodes and determine the extent of immune system activation by measuring viral load and the number of each cell type over time. Figure 7 shows a graphical representation of the change in the lung epithelium in response to viral infection, as well as the proliferation of B and T cells in the lymph node. Importantly, the researchers found that viral loads did not result in a hyperactive immune system or in complete tissue destruction, but yielded results consistent with what was predicted by another robust mathematical model of the spread of influenza A infection.

The ABM also enables prediction of the immune system's adaptive capabilities,

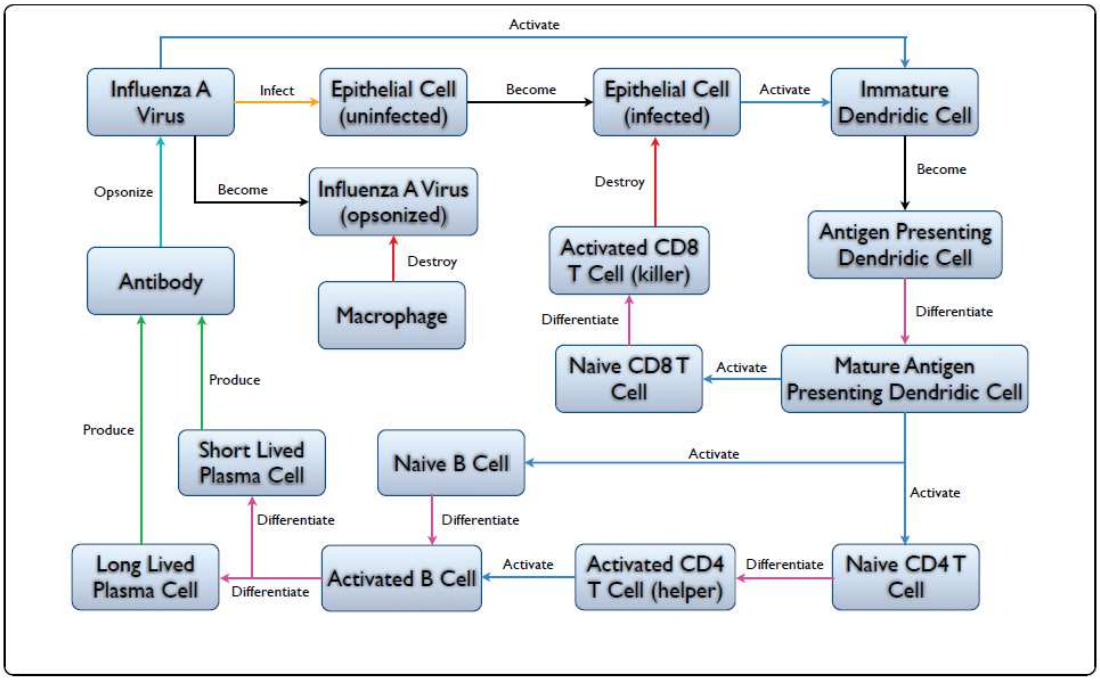

Figure 6: Schematic illustrating the rules governing agent interactions in the immune system ABM. Different colors indicate different types of interactions. Modified from [255]

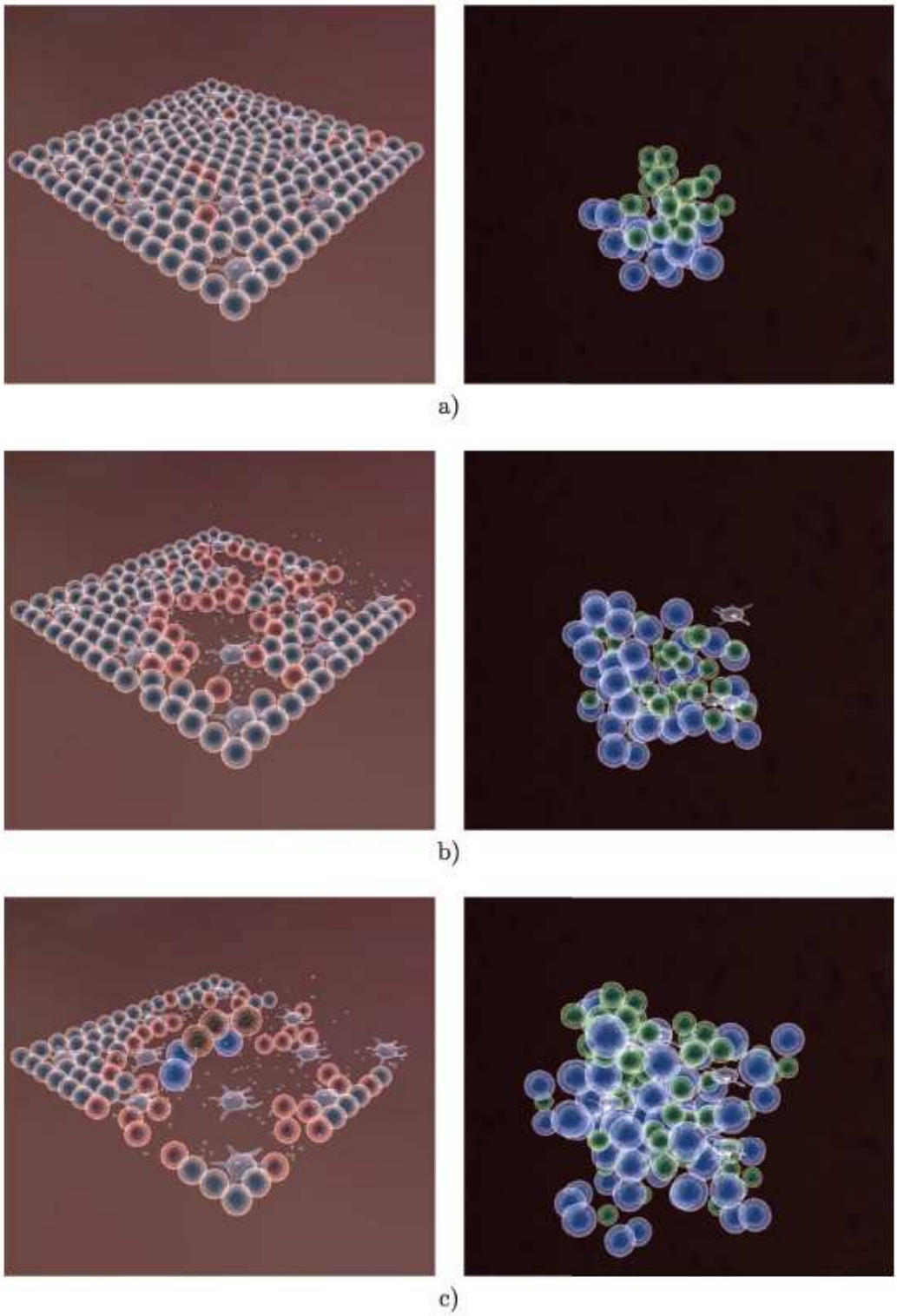

Figure 7: Images of the immune system ABM's tissue (left) and lymph node (right) environments over time in response to influenza infection. Blue and green spherical cells represent healthy cells, while red cells indicate infected cells. Modified from [255]

measured here by how the system responds to a second viral exposure. They observed a distinctive response relative to the response triggered by the first exposure, as shown in Figure 8, with significantly less damage and a lower maximal viral load. The cell-mediated reactions also started earlier and were significantly less intense, and the overall timecourse of the adaptive response is consistent with what has been reported in multiple immunology textbooks. While these are preliminary results, they nevertheless illustrate how complex immune processes can be visualized and studied over time across multiple organs and regions.

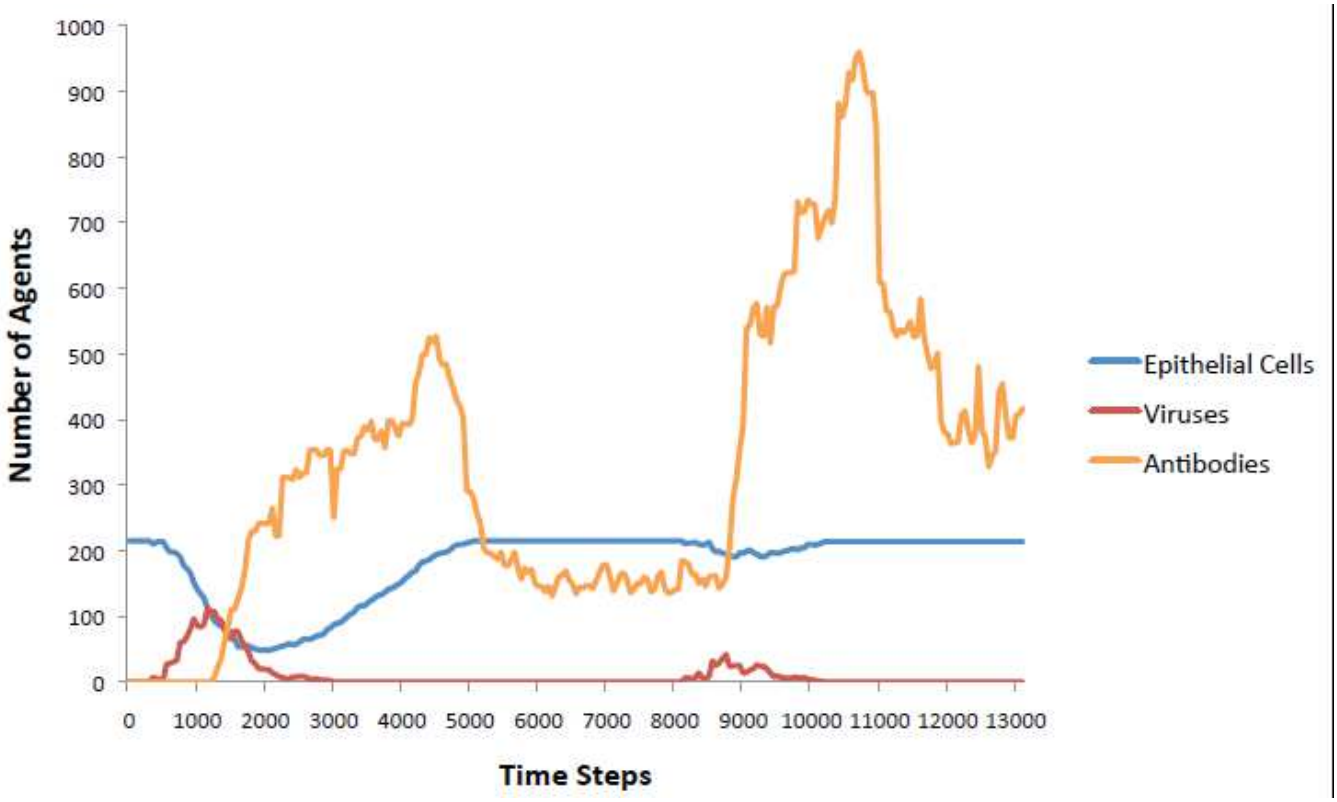

Figure 8: Number of agents over the timecourse of the immune system ABM simulation, with reintroduction of the virus at time step 8000. Modified from [255]

2.4.3. Melanoma

We now examine an ABM of melanoma behavior and associated angiogenesis [258]. Melanoma is the most malignant type of skin cancer, responsible for 3/4 of all skin-cancer-related deaths. While there is interest in a chemotherapy treatment, there have been drastic differences between *in vitro* and *in vivo* success of drugs due to issues in absorption, distribution, metabolism and toxicity.

To address this, the researchers focused on the effects of different drugs on both the behavior of melanoma cells and the development of new capillary sprouts. They focused on the latter factor, though less intuitive, because angiogenesis enables more nutrients and oxygen to be brought to the tumor and thus is significant in its growth and survival, and because the shape of a tumor's underlying vasculature affects the distribution of the drug. To more fully understand these effects, they wanted to observe the effects at multiple scales: intracellular, intercellular and tissue. Given the difficulty of generating an experimental protocol that would allow observation of each scale at every instant in time, they developed a 3D ABM containing these three scales, which they noted was the first of its kind at the time of publication.

In this model, the agents are melanoma and endothelial cells, which can both exist in active (migratory or proliferative), dead (apoptotic) or quiescent phenotypic states. Both can grow into tumor and vasculature, respectively, within a 3D cube environment that simulates a slice of tumor extracellular matrix (ECM). The model is initialized with 100 active melanoma cells distributed as a sphere in the center of the cube, along with 16

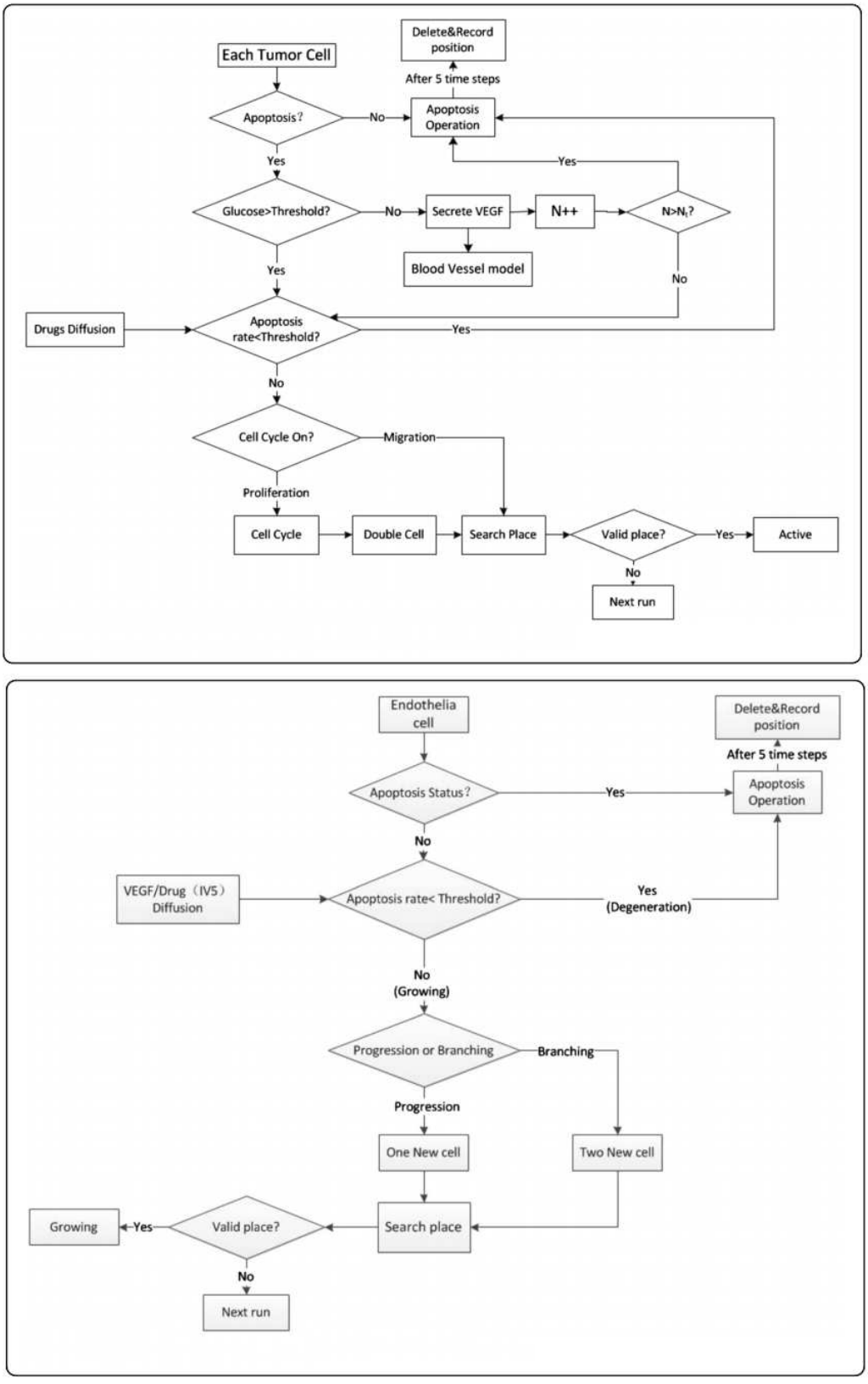

Figure 9: Schematic showing the states and behavioral rules for tumor cells (top) and endothelial cells (bottom) in the melanoma ABM. Modified from [256]

endothelial cells distributed on the surface of the ECM. VEGF and glucose are required for growth, and are normally distributed throughout the cube when the model is initialized. The vasculature can also deliver oxygen, cytokines and glucose to the tumor's melanoma cells, which may undergo phenotypic switching in response to the cytokines, and which can secrete VEGF once there is a drop in glucose and oxygen. A drop in the latter induces blood vessel sprouts to branch outward. A graphical layout of the rules for the tumor and endothelial cells in the model is shown in Figure 9. Equations regulating apoptosis follow an exponential distribution, while the levels of glucose, VEGF, or drugs at any location and moment in time follow a recursive function dependent on the levels at that location and on its six neighbors (Von Neumann neighbors) at the previous instance in time.

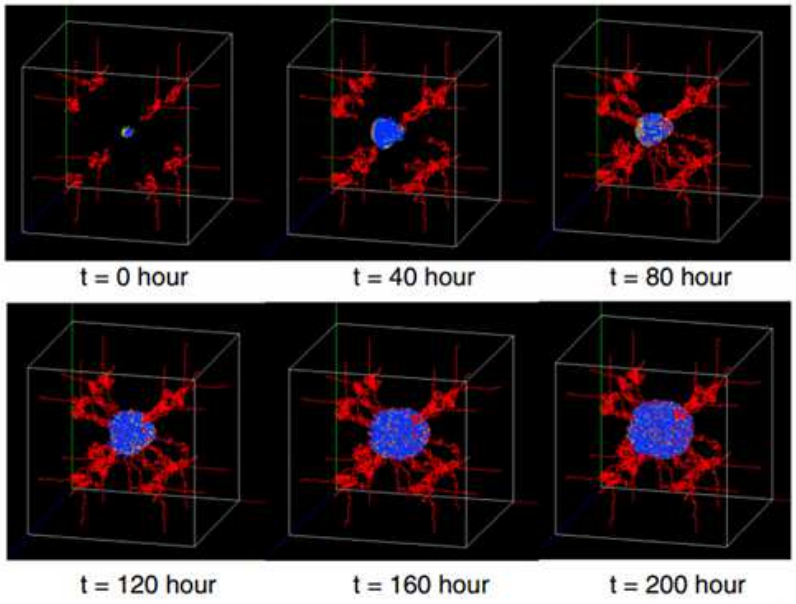

Figure 10: 3D images of the melanoma ABM at different timepoints, indicating the tumor (central mass) and associated vasculature composed of endothelial cells (colored in red). The tumor is composed of cells that are quiescent (blue), active (yellow), or dead (gray). Modified from [256]

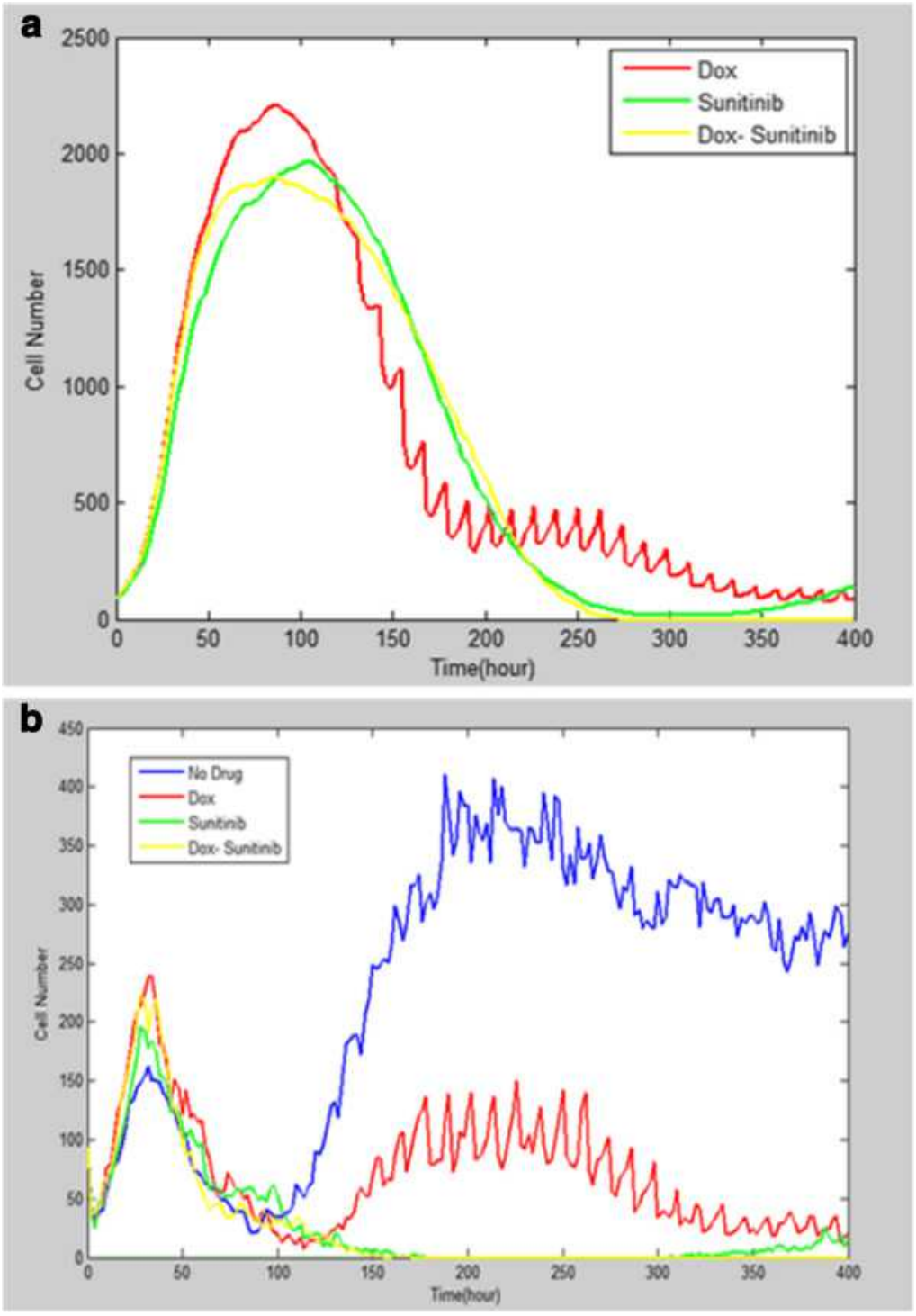

Figure 11: For the melanoma ABM, a) Total number of cells following no drug (control), doxorubicin, sunitinib or both doxorubicin and sunitinib over the timecourse of the simulation. b) Number of active cells under the different drug treatments over the timecourse of the simulation. Modified from [256]

The model also tests two drugs: doxorubicin, an anti-tumor drug that increases the rate of apoptosis by directly incrementing appropriate model parameters, and sunitinib, an anti-angiogenesis drug that prevents endothelial cell receptors from receiving the VEGF produced by fast growing melanoma cells, thereby increasing the rate of apoptosis of the endothelial cell tip. The researchers investigated the effects of these two drugs both alone and in combination to determine the most efficacious treatments for inducing melanoma apoptosis. Each experiment in the model was performed 20 times and was run for 200 time steps, calibrated to be the equivalent of 400 hours.

Using the model, the researchers generated hypotheses regarding the behavior of the individual cells and the tumor. For instance, they observed that near blood vessels, quiescent tumor cells often switch to a migratory or proliferative mode. They also compared the 3-D volume of the tumor over the timecourse of the simulation against experimental measurements of tumor growth to illustrate a comparable growth curve. Figure 10 shows representative images of the tumor at various timepoints in the simulation. Using these, they determined the appearance of the surrounding vasculature and the states of all the cells in the model over time. Utilizing the angiogenesis-targeted sunitinib was significantly more effective than the anti-tumor drug Doxorubicin at decreasing the size of the tumor. However, the two drugs in combination had a synergistic effect that both increased the rate of apoptosis and decreased the amount of nutrients delivered to the tumor (Figure 11). The researchers used a sensitivity analysis of the model parameters to confirm a high correlation between blood delivery rates of nutrients and drugs and the outcome of regression and death of the tumor. This suggests

these two drugs may serve as an effective treatment for melanoma, and can now be evaluated experimentally for their efficacy.

2.4.4. Pressure Ulcer Formation

The next ABM we consider studied the dynamics of skin blood flow and pressure ulcer formation [259]. The underlying motivation is care of patients with spinal cord injury (SCI), for whom total cost of care in the United States alone amounts to $7 billion each year. In this population, there is a high prevalence of pressure ulcers due to multiple factors such as impaired mobility, sensation and vascularization. Of the potential pathways, the researchers identify pressure-induced tissue ischemia as the most important in determining formation of the ulcer. Interestingly, tissue ischemia paradoxically leads to an increase in skin blood flow, a phenomenon known as ischemia-induced hyperemia. Yet as the ischemia is prolonged, it ultimately results in local inflammation and the necrosis that forms the ulcer. The researchers wanted to use this known biological behavior to develop a tool that could directly improve patient care. In particular, they were interested in determining how often bedridden SCI patients must be turned to prevent ulcer formation. Computational modeling was thus appealing to them since it provided a rapid means of performing turning studies that could not be easily performed in human subjects.

The researchers had previously determined a set of differential equations governing blood flow in skin, but this lacked information regarding the epithelial spatial features over the timecourse of the ischemic response. Thus they incorporated these

equations as rules regarding blood flow into an ABM of a tissue region that incorporated multiple biological insights regarding skin injury, inflammation and healing. While this ABM is necessarily a simplified version of the *in vivo* system, it nevertheless contains what they determined to be the most important features of the environment and the agent behavior, thus enabling them to capture both local and global features involved in the response to ischemia. Furthermore, this model has a degree of complexity that makes its predictions only realizable through computer implementation.

In this ABM, the environment is a 2D segment of tissue composed of square epithelial cells, with blood vessels distributed in a uniform grid pattern. Epithelial cells can be damaged both by pressure and by chemical signals, and have an individual life value initialized at the maximum value of 100. If the cell's life value ever drops to 0, it dies. If its life drops below a critical value (set at 80), the epithelial cell will release TNF (a coarse-grained version of all pro-inflammatory cytokines) into the environment. The surrounding vessels release oxygen (which diffuses into the eight surrounding patches) and can bring macrophages into the environment. Macrophages are chemoattracted by TNF or else will traverse the environment randomly. These cells can release either TNF or TGF-β (a coarse-grained version of all anti-inflammatory and pro-healing cytokines), which directly damage or repair epithelial cells, respectively. In considering where to move, a macrophage considers three potential locations in the vector of its current direction: directly ahead, ahead and to the left, or ahead and to the right. The rules governing blood flow, and thus the supply of oxygen and macrophages, are governed by the previously determined ordinary differential equation (ODE) system, which receives

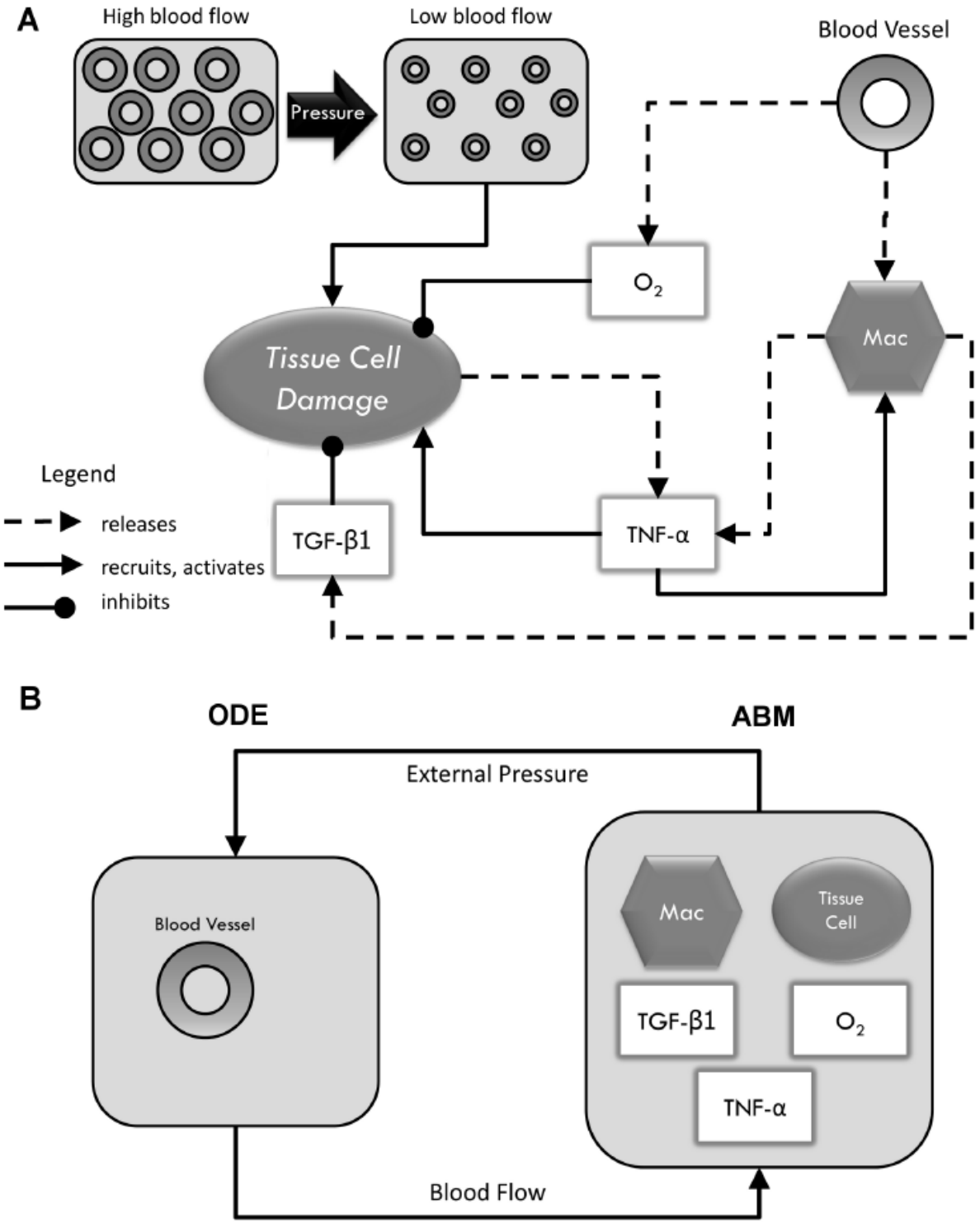

Figure 12: A) shows the main components and interactions in the pressure ulcer ABM (with Mac indicating macrophages, representative of inflammatory cells). B) shows the ODE system is connected to the ABM. Modified from [257]

the ABM's frequency of the applied pressure as an input. We show a diagram summarizing the model setup and the underlying rules in Figure 12. The model was then calibrated using blood flow data for patients with and without SCI, with the latter group functioning as a control. Following calibration of the model parameters for each patient, the researchers then applied different pressure intervals to the model over a timecourse of 2000 time steps.

Simulated SCI patients had substantial death of multiple epithelial cells at lower pressure intervals relative to control patients, as seen in Figure 13. The researchers then tested different turning frequencies for both the SCI and control models, and then tested different turning frequencies in SCI and non-SCI patients, as shown in Figure 14. In both groups, turning every 80 time steps resulted in a stable pattern in the overall health of the epithelial tissue, whereas waiting longer periods of time to turn resulted in a substantial

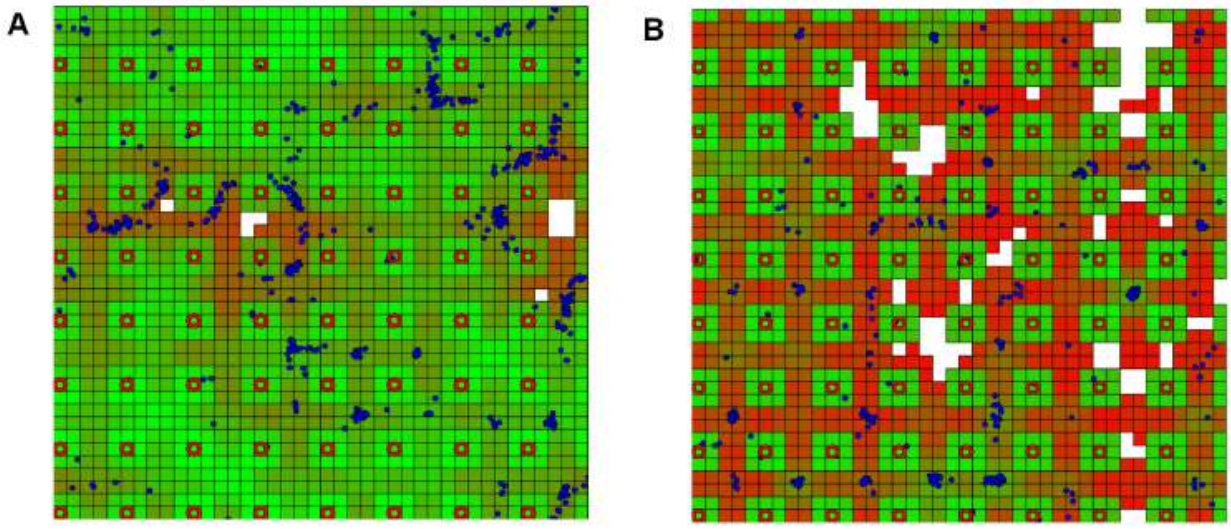

Figure 13: Image of the pressure ulcer ABM after 2000 time steps for A) the control group with a pressure interval of 210 time steps, and B) the spinal cord injury (SCI) group with a pressure interval of 107 time steps. Here, green squares represent healthy epithelial cells, while red squares represent damaged epithelial cells and white squares represent dead cells. Red circles represent blood vessels, and blue circles represent macrophages. Modified from [257]

decrease in the tissue's health, implying a higher likelihood of ulceration. As the timescale of this model is arbitrary, further work must be done to calibrate it to determine clinically appropriate turning frequencies. Nevertheless, it represents a first step in moving towards an ABM that can improve individual patient care.

2.4.5. Blood Vessel Development

The next agent-based model we consider simulated vascular development and disruption during embryogenesis [260]. Its focus is on microenvironmental cues and

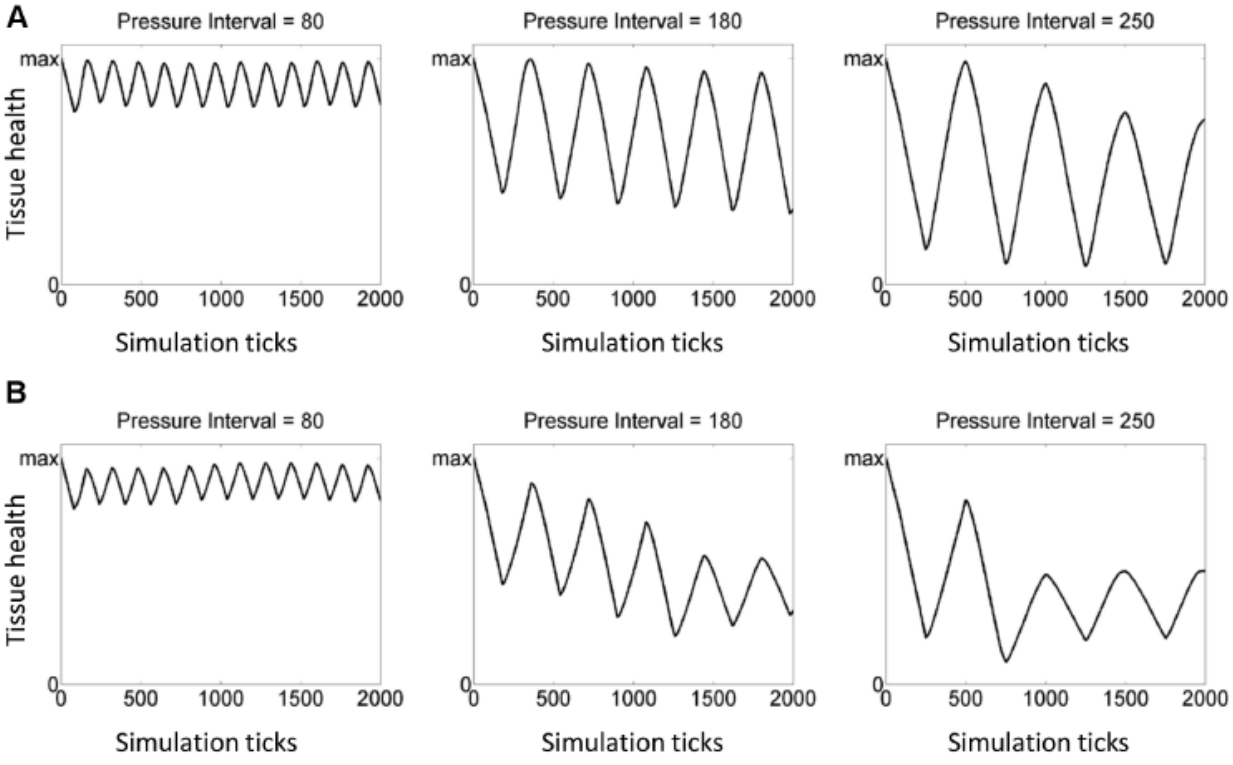

Figure 14: Average tissue health, which decreases as epithelial cells undergo apoptosis, over the timecourse of the simulation of the pressure ulcer ABM for different pressure intervals` for A) control group and B) spinal cord injury (SCI) group. Each group is averaged using the outputs from the model's outputs for six different individuals. Modified from [257]

events that promote or disrupt the growth of capillary plexi. The researchers note that the events involved in the embryo vasculogenesis are similar to those involved in pathological vessel growth, meaning such modeling efforts could ultimately have applications in wound healing and tumor angiogenesis, for instance.

Agent-based modeling was advantageous in this study because of the complexity of the processes involved. Predicting embryonic behavior requires accounting for a large amount of biological data regarding complex cell-cell and cell-environment interactions across multiple biological pathways, as well as the coordinated regulation of cellular behavior such as mitosis, migration, contractility and extracellular matrix (ECM) remodeling. Thus the researchers argued that a thorough understanding necessitated a multiscale modeling approach that incorporated this knowledge to allow for the possibility of emergent behavior, which can then be evaluated for biological insight. Furthermore, by developing a model that can simulate normal growth, the researchers could then simulate the effects of different chemicals to determine if they disrupt normal vessel growth, and if so, how. This ultimately could help them further determine the most critical events in normal capillary formation.

To do this, the investigators developed a 2D cellular ABM that simulates lateral splanchnic mesoderm as a flat plane upon which developing vessels can grow. The agents in this model are inflammatory cells (ICs), apoptotic cells, mural cells (MCs), endothelial-tip cells (EC-tip) and endothelial-stalk (EC-stalk) cells. In order to both determine the major cellular signals and parameterize the model appropriately, they

constructed an e-library to retrieve relevant articles on embryonic and fetal blood growth and development. They then selected 12 chemical signals that influence cellular behavior either alone or in combination. Seven of these are represented as biochemical fields with diffusion equations, while the other five are represented by their effects on cellular behaviors (e.g. engraftment, motility). The rules governing these signals' effects on the cellular behaviors are shown in Figure 15. The physical features of cells (e.g. cellular volume) and their behaviors (e.g. chemotaxis) are modeled as a system of equations utilizing the features of surrounding cells.

Cell Type	Behavior	Signal
Endothelial Tip Cell (EC_t)	migration up chemotactic gradients	VEGF165, VEGF121, CCL2
	secretion of proteases that break down ECM and release growth factors	PAI1, Proteases, VEGF165
	expression of chemokines	CCL2
	motility along the ECM	uPAR, VCAM1
	Apoptosis	
Endothelial Stalk Cell (EC_s)	proliferation in response to growth factors	VEGF165, VEGF121
	inhibition of proliferation	CXCL10
	secretion of proteases that break down ECM and release growth factors	PAI1, Proteases, VEGF165
	secretion of soluble decoy receptors that bind and sequester growth factor	sVEGFR1
	adhesion to other cell types	Tie2, VCAM1
	assumption of tip cell type based on free surface area and growth factor concentration	VEGF165, VEGF121
	motility along the ECM	uPAR, VCAM1
	quiescence based on shared surface area with other cells	
	Apoptosis	
Inflammatory Cell (IC)	migration up chemotactic gradients	CCL2
	expression of chemokines/growth factors	VEGF121, CCL2, CXCL10
	interaction with the ECM to release bound growth factor	VEGF165
	adhesion to other cell types	VCAM1
	Apoptosis	
Mural Cell (MC)	expression of chemokines/growth factors	VEGF165, VEGF121, CCL2
	adhesion to other cell types	ANG1, VCAM1
	motility along the ECM	PAI1
	promotion of endothelial quiescence based on shared surface area	
	Apoptosis	

Figure 15: List of all cell types, along with their associated behaviors and signals in the vasculogenesis ABM. Modified from [258]

From the model, they observed that capillary networks indeed emerge as a result of environmental cues and cellular behavior. As shown in Figure 16, an initial network forms as a result of EC-tip cellular exploration of the local environment, which is then followed behind by EC-stalk cells that subsequently proliferate. The network subsequently grows and reaches a steady state in which the total number of cells remains the same while the network nevertheless continues to grow and remodel, leading to increased vessel thickness and proliferation stabilized by surrounding MCs. This activity results in part via bridging of the EC-tip cells, a consequence of both signal concentration fields and cellular adhesions.

The researchers then used the ABM to explore how vasculogenesis is disrupted by

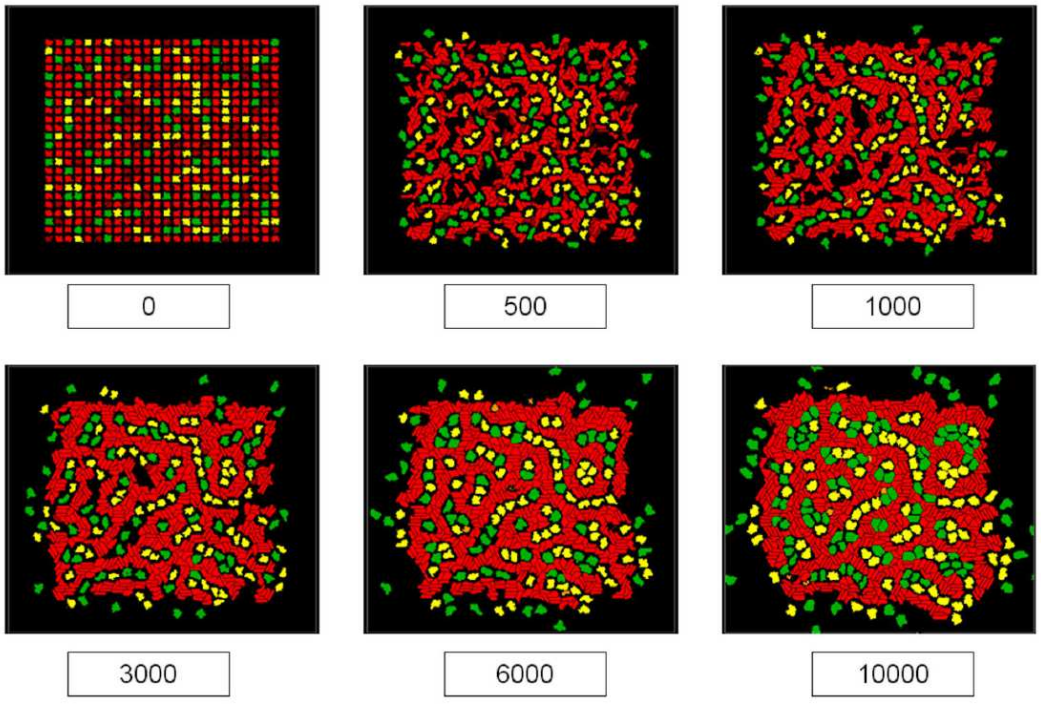

Figure 16: Snapshots of the control-calibrated vasculogenesis ABM at six different timepoints over 10,000 time steps (or 3 computational hours). Red cells represent endothelial cells, green cells represent mural cells, and inflammatory cells represent yellow cells. Modified from [258]

5HPP-33, a reference molecule known to be anti-angiogenic. They determined several molecular effects of 5HPP-33 using a high-throughput screening (HTS) assay, which were simulated by perturbing associated model parameters accordingly. Snapshots of the model treated with varying levels of 5HPP-33 were compared against experimental images of human umbilical vein endothelial cells (HUVECs) stimulated to undergo vasculogenesis and subsequently exposed to different concentrations of 5HPP-33. These comparisons were made both qualitatively and quantitatively, as shown in Figure 17, through image analysis software known as Angiotool. These indicate similar features in the resulting computational and experimental networks, such as increased vessel plexus disruption and cellular clustering as the concentrations of 5HPP-33 are increased. While

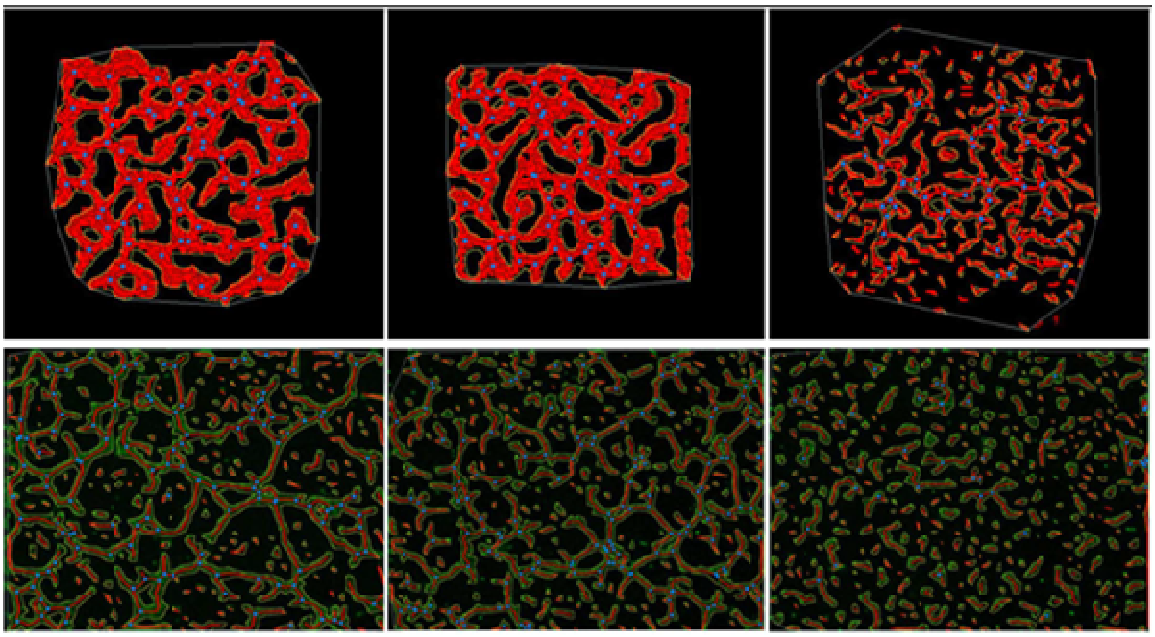

Figure 17: Top row shows snapshots of the vasculogenesis ABM in response to 0 µM (control), 4.44 µM (low) and 40 µM (high) concentrations of 5HPP-33 from left to right, respectively. Bottom row shows images of experimental images of human umbilical vein endothelial cells stimulated to undergo angiogenesis in the presence of 0, 4.44 and 40 µM of 5HPP-33. Both rows were analyzed using AngioTool software to show staining and segmenting of endothelial cells (ECs), with non-ECs set to black. Modified from [258]

this experiment thus serves as a proof-of-concept of the ABM, it nevertheless indicates how other molecules could be rapidly studied using the ABM following calibration with HTS results in order to generate hypotheses regarding their effects on vasculogenesis.

2.4.6. Muscle Atrophy

The next ABM investigated changes in muscle behavior in response to atrophy [261]. Muscle atrophy causes 1.5% ($18.5 billion) of healthcare costs for elderly in the United States, and is an important factor in medically-related bed rest or immobilization. The researchers note that muscle response is well-characterized in terms of the many cellular and molecular consequences resulting from cellular interactions within the responding muscle. The difficulty lies in integrating this knowledge to predict how any individual muscle responds to disuse, which prompted the adoption of an agent-based computational model.

We show an image of the model in Figure 18, along with the different agents and their respective rules in Figures 19 and 20, respectively. Briefly, the model is of a 3 μm-thick cross-section of muscle, made of a single muscle fascicle composed of 14 muscle

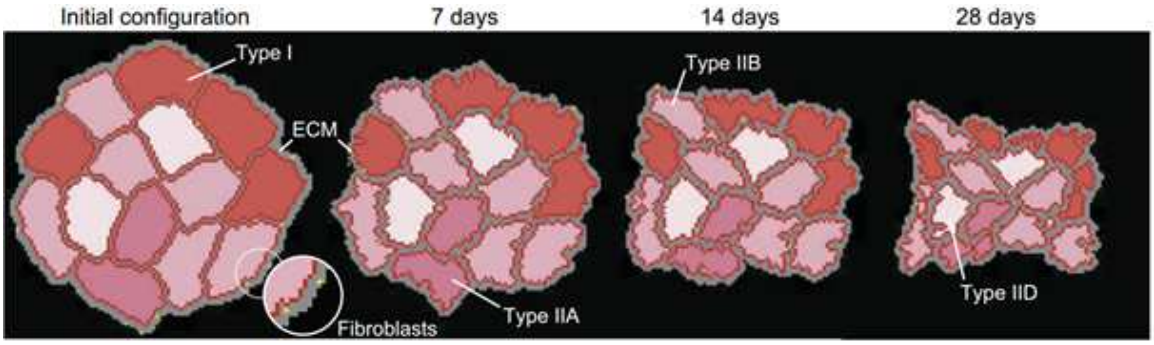

Figure 18: Representative images of muscle atrophy ABM at 0, 7, 14 and 28 computational days. Modified from [259]

Behaviors	IGF-1	TNF-α	TGF-β	PDGF
Fibroblasts				
Secretions	$8.8e^{-5}$ pg/cell per h (45)	$4.9e^{-6}$ pg/cell per h (78)	$1.7e^{-6}$ pg/cell per h (41)	$0.4e^{-6}$ pg/cell per h (59)
Migration, 31 μm/h (11, 57)	Increase_{E1} (44, 57)	No effect	No effect	Increase_{E2} (44)
Proliferation, 1 cell/10 days	Increase_{E3} (22, 39)	Increase_{E4} (5, 22)	Decrease_{E5} (39)	Increase_{E6} (22, 39)
Apoptosis, 1 cell/15 days	Decrease_{E7} (42)	Increase_{E8} (1)	Increase_{E9} (77)	Decrease_{E10} (49)
Muscle fibers				
Secretions	$5.1e^{-5}$ pg/cell per h (45)	None	None	None
Protein synthesis, β_D	Increase_{E11} (14)	No effect	No effect	No effect
Protein degradation (β_S)	No effect	Increase_{E12} (35)	No effect	No effect

Baseline values are in parentheses. Subscripts indicate the corresponding equation for a given rule found in Table 2. IGF, insulin growth factor; PDGF, platelet derived growth factor; TNF, tumor necrosis factor; TGF, transforming growth factor.

Figure 19: List of cellular behaviors in response to chemical signals in the muscle atrophy ABM. Modified from [259]

Equation Number (From Table 1)	Equations As Implemented in Netlogo
Migration	Initial S = 31 μm/h, persistence magnitude is in min
E1	When IGF is between 0.01 and 1 ng/ml S = S + $-0.0284 * (\log IGF1)^3 - 0.0124 * (\log IGF1)^2 + 0.0906 * (\log IGF1) + 0.4205$ Magnitude of $<p> = -0.1145 * (\log IGF1)^3 - 0.0186 * (\log IGF1)^2 + 0.4221 * (\log IGF1) + 24.192$ When IGF is 1 or greater, with a maximum of 320 ng/ml S = S + $-0.7332 * (\log IGF1)^3 + 2.6171 * (\log IGF1)^2 - 2.0028 * (\log IGF1) + 24.586$ Magnitude of $<p> = -0.1087 * (\log IGF1)^3 + 0.3878 * (\log IGF1)^2 - 0.2949 * (\log IGF1) + 0.4838$
E2	When PDGF is between 0.1 and 1 ng/ml Magnitude of $<p> = 25.9$ When PDGF is 1 or greater, with a maximum of 1,000 ng/ml S = S + $-0.864 * (\log PDGF)^2 + 2.592 * (\log PDGF) + 25.92$ Magnitude of $<p> = -0.0692 * (\log PDGF)^2 + 0.2947 * (\log PDGF) + 2e^{-16}$
Proliferation	Fibroblast agents have a chance to proliferate (100 out of 24,000 or once every 10 days); factors that altered this were either added to the original chance or modified the entire probability
E3	When IGF is between 1 and a maximum of 100 ng/ml Proliferation = Proliferation + $[1.15 * (\log IGF1) + 1] * 100 - 100$
E4	When TNF is between 0.1 and a maximum of 10 ng/ml Proliferation = Proliferation + $[0.43 * (\log TNF) + 1.43] * 100 - 100$
E5	When TGF is between 0.1 and a maximum of 10 ng/ml Proliferation = $[-0.25 * (\log TGF) + 0.75]$ * Proliferation
E6	When PDGF is between 0.1 and a maximum of 100 ng/ml Proliferation = Proliferation + $[(\log PDGF) + 2] * 100 - 100$
Apoptosis	Fibroblast agents have a chance to apoptose (100 out of 36,000 or once every 15 days); factors that altered this were either added to the original chance or modified the entire probability
E7	When IGF is between 1 and a maximum of 100 ng/ml Apoptosis = $[-0.14 * (\log IGF1) + 1]$ * Apoptosis
E8	When TNF is between 0.2 and a maximum of 20 ng/ml Apoptosis = Apoptosis + $[2.5 * (\log TNF) + 2.75] * 100 - 100$
E9	When TGF is between 0.05 and a maximum of 5 ng/ml Apoptosis = Apoptosis + $[0.5 * (\log TGF) + 1.65] * 100 - 100$
E10	When PDGF is between 0.5 and a maximum of 50 ng/ml Apoptosis = Apoptosis + $[-0.25 * (\log PDGF) + 0.92] * 100 - 100$
Protein Turnover	We utilized the Euler method for solving the balance between synthesis and degradation $CSA(t + \text{timestep}) = CSA(t) + x * \beta_S * \text{timestep} - y * \beta_D * CSA(t) * \text{timestep}$
E11	When IGF is between 0.2 and a maximum of 40 ng/ml $x = [(0.09 * (\log IGF) + 1.1]$ Otherwise, $x = 1$
E12	When TNF is between 1 and a maximum of 6 ng/ml $y = (0.035 * TNF + 0.97)$ Otherwise, $y = 1$

When the concentration of a factor is above the maximum concentration for a given equation, the maximum concentration is used in the calculation. ABM, agent-based model; CSA, cross-sectional area.

Figure 20: Equations for the behavioral rules used by the cells in the muscle atrophy ABM. Modified from [259]

fibers. Fibers are agents that can exist as one of four types (I, IIA, IIB or IID) with a defined cross-sectional area, and that can secrete IGF or undergo protein synthesis or degradation. The muscle exists in a cube environment with fibroblast agents. Each fibroblast can be thought of as existing in the center patch of a 3x3 patch grid, meaning the eight surrounding patches serve as the agent's local neighborhood. Fibroblasts can undergo proliferation or apoptosis, migrate across the muscle and/or produce chemical signals such as IGF, TGF, PDGF and TNF. The effects of these signals on the muscle behavior are specified through a set of equation rules, which can affect cell migration, cellular proliferation, cellular apoptosis, protein synthesis and protein degradation. Utilizing previously published experimental data regarding muscle fiber composition and geometry, the researchers tailored the muscle fiber to represent a variety of muscles across the body, and then simulated their atrophy over time. Each model time step corresponds to 1 hour, with simulations running for 28 days of model time. All results were the average of 10 simulations, which allows for a total of 140 fibers in order for the fiber number to fall within the range of published experimental studies.

Many of their model findings addressed current questions governing muscle behavior. For instance, while muscles from the same region experienced a similar degree of atrophy, none of their individual muscle architecture parameters could predict the degree of atrophy for an individual muscle. These parameters include the percent composition of each fiber type and the initial average cross-sectional area for each fiber type. This suggests that the extent of atrophy is an emergent feature resulting from the

combination of muscle architecture parameters, and that the underlying rules governing an individual's muscle behavior are the same, regardless of its location.

The researchers also used the model to construct theoretical muscles composed purely of individual fiber types to better understand the behavior of the fibers. For instance, they determined that muscles composed purely of IIB fibers underwent less atrophy than those composed entirely of type I. The researchers also used their model to address muscle behavior at the cellular level. As shown in Figure 21, increasing the initial

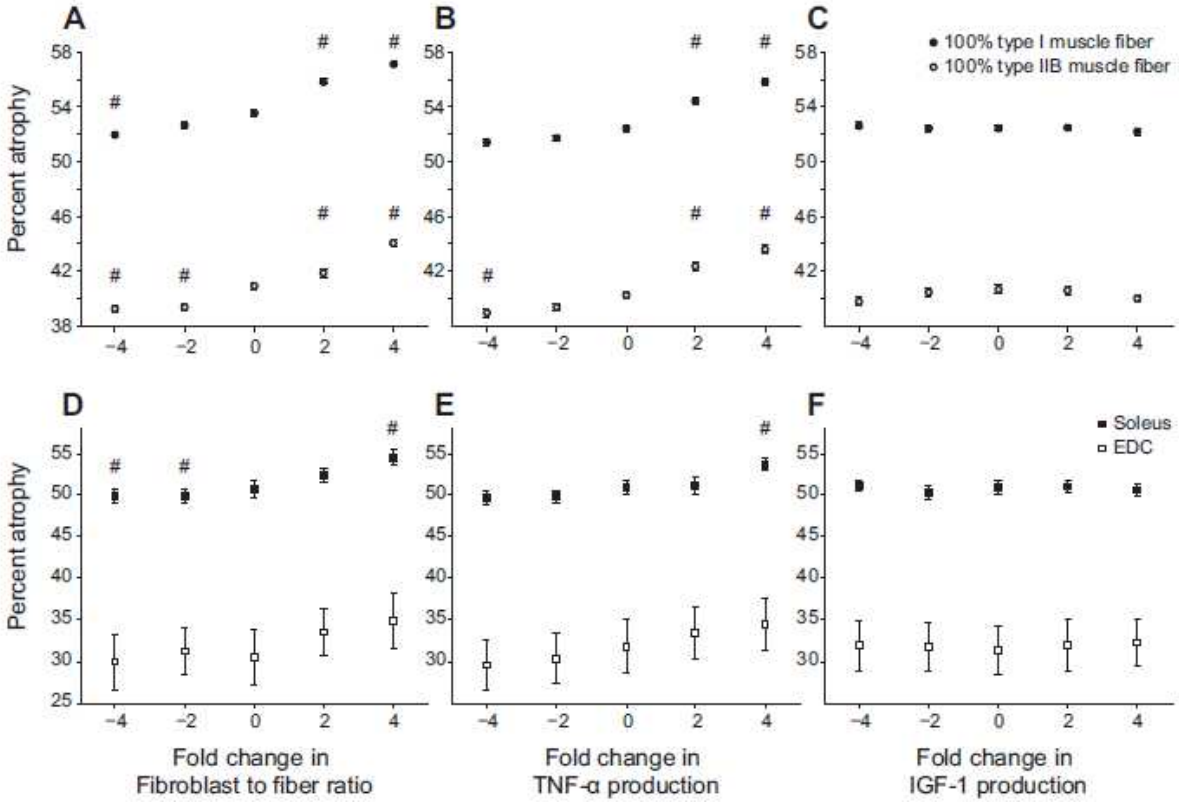

Figure 21: Percent of muscle atrophy in response to differing fibroblast to fiber ratios (A, D), TNF production (B, E) and IGF-1 production (C, F) in different fiber types (A-C) and different muscles (D-F) in the muscle atrophy ABM. All measurements are averages of 10 simulations. # indicates a statistically significant difference relative to the baseline value at x=0, as determined by a 1-way ANOVA, $p < 0.01$. Modified from [259]

number of fibroblasts increased the degree of atrophy for all fiber types within the model, while decreasing this number resulted in less atrophy in only two of the fiber types. Interestingly, increasing or decreasing IGF-1 production by muscle fibers and fibroblasts had no significant effect on atrophy, while increasing the amount of TNF released by fibroblasts resulted in increased atrophy. The researchers emphasized that this notion of fibroblasts and their secreted factors having critical effects on muscle atrophy is one that could now be further explored.

2.4.7. Lung Inflammation And Fibrosis

The final model we examine is a 2011 model of inflammation and fibrosis in the lung [262], aimed at determining how inhalation of particulate matter leads to different inflammatory lung diseases such as chronic obstructive pulmonary disease (COPD). Though chronic airway disease is often linked to repeated inhalation of particulate matter such as cigarette smoke or pollutants, this is not always the case, underscoring the need to better understand the inflammatory response in the lung to determine the factors that lead to disease states.

The researchers note that while there have been many *in vitro, in vivo and ex vivo* models of chronic airway disease, none of them seem to have the potential to fully recapitulate the development of COPD in humans. While *in vivo* and *ex vivo* models can answer focused questions about the details of cellular behaviors, they do not contain the complete set of cells activated in COPD. *In vivo* animal models are closer to the human model, but still differ in multiple respects such as anatomy, genetics, and the details of the immune

system. An *in silico* approach would thus enable them to more fully incorporate all the components of the inflammatory response in the lung. Agent-based modeling was proposed because it could enable them to rapidly modulate multiple variables and observe the effects on the lung.

As a first step in creating a rigorous model of the response, the researchers created a relatively simple "lumped parameter" ABM that simplifies the geometry of the lung and collapses multiple cells and parameters into single types. The environment is a 50 x 50 patch grid upon which cells can migrate. Key chemical signals released into this environment include TNF (a lumped version of all pro-inflammatory cytokines and a surrogate for proteases and reactive oxygen species that damage lung tissue) and TGF-β

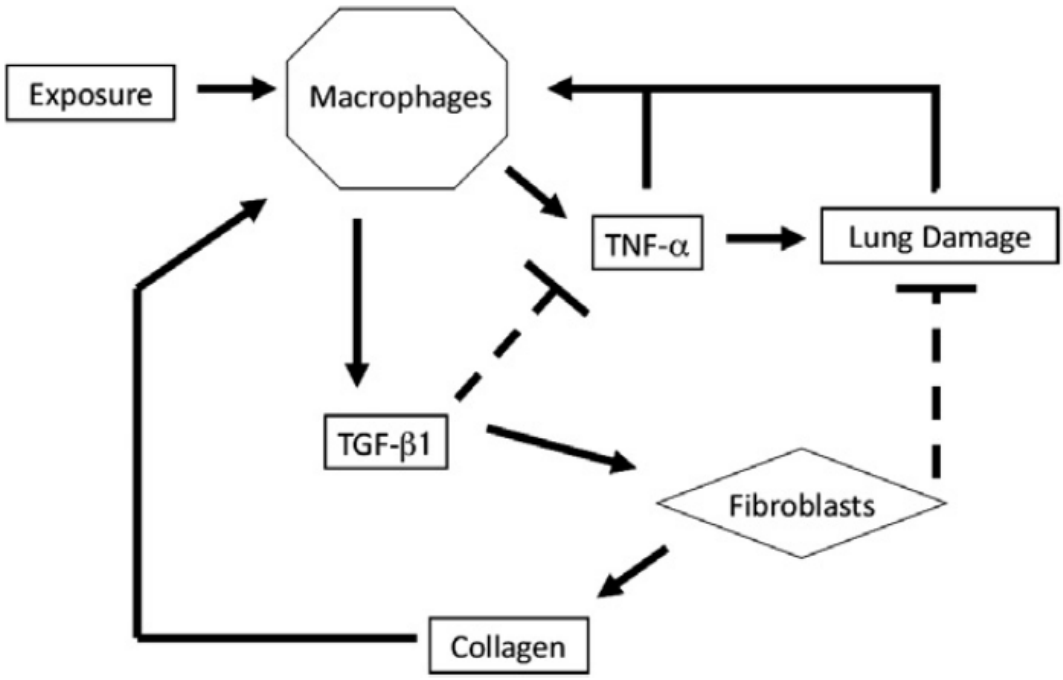

Figure 22: Schematic showing the interactions in the lung inflammation ABM. Macrophages and fibroblasts are model agents. TNF and TGF-β1 are released by macrophages, while collagen is released by fibroblasts. Modified from [260]

(a lumped version of anti-inflammatory cytokines, pro-fibrotic cytokines and growth factors). The cellular agents include macrophages (a lumped version of macrophages, neutrophils, lymphocytes and other inflammatory cells), fibroblasts, and particulate matter. A schematic of the key interactions is shown in Figure 22. Briefly, encounter with particulate matter makes macrophages enter an activated state in which they release TNF, which draws in additional macrophages and deals direct damage to the tissue patch on which it is released. Once the particulate matter is cleared, the macrophages release TGF-β, which antagonizes TNF production and serves as a chemoattractant for fibroblasts, which repair patches with tissue damage and deposit collagen onto the patches. Both macrophages and fibroblasts consider three patches at each timepoint: the

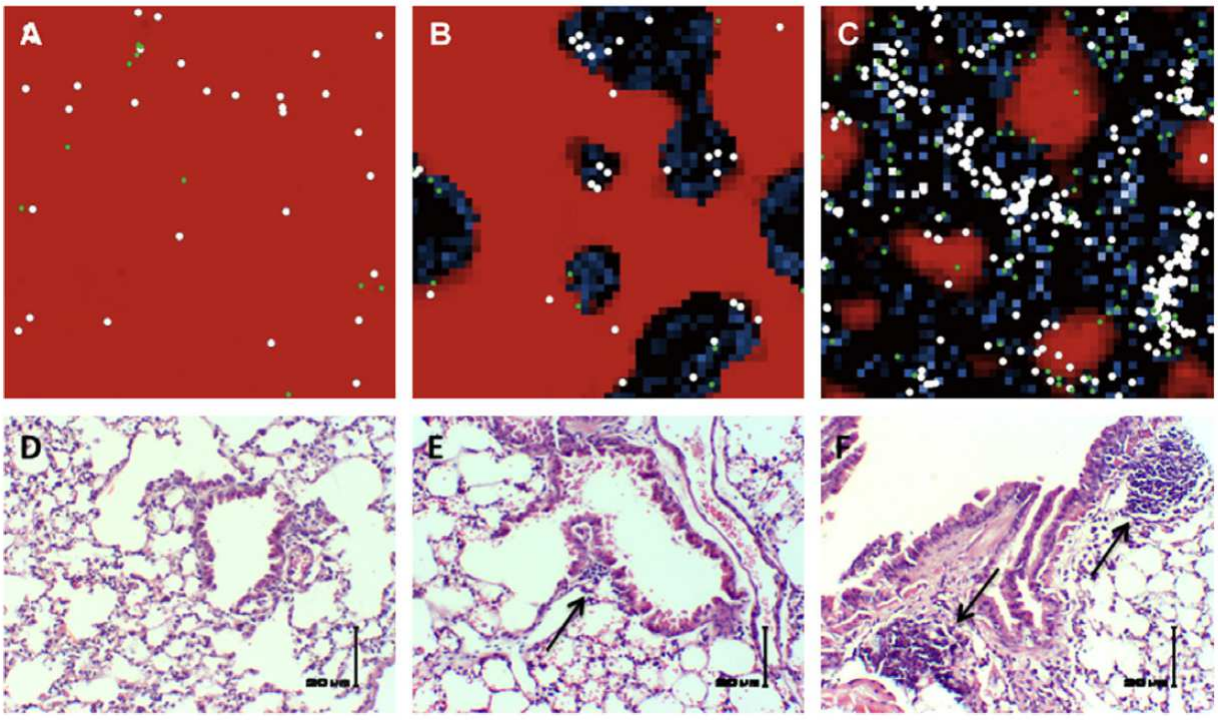

Figure 23: A, B, and C show the lung inflammation ABM during the self-resolving state, localized damage and fibrosis state and widespread damage and fibrosis state, respectively. D-F show lung slices gathered from mice exposed to cigarette smoke for 5 weeks. Arrows in E and F show inflammatory aggregates within the slice. Modified from [260]

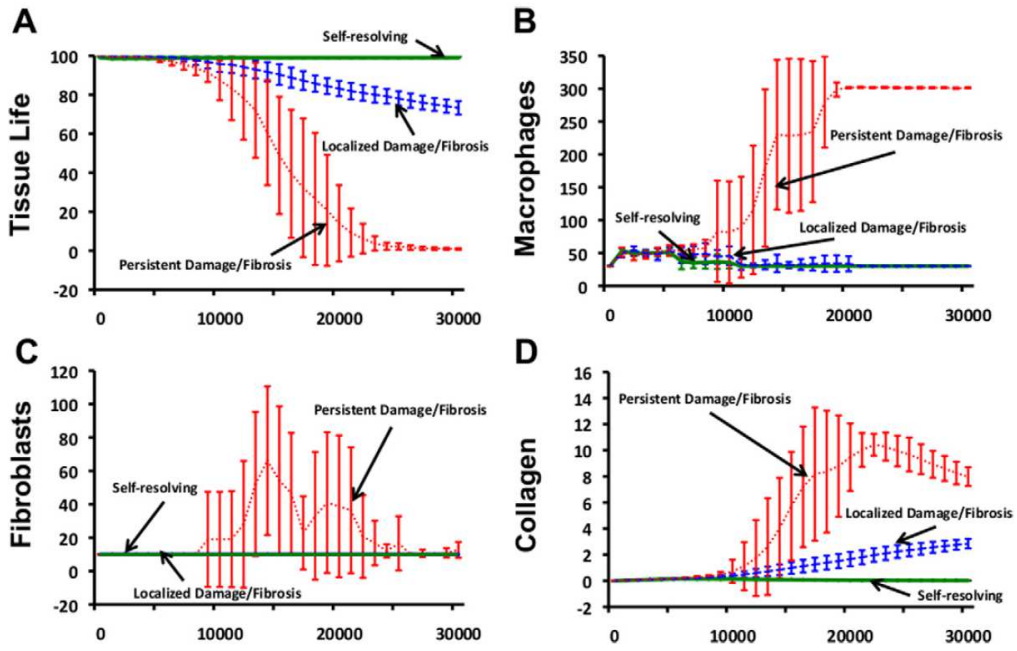

Figure 24: Mean ± standard deviations for (A) tissue life (a marker of inflammation measured by averaging the health of each environment patch, where 100 indicates complete health and 0 indicates complete damage), and total number of (B) macrophages, (C) fibroblasts and (D) collagen in the model for each of the three model states throughout the timecourse of the simulation in the lung inflammation ABM. Each result is an average of 10 representative simulations for each state. All numbers are in arbitrary units. Modified from [260]

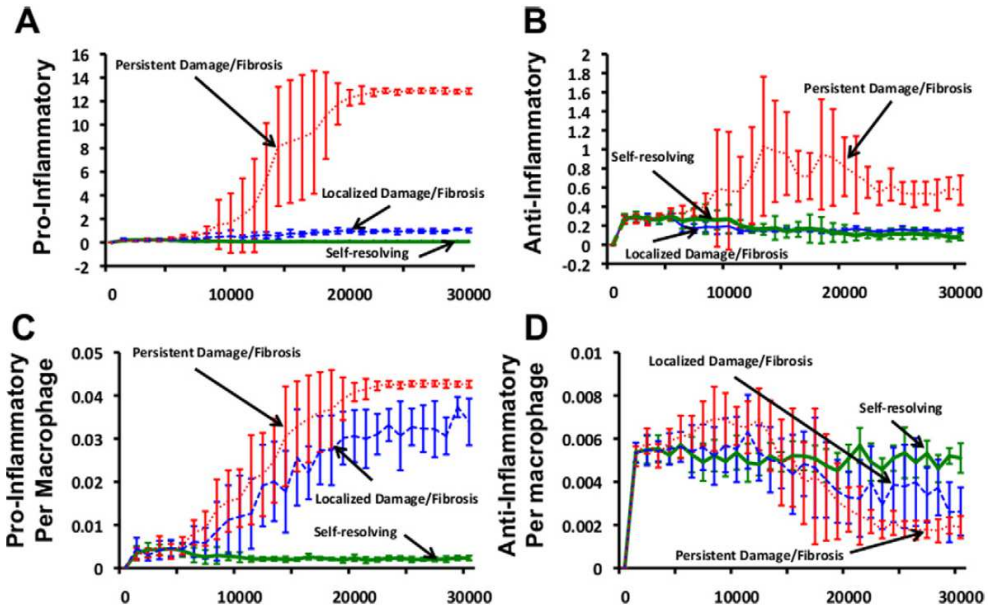

Figure 25: Mean ± standard deviations for total number of (A) pro-inflammatory cytokines, (B) anti-inflammatory cytokines, (C) pro-inflammatory cytokines per macrophage and (D) anti-inflammatory cytokines per macrophage for each of the three model states throughout the timecourse of the simulation in the lung inflammation ABM. Each result is an average of 10 representative simulations for each state. All numbers are in arbitrary units. Modified from [260]

patch directly ahead of their current direction, as well as the patches left and right of that patch. The rules governing the behaviors are based on known biological behavior in chronic airway diseases as well as insights from previous models of inflammation and wound healing. Five, 10, 15 or 20 particles were randomly distributed throughout the airway every 50, 100 or 200 time steps, with a maximum particulate exposure of 50, 100 or 200 times. Each of these potential combinations was run for 40 times, each for 10,000 time steps to determine if any result in a disease state.

Interestingly, these experimental results indicated three distinct model states, as shown qualitatively in Figures 23 and quantitatively in Figures 24 and 25. In the first, described as self-resolving, by the end of the simulation the model had cleared the particles without sustained tissue damage over time. In the second state, described as localized damage and fibrosis, regions of tissue damage slowly emerged throughout the model environment, with a gradual increase in inflammation and local damage that continued even after exposure had ceased. Macrophages and fibroblasts remained localized to the periphery of the sites of damage, along with the majority of collagen deposition. Interestingly, only pro-inflammatory cytokines remained elevated at the end of the simulation while anti-inflammatory cytokines were absent. The third state was described as systemic damage and fibrosis, with rampant tissue damage and a random distribution of collagen deposition throughout the environment. This state is marked by an early period of gradual tissue damage, followed by a rapid period of significant damage that results in complete destruction of the tissue region. Furthermore, both pro-inflammatory and anti-inflammatory cytokines remained elevated at the end of the

simulation, and there was a significantly elevated number of macrophages and fibroblasts.

Thus even with this very simplified model, the researchers produced three distinct states of the lung in response to chronic particulate exposure. Interestingly, the researchers had not anticipated the localized damage state arising from the interactions in their model, further indicating the ABM's ability to give rise to emergent phenomena. The researchers also noted that increased particulate exposure at higher frequencies and shorter intervals increases the likelihood of the lung falling into a localized or systemic damage state. They speculated that the second and third states correspond most closely to granulomas and COPD, respectively. In order to increase the model's utility, they proposed expanding the range of cells included in the model (including breaking the lumped cell types into their constitutive components), and updating the environment to more closely mimic specific lung tissue structures of interest. Nevertheless, this was an important first step in demonstrating that ABM's can lead to multiple, emergent disease states within the lung.

2.5. Conclusions

We have highlighted seven different ABMs of biological systems that explore the underlying spatiotemporal dynamics of a variety of biomedical systems. Some of these models test notions about the behavior of the system that were previously tested experimentally, generating results consistent with what had been observed. This indicates

the power of this form of modeling to rapidly test hypotheses and generate results that are consistent with *in vivo* experiments. Other models presented here critically test the systems in ways that would be difficult (if not impossible) to determine experimentally, leading to proposed insights about the underlying biological behavior. These models also reveal important emergent phenomena, in some cases indicating behavior that is governed by the unique combination of multiple parameters. This highlights the need to account for all of these interactions in hypothesis testing—as this form of modeling allows—in order to generate experimentally useful results. The ability of agent-based modeling to have emergent behavior arise naturally from simple rules without prior knowledge that this will happen is a key advantage of this form of modeling, illustrating the utility of ABM's at the initial stages of biomedical investigation.

While the field of medically oriented ABMs yields great promise, in many instances we are still in the early stages of using them to advance clinical knowledge. Many of the published studies shown here serve as a proof of concept by recapitulating known experimental findings, or are exploratory into the nature of the biological behavior and require further development and testing to yield clinically useful insights. The breast cancer and melanoma ABMs stand in contrast, perhaps due to the relatively more widespread use of ABMs in the study of cancer. The breast cancer findings led to the identification of a gene not previously considered as a critical player in determining the type of breast tumors that arise in an individual, while the melanoma ABM led to identification of a potential treatment and its effects on the tumor. This comes closest to indicating the true power of agent-based modeling: to test concrete, novel predictions

regarding the nature and treatment of clinical diseases using insights derived from previous literature.

In conclusion, we have shown that agent-based modeling is a powerful form of virtual experimentation that enables us to model a wide range of biological systems. It is our hope that more biological researchers will consider ABM's as a first step in critically vetting hypotheses about the system behavior prior to experimental work in the lab, in order to accelerate the advancement of novel, useful insights into biomedical systems.

2.6. References

1. Feuerstein GZ, Chavez J. Translational medicine for stroke drug discovery: the pharmaceutical industry perspective. Stroke 2009; 40(3 Suppl): S121-125.
2. Shiang K, Kandeel F. A Computational Model of the Human Glucose-Insulin Regulatory System. Journal of Biomedical Research 2016 Jan; 24.5 (2010): 347–364.
3. Wu H. A Case Study of Type 2 Diabetes Self-Management. BioMedical Engineering OnLine 2016 Jan; 4 (2005): 4.
4. Cruz J, Barahona P. An interval constraint approach to handle parametric ordinary differential equations for decision support, Online available from the World Wide Web: http://centria.di.fct.unl.pt/~pb/papers/cruz_ekdb99.pdf and http://centria.di.fct.unl.pt/~pb/papers/cruz_cp99.pdf.

5. Bolie VW. Coefficients of normal blood glucose regulation. J Appl Physiol. 1961;16:783–8.

6. Ackerman E, Gatewood LC, Rosevear JW, Molnar GD. Model studies of blood glucose regulation. Bull Math Biophys. 1965;27:21–37.

7. Ackerman E, Gatewood LC, Rosevear JW, Molnar GD. Concepts and Models of Biomathematics.Marcel Dekker; 1969. Blood glucose regulation and diabetes; pp. 131–56.

8. Ackerman E, Rosevear JW, McGuckin WF. A mathematical model of the glucose tolerance test. Phys Med Biol. 1964;9:202–13.

9. Kholodenko BN, Demin OV, Moehren G, Hoek JB. Quantification of short term signaling by the epidermal growth factor receptor. J. Biol. Chem. 1999;274:30169–30181.

10. Brightman FA, Fell DA. Differential feedback regulation of the MAPK cascade underlies the quantitative differences in EGF and NGF signalling in PC12 cells. FEBS Lett. 2000;482:169–174.

11. Schoeberl B, Eichler-Jonsson C, Gilles ED, Muller G. Computational modeling of the dynamics of the MAP kinase cascade activated by surface and internalized EGF receptors. Nat. Biotechnol. 2002;20:370–375.

12. Zhao CY, Greenstein JL, Winslow RL. Roles of phosphodiesterases in the regulation of the cardiac cyclic nucleotide cross-talk signaling network, Journal of Molecular and Cellular Cardiology, Volume 91, February 2016, Pages 215-227, ISSN 0022-2828.

13. Batchelor AM, Bartus K, Reynell C, Constantinou S, Halvey EJ, Held KF, Dostmann WR, Vernon J, Garthwaite J. Exquisite sensitivity to subsecond, picomolar nitric oxide transients conferred on cells by guanylyl cyclase-coupled receptors. Proc. Natl. Acad. Sci., 107 (2010), pp. 22060–22065.

14. Van Vo T, Hammer PE, Hoimes ML, Nadgir S, Fantini, S. Mathematical Model for the Hemodynamic Response to Venous Occlusion Measured With Near-Infrared Spectroscopy in the Human Forearm. Biomedical Engineering. IEEE Transactions 2007 April; 54 (4): pp.573-584.

15. de Mul FF, Morales F, Smit AJ, Graaff R. A model for post-occlusive reactive hyperemia as measured with laser-Doppler perfusion monitoring. IEEE Trans Biomed Eng 2005; 52: 184–190.

16. Deshpande RS, Grayson WL, Spector AA. A Modeling Insight into Adipose-Derived Stem Cell Myogenesis. PLoS One 2015; 10(9): e0137918.

17. Krinner A, Roeder I, Loeffler M, Scholz M. Merging concepts - coupling an agent-based model of hematopoietic stem cells with an ODE model of granulopoiesis. BMC Syst Biol 2013; 7: 117.

18. Wichmann H, Loeffler M. Mathematical Modeling of Cell Proliferation: Stem Cell Regulation in Hemopoiesis. BocaRaton, Florida: CRC Press; 1985.

19. Engel C, Scholz M, Loeffler M. A computational model of human granulopoiesis to simulate the hematotoxic effects of multicycle polychemotherapy. Blood. 2004;104:2323–2331.

20. Scholz M, Engel C, Loeffler M. Modelling human granulopoiesis under poly-chemotherapy with G-CSF support. J Math Biol. 2005;50:397–439. doi: 10.1007/s00285-004-0295-1.

21. González PP, Cárdenas M, Gershenson C, Lagunez J. Advances in Systems Science: Measurement. Athens, Greece: Circuits and Control, WSES Press; 2001. Integration of computational techniques for the modelling of signal transduction; pp. 400–411.

22. Monteagudo A, Santos J. Treatment Analysis in a Cancer Stem Cell Context Using a Tumor Growth Model Based on Cellular Automata. PLoS One 2015; 10(7): e0132306.

23. Morton CI, Hlatky L, Hahnfeldt P, Enderling H. Non-Stem Cancer Cell Kinetics Modulate Solid Tumor Progression. Theoretical Biology & Medical Modelling 2016; 8 (2011): 48.

24. Enderling H, Anderson ARA, Chaplain MAJ, Beheshti A, Hlatky L, Hahnfeldt P. Paradoxical dependencies of tumor dormancy and progression on basic cell

kinetics. Cancer Res. 2009;69:8814–8821. doi: 10.1158/0008-5472.CAN-09-2115.

25. Vainstein V, Kirnasovsky OU, Kogan Y, Agur Z. Strategies for cancer stem cell elimination: Insights from mathematical modeling. Journal of Theoretical Biology. 2012;298:32–41.

26. Santos J, Monteagudo A. Analysis of behaviour transitions in tumour growth using a cellular automaton simulation. IET Syst Biol 2015; 9(3): 75-87.

27. Gevertz JL, Torquato S. Modeling the effects of vasculature evolution on early brain tumor growth. J Theor Biol 2006; 243(4): 517-531.

28. Alarcon T, Byrne HM, Maini PK. A cellular automaton model for tumour growth in inhomogeneous environment. J Theor Biol. 2003;225(2): 257–74.

29. Gevertz JL, Gillies GT, Torquato S. Simulating tumor growth in confined heterogeneous environments. Phys Biol. 2008;5: 036010.

30. Kansal AR, Torquato S, Harsh GR IV, Chiocca EA, Deisboeck TS. Simulated brain tumor growth using a three-dimensional cellular automaton. J Theor Biol. 2000;203(4): 367–82.

31. Al-Husari M, Murdoch C, Webb SD. A cellular automaton model examining the effects of oxygen, hydrogen ions and lactate on early tumour growth. J Math Biol 2014; 69(4): 839-873.

32. Poleszczuk J, Hahnfeldt P, Enderling H. Evolution and phenotypic selection of cancer stem cells. PLoS Comput Biol 2015; 11(3): e1004025.

33. Bankhead A III, Heckendorn RB. Using evolvable genetic cellular automata to model breast cancer. Genet Program Evolvable Mach. 2007;8(4): 381–393.

34. Anderson AR, Weaver AM, Cummings PT, Quaranta V. Tumor morphology and phenotypic evolution driven by selective pressure from microenvironment. Cell. 2006;127(5): 905–15.

35. Gevertz JL, Torquato S. Growing heterogeneous tumors in silico. Phys Rev E Stat Nonlin Soft Matter Phys. 2009;80: 051910.

36. Schmitz JE, Kansal AR, Torquato S. A Cellular Automaton Model of Brain Tumor Treatment and Resistance. J Theor Med. 2002;4: 223–239.

37. Kansal AR, Torquato S, Chiocca EA, Deisboeck TS. Emergence of a subpopulation in a computational model of tumor growth. J Theor Biol. 2000;207(3): 431–41.

38. Patel AA, Gawlinsky ET, Lemieux SK, Gatenby RA. Cellular automaton model of early tumour growth and invasion: the effects of native tissue vascularity and increased anaerobic tumour metabolism. J. Theor. Biol. 2001; 213: 315–331.

39. Anderson AR. A hybrid mathematical model of solid tumor invasion: the important of cell adhesion. Math Med Biol. 2005;22: 163–86.

40. Zhu J, Liang L, Jiao Y, Liu L. Enhanced invasion of metastatic cancer cells via extracellular matrix interface. PLoS One 2015; 10(2): e0118058.

41. Precharattana M. Stochastic modeling for dynamics of HIV-1 infection using cellular automata. J Bioinform Comput Biol 2015: 1630001.

42. Young RC, Barendse P. Linking myometrial physiology to intrauterine pressure; how tissue-level contractions create uterine contractions of labor. PLoS Comput Biol 2014; 10(10): e1003850.

43. Sabzpoushan SH, Pourhasanzade F. A Cellular Automata-based Model for Simulating Restitution Property in a Single Heart Cell. J Med Signals Sens 2011; 1(1): 19-23.

44. Gao J, Du P, O'Grady G, Archer R, Gibbons SJ, Farrugia G, Cheng LK. Cellular automaton model for simulating tissue-specific intestinal electrophysiological activity. Conf Proc IEEE Eng Med Biol Soc 2013: 5537-5540.

45. Lammers WJEP, Al-Bloushi HM, Al-Eisaei SA, Al-Dhaheri FA, Stephen B, John R, Dhanasekaran S, Karam SM. Slow wave propagation and plasticity of interstitial cells of Cajal in the small intestine of diabetic rats. Exp Physiol. 2011;96:1039–1048.

46. Du P, O'Grady G, Windsor JA, Cheng LK, Pullan AJ. A tissue framework for simulating the effects of gastric electrical stimulation and in vivo validation. IEEE Trans Biomed Eng. 2009;56:2755–2761.

47. OReilly A, Hankenson KD, Kelly DJ. A computational model to explore the role of angiogenic impairment on endochondral ossification during fracture healing. Biomech Model Mechanobiol. 2016.

48. Burke D, Dishowitz M, Sweetwyne M, Miedel E, Hankenson KD, Kelly DJ. The role of oxygen as a regulator of stem cell fate during fracture repair in TSP2-null mice. J Orthop Res 2013; 31(10): 1585-1596.

49. Sun W, Martin C, Pham T. Computational modeling of cardiac valve function and intervention. Annu Rev Biomed Eng 2014; 16: 53-76.

50. Cataloglu A, Clark RE, Gould PL. Stress analysis of aortic valve leaflets with smoothed geometrical data. J. Biomech. 1977; 10:153–58.

51. Gould PL, Cataloglu A. Stress analysis of the human aortic valve. Comput. Struct. 1973; 3:377–78, IN1–2, 379–84.

52. Cataloglu A, Gould PL, Clark RE. Validation of a simplified mathematical model for the stress analysis of human aortic heart valves. J. Biomech. 1975; 8:347–48.

53. Jermihov PN, Jia L, Sacks MS, Gorman RC, Gorman JH III, Chandran KB. Effect of geometry on the leaflet stresses in simulated models of congenital bicuspid aortic valves. Cardiovasc. Eng. Technol. 2011; 2:48–56.

54. Conti C, Della Corte A, Votta E, Del Viscovo L, Bancone C, De Santo LS, Redaelli A. Biomechanical implications of the congenital bicuspid aortic valve: a

finite element study of aortic root function from in vivo data. J. Thorac. Cardiovasc. Surg. 2010; 140:890–96.

55. Katayama S, Umetani N, Hisada T, Sugiura S. Bicuspid aortic valves undergo excessive strain during opening: a simulation study. J. Thorac. Cardiovasc. Surg. 2013; 145:1570–76.

56. Grande KJ, Cochran RP, Reinhall PG, Kunzelman KS. Mechanisms of aortic valve incompetence: finite element modeling of aortic root dilatation. Ann. Thorac. Surg. 2000; 69:1851–5.

57. Grande-Allen KJ, Cochran RP, Reinhall PG, Kunzelman KS. Mechanisms of aortic valve incompetence: finite-element modeling of Marfan syndrome. J. Thorac. Cardiovasc. Surg. 2001; 122:946–54.

58. Cacciola G, Peters GW, Baaijens FP. A synthetic fiber-reinforced stentless heart valve. J. Biomech. 2000; 33:653–58.

59. Cacciola G, Peters GW, Schreurs PJ. A three-dimensional mechanical analysis of a stentless fibre reinforced aortic valve prosthesis. J. Biomech. 2000; 33:521–30.

60. Krucinski S, Vesely I, Dokainish MA, Campbell G. Numerical simulation of leaflet flexure in bioprosthetic valves mounted on rigid and expansile stents. J. Biomech. 1993; 26:929–43.

61. Martin C, Sun W. Simulation of long-term fatigue damage in bioprosthetic heart valves: effect of leaflet and stent elastic properties. Biomech. Model. Mechanobiol. 2013; doi: 10.1007/s10237-013-0532-x.

62. Labrosse MR, Boodhwani M, Sohmer B, Beller CJ. Modeling leaflet correction techniques in aortic valve repair: a finite element study. J. Biomech. 2011; 44:2292–98.

63. Grande-Allen K, Cochran R, Reinhall P, Kunzelman K. Finite-element analysis of aortic valvesparing: influence of graft shape and stiffness. IEEE Trans. Biomed. Eng. 2001; 48:647–59.

64. Soncini M, Votta E, Zinicchino S, Burrone V, Mangini A, Lemma M, Antona C, Redaelli A. Aortic root performance after valve sparing procedure: a comparative finite element analysis. Med. Eng. Phys. 2009; 31:234–43.

65. Totaro P, Morganti S, Ngo Yon C, Dore R, Conti M, Auricchio F, Vigano M. Computational finite element analyses to optimize graft sizing during aortic valve-sparing procedure. J. Heart Valve Dis. 2012; 21:141–47.

66. Ranga A, Bouchot O, Mongrain R, Ugolini P, Cartier R. Computational simulations of the aortic valve validated by imaging data: evaluation of valve-sparing techniques. Interact. Cardiovasc. Thorac. Surg. 2006; 5:373–78.

67. Beck A, Thubrikar M, Robicsek F. Stress analysis of the aortic valve with and without the sinuses of Valsalva. J. Heart Valve Dis. 2001; 10:1–11.

68. Wang Q, Sirois E, Sun W. Patient-specific modeling of biomechanical interaction in transcatheter aortic valve deployment. J. Biomech. 2012; 45:1965–71.

69. Capelli C, Bosi GM, Cerri E, Nordmeyer J, Odenwald T, Bonhoeffer P, Migliavacca F, Taylor AM, Schievano S. Patient-specific simulations of transcatheter aortic valve stent implantation. Med. Biol. Eng. Comput. 2012; 50:183–92.

70. Auricchio F, Conti M, Morganti S, Reali A. Simulation of transcatheter aortic valve implantation: a patient-specific finite element approach. Comput. Methods Biomech. Biomed. Eng. 2014; 17:1347–57.

71. Chand R, Haug E, Rim K. Stresses in the human knee joint. Journal of Biomechanics. 1976;9(6):417–422.

72. Heegaard J, Leyvraz PF, Curnier A, Rakotomananaa L, Huiskes R. The biomechanics of the human patella during passive knee flexion. Journal of Biomechanics. 1995;28(11):1265–1279.

73. Besier TF, Gold GE, Beaupré GS, Delp SL. A modeling framework to estimate patellofemoral joint cartilage stress in vivo. Medicine and Science in Sports and Exercise. 2005;37(11):1924–1930.

74. Besier TF, Gold GE, Delp SL, Fredericson M, Beaupré GS. The influence of femoral internal and external rotation on cartilage stresses within the patellofemoral joint. Journal of Orthopaedic Research.2008;26(12):1627–1635.

75. Moglo KE, Shirazi-Adl A. Cruciate coupling and screw-home mechanism in passive knee joint during extension-flexion. Journal of Biomechanics. 2005;38(5):1075–1083.

76. Mesfar W, Shirazi-Adl A. Biomechanics of the knee joint in flexion under various quadriceps forces. Knee. 2005;12(6):424–434.

77. Donahue TLH, Hull ML, Rashid MM, Jacobs CR. A finite element model of the human knee joint for the study of tibio-femoral contact. Journal of Biomechanical Engineering. 2002;124(3):273–280.

78. Haut Donahue TL, Hull ML, Rashid MM, Jacobs CR. How the stiffness of meniscal attachments and meniscal material properties affect tibio-femoral contact pressure computed using a validated finite element model of the human knee joint. Journal of Biomechanics 2003;36(1):19–34.

79. Hao Z, Jin D, Zhang Y, Zhang J. A finite element 3D model of in vivo human knee joint based on MRI for the tibiofemoral joint contact analysis. Proceedings of the 1st international conference on Digital human modeling 2007; Beijing, China. pp. 616–622.

80. Beillas P, Papaioannou G, Tashman S, Yang KH. A new method to investigate in vivo knee behavior using a finite element model of the lower limb. Journal of Biomechanics. 2004;37(7):1019–1030.

81. Shirazi R, Shirazi-Adl A, Hurtig M. Role of cartilage collagen fibrils networks in knee joint biomechanics under compression. Journal of Biomechanics. 2008;41(16):3340–3348.

82. Peña E, Calvo B, Martínez MA, Doblaré M. A three-dimensional finite element analysis of the combined behavior of ligaments and menisci in the healthy human knee joint. Journal of Biomechanics.2006;39(9):1686–1701.

83. Dhaher YY, Kwon TH, Barry M. The effect of connective tissue material uncertainties on knee joint mechanics under isolated loading conditions. Journal of Biomechanics. 2010;43(16):3118–3125.

84. Sibole SC, Erdemir A. Chondrocyte deformations as a function of tibiofemoral joint loading predicted by a generalized high-throughput pipeline of multi-scale simulations. PLoS One 2012;7(5)e37538.

85. Papaioannou G, Demetropoulos CK, King YH. Predicting the effects of knee focal articular surface injury with a patient-specific finite element model. Knee 2010;17(1):61–68.

86. Shirazi R, Shirazi-Adl A. Computational biomechanics of articular cartilage of human knee joint: effect of osteochondral defects. Journal of Biomechanics 2009;42(15):2458–2465.

87. Peña E, Calvo B, Martínez MA, Doblaré M. Effect of the size and location of osteochondral defects in degenerative arthritis. A finite element simulation. Computers in Biology and Medicine 2007;37(3):376–387.

88. Mononen ME, Julkunen P, Töyräs J, Jurvelin JS, Kiviranta I, Korhonen RK. Alterations in structure and properties of collagen network of osteoarthritic and repaired cartilage modify knee joint stresses. Biomechanics and Modeling in Mechanobiology 2011;10(3):357–369.

89. Mononen ME, Mikkola MT, Julkunen P, Ojala R, Nieminen MT, Jurvelin JS, Korhonen RK. Effect of superficial collagen patterns and fibrillation of femoral articular cartilage on knee joint mechanics-a 3D finite element analysis. Journal of Biomechanics 2012;45(3):579–587.

90. Galie P, Spilker RL.. A two-dimensional computational model of lymph transport across primary lymphatic valves. J Biomech Eng 2009; 131(11): 111004.

91. Wilson JT, van Loon R, Wang W, Zawieja DC, Moore JE Jr. Determining the combined effect of the lymphatic valve leaflets and sinus on resistance to forward flow. J Biomech 2015; 48(13): 3593-3599.

92. Teplitzky, B A, Connolly AT, Bajwa JA, Johnson MD. Computational modeling of an endovascular approach to deep brain stimulation. J Neural Eng 2014; 11(2): 026011.

93. Miocinovic S, Parent M, Butson CR, Hahn PJ, Russo GS, Vitek JL, McIntyre CC. Computational analysis of subthalamic nucleus and lenticular fasciculus activation during therapeutic deep brain stimulation J. Neurophysiol 2006; 96 1569–80.

94. McIntyre CC, Grill WM, Sherman DL, Thakor NV. Cellular effects of deep brain stimulation: model-based analysis of activation and inhibition J. Neurophysiol 2004; 91 1457–69.

95. Johnson MD, McIntyre CC. Quantifying the neural elements activated and inhibited by globus pallidus deep brain stimulation J. Neurophysiol 2008; 100 2549–63.

96. Barnes D, Chu D. Introduction to Modeling for Biosciences. London: Springer; c2010. Chapter 2: Agent-Based Modeling; p.15-77.

97. Gilbert, N. Agent-Based Models. London: SAGE Publications; c2007. Chapter 1: The Idea of Agent-Based Modeling; p.1-20.

98. Railsback S, Grimm V. Agent-Based and Individual-Based Modeling: A Practical Introduction. Princeton: Princeton University Press; c2011. Chapter 1: Models, Agent-Based Models, and the Modeling Cycle; p.3-13.

99. Schelling, TC. Dynamic models of segregation. The Journal of Mathematical Sociology 1971; 1(2): 143-186.

100. Scholl, HJ. Agent-based and system dynamics modeling: a call for cross study and joint research. System Sciences, 2001. Proceedings of the 34th Annual Hawaii International Conference on. IEEE, 2001.

101. Klatt J, Marsella S, Krämer NC. Negotiations in the context of AIDS prevention: an agent-based model using theory of mind. Intelligent virtual agents. Springer Berlin Heidelberg, 2011.

102. Gotts NM, Polhill JG, Law ANR. Agent-based simulation in the study of social dilemmas. Artificial Intelligence Review 2003; 19.1: 3-92.

103. Zhang T, Zhang D. Agent-based simulation of consumer purchase decision-making and the decoy effect. Journal of Business Research 2007; 60.8: 912-922.

104. Nilsson F, Darley V. On complex adaptive systems and agent-based modelling for improving decision-making in manufacturing and logistics settings: Experiences from a packaging company. International Journal of Operations & Production Management 2006; 26.12: 1351-1373.

105. Roozmand O, Ghasem-Aghaee N, Hofstede GJ, Nematbakhsh MA, Baraani A, Verwaat T. Agent-based modeling of consumer decision making process based on power distance and personality. Knowledge-Based Systems 2011; 24.7: 1075-1095.

106. Lim K, Deadman PJ, Moran E, Brondizio E, McCracken S. Agent-based simulations of household decision making and land use change near Altamira, Brazil. Integrating Geographic Information Systems and Agent-Based Modeling: Techniques for Simulating Social and Ecological Processes 2002: 277-310.

107. Benenson I. Agent-based modeling: From individual residential choice to urban residential dynamics. Spatially Integrated Social Science 2004: 67-95.

108. Deadman P, Robinson D, Moran E. Colonist household decisionmaking and land-use change in the Amazon Rainforest: an agent-based simulation. Environment and Planning B: Planning and Design 2004; 31.5: 693-709.

109. Becu N, Neef A, Schreinemachers P, Sangkapitux C. Participatory computer simulation to support collective decision-making: Potential and limits of stakeholder involvement. Land use policy 2008; 25.4: 498-509.

110. Campbell KC, Cooper WW Jr., Greenbaum DP, Wojcik LA. Modeling distributed human decision making in traffic flow management operations. Progress In Astronautics And Aeronautics 2001; 193: 227-238.

111. North MJ, Macal CM, St. Aubin J, Thimmapuram P, Bragen M, Hahn J, Karr J, Brigham N, Lacy ME, Hampton D Multiscale agent-based consumer market modeling. Complexity 2010; 15.5: 37-47.

112. Ng TL, Eheart JW, Cai X, Braden JB. An agent-based model of farmer decision-making and water quality impacts at the watershed scale under markets

for carbon allowances and a second-generation biofuel crop. Water Resources Research 2011; 47.9.

113. Sueyoshi T, Tadiparthi GR. An agent-based decision support system for wholesale electricity market. Decision Support Systems 2008; 44.2: 425-446.

114. Twomey P, Cadman R. Agent-based modelling of customer behaviour in the telecoms and media markets. Emerald Insight 2002; 4.1: 56-63.

115. An L. Modeling human decisions in coupled human and natural systems: review of agent-based models. Ecological Modelling 2012; 229: 25-36.

116. Garcia R. Uses of agent-based modeling in innovation/new product development research. Journal of Product Innovation Management 2005; 22.5: 380-398.

117. Said LB, Bouron T, Drogoul A. Agent-based interaction analysis of consumer behavior. Proceedings of the first international joint conference on Autonomous agents and multiagent systems: part 1. ACM, 2002.

118. Bohlmann, JD, Calantone RJ, Zhao M. The effects of market network heterogeneity on innovation diffusion: An agent-based modeling approach. Journal of Product Innovation Management 2010; 27.5: 741-760.

119. Amini M, Wakolbinger T, Racer M, Nejad MG. Alternative supply chain production–sales policies for new product diffusion: An agent-based modeling

and simulation approach. European Journal of Operational Research 2012; 216.2: 301-311.

120. Axelrod R. The dissemination of culture a model with local convergence and global polarization. Journal of Conflict Resolution 1997; 41.2: 203-226.

121. Zhang T, Gensler S, Garcia R. A Study of the Diffusion of Alternative Fuel Vehicles: An Agent-Based Modeling Approach. Journal of Product Innovation Management 2011; 28.2: 152-168.

122. Kiesling E, Günther M, Stummer C, Wakolbinger L. Agent-based simulation of innovation diffusion: a review. Central European Journal of Operations Research 2012; 20.2: 183-230.

123. Garcia R, Jager W. From the Special Issue Editors: Agent-Based Modeling of Innovation Diffusion. Journal of Product Innovation Management 2011; 28.2: 148-151.

124. Schreinemachers P, Berger T, Sirijinda A, Praneetvatakul S. The Diffusion of Greenhouse Agriculture in Northern Thailand: Combining Econometrics and Agent-Based Modeling. Canadian Journal of Agricultural Economics/Revue Canadienne d'agroeconomie 2009; 57.4: 513-536.

125. Hui C, Goldberg M, Magdon-Ismail M, Wallace WA. Simulating the diffusion of information: An agent-based modeling approach. International Journal of Agent Technologies and Systems 2010; 2.3: 31-46.

126. Tang W, Bennett DA. Reprint of: Parallel agent-based modeling of spatial opinion diffusion accelerated using graphics processing units. Ecological Modelling 2012; 229: 108-118.

127. Schramm ME, Trainor KJ, Shanker M, Hu MY. An agent-based diffusion model with consumer and brand agents. Decision Support Systems 2010; 50.1: 234-242.

128. Günther M, Stummer C, Wakolbinger LM, Wildpaner M. An agent-based simulation approach for the new product diffusion of a novel biomass fuel. Agent-Based Modeling and Simulation. Palgrave Macmillan UK, 2014. 61-77.

129. Sopha BM, Klöckner CA, Hertwich EG. Adoption and diffusion of heating systems in Norway: coupling agent-based modeling with empirical research. Environmental Innovation and Societal Transitions 2013; 8: 42-61.

130. Laciana CE, Rovere SL. Ising-like agent-based technology diffusion model: Adoption patterns vs. seeding strategies. Physica A: Statistical Mechanics and its Applications 2011; 390.6: 1139-1149.

131. Namatame A, Morita H, Matsuyama K. Agent-based modeling for the study of diffusion dynamics. Proceedings of the 2009 Spring Simulation Multiconference. Society for Computer Simulation International, 2009.

132. Orr MG, Evans CR. Understanding long-term diffusion dynamics in the prevalence of adolescent sexual initiation: A first investigation using agent-based modeling. Research in Human Development 2011; 8.1: 48-66.

133. Rapaport O, Levi-Faur D, Miodownik D. The Puzzle of the Diffusion of Central-Bank Independence Reforms: Insights from an Agent-Based Simulation. Policy Studies Journal 2009; 37.4: 695-716.

134. Kuandykov L, Sokolov M. Impact of social neighborhood on diffusion of innovation S-curve. Decision Support Systems 2010; 48.4: 531-535.

135. Peres R, Muller E, Mahajan V. Innovation diffusion and new product growth models: A critical review and research directions. International Journal of Research in Marketing 2010; 27.2: 91-106.

136. Kowalska-Pyzalska A, Maciejowska K, Sznajd-Weron K, Weron R. Going Green: Agent-based modeling of the diffusion of dynamic electricity tariffs. No. HSC/13/05. Hugo Steinhaus Center, Wroclaw University of Technology, 2013.

137. Manson SM. Agent-based modeling and genetic programming for modeling land change in the Southern Yucatan Peninsular Region of Mexico. Agriculture, Ecosystems & Environment 2005; 111.1: 47-62.

138. Brown DG, Page S, Riolo R, Zellner M, Rand W. Path dependence and the validation of agent-based spatial models of land use. International Journal of Geographical Information Science 2005; 19.2: 153-174.

139. Manson SM, Evans T. Agent-based modeling of deforestation in southern Yucatán, Mexico, and reforestation in the Midwest United States. Proceedings of the National Academy of Sciences 2007; 104.52: 20678-20683.

140. Guzy MR, Smith CL, Bolte JP, Hulse DW, Gregory SV. Policy research using agent-based modeling to assess future impacts of urban expansion into farmlands and forests. Ecology and Society 2008; 13.1: 37.

141. Heppenstall, AJ, Crooks AT, See LM, Batty M, eds. Agent-based models of geographical systems. Springer Science & Business Media; 2011.

142. Parker DC, Filatova T. A conceptual design for a bilateral agent-based land market with heterogeneous economic agents. Computers, Environment and Urban Systems 2008; 32.6: 454-463.

143. Valbuena D, Verburg PH, Bregt AK, Ligtenberg A. An agent-based approach to model land-use change at a regional scale. Landscape Ecology 2008; 25.2: 185-199.

144. Xie Y, Batty M, Zhao K. Simulating emergent urban form using agent-based modeling: Desakota in the Suzhou-Wuxian region in China. Annals of the Association of American Geographers 2007; 97.3: 477-495.

145. Parker DC, Manson SM, Janssen MA, Hoffmann MJ, Deadman P. Multi-agent systems for the simulation of land-use and land-cover change: a review. Annals of the association of American Geographers 2003; 93.2: 314-337.

146. Brown DG, Robinson DT. Effects of heterogeneity in residential preferences on an agent-based model of urban sprawl. Ecology and society 2006; 11.1: 46.

147. Jiang B, Gimblett HR. An agent-based approach to environmental and urban systems within geographic information systems. Integrating Geographic Information Systems and Agent-based Modeling Techniques for Simulating Social and Ecological Processes 2002; 171-189.

148. Hosseinali F, Alesheikh AA, Nourian F. Agent-based modeling of urban land-use development, case study: Simulating future scenarios of Qazvin city. Cities 2013; 31: 105-113.

149. Fontaine CM, Rounsevell MDA. An agent-based approach to model future residential pressure on a regional landscape. Landscape Ecology 2009; 24.9: 1237-1254.

150. Zhang H, Zeng Y, Bian L, Yu X. Modelling urban expansion using a multi agent-based model in the city of Changsha. Journal of Geographical Sciences 2010; 20.4: 540-556.

151. Kim D, Batty M. Modeling Urban Growth: An Agent Based Microeconomic Approach to Urban Dynamics and Spatial Policy Simulation. Vol. 165. Working Paper Series, 2011.

152. Ligmann-Zielinska A, Jankowski P. Exploring normative scenarios of land use development decisions with an agent-based simulation laboratory. Computers, Environment and Urban Systems 2010; 34.5: 409-423.

153. d'Aquino P, August P, Balmann A, Berger T, Bousquet F, et al. Agent-based models of land-use and land-cover change. Proc. of an International Workshop. 2002.

154. Jjumba A, Dragićević S. High resolution urban land-use change modeling: Agent iCity approach. Applied Spatial Analysis and Policy 2012; 5.4: 291-315.

155. Le QB, Seidl R, Scholz RW. Feedback loops and types of adaptation in the modelling of land-use decisions in an agent-based simulation. Environmental Modelling & Software 2012; 27: 83-96.

156. Ligmann-Zielinska A, Sun L. Applying time-dependent variance-based global sensitivity analysis to represent the dynamics of an agent-based model of land use change. International Journal of Geographical Information Science 2010; 24.12: 1829-1850.

157. Millington J, Romero-Calcerrada R, Wainwright J, Perry G. An agent-based model of Mediterranean agricultural land-use/cover change for examining wildfire risk. Journal of Artificial Societies and Social Simulation 2008; 11.4: 4.

158. Singer HM, Singer I, Herrmann HJ. Agent-based model for friendship in social networks. Physical Review E 2009; 80.2: 026113.

159. Hassan S, Salgado M, Pavon J. Friends forever: Social relationships with a fuzzy agent-based model. Hybrid Artificial Intelligence Systems. Springer Berlin Heidelberg 2008. 523-532.

160. Smaldino P, Pickett C, Sherman J, Schank J. An agent-based model of social identity dynamics. Journal of Artificial Societies and Social Simulation 2012; 15.4: 7.

161. Hamill L, Gilbert N. Social circles: A simple structure for agent-based social network models. Journal of Artificial Societies and Social Simulation 2009; 12.2: 3.

162. Hamill L, Gilbert N. A simple but more realistic agent-based model of a social network. Conf. European Social Simulation Assoc. 2008.

163. Gaston ME, desJardins M. Agent-organized networks for dynamic team formation. Proceedings of the fourth international joint conference on Autonomous agents and multiagent systems. ACM, 2005.

164. Marsella SC, Pynadath DV, Read SJ. PsychSim: Agent-based modeling of social interactions and influence. Proceedings of the international conference on cognitive modeling. Vol. 36. 2004.

165. Lustick IS. Agent-based modelling of collective identity: testing constructivist theory. Journal of Artificial Societies and Social Simulation 2000; 3.1: 1.

166. Billari FC Prskawetz A, Diaz BA, Fent T. The "Wedding-Ring": An agent-based marriage model based on social interaction. Demographic Research 2008; 17.3: 59-82.

167. Keller JP, Desouza KC, Lin Y. Dismantling terrorist networks: Evaluating strategic options using agent-based modeling. Technological Forecasting and Social Change 2010; 77.7: 1014-1036.

168. Fioretti G. Agent-based simulation models in organization science. Organizational Research Methods 2013; 16.2: 227-242.

169. Helbing, Dirk, ed. Social self-organization: Agent-based simulations and experiments to study emergent social behavior. Springer, 2012.

170. Ko TH, Berry NM. Agent-based modeling with social networks for terrorist recruitment. AAAI. 2004.

171. Korobow A, Johnson C, Axtell R. An agent–based model of tax compliance with social networks. National Tax Journal 2007: 589-610.

172. Madey G, Gao Y, Freeh V, Tynan R, Hoffman C. Agent-based modeling and simulation of collaborative social networks. AMCIS 2003 Proceedings: 237.

173. Dixon DS. Preliminary results from an agent-based adaptation of friendship games. 86th Annual Conference of the Western Economics Association International. 2011.

174. Garrison LA, Babcock DS. Alcohol consumption among college students: An agent-based computational simulation. Complexity 2009; 14.6: 35-44.

175. Giabbanelli P, Crutzen R. An agent-based social network model of binge drinking among Dutch adults. Journal of Artificial Societies and Social Simulation 2013; 16.2: 10.

176. Abbas SMA. An agent-based model of the development of friendship links within Facebook. Computational and Mathematical Organization Theory 2013; 19.2: 232-252.

177. Zhao K, Yen J, Ngamassi L, Maitland C, Tapia AH. Simulating inter-organizational collaboration network: a multi-relational and event-based approach. Simulation 2011: 0037549711421942.

178. Dishion TJ. Stochastic Agent-Based Modeling of Influence and Selection in Adolescence: Current Status and Future Directions in Understanding the Dynamics of Peer Contagion. Journal of Research on Adolescence 2013; 23.3: 596-603.

179. Srbljinovic A, Penzar D, Rodik P, Kardov K. An agent-based model of ethnic mobilisation. Journal of Artificial Societies and Social Simulation 2013; 6.1: 1.

180. Cederman L. Endogenizing geopolitical boundaries with agent-based modeling. Proceedings of the National Academy of Sciences 2002; 99.suppl 3: 7296-7303.

181. Epstein JM. Modeling civil violence: An agent-based computational approach. Proceedings of the National Academy of Sciences 2002; 99.suppl 3: 7243-7250.

182. Cioffi-Revilla C, Rouleau M. MASON RebeLand: An Agent-Based Model of Politics, Environment, and Insurgency. International Studies Review 2010; 12.1: 31-52.

183. Lustick I. PS-I: A user-friendly agent-based modeling platform for testing theories of political identity and political stability. Journal of Artificial Societies and Social Simulation 2002; 5.3.

184. Cioffi-Revilla C, Luke S, Parker DC, Rogers D, Fitzhugh WW, Honeychurch W, Frohlich B, DePriest P, Amartuvshin C. Agent-based modeling simulation of social adaptation and long-term change in inner Asia. Advancing Social Simulation: The First World Congress. Springer Japan 2007.

185. Kuznar LA, Sedlmeyer R. Collective violence in Darfur: An agent-based model of pastoral nomad/sedentary peasant interaction. Human Complex Systems 2005; 1(4).

186. Geller A, Alam SJ. A Socio-Political and-Cultural Model of the War in Afghanistan. International Studies Review 2010; 12.1: 8-30.

187. Ravi B, Miodownik D, Nart J. REsCape: an agent-based framework for modeling resources, ethnicity, and conflict. The Journal of Artificial Societies and Social Simulation 2008; 11.27.

188. Hailegiorgis AB, Balan GC, Bassett JK, Gulden T, Kennedy WG. An agent based model of climate change and conflict among pastoralists in East Africa. Proceedings of the International Congress on Environmental Modeling and Software. 2010.

189. Kennedy WG, Hailegiorgis AB, Rouleau M, Bassett JK, Coletti M, Balan BC, Gulden T. An agent-based model of conflict in East Africa and the effect of watering holes. Proceedings of the 19th Conference on Behavior Representation in Modeling and Simulation. 2010.

190. Rouleau M, Coletti M, Bassett JK, Hailegiorgis AB, Gulden T, Kennedy WG. Conflict in complex socio-natural systems: Using agent-based modeling to understand the behavioral roots of social unrest within the Mandera Triangle. Human Behavior-Computational Modeling and Interoperability Conference, 2009.

191. Kuznar LA, Frederick W. Simulating the effect of nepotism on political risk taking and social unrest. Computational and Mathematical Organization Theory 2007; 13.1: 29-37.

192. Chaturvedi AR, Dolk D, Chaturvedi R, Mulpuri M, Lengacher D, Mellema S, Poddar P, Foong C, Armstrong B. Understanding insurgency by using agent-based computational experimentation: Case study of Indonesia. Proceedings of the Agent 2005 Conference on Generative Social Processes, Models, and Mechanisms. 2005.

193. Lemos C, Coelho H, Lopes RJ. Agent-based Modeling of Social Conflict, Civil Violence and Revolution: State-of-the-art-review and Further Prospects. EUMAS. 2013.

194. Banks CM, Sokolowski JA. Modeling the Niger Delta Insurgency. The Social Science Journal 2010; 47.2: 271-293.

195. Weidmann, NB, Salehyan I. Violence and ethnic segregation: a computational model applied to Baghdad. International Studies Quarterly 2013; 57.1: 52-64.

196. Zou Y, Vladimir A, Fonoberov MF, Mezic I, Kevrekidis IG. Model reduction for agent-based social simulation: coarse-graining a civil violence model. Physical Review 2012; E 85.6: 066106.

197. Robbins MM, Robbins AM. Simulation of the population dynamics and social structure of the Virunga mountain gorillas. Am J Primatol 2004; 63(4): 201-223.

198. Jackson D, Holcombe M, Ratnieks F. Coupled computational simulation and empirical research into the foraging system of Pharaoh's ant (Monomorium pharaonis). Biosystems 2004; 76.1: 101-112.

199. Mach R, Schweitzer F. Modeling vortex swarming in daphnia. Bulletin of mathematical biology 2007; 69.2: 539-562.

200. Campos D, Llebot JE, Méndez V. Limited resources and evolutionary learning may help to understand the mistimed reproduction in birds caused by climate change. Theoretical population biology 2008; 74.1: 16-21.

201. Robinson EJH, Ratnieks FLW, Holcombe M. An agent-based model to investigate the roles of attractive and repellent pheromones in ant decision making during foraging. Journal of Theoretical Biology 2008; 255.2: 250-258.

202. Johnson BR. Pattern formation on the combs of honeybees: increasing fitness by coupling self-organization with templates. Proceedings of the Royal Society of London B: Biological Sciences 2009; 276.1655: 255-261.

203. Padmanabha H, Correa F, Rubio C, Baeza A, Osorio S, Mendez J, Jones JH, Diuk-Wasser MA. Human Social Behavior and Demography Drive Patterns of Fine-Scale Dengue Transmission in Endemic Areas of Colombia. PloS One 2015; 10.12: e0144451.

204. Masuda N, O'shea-Wheller TA, Doran C, Franks NR. Computational model of collective nest selection by ants with heterogeneous acceptance thresholds. Royal Society open science 2015; 2.6: 140533.

205. Lin Y, Abaid N. Modeling perspectives on echolocation strategies inspired by bats flying in groups. Journal of Theoretical Biology 2015; 387: 46-53.

206. Filatova OA, Miller PJO. An agent-based model of dialect evolution in killer whales. Journal of Theoretical Biology 2015; 373: 82-91.

207. Becher MA, Grimm V, Thorbek P, Horn J, Kennedy PJ, Osborne JL. BEEHAVE: a systems model of honeybee colony dynamics and foraging to explore multifactorial causes of colony failure. Journal of applied ecology 2014; 51.2: 470-482.

208. Strömbom D, Mann RP, Wilson AM, Hailes S, Morton AJ, Sumpter DJ, King AJ. Solving the shepherding problem: heuristics for herding autonomous,

interacting agents. Journal of The Royal Society Interface 2014; 11.100: 20140719.

209. Senior AM, Nakagawa S, Grimm V. The Evolutionary Consequences of Disrupted Male Mating Signals: An Agent-Based Modelling Exploration of Endocrine Disrupting Chemicals in the Guppy. PloS One 2014; 9.7: e103100.

210. Czaczkes TJ. How to not get stuck—Negative feedback due to crowding maintains flexibility in ant foraging. Journal of Theoretical Biology 2014; 360: 172-180.

211. Lotem A, Biran-Yoeli I. Evolution of learning and levels of selection: A lesson from avian parent–offspring communication. Theoretical Population Biology 2014; 91: 58-74.

212. Franz M, Schülke O, Ostner J. Rapid evolution of cooperation in group-living animals. BMC Evolutionary Biology 2013; 13.1: 235.

213. Grueter C, Schürch R, Czaczkes TJ, Taylor K, Durance T, Jones SM. Negative feedback enables fast and flexible collective decision-making in ants. PLoS One 2012; 7.9: e44501.

214. Perna A, Granovskiy B, Garnier S, Nicolis SC, Labédan M, Theraulaz G, Fourcassié V, Sumpter DJT. Individual rules for trail pattern formation in Argentine ants (Linepithema humile). PLoS Comput Biol 2012; 8.7: e1002592.

215. Karsai I, Phillips MD. Regulation of task differentiation in wasp societies: A bottom-up model of the "common stomach". Journal of Theoretical Biology 2012; 294: 98-113.

216. Franz M, van der Post D, Schülke O, Ostner J. The evolution of cooperative turn-taking in animal conflict. BMC Evolutionary Biology 2011; 11.1: 1.

217. Galla T. Independence and interdependence in the nest-site choice by honeybee swarms: agent-based models, analytical approaches and pattern formation. Journal of Theoretical Biology 2010; 262.1: 186-196.

218. Duca KA, Shapiro M, Delgado-Eckert E, Hadinoto V, Jarrah AS, Laubenbacher R, Lee K, Luzuriaga K, Polys NF, Thorley-Lawson DA. A virtual look at Epstein–Barr virus infection: biological interpretations. PLoS Pathog 2007; 3.10: e137.

219. Muller G, Grébaut P, and Gouteux J. An agent-based model of sleeping sickness: simulation trials of a forest focus in southern Cameroon. Comptes Rendus Biologies 2004; 327.1: 1-11.

220. Lee BY, Bedford VL, Roberts MS, Carley KM. Virtual epidemic in a virtual city: simulating the spread of influenza in a US metropolitan area. Translational Research 2008; 151.6: 275-287.

221. Sander B, Nizam A, Garrison LP Jr, Postma MJ, Halloran ME, Longini IM Jr. Economic evaluation of influenza pandemic mitigation strategies in the United States using a stochastic microsimulation transmission model. Value in Health 2009; 12.2: 226-233.

222. Escobar E, Durgham R, Dammann O, Stopka TJ. Agent-based computational model of the prevalence of gonococcal infections after the implementation of HIV pre-exposure prophylaxis guidelines. Online Journal of Public Health Informatics 2015; 7.3.

223. Siettos CI, Anastassopoulou C, Russo L, Grigoras C, Mylonakis E.. Forecasting and control policy assessment for the Ebola virus disease (EVD) epidemic in Sierra Leone using small-world networked model simulations. BMJ Open 2016; 6.1: e008649.

224. Lin S, DeVisser MH, Messina JP. An agent-based model to simulate tsetse fly distribution and control techniques: A case study in Nguruman, Kenya. Ecological Modelling 2015; 314: 80-89.

225. Poore KD, Bauch CT. The impact of aggregating serogroups in dynamic models of Neisseria meningitidis transmission. BMC Infectious Diseases 2015; 15.1: 1.

226. Pollmächer J, Figge MT. Deciphering chemokine properties by a hybrid agent-based model of Aspergillus fumigatus infection in human alveoli. Frontiers in Microbiology 2015; 6:503.

227. Zhu L, Qualls WA, Marshall JM, Arheart KL, DeAngelis DL, McManus JW, Traore SF, Doumbia S, Schlein Y, Müller GC, Beier JC. A spatial individual-based model predicting a great impact of copious sugar sources and resting sites on survival of Anopheles gambiae and malaria parasite transmission. Malar J 2015; 14: 59.

228. Manore CA, Hickmann KS, Hyman JM, Foppa IM, Davis JK, Wesson DM, Mores CN.. A network-patch methodology for adapting agent-based models for directly transmitted disease to mosquito-borne disease. Journal of Biological Dynamics 2015; 9.1: 52-72.

229. McCreesh N, Nikulin G, Booth M. Predicting the effects of climate change on Schistosoma mansoni transmission in eastern Africa. Parasites & Vectors 2015; 8.1: 1-9.

230. Arifin SM, Zhou Y, Davis GJ, Gentile JE, Madey GR, Collins FH. An agent-based model of the population dynamics of Anopheles gambiae. Malaria journal 2014; 13.1: 1-20.

231. Gotteland C, McFerrin BM, Zhao X, Gilot-Fromont E, Lélu M. Agricultural landscape and spatial distribution of Toxoplasma gondii in rural

environment: an agent-based model. International journal of health geographics 2014; 13.1: 1.

232. Saul A, Smith T, Maire N. Stochastic simulation of endemic Salmonella enterica serovar Typhi: the importance of long lasting immunity and the carrier state. PloS One 2013; 8.9: e74097.

233. McCreesh N, Booth M. The effect of simulating different intermediate host snail species on the link between water temperature and schistosomiasis risk. PloS One 2014; 9.7: e87892.

234. Groner ML, Cox R, Gettinby G, Revie CW. Use of agent-based modelling to predict benefits of cleaner fish in controlling sea lice, Lepeophtheirus salmonis, infestations on farmed Atlantic salmon, Salmo salar L. Journal of Fish Diseases 2013; 36.3: 195-208.

235. Havas KA, Boone RB, Hill AE, Salman MD. A Brucellosis Disease Control Strategy for the Kakheti Region of the Country of Georgia: An Agent-Based Model. Zoonoses and Public Health 2014; 61.4: 260-270.

236. Devillers H, Lobry JR, Menu F. An agent-based model for predicting the prevalence of Trypanosoma cruzi I and II in their host and vector populations. Journal of Theoretical Biology 2008; 255.3: 307-315.

237. Huang L, Huang Y, Wang Q, Xiao N, Yi D, Yu W, Qiu D. An agent-based model for control strategies of Echinococcus granulosus. Veterinary Parasitology 2011; 179.1: 84-91.

238. Mansury Y, Kimura M, Lobo J, Deisboeck TS. Emerging patterns in tumor systems: simulating the dynamics of multicellular clusters with an agent-based spatial agglomeration model. Journal of Theoretical Biology 2002; 219.3: 343-370.

239. Mansury Y, Deisboeck TS. The impact of "search precision" in an agent-based tumor model. Journal of Theoretical Biology 2003; 224.3: 325-337.

240. Athale C, Mansury Y, Deisboeck TS. Simulating the impact of a molecular 'decision-process' on cellular phenotype and multicellular patterns in brain tumors. Journal of Theoretical Biology 2005; 233.4: 469-481.

241. Zhang L, Athale CA, Deisboeck TS. Development of a three-dimensional multiscale agent-based tumor model: simulating gene-protein interaction profiles, cell phenotypes and multicellular patterns in brain cancer. Journal of Theoretical Biology 2007; 244.1: 96-107.

242. Wang Z, Zhang L, Sagotsky J, Deisboeck TS. Simulating non-small cell lung cancer with a multiscale agent-based model. Theoretical Biology & Medical Modelling. 2007;4:50. doi:10.1186/1742-4682-4-50.

243. Fox, BM, Moffitt RA, Wang MD. An agent-based stochastic tumor model for predicting mitotic arrest drug response. Engineering in Medicine and Biology Society, 2008. EMBS 2008. 30th Annual International Conference of the IEEE. IEEE, 2008.

244. Wang Z, Birch CM, Sagotsky J, Deisboeck TS. Cross-scale, cross-pathway evaluation using an agent-based non-small cell lung cancer model. Bioinformatics 2009; 25.18: 2389-2396.

245. Chen, LL, Ulmer S, and Deisboeck TS. An agent-based model identifies MRI regions of probable tumor invasion in a patient with glioblastoma. Physics in medicine and biology 2009; 55.2: 329.

246. Zhang L, Chen LL, Deisboeck TS. Multi-scale, multi-resolution brain cancer modeling. Mathematics and Computers in Simulation 20098; 79.7: 2021-2035.

247. Chen J, Sprouffske K, Huang Q, Maley CC. Solving the puzzle of metastasis: the evolution of cell migration in neoplasms. PLoS One 2011; 6.4: e17933.

248. Krepkin K, Costa J. Defining the role of cooperation in early tumor progression. Journal of Theoretical Biology 2011; 285.1: 36-45.

249. Zhang L, Jiang B, Wu Y, Strouthos C, Sun PZ, Su J, Zhou X. Developing a multiscale, multi-resolution agent-based brain tumor model by graphics processing units. Theoretical Biology and Medical Modelling 2011; 8.1: 46.

250. Macklin P, Edgerton ME, Thompson AM, Cristini V. Patient-calibrated agent-based modelling of ductal carcinoma in situ (DCIS): from microscopic measurements to macroscopic predictions of clinical progression. Journal of Theoretical Biology 2012; 301: 122-140.

251. Narang V, Wong SY, Leong SR, Harish B, Abastado JP, Gouaillard A. Selection of Mesenchymal-Like Metastatic Cells in Primary Tumors-An in silico Investigation. Front Immunol 2012; 3: 88.

252. Masoudi-Nejad A, Bidkhori G, Hosseini Ashtiani S, Najafi A, Bozorgmehr JH, Wang E. Cancer systems biology and modeling: Microscopic scale and multiscale approaches. Seminars in cancer biology. Vol. 30. Academic Press, 2015.

253. Wang Z, Butner JD, Kerketta R, Cristini V, Deisboeck TS. Simulating cancer growth with multiscale agent-based modeling. Seminars in cancer biology. Vol. 30. Academic Press, 2015.

254. Chen Y, Wang H, Zhang J, Chen K, Li Y. Simulation of avascular tumor growth by agent-based game model involving phenotype-phenotype interactions. Sci Rep 2015; 9:5:17992. Epub 2015 Dec 9.

255. Qiao M, Wu D, Carey M, Zhou X, Zhang L. Multi-Scale Agent-Based Multiple Myeloma Cancer Modeling and the Related Study of the Balance between Osteoclasts and Osteoblasts. PloS One 10.12 (2015): e0143206.

256. Chapa J, Bourgo RJ, Greene GL, Kulkarni S, An G. Examining the pathogenesis of breast cancer using a novel agent-based model of mammary ductal epithelium dynamics. PLoS One 2013; 8(5): e64091.

257. Sarpe V, Jacob C. Simulating the decentralized processes of the human immune system in a virtual anatomy model. BMC Bioinformatics 2013; 14 Suppl 6: S2.

258. Wang J, Zhang L, Jing C, Ye G, Wu H, Miao H, Wu Y, Zhou X. Multi-scale agent-based modeling on melanoma and its related angiogenesis analysis. Theor Biol Med Model 2013; 10: 41.

259. Solovyev A, Mi Q, Tzen YT, Brienza D, Vodovotz Y. Hybrid equation/agent-based model of ischemia-induced hyperemia and pressure ulcer formation predicts greater propensity to ulcerate in subjects with spinal cord injury. PLoS Comput Biol 2013; 9(5): e1003070.

260. Kleinstreuer N, Dix D, Rountree M, Baker N, Sipes N, Reif D, Spencer R, Knudsen T. A computational model predicting disruption of blood vessel development. PLoS Comput Biol 2013; 9(4): e1002996.

261. Martin KS, Blemker SS, Peirce SM. Agent-based computational model investigates muscle-specific responses to disuse-induced atrophy. Journal of Applied Physiology 2015; 118(10): 1299-1309.

262. Brown BN, Price IM, Toapanta FR, DeAlmeida DR, Wiley CA, Ross TM, Oury TD, Vodovotz Y. An agent-based model of inflammation and fibrosis following particulate exposure in the lung. Math Biosci. 2011 Jun;231(2):186-96.

CHAPTER 3: THE INFLAMMATORY TWITCH

3.1. Introduction

The inflammatory response is a general biological defense mechanism for battling invading microbes or attending to injury. The symptomatic manifestations of inflammation, namely *tumor*, *rugor*, *calor* and *dolor*, reflect myriad molecular events that orchestrate a variety of resident and recruited cell types to operate in a specific manner within the affected tissue [1]. Clearly, turning on an appropriate inflammatory response in time of need is critical to an organism's survival. However, turning the response off again when it is no longer needed is equally important. Indeed, failure to resolve the inflammatory response is presumably behind the chronic inflammatory conditions that characterize many common diseases. This raises the general question as to what strategy the body uses to control both the up regulation and the down regulation of inflammation. Negative feedback has been proposed as a means for controlling the extent of allergic inflammation [2]. However, recent work suggests this does not adequately explain the relationship between the stimulus and the allergic response [3]. Another possibility is that these two events are subject to independent decision criteria; up regulation of inflammation is directed by a control mechanism that reacts to the appearance of a threat, while down regulation is controlled by a separate mechanism that detects the threat's disappearance. This scenario is compelling because of its ready analogy to the fighting of military battles. However, it is not the only possibility.

An alternative control strategy for the inflammatory response is suggested by the formal similarity of its task structure to that of skeletal muscle. The inflammatory response is something that an organism must be ready to invoke, without warning, any time a threat arises, and yet it must dissipate when no longer needed. The same applies to muscle activation; muscles must be ready to generate force whenever the brain decides to undertake some task, but must cease to do so as soon as the task is completed. However, force generation and cessation in muscle are not subject to separate decision processes, but rather are controlled jointly via frequency modulation. Specifically, a muscle continues to do the job asked of it so long as it receives a steady stream of periodic electrical impulses, the frequency of the impulses dictating the level of force. Once the need for the task has passed, however, the impulses stop and the muscle returns to quiescence. The functional unit of this control strategy is the muscle twitch, a transient manifestation of force driven by a sequence of events that includes not only those that cause force to escalate, but also those that bring about its subsequent resolution. In other words, the termination of a muscle twitch is an inevitable consequence of its initiation, so continuation and/or escalation of force is simply a consequence of how individual twitches summate when invoked in rapid succession. The singular advantage of this type of control strategy is that it obviates the need for additional decision resources beyond those involved in activation.

The above reasoning leads us to contemplate the possibility that inflammation might be controlled in a similar manner to skeletal muscle, that is, via the repetitive generation of self-limited transient unitary responses. This analogy implies the existence

of an “inflammatory twitch”, an inevitably resolving sequence of cellular events having formal similarity to a muscle twitch, albeit it over a greatly extended time scale. Further questions then arise as to the extent of this analogy. What is the duration of an inflammatory twitch? Can multiple inflammatory twitches summate in the same manner as muscle twitches? Do inflammatory twitches give rise to a post-initiation refractory period? Answering these questions might elucidate important aspects of how the general host inflammatory response is controlled, and possibly even how its control might fail in disease.

Accordingly, the goal of the present study was to investigate the plausibility of the inflammatory twitch hypothesis. We focused in particular on allergic inflammation in the lung because this condition has been well characterized in terms of the cell types involved [1]. Also, we have previously observed that when allergically sensitized mice are continuously challenged with antigen over a period of weeks, their inflammatory response does not continue indefinitely but instead eventually resolves toward baseline [4]. Furthermore, if antigen challenge is interrupted for several weeks and then reinitiated, the animals again mount a vigorous inflammatory response [5]. These observations appear to be consistent with our notion of the inflammatory twitch, but they do not demonstrate that it is feasible relative to the interactions of all the cells involved. Allergic inflammation in the lung is a complex event, localized around the lung and its associated mediastinal lymph nodes, yet involving a variety of cells recruited at different times from outside the organ [6-7]. It is not immediately obvious that a twitch-like self-

limited response to the appearance of an antigen in the lung could actually manifest from a system with these features.

Testing the plausibility of the inflammatory twitch hypothesis thus requires that the spatiotemporal dynamics of the various cellular players and chemical signals involved be taken into account. In the present study we undertook this task computationally, employing a modeling technique that appears ideally suited to this purpose. This technique, known as agent-based modeling, allowed us to simulate the dynamic environment comprising the pulmonary capillary and its associated alveolar compartment, and to determine if something akin to an inflammatory twitch is indeed possible, and what its temporal and spatial morphology might look like.

3.2. Computational Methods

3.2.1. Model Structure

We used NetLogo 4.1.3 freeware [8] to design an agent-based model that simulates allergic inflammation in an alveolus of the lung in response to antigen stimulation. The model uses two types of variables known respectively as patches and agents. Patches represent fixed pieces of the local environment, and thus contain local variables representing information about that area. In our model of the allergic inflammatory response, the patches represent the capillary and alveolus as well as the endothelial barrier between them. (The sizes of the capillary and alveolar spaces are arbitrary.) Each alveolar patch has a local parameter known as “tissue-life”, which indicates the amount of tissue damage that has occurred on that patch. It is set between 0

and 100, where 100 corresponds to full health and 0 indicates a fully destroyed patch. Thus the average health of all alveolar patches represents the average health of the alveolus.

In contrast to patches, which represent the environment, agents represent individual entities capable of moving across patches and interacting with surrounding patches and with other agents. The agents in our model are the multiple cell types involved in the allergic inflammatory response in the lung. The behavior of the model is thus determined by the collection of rules that each agent obeys.

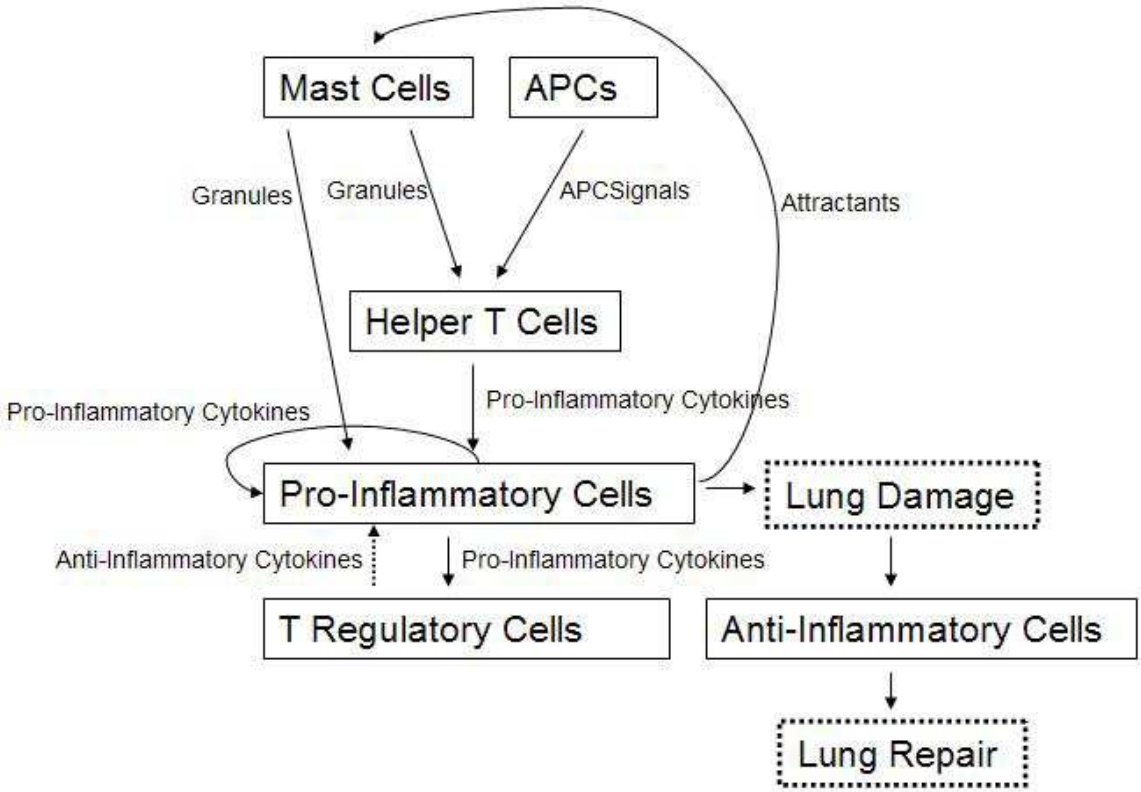

Figure 26: Schema for allergic inflammation in the lung. Mast cells and APCs are activated upon encountering Particles (i.e. antigen), which then leads to the indicated cascades

Our overall schema for the allergic response is shown in Figure 26, and includes what we believe to be the key mechanisms and cell types that are involved. To increase the manageability of the model we have not included all known details of allergic inflammation in this schema. For example, following the approach of Brown et al. [8], we lumped dendritic cells, B cells and macrophages together into a single Antigen Presenting Cell (APC) type. Similarly, neutrophils, eosinophils and other cell types that cause local tissue damage are merged into a single Pro-Inflammatory Cell (PIC) type, while fibroblasts and other cells that are involved in tissue repair are combined into a single Anti-Inflammatory Cell (AIC) type. This grouping of cell types is, of course, a gross over simplification of reality, but we believe it represents the greatest degree of coarse-graining that could reasonably be applied to the cellular community so that it still retains the ability to exhibit competition between inflammatory and reparative processes.

The inflammatory response is initiated by the sudden presence of Particles at random locations in the alveolar space. Both Mast Cells and APCs are involved in this initiation. We focus on these two cell types because *in vivo*, mast cells release both preformed and synthesized chemical mediators such as prostaglandins, leukotrienes and vasoactive amines upon cross-linking of their receptors by bound antigen [1]. This leads to many of the symptoms that are observed in the allergic inflammatory response, such as vasodilation and bronchoconstriction [1]. In addition, APCs process antigen particles via pattern-recognition receptors, such as Toll-like receptors, and subsequently become activated. This affects cytokine production in such a way as to ultimately affect the T-cell

population, leading to amplification and perpetuation of the inflammatory phase of the allergic response [9].

The model was initialized with 5 Mast Cells, 10 APCs and 10 PICs in the alveolus, and the same numbers in the capillary. The alveolus was also initialized with 20 AICs, 10 helper T-cells and 10 regulatory T-cells, while the capillary contained 5 helper-T and regulatory T-Cells. The capillary acts as a reservoir of cells, so if any of these cells dropped below these baseline values in the capillary, the appropriate number of additional cells was randomly added to the capillary space. The capillary effectively acts as a source and sink for cells in the alveolus. Thus while the size of these spaces are arbitrary, changing the size of the capillary would not have a significant effect on the model.

The model includes an endothelial barrier between the capillary and the alveolus. Pores in the barrier allow restricted cell movement between the two spaces. If the sum of various pro-inflammatory chemical signals, namely Granules and Pro-Inflammatory Cytokines (PI Cytokines) in the lung space is greater than a critical value (arbitrarily chosen as 200 for this model), the barrier is removed. This simulates the effects of vasodilation and endothelial leak by allowing uninhibited cell movement between the capillary and alveolar spaces.

3.2.2. Model Dynamics

Inflammation in the model is initiated by random placement of a certain number of Particles throughout the alveolus [8]. Additional Particles may be placed at any later time point in order to simulate continual stimulation of the inflammatory response.

All cell movement in the model is probabilistic. If there is no reason for a cell to move in any particular direction, the cell moves a distance of one patch either forward, back, right or left with equal probability at each time step. However, if a patch contains a signal to which the cell is responsive, the probability of movement to that patch will be increased proportional to the strength of the signal. Thus, while on average a cell will move in the direction of the strongest signal, the movement at any particular time step may not be in this direction.

Diffusion of chemical signals (i.e. Granules, PI Cytokines and AI Cytokines) is simulated by randomly distributing a specified fraction of each signal on a patch to its adjacent patches at each time step. Removal of these substances by enzymes, blood flow, etc. is simulated by having their strengths decrease by set proportions (specific for each substance) at each time step [8].

The lifespan of each cell type in the model follows an exponential distribution that is implemented as follows. At each time step, and for each cell in the model, we generate a random number on the uniform distribution between 0 and 1. If this number is greater than a critical value specific for the cell type in question then the cell is eliminated. Mast Cells and APCs are relatively long-lived compared to most of the other cell types [6, 10]. (While the most abundant CD4 T-cell type, memory T cells, are also

long-lived, we do not consider them long-lived in our model because they may only be active for a shorter period of time following antigen exposure.) We thus chose the critical value for Mast Cells and APCs to be 0.9997 giving them an estimated mean life span of 2500 time steps, while the critical value for all the other cell types except the AICs was 0.9978 giving them an estimated mean lifespan of 200 time steps. The AICs were allowed to live indefinitely since fibroblasts are known to be very long-lived relative to the other cell types [11-12].

3.2.3. Agent Rules

The overall behavior of the model is a consequence of the way in which its agents (the cell types described above) behave. The behavior of each agent is governed by a set of rules designed to capture the essential elements of actual biological behavior. The various agents in our model are listed in Table 1 together with the signals to which they respond and the rules that govern their behavior. The rule sets for each cell type are generally similar in that they cause the cells to move towards and become activated by certain chemical signals, and then release chemical signals of their own into the surrounding patches.

The initial cell types involved in the allergic response are Mast Cells and APCs, which both respond to Particles and release chemical signals that initiate the subsequent events of the allergic response. Mast Cells accomplish this task by binding Particles on

Table 1: Summary of all agents and their respective rules included in the model

Cell Type	Moves Towards	Rule
Mast Cell (immature)	Attractants	Moves preferentially to attractants, or randomly if there are no attractants
Mast Cell (mature)	Particles, Attractants	Upon binding Particle, releases Granules for 10 time steps. Becomes inactive for user-set time if encounters user-set number of Particles
APC	Particles	While digesting Particle, releases APC Signals. Becomes inactive for user-set time if encounters user-set number of Particles
Helper T Cell	Granules, APCSignals	If moving towards Granules and/or APCs, releases Pro-Inflammatory Cytokines for 10 time steps. Afterwards, if there is a strong chemical signal on the current patch, converts into a Pro-Inflammatory Cell
Pro-Inflammatory Cell	Pro-Inflammatory Cytokines, Granules	If moving towards Pro-Inflammatory Cytokines and/or Granules, become activated for 10 time steps. While activated, release Pro-Inflammatory Cytokines and Attractants. Also, subtract 5 from the health of the patch currently on if cell has moved towards a chemical signal, or 2 if not. At the end of activation, the cell dies if there is a chemical signal on the current patch
T-Regulatory Cell	Pro-Inflammatory Cytokines	If moving towards Pro-Inflammatory Cytokines, release Anti-Inflammatory Cytokines
Anti-Inflammatory Cell	Patches with Health < 100	If on a patch with health < 100, add 1 to that patch's health parameter at each time step

the patch they are currently on and then releasing a user-specified number of Granules into the surrounding patches for 10 time steps [1]. Mast Cells initially exist in an immature state until a user-specified amount of time has passed, at which point they become mature and functional. Mature Mast Cells move towards Particles on adjacent patches, while immature Mast Cells move towards released Attractants or else they move randomly [13-14]. In contrast, APCs eliminate Particles on the patch they are currently

on, releasing APC Signals into the surrounding patches in the process [15]. When either a PIC or a Mast Cell encounters a particle, it becomes sensitized. However, previous studies have shown that Mast Cells and APCs become desensitized after a period of continual stimulation (13). Accordingly, we allow Mast Cells and APCs in the model to be sensitized so long as they have encountered fewer than 5 particles, but they revert to a quiescent state otherwise.

Granules and APCSignals serve as chemical signals for helper T-cells, i.e. these cells preferentially move towards patches with high concentrations of these chemicals. Upon landing on these patches, helper T-cells are activated for 10 time steps during which they release PI Cytokines [1]. Afterwards they convert to PICs if they are still on patches with high PI Cytokine levels.

PICs are signaled by both Granules and PI Cytokines, and become activated upon landing on a patch with high concentrations of these signals. They release PI Cytokines and Attractants for 10 activation steps and then die afterwards. If activated PICs sense a strong signal on at least one of the nearby patches, they subtract 5 from the tissue-life parameter of the patch they are currently on. Otherwise, they subtract 2.

The combination of both helper-T cell and PIC actions creates a positive feedback loop of PIC recruitment and PI Cytokine release. This loop is ultimately hindered by T-Regulatory cells that respond to the PI Cytokine chemical signal. Unlike PICs or helper T-cells, however, T-Regulatory cells remained permanently activated. Whenever they move towards PI Cytokines, T-Regulatory cells release AI Cytokines that subtract from

the amount of PI Cytokines on a patch and thus dampen the pro-inflammatory signal and its effect [1].

In contrast to the other cell types, AICs move preferentially towards damaged tissue, i.e. any patch with a tissue-life parameter less than 100. Upon reaching a damaged tissue patch, an AIC will remain there and with each time step will add 1 to the Tissue-Life parameter of the patch until it reaches 100. At that point, the cells will either move towards another patch with a tissue-life parameter less than 100 or else it will move randomly. This behavior comes directly from the agent-based model developed by Brown et al. [8].

Figure 27 shows an example output of the model. The baseline state of the model prior to application of any Particles is shown in Panel 1, where the light gray color

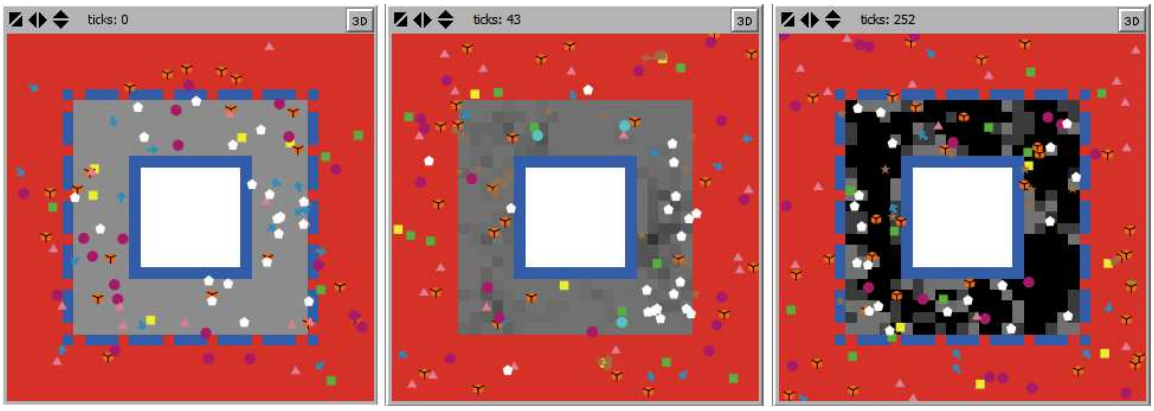

Figure 27: Three snapshots of the model at rest, with increasing levels of lung damage from left to right. The red area is the blood, the gray area represents the alveolus, the white area represents air, and the blue outlines are barriers between these respective spaces. The leaky barrier between the blood and alveolus can disappear during an allergic reaction (as seen in the middle figure), representing vasodilation. Darker gray areas indicate damaged lung tissue. The other shapes dispersed throughout the blood and alveolus spaces represent different cell types included in the model

corresponds to full tissue health. Panels 2 and 3 show increasing levels of lung damage indicated by the progressively darkening alveolar patches.

3.3. Results

All model simulations began with a run-in period of 250 time steps with no stimulation, which was found was sufficient to have the model achieve steady state. Figure 28 shows the time course of Tissue Health over 15,000 times steps after the run-in period (average of 10 independent simulations) resulting from stimulating the model with 85 Particles placed randomly within the Alveolar Space every 20 times steps. This caused

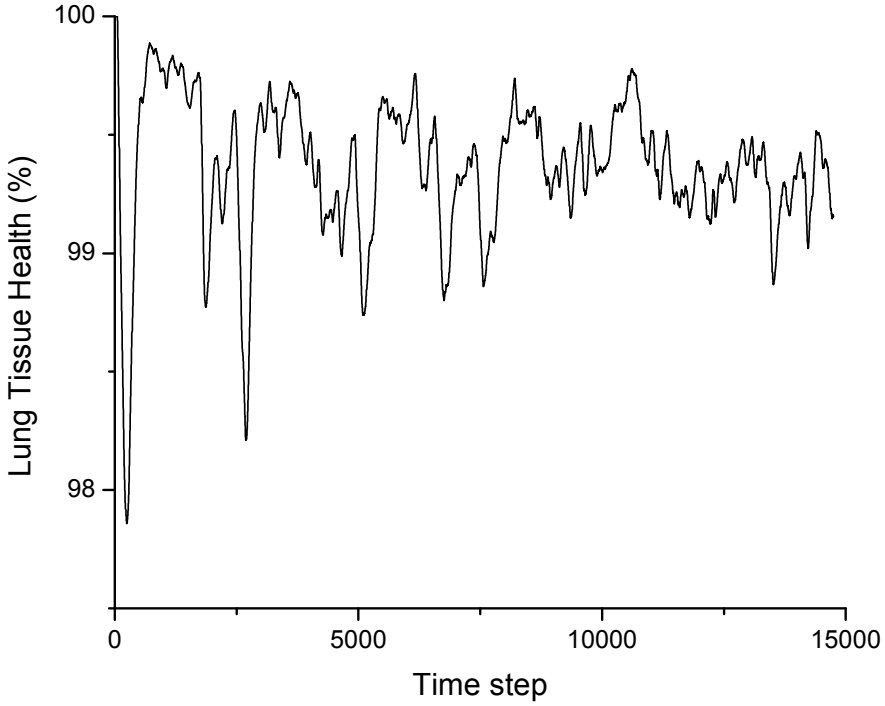

Figure 28: Average of 10 simulations of Tissue Health (defined as 0 for totally damaged and 100 for completely healthy) for the Alveolar Space of the model a function of the number of time steps when 85 Particles are placed randomly within the Alveolar Space every 20 time steps

oscillations in Tissue Health of progressively decreasing amplitude. Figure 29 shows an expanded view of the initial portion of the simulation upon which we have superimposed data taken from a study by Tanaka et al. [3] who subjected ovalbumin-sensitized mice to 3 weeks of daily stimulation with ovalbumin aerosol. The inflammatory status of the mice, including a variety of cell types in bronchoalveolar lavage fluid, were measured at 4 time points during this period to provide a time-course for the inflammatory response. The data shown consist of the counts of pro-inflammatory cell types in Fig. 29A (leukocytes plus lymphocytes), and macrophages (taken to represent anti-inflammatory cells) in Fig. 29B. The two cell type counts from Tanaka et al. [3] shown in Fig. 29 have been scaled to be comparable to the simulated cell counts for ease of comparison of the shapes of these relationships with time. In addition, the time scales of the simulations have been adjusted so that 100 time steps equals 1 week of real time, which leads to a good match between the simulated and experimental cell count profiles.

Figure 30 shows the model behavior when it was subjected to the same stimulation regimen as used by Riesenfeld et al. [5], namely 3 consecutive daily exposures to antigen followed by a single exposure one month later. The dip in Tissue Health seen with the 3 early Particle administrations is recapitulated, albeit it to a somewhat reduced degree, when Particles are administered again after the break. This shows that, given sufficient time, the model will recover sufficiently towards it naïve state that it can mount a second response when re-stimulated.

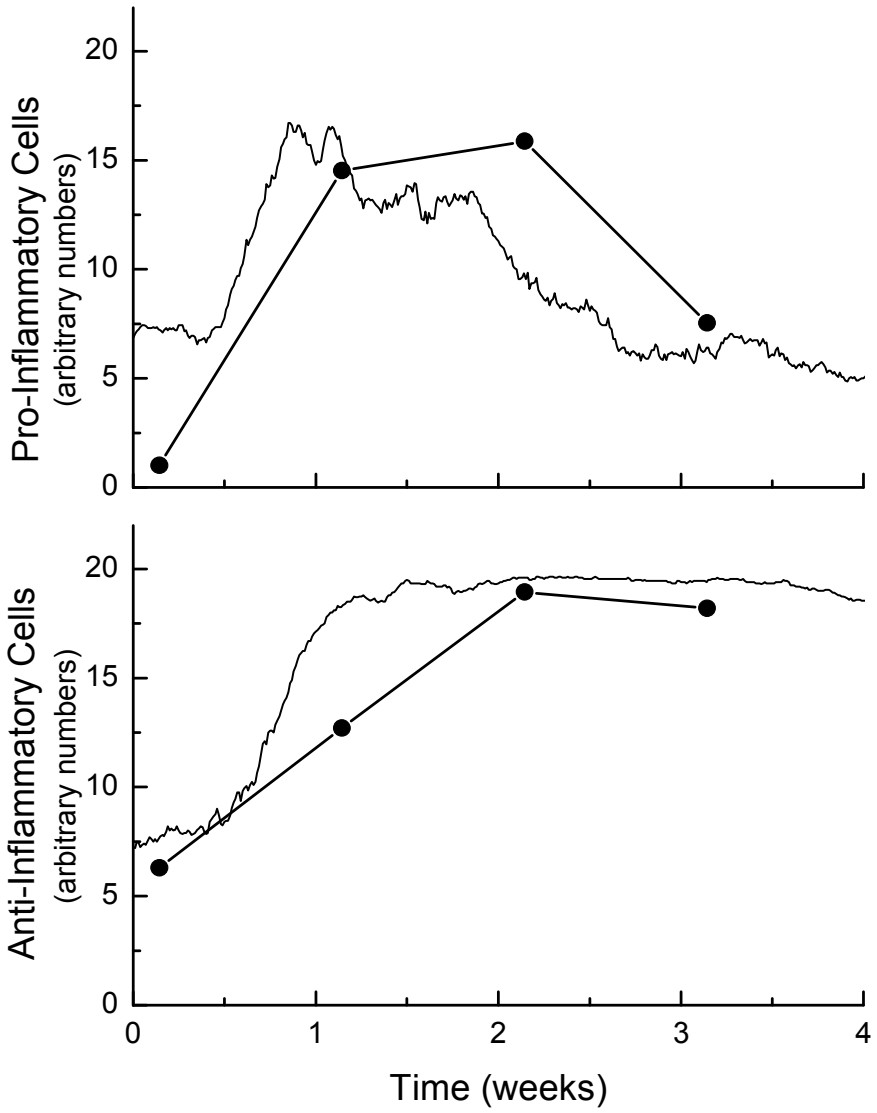

Figure 29: Pro- (top) and anti- (bottom) inflammatory cell types from the early portion of the simulation shown in Fig. 3, together with counts of pro-inflammatory cells (leukocytes and lymphocytes) and a nominal anti-inflammatory cell type (macrophages) from bronchalveolar lavage fluid determined experimentally by Tanaka et al. (3) in sensitized mice exposed to ovalbumin daily for 3 weeks. The experimental counts have been scaled vertically for ease of comparison of their temporal relationships to the simulated data. The simulated time base (i.e. number of time steps) have been divided by 100 to convert to real time in weeks

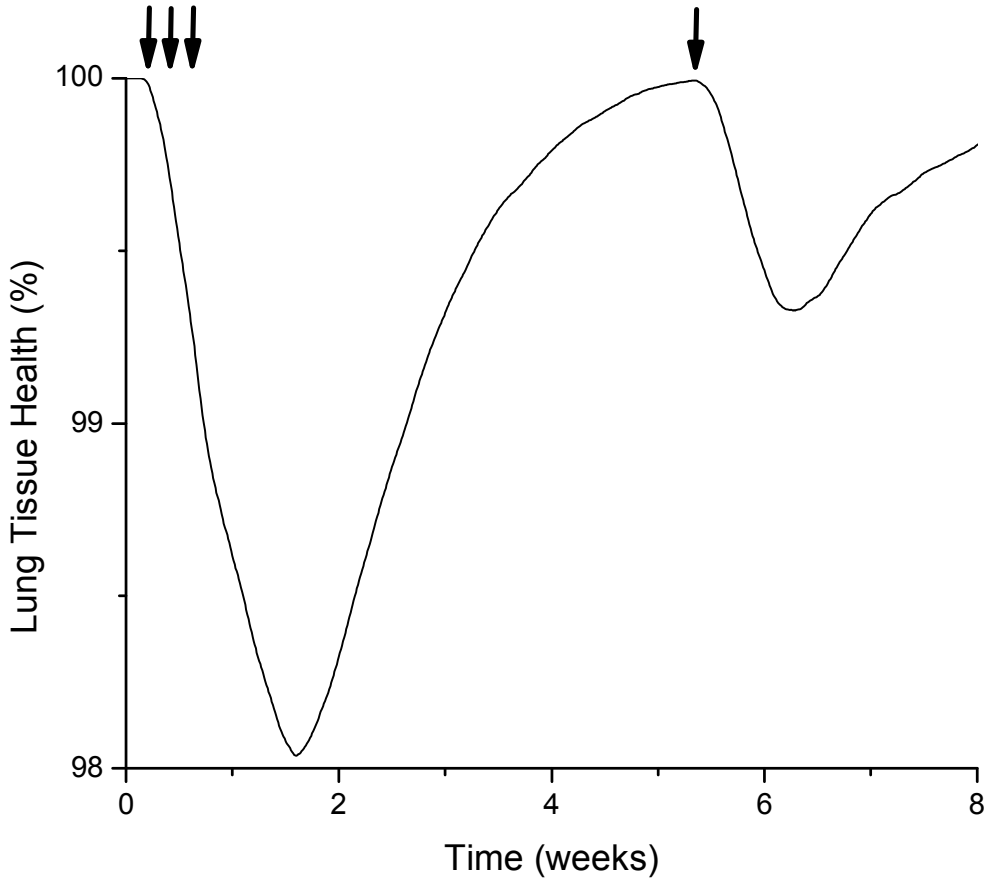

Figure 30: Average of ten simulations in which 3 Particle challenges were placed in the Alveolar Space at roughly once per day followed by a 4th challenge one month later (the vertical arrows indicate the times of challenge)

Finally, Figure 31 shows what happens to Tissue Health when the interval between application of Particles is varied. Stimulation periods of 0.5, 1 and 2 weeks yield rather similar results, characterized by an initial pronounced dip in Tissue Health followed by decreasing dips and more chaotic behavior as time progresses. By contrast, an application interval of 10 weeks produces regular marked oscillations in Tissue Health that continue unabated.

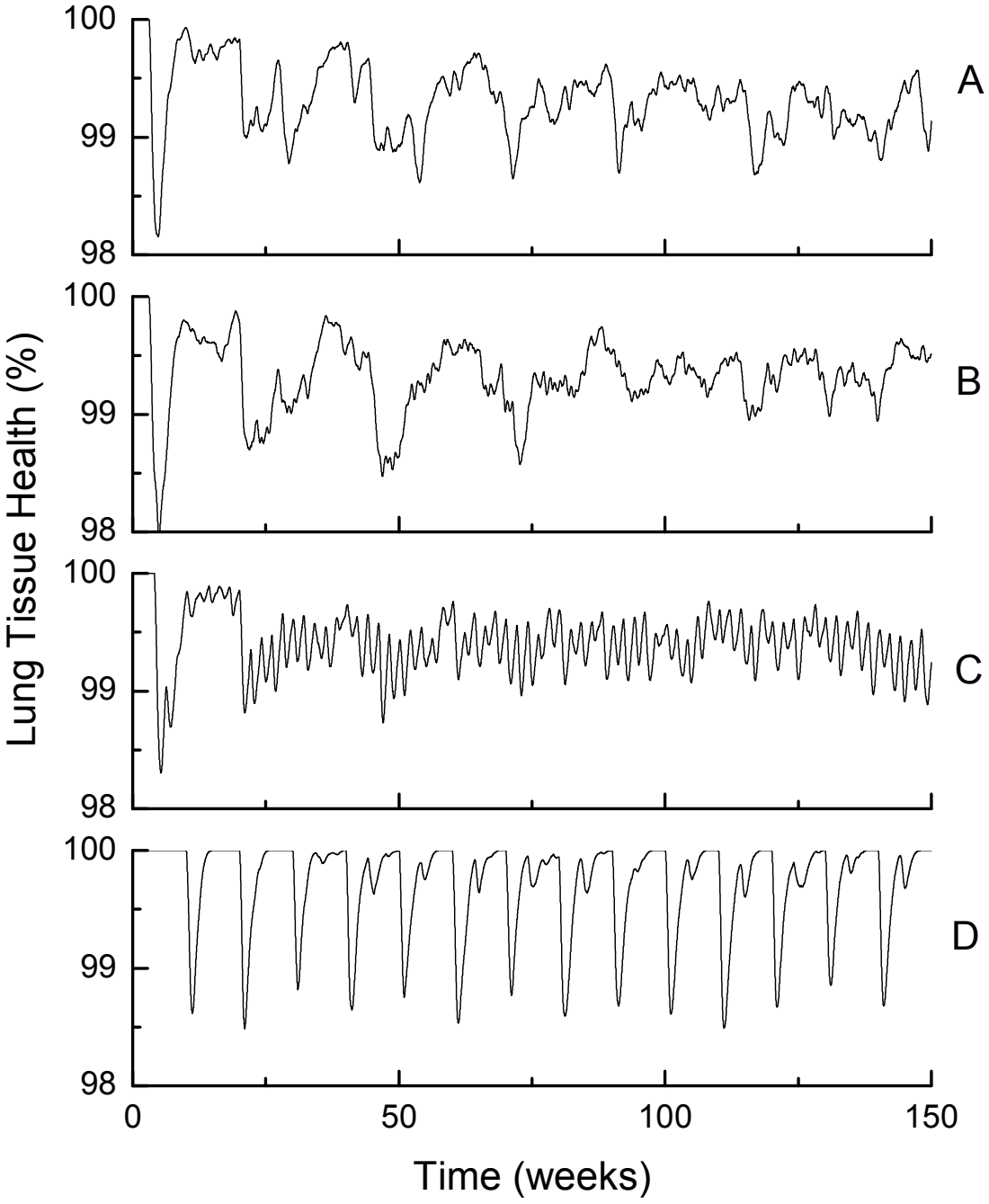

Figure 31: Tissue Health versus number of time steps when Particles were placed in the Alveolar Space every A) 0.5, B) 1, C) 2 and D) 10 weeks. All plots are an average of ten simulations

3.4. Discussion

From the perspective of survival, turning off the body's defense mechanisms when they are no longer needed is just as important as turning them on in response to a threat. Indeed, many chronic and debilitating diseases appear to be manifestations of a host response that fails to resolve when it should. Elucidating the pathophysiology of these diseases amounts in large part to finding out why control of the host response fails, and this begins with consideration of how it is controlled normally. Our thinking on this subject tends to be influenced by the common view of the host response as the waging of a military battle in which an army of defenders attempts to vanquish an invading foe. The danger with this analogy, however, is that it leads to the supposition of top-down command, yet there is no obvious analog in living organisms of the General who surveys a battle scene and gives orders based on what is perceived to be happening.

Even more problematic, the military analogy suggests separate command and control systems for turning on the host response when it is needed, and then turning it off again when its job is done. Turning the response on presents no particular conceptual difficulty because it merely requires detection of a threat, and the various specialized cells of the immune system do just that. Turning the response off again via a separate controller is a problem, however, because this would require detection of the absence of a threat, something that can only be done either by an intelligent entity capable of remembering all possible threats or by an innate sentinel poised to recognize molecular patterns indicative of "health" or threat absence, neither of which seems very likely. These considerations led us to postulate that the host response, and the allergic

inflammatory response in particular, is controlled in a manner similar to that employed by the nervous system to control the force exerted by skeletal muscles. This control is achieved by the repetitive invocation of a unitary event of short duration whose resolution is built into its initiation, namely the muscle twitch. Force persists so long as twitches keep being initiated by neuronal action potentials, which themselves are instigated by the brain's desire to move some part of the body. Control of muscle force thus requires only detection of the presence of something, but not detection of the absence of something.

This line of reasoning leads immediately to the notion of the inflammatory twitch as the unit of response of the immune system to an invader, but it brings with it some ancillary analogs. Most obvious is refractoriness, a period following twitch initiation during which a second twitch cannot be instigated. Refractoriness is a necessary requirement for twitch morphology because it ensures that the events involved in generating the twitch are properly turned off before they can be reinitiated. In the case of muscle force, the timing of refractoriness may allow for stacking (summation) of the forces from multiple twitches as occurs in skeletal muscle, or it may prevent stacking as is the case for cardiac muscle. It is not obvious *a priori* which strategy the immune system would choose, but we have previously obtained evidence from sensitized mice treated with sequential daily exposures to a foreign protein (ovalbumin) that the latter situation may pertain to allergic inflammation of the lung. Inflammation peaks after about 3 days of exposure, and then gradually abates as exposures are continued over days to weeks [4-5]. This is referred to as tolerization [16], and is thought to involve T-regulatory

cells. Resting the animals for several weeks, however, allows them to once again respond vigorously to a subsequent ovalbumin challenge [5], suggesting that the inflammatory twitch in these animals lasts on the order of weeks and has a refractory character that prevents them from stacking.

These findings are recapitulated by the agent-based model we developed in the present study, which exhibits clear oscillatory behavior following continual stimulation with Particles (the analog of antigen exposure in mice). Of particular note is the fact that, for most stimulation regimens, the largest and most well defined oscillations are observed early on, and these are followed by behavior that becomes progressively more chaotic with less well defined peaks (Figs. 28 and 31). On the other hand, if the period between successive stimulations is long enough to allow resolution of the response to each challenge, the oscillations remain sharply defined with time (Fig. 30d), resembling a series of well separated twitches that are unable to summate. The twitch hypothesis is further supported in the model by our finding that allowing the model to rest for a period of time results in a reiteration of the initial peaked response upon re-stimulation (Fig. 30), similar to our previous observations in mice [5].

Inferences drawn from the behavior of our agent-based model must be viewed in light of its numerous simplifying assumptions, which were made in the interests of conceptual and computational tractability. Many of these assumptions relate to the way in which individual biological entities behave. For example, we assume that cells have infinite stores of the chemical signals they release, and that the epithelium plays a purely

passive role as a physical barrier to cell movement, which from our own work [17] and that of others [18] is clearly an oversimplification. Furthermore, the alveolar airspace in the model is inaccessible to any cell type, whereas in reality cells do cross the epithelial barrier and some are cleared via the airways, which creates an additional sink for cells from the alveolar compartment. This might affect the magnitude and/or dynamics of predicted inflammatory oscillations, but would likely not affect their actual existence. Similar remarks can be made with respect to our model assumption that cells do not divide. Fibroblasts, for example, actively divide during the repair phase of the allergic response [19], which might not significantly affect the prediction of the early inflammatory oscillations but could result in greater suppression of the subsequent inflammatory activity (such as beyond 5000 time steps in Fig. 28).

The most important assumptions in the model, however, relate to the way in which we coarse-grain the myriad details of reality into a much smaller number of independent components. Coarse graining is a hierarchical process, the success of which depends on appropriate binning of the underlying biological details into their various model groups. In our model, for example, we coarse-grain the dynamics of cell movement by lumping all the different movement velocities into a single average rate of random movement from location to location, regardless of whether or not the cells are activated. This presupposes that cell movement *per se* is the most important feature of the ability of cells to travel between different locations, and that different cells moving at different velocities is of secondary importance, following the approach taken by Brown et al. [8]. In reality, for example, fibroblasts tend to remain localized to fixed locations

within the lung, which could mean that nearby regions could be maintained on average in a more healthy state compared to regions far from a fibroblast, which could increase the topographical heterogeneity of predicted tissue damage in the model. We also coarse-grain cell size by assuming it is the same for all cell types.

Similarly, by lumping multiple cell types into only two functional groups, the PIC's and AIC's, we assume that it is simply the existence of competing cell types that is paramount, while the existence of different phenotypes within each cell group is of secondary importance. For example, we ignore differences in lifespan and behavior between cells neutrophils and eosinophils, both of which are lumped together into the PIC category. The question thus remains as to whether such a crude level of coarse-graining causes us to miss some crucial detail of overall system behavior that would have become apparent had we divided the PIC and AIC groups into sub-groups with different properties. There are many known details of cell behavior that could be investigated in this regard. For example, the alveolar macrophage has a lifespan between that of other PICs and AICs, and can initially behave as a PIC but then switch to an AIC depending on environmental stimuli [20], and indeed we invoked the macrophage data from Tanaka et al. [3] as representative anti-inflammatory cell types in Fig. 4. Mast cells and APCs can signal to cells such as monocytes and macrophages, causing them to turn into PICs [21-22]. Some pro-inflammatory cytokines, such as TNF-alpha, inhibit their own synthesis which self-limits their production [23]. Thus, the number of ways in which we might delve into a finer level of model coarse-graining is enormous. For the time being, however, we will let ourselves be guided by the notion that it is the competition between

temporally offset pro- and anti-inflammatory processes that gives rise to the inflammatory oscillations predicted by our model, and which support the inflammatory twitch hypothesis. Accordingly, we take the position that the details alluded to above, while clearly important for refining the details of the model predictions, are not crucial to the prediction of their actual existence.

The behavior of our model can thus not be taken to constitute proof or otherwise of a biological theory. However, it does provide a test of plausibility to an extent that is impossible to achieve through any other approach. The allergic inflammatory response involves a large number of mutually interacting cell types, each playing different roles. Determining the details of the ensemble behavior of such a complex system defies human intuition. Agent-based computational modeling, on the other hand, allows one to estimate how the system might possibly behave within its spatiotemporal constraints. This approach has been exploited convincingly by Vodovotz and colleagues in the exploration of a number of aspects of the inflammatory response [8]. In the case of the present model, we have demonstrated that the major cell types involved in the allergic inflammatory response could indeed conspire to produce collective behavior in the lung that is formally similar in many important respects to the muscle twitch.

An important feature of the muscle twitch is the fact that it manifests in cycles where stimulation is continual. Support for the inflammatory twitch hypothesis in this regard comes from the experimental work by Tanaka et al. [24] showing that mice undergoing chronic antigen challenge have cytokine levels that peak 1 week after

initiation of the antigen challenge and then decrease for up to 3 weeks afterward. These cyclic biomarkers are consistent with the waxing and waning of the hyperresponsive phenotype that occurs in allergic mice [5]. Such observations are consistent with the duration of this inflammation and resolution event being on the order of 4 weeks, allowing us to propose that this time period corresponds to about 400 time steps in our model (Figs. 28 and 29).

Another key feature of the muscle twitch is its refractory period, and this is borne out in our model simulations (Figs. 28 and 31D illustrate this most clearly). Experimental support for the existence of a refractory period in the inflammatory response is evident in the data of Dienz et al. [25] who showed that when mice deficient in IL-6 are exposed to influenza virus, they experience significantly higher mortality around day 9 of the infection with fewer neutrophils recruited to the lung, compared with wild-type controls. In both deficient and wild-type strains, however, neutrophils disappeared from the lung around day 9. These data are consistent with the triggering of an immune response twitch having an active duration of about 9 days. Interestingly, mice (and humans) are known to be particularly susceptible to secondary bacterial infections following this initial immune response to virus [26], suggesting that they enter a period of refractoriness to re-initiation of the immune response beginning around the time when the neutrophils disappear. The duration of the combined active inflammatory phase and the subsequent refractory phase in our model appears to be in the order of weeks (Figs. 30 and 31). Interestingly, we have previously observed [27] that ovalbumin challenge in mice results in cyclical levels of Nuclear Factor-κB in bronchial epithelial cells with a period of two to six hours. While

this is clearly far too short to correspond to the period of the inflammatory twitch, it does suggest that frequency modulation may be a strategy employed by living organisms to control metabolic processes manifesting over a wide range of length and time scales.

In conclusion, we have advanced a hypothesis in which a unitary self-resolving event that we call the inflammatory twitch serves as the basis for control of the host response to an insult from the environment. We developed an agent-based model of allergic inflammation in the lung that exhibits key features predicted by this hypothesis, including refractoriness to continued stimulation leading to cycles of inflammation and repair. An implication of this hypothesis is that chronic inflammatory diseases may reflect a failure of the inflammatory twitch to resolve toward baseline.

3.5. Acknowledgements

This work was supported by NIH grants R01 HL103405, P30 GM103532 and T32 HL076122.

3.6. References

1. Barnes, P. J. Pathophysiology of allergic inflammation. Immunol Rev 242: 31-50.

2. Haczku, A., Y. Cao, G. Vass, S. Kierstein, P. Nath, E. N. Atochina-Vasserman, S. T. Scanlon, L. Li, D. E. Griswold, K. F. Chung, F. R. Poulain, S. Hawgood, M. F. Beers, and E. C. Crouch. 2006. IL-4 and IL-13 form a negative feedback circuit with surfactant protein-D in the allergic airway response. J Immunol 176: 3557-3565.

3. Tanaka, H., T. Masuda, S. Tokuoka, Y. Takahashi, M. Komai, K. Nagao, and H. Nagai. 2002. Time course study on the development of allergen-induced airway remodeling in mice: the effect of allergen avoidance on established airway remodeling. Inflamm Res 51: 307-316.

4. Cojocaru, A., C. G. Irvin, H. C. Haverkamp, and J. H. Bates. 2008. Computational assessment of airway wall stiffness in vivo in allergically inflamed mouse models of asthma. J Appl Physiol 104: 1601-1610.

5. Riesenfeld EP, A. G., Bates JHT, Poynter ME, Wu M, Aimi S and LK Lundblad. 2012. The Temporal Evolution of Airways Hyperresponsiveness and Inflammation. Allergy & Therapy S1.

6. Ekoff, M., and G. Nilsson. Mast cell apoptosis and survival. Adv Exp Med Biol 716: 47-60.

7. Wolterink, R. G., A. Kleinjan, M. van Nimwegen, I. Bergen, M. de Bruijn, Y. Levani, and R. W. Hendriks. Pulmonary innate lymphoid cells are major producers of IL-5 and IL-13 in murine models of allergic asthma. Eur J Immunol 42: 1106-1116.

8. Brown, B. N., I. M. Price, F. R. Toapanta, D. R. DeAlmeida, C. A. Wiley, T. M. Ross, T. D. Oury, and Y. Vodovotz. An agent-based model of inflammation and fibrosis following particulate exposure in the lung. Math Biosci 231: 186-196.

9. Islam, S. A., and A. D. Luster. T cell homing to epithelial barriers in allergic disease. Nat Med 18: 705-715.

10. Hammad, H., and B. N. Lambrecht. Dendritic cells and airway epithelial cells at the interface between innate and adaptive immune responses. Allergy 66: 579-587.

11. Kang, H. T., H. I. Lee, and E. S. Hwang. 2006. Nicotinamide extends replicative lifespan of human cells. Aging Cell 5: 423-436.

12. Simon, H. U. 2009. Cell death in allergic diseases. Apoptosis 14: 439-446.

13. Akdis, C. A. Therapies for allergic inflammation: refining strategies to induce tolerance. Nat Med 18: 736-749.

14. Collington, S. J., J. Hallgren, J. E. Pease, T. G. Jones, B. J. Rollins, J. Westwick, K. F. Austen, T. J. Williams, M. F. Gurish, and C. L. Weller. The role of the CCL2/CCR2 axis in mouse mast cell migration in vitro and in vivo. J Immunol 184: 6114-6123.

15. Nakanishi, K. Basophils are potent antigen-presenting cells that selectively induce Th2 cells. Eur J Immunol 40: 1836-1842.

16. Natarajan, P., A. Singh, J. T. McNamara, E. R. Secor, Jr., L. A. Guernsey, R. S. Thrall, and C. M. Schramm. Regulatory B cells from hilar lymph nodes of tolerant mice in a murine model of allergic airway disease are CD5(+), express TGF-beta, and co-localize with CD4(+)Foxp3(+) T cells. Mucosal Immunol.

17. Janssen-Heininger, Y. M., M. E. Poynter, S. W. Aesif, C. Pantano, J. L. Ather, N. L. Reynaert, K. Ckless, V. Anathy, J. van der Velden, C. G. Irvin, and A. van der Vliet. 2009. Nuclear factor kappaB, airway epithelium, and asthma: avenues for redox control. Proc Am Thorac Soc 6: 249-255.

18. Lambrecht, B. N., and H. Hammad. The airway epithelium in asthma. Nat Med 18: 684-692.

19. Reed, C. E., and H. Kita. 2004. The role of protease activation of inflammation in allergic respiratory diseases. J Allergy Clin Immunol 114: 997-1008; quiz 1009.

20. Balhara, J., and A. S. Gounni. 2012. The alveolar macrophages in asthma: a double-edged sword. Mucosal Immunol 5: 605-609.

21. Kitawaki, T., N. Kadowaki, N. Sugimoto, N. Kambe, T. Hori, Y. Miyachi, T. Nakahata, and T. Uchiyama. 2006. IgE-activated mast cells in combination with pro-inflammatory factors induce Th2-promoting dendritic cells. International Immunology 18: 1789-1799.

22. Minnicozzi, M., R. T. Sawyer, and M. J. Fenton. Innate immunity in allergic disease. Immunol Rev 242: 106-127.

23. Flammiger, A., W. Fiedler, U. Bacher, C. Bokemeyer, M. Schneider, and M. Binder. 2012. Critical imbalance of TNF-alpha and soluble TNF receptor 1 in a patient with macrophage activation syndrome: potential implications for diagnostics and treatment. Acta Haematol 128: 69-72.

24. Tanaka, H., T. Masuda, S. Tokuoka, Y. Takahashi, M. Komai, K. Nagao, and H. Nagai. 2002. Time course study on the development of allergen-induced airway remodeling in mice: the effect of allergen avoidance on established airway remodeling. Inflamm Res 51: 307-316.

25. Dienz, O., J. G. Rud, S. M. Eaton, P. A. Lanthier, E. Burg, A. Drew, J. Bunn, B. T. Suratt, L. Haynes, and M. Rincon. Essential role of IL-6 in protection against H1N1 influenza virus by promoting neutrophil survival in the lung. Mucosal Immunol 5: 258-266.

26. Chen, W. H., F. R. Toapanta, K. A. Shirey, L. Zhang, A. Giannelou, C. Page, M. B. Frieman, S. N. Vogel, and A. S. Cross. Potential role for alternatively activated macrophages in the secondary bacterial infection during recovery from influenza. Immunol Lett 141: 227-234.

27. Poynter, M. E., C. G. Irvin, and Y. M. Janssen-Heininger. 2002. Rapid activation of nuclear factor-kappaB in airway epithelium in a murine model of allergic airway inflammation. Am J Pathol 160: 1325-1334.

CHAPTER 4: BREAKING THE INFLAMMATORY TWITCH

4.1. Introduction

Allergic airway diseases such as asthma still prove difficult for clinicians to effectively manage [1]. The current framework for understanding these diseases is of a type I hypersensitivity reaction in which allergen cross-links IgE-laden FcεRI receptors on mast cells to trigger the release of mediators that signal other cells, ultimately leading to inflammation [2]. While this framework provides an intuitively reasonable notion of how inflammation is instigated, it does not explain how inflammation is eventually resolved. Furthermore, it does not account for the wide range of symptomatic behavior observed in patients. Some individuals with asthma have continual progression of inflammatory disease [3], while others have an intermittent clinical presentation characterized by alternating asymptomatic and symptomatic periods [4]. This suggests that allergic inflammation should be viewed as a dynamic process that not only has a beginning signaled by a need for host defense, but that also (hopefully) has an end that occurs when the need for defense is no longer present.

To this end, we have recently proposed a hypothesis about the nature of the normal allergic inflammatory response that centers on what we refer to as the "inflammatory twitch" [5]. Specifically, we posit that stimulation with allergen sets into motion a sequence of events that includes both factors that induce inflammation as well as those that ultimately bring about its resolution to the baseline state. A key corollary of the inflammatory twitch hypothesis is that there should exist a refractory period during

which the capacity to re-instigate inflammation is suppressed, akin to the refractory period associated with muscle twitches and neuronal action potentials. We have tested the plausibility of this hypothesis at the alveolar-capillary interface in the lung using an agent-based computational model that enabled us to investigate both the spatial and temporal behaviors of the various cellular players involved [5-6]. Following calibration against the experimental data of Tanaka et al. [7], we showed that this model can mimic the dynamics of allergic inflammation in mice [5], supporting the notion that there is a natural finite timescale to the normal inflammatory response.

The possible existence of an inflammatory twitch, however, immediately raises an important question: what defects in the twitch mechanism could cause it to fail to resolve back to baseline? Such defects might, for example, be behind the chronic inflammatory conditions that seem to characterize allergic asthma. Investigating this question was, accordingly, the goal of the present study. Again, a previously calibrated agent-based computational model provides a convenient platform for addressing this question because it serves as a virtual laboratory in which we can rapidly test the consequences of behavioral defects in any of the cells represented in the model [5-6], hopefully helping to focus the intent of subsequent laboratory investigation. We focus in particular on defects that cause the twitch to either become prolonged in duration or to fail to resolve altogether, the ultimate hope being that this will identify therapeutic targets.

4.2. Materials and Methods

4.2.1. Computational Model

We have previously developed an agent-based computational model of the allergic inflammatory response in an alveolar-capillary cross-section using NetLogo 4.1.3 freeware. Further details of this model are presented in a previous publication [5]. Briefly, our model of the normal allergic inflammatory response includes separate agents representing mast cells, APCs (antigen-presenting cells, representing the combination of dendritic cells, B-cells and macrophages), helper T-cells, T-regulatory cells, pro-inflammatory cells (representing the combination of neutrophils, eosinophils and other cell types involved in causing local tissue damage), and anti-inflammatory cells

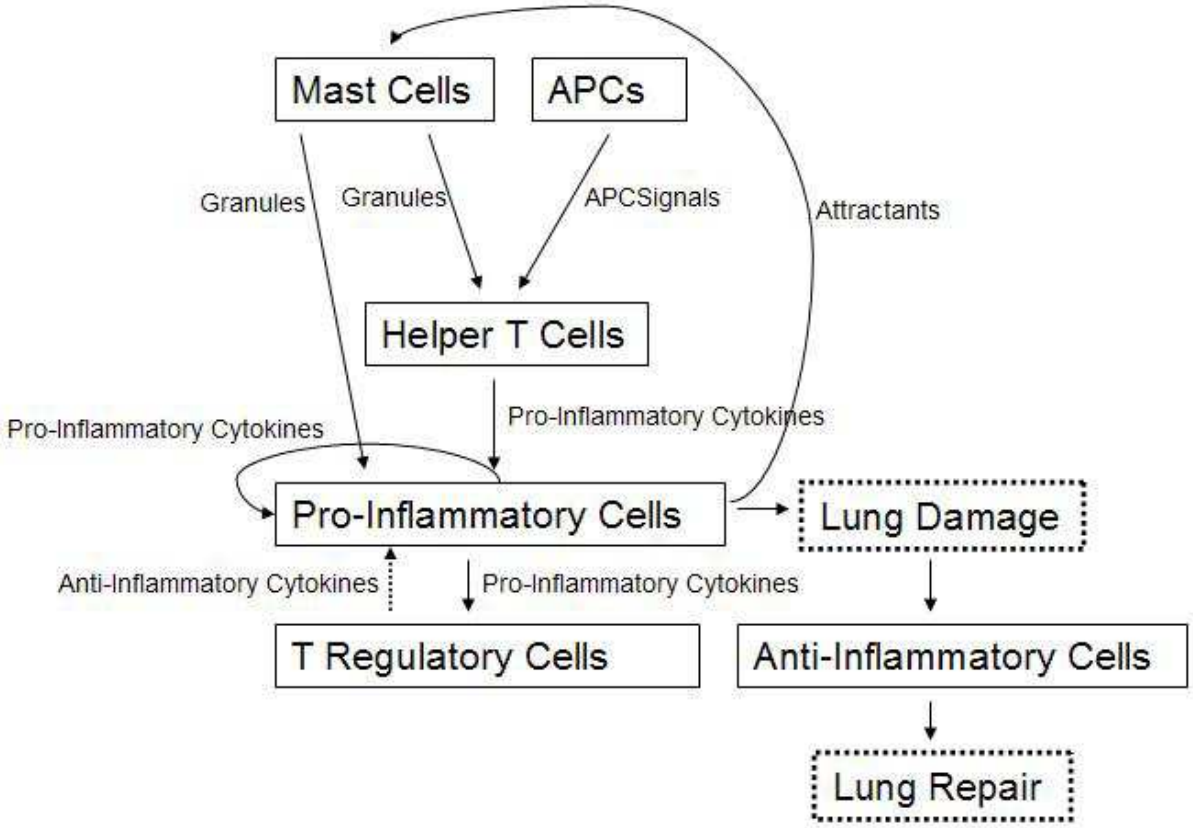

Figure 32: Mechanism for allergic inflammation in the lung. The initial cells of the response (Mast cells and APCs) activate after encountering Particles (i.e. antigen), resulting in the indicated cascades

(representing fibroblasts and other cells involved in tissue repair). The model is initialized with certain numbers of these cells, each of which obeys a set of rules that stipulates how the cell moves around in the alveolar-capillary environment, what actions it performs and when, and how long it lives. Inflammation is triggered through the application of a certain number of randomly placed particles (representing antigen) in the alveolar region. The inflammatory cascade ensues as the various cell types encounter these particles during their exploration of the environment. Figure 32 shows the scheme

Table 2: Summary of all agents and their respective rules included in the model

Cell Type	Moves Towards	Rule
Mast Cell (immature)	Attractants	Moves preferentially to attractants, or randomly if there are no attractants
Mast Cell (mature)	Particles, Attractants	Upon binding Particle, releases Granules for 10 time steps. Becomes inactive for user-set time if encounters user-set number of Particles
APC	Particles	While digesting Particle, releases APC Signals. Becomes inactive for user-set time if encounters user-set number of Particles
Helper T Cell	Granules, APCSignals	If moving towards Granules and/or APCs, releases Pro-Inflammatory Cytokines for 10 time steps. Afterwards, if there is a strong chemical signal on the current patch, converts into a Pro-Inflammatory Cell
Pro-Inflammatory Cell	Pro-Inflammatory Cytokines, Granules	If moving towards Pro-Inflammatory Cytokines and/or Granules, become activated for 10 time steps. While activated, release Pro-Inflammatory Cytokines and Attractants. Also, subtract 5 from the health of the patch currently on if cell has moved towards a chemical signal, or 2 if not. At the end of activation, the cell dies if there is a chemical signal on the current patch
T-Regulatory Cell	Pro-Inflammatory Cytokines	If moving towards Pro-Inflammatory Cytokines, release Anti-Inflammatory Cytokines
Anti-Inflammatory Cell	Patches with Health < 100	If on a patch with health < 100, add 1 to that patch's health parameter at each time step

interactions recapitulated in the model, while Table 2 lists the rules of behavior for the different cell types. We also show a snapshot of the model during the peak inflammatory period in Fig. 33.

The primary output of the model is a parameter we term average lung tissue health, which is the mean value of tissue health for each patch in the model (Fig. 33). The tissue health parameter for each patch is merely an empirical representation of the overall local level of those various tissue abnormalities that accompany an inflammatory

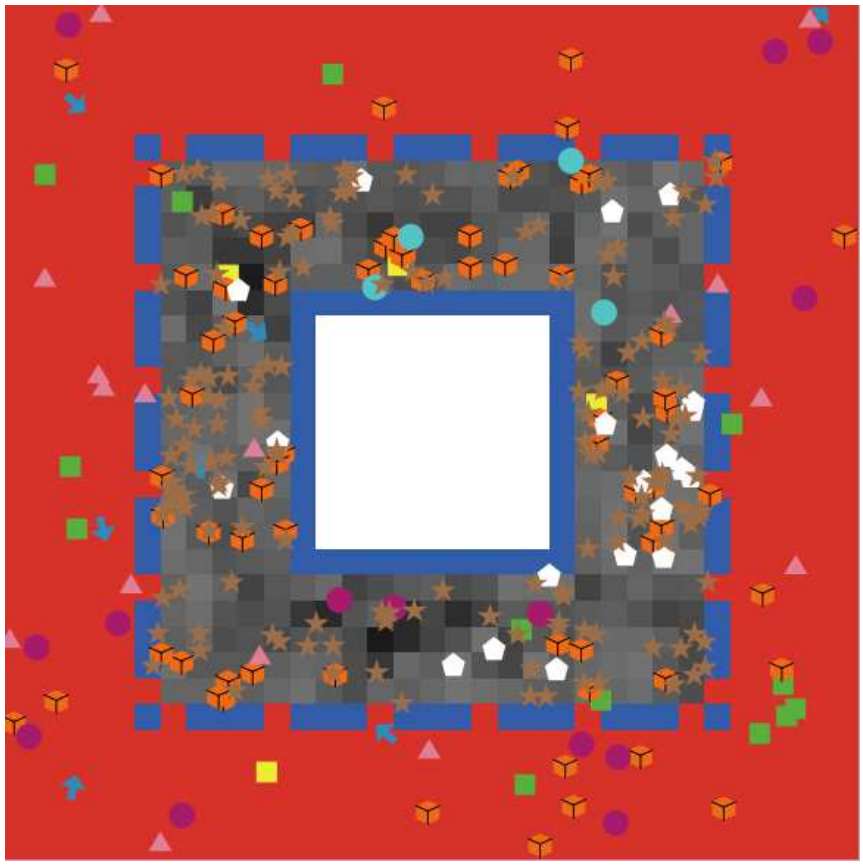

Figure 33: Snapshot of the normal allergic inflammatory twitch response during a selected timepoint. The red space represents the capillary, the blue dashed region represents the endothelial barrier, and the patchy gray region represents the alveolar tissue, which can be tiled into patches. A darker patch indicates a higher amount of damage that has occurred to the tissue at that location. The brown stars represent Particles (antigen), and all the other shapes represent cells involved in the allergic response

response in the lung, including edema formation, mucus secretion, and bronchospasm. While these tissue abnormalities result directly from the dynamic cellular events represented in the model, specifically representing the abnormalities themselves in the model is beyond the scope of our study.

Tissue health is increased in the presence of anti-inflammatory cells and decreased by pro-inflammatory cells as indicated in Fig. 31. In other words, tissue health is simply a global measure of the integrated consequences of tissue destruction and repair, and is given an arbitrary scale between 0 and 100. A value of 100 represents perfect tissue health, while the degree of tissue damage is reflected in the amount by which health has a value less than 100. Thus, a decrease in tissue health corresponds to the inflammatory phase of the allergic response, while an increase in tissue health corresponds to the resolution phase. Under normal circumstances, this parameter exhibits a transient decrement in response to particle stimulation, and which is the manifestation of the inflammatory twitch.

We have previously calibrated the dynamics of the inflammatory twitch in the model to published experimental data in mice from Tanaka et al., [5, 7]. This enabled us to determine that 15 time steps in the model correspond to 1 day of actual time. Accordingly, the simulation results presented in this study are plotted against time in days.

4.2.2. Experimental Protocol

Table 3: List of modifications made to the agent rules of the original model

Removed all mast cells
Removed of all antigen-presenting cells
Removed of all helper T-cells
Doubled number of mast cells
Doubled the number of particles the mast cells had to encounter before becoming desensitized
Doubled number of particles the antigen-presenting cells had to encounter before becoming desensitized
Halved the amount of sensitization time of mast cells and antigen-presenting cells following an encounter with a particle
Increased the lifespan of activated pro-inflammatory cells by 5x
Decreased apoptosis of antigen-presenting cells
Decreased the amount of repair performed by anti-inflammatory cells by a factor of 5
Decreased the amount of anti-inflammatory cytokines released by T-regulatory cells
Decreased the speed of movement of all T-regulatory cells by a factor of 2
Decreased the speed of movement of anti-inflammatory cells by AICs by a factor of 2

inflammatory response to particle stimulation, as in our previous study [5], but with specific alterations to the rules assigned to the various cell types. Stimulation was continual throughout the simulations, with 85 particles being applied to the model every 15 time steps. The original model served as the control. The interventions we investigated fell into four general categories: 1) knockout of specific cell types, 2) alterations to the mobility of specific cell types, 3) changes to the actions performed by specific cell types, and 4) changes to the lifetimes or activation times of specific cell types. We did not investigate every conceivable example of these interventions because some lead to trivial insights. For example, knocking out all the pro-inflammatory cells would obviously eliminate the possibility for any kind of inflammatory response at all. Similarly, knocking out anti-inflammatory cells eliminates the possibility for any kind of tissue repair and would automatically condemn the model to interminable inflammation. The full list of interventions we investigated is provided in Table 3. For each intervention we ran the

model 100 times, each time for 6000 time-steps and ensemble-averaged the resulting simulations of tissue health.

4.3. Results

We first simulated a "normal" inflammatory twitch in response to continual particle stimulation. The result serves as the control for our subsequent simulations, and consists of a transient decrease in tissue health that resolves toward baseline over about 6

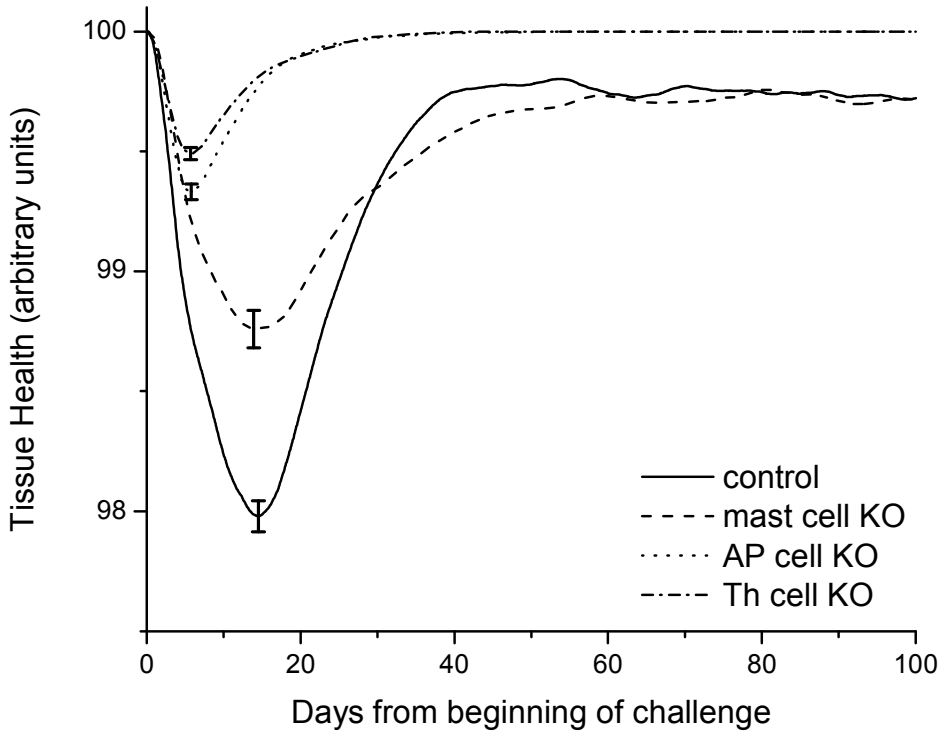

Figure 34: The control inflammatory twitch simulated by the original model together with the twitches produced after knocking out mast cells (mast), antigen-presenting cells (APC), and T-helper cells (Th). Stimulation of the model by particles began at t = 0 days and continued daily throughout the subsequent 100 days, as in Figs. 4-8. Each of the curves shown is the ensemble average of 100 simulations obtained under identical conditions, and the error bars at the peaks of each response indicate standard errors. These errors were essentially identical in all other simulations (Figs. 4-8); two curves are thus significantly different when they are separated by more than about 2 standard errors

weeks. This is the characteristic shape of the inflammatory twitch that we have previously described [5]. We show a snapshot of the model during the peak of the initial inflammatory response in Figure 33, and show the resulting behavior along with the standard error at this maximal peak of inflammation in Figure 34. Continuing the simulation for longer durations causes additional twitches to occur, with the return to baseline between each twitch representing a refractory period during which the inflammatory response in the model cannot be initiated.

We then applied a series of biologically motivated interventions to the model to see how this would affect the inflammatory twitch, where our unaltered twitch model functions as our control. We began by simulating the knock-out of certain key cell types, achieved simply by eliminating these cells from the model. Figure 34 shows that elimination of mast cells reduces the amplitude of the inflammatory twitch by nearly a factor of 2, while elimination of either antigen-presenting cells or T-helper cells reduces it by about 3-fold. Next, we discovered that the twitch is affected in only a rather minor way by alterations in key anti-inflammatory processes in the model. Specifically, we found that reducing the speed of movement of either the T-regulatory cells or the anti-inflammatory cells has essentially no effect on the shape of the inflammatory twitch, either in terms of its magnitude or duration (Fig. 35). Similarly unremarkable effects were produced by reducing either the degree of tissue repair produced by anti-

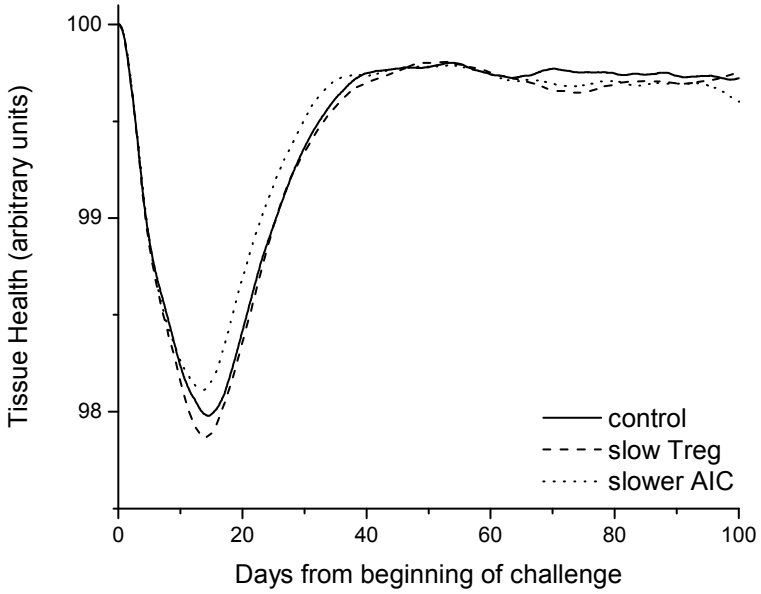

Figure 35: Effects on the inflammatory twitch of halving the speed of movement of T-regulatory cells (Treg) and anti-inflammatory cells (AIC), relative to the control twitch

inflammatory cells or the amount of release of anti-inflammatory cytokines (Fig. 36).

By contrast, the inflammatory twitch is more sensitive to certain alterations in the behaviors of the pro-inflammatory processes in the mode. Both mast cells and antigen-presenting cells become desensitized for a period of time after encountering a certain number of particles [8-9]. A 4-fold increase in this number of particles for the antigen-presenting cells has a major accentuating and prolonging effect on the twitch, but a similar increase in particle number for the mast cells has minimal effect (Fig. 37). Doubling the number of mast cells in the model also results in a minimal effect (Fig. 37). Also, once the critical number of particles has been encountered, both cell types remain desensitized for a certain period of time, and halving this desensitization period for both mast cells and antigen-presenting cells simultaneously has minimal effect on the twitch (Fig. 37). Similarly unremarkable is the result of increasing the lifetime of the antigen-presenting cells (Fig. 38). The twitch is most profoundly affected, however, by increases in the duration of pro-inflammatory activity in the model, which causes a major increase

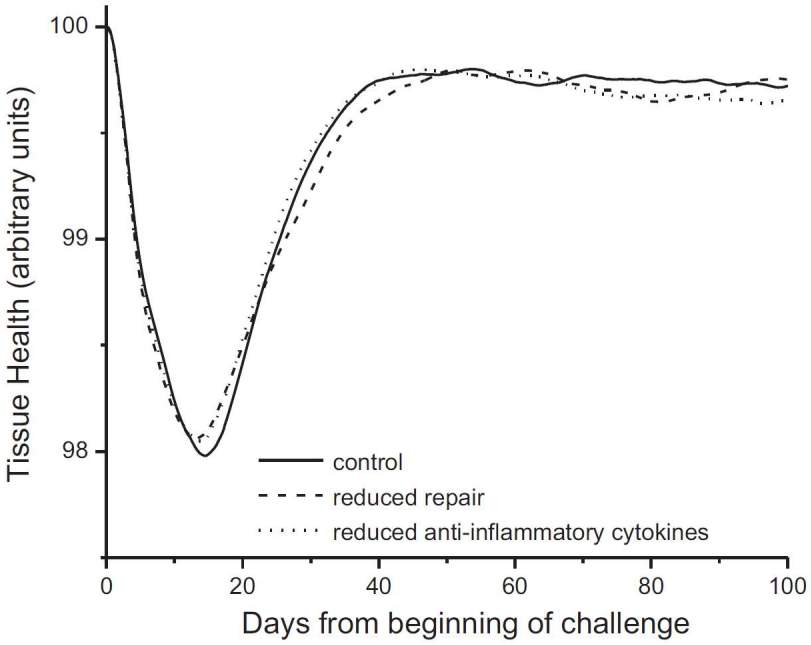

Figure 36: Effects on the inflammatory twitch of 80% reductions in the degree of repair produced by anti-inflammatory cells (repair) and in the release of anti-inflammatory cytokines (cytokines)

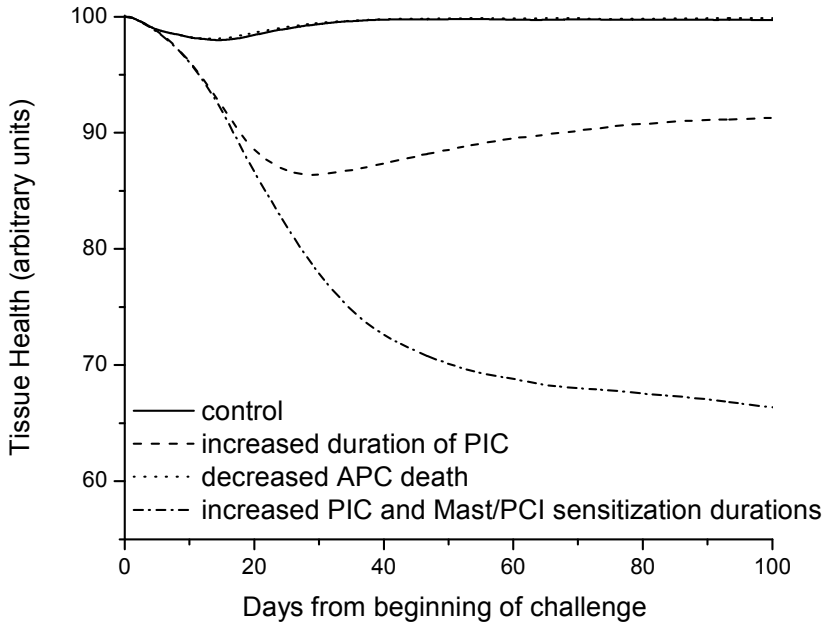

Figure 37: Effect on the inflammatory twitch of four-fold increases in the number of particles that either mast cells (mast) or antigen-presenting cells (APC) must encounter before becoming desensitized. Also shown are the results of doubling the number of mast cells, and of halving the duration over which both mast cells and APCs remained desensitized for (duration)

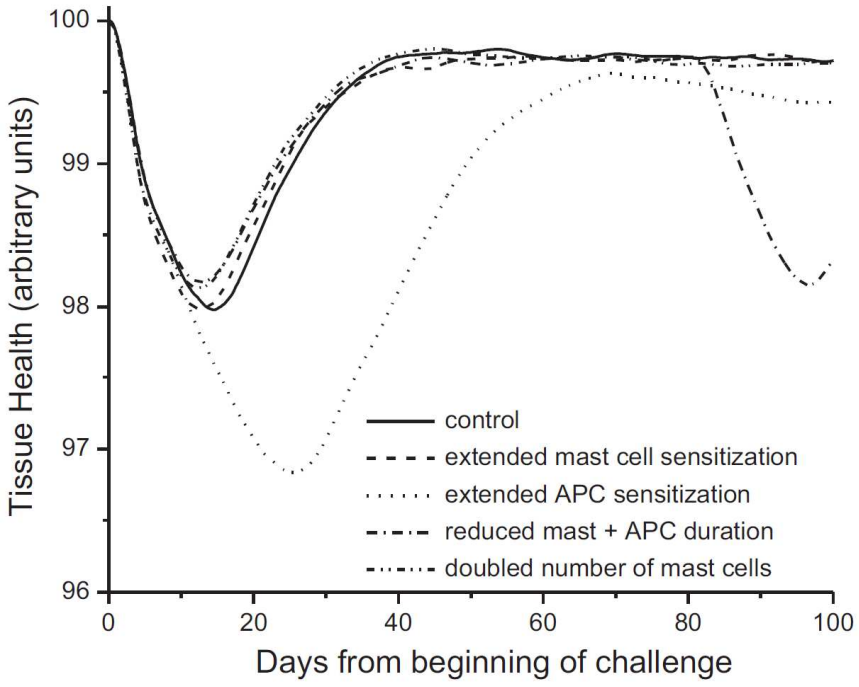

Figure 38: Effects on the inflammatory twitch of a 5-fold increase in the duration of activation of pro-inflammatory cells (PIC), an 50% decrease in the probability that antigen-presenting cells will die at each time step (APC), and the combination of a 5-fold increase in the duration of activation of PICs with a four-fold increase in the number of particles that both mast cells and antigen-presenting cells must encounter before becoming desensitized (Combination)

in twitch amplitude and prevents its return to baseline (Fig. 38). These effects are even more pronounced when combined with an increased duration of activation of mast cells and APCs (Fig. 38).

Finally, we examined the effects of applying simulated therapies to the inflammatory response caused by increasing the duration of activation of pro-inflammatory cells. Knocking out mast cells has little benefit, but either knocking out T-helper cells or reducing the lifetime of pro-inflammatory cells returns the inflammatory twitch almost back to the unaltered twitch control (Fig. 39).

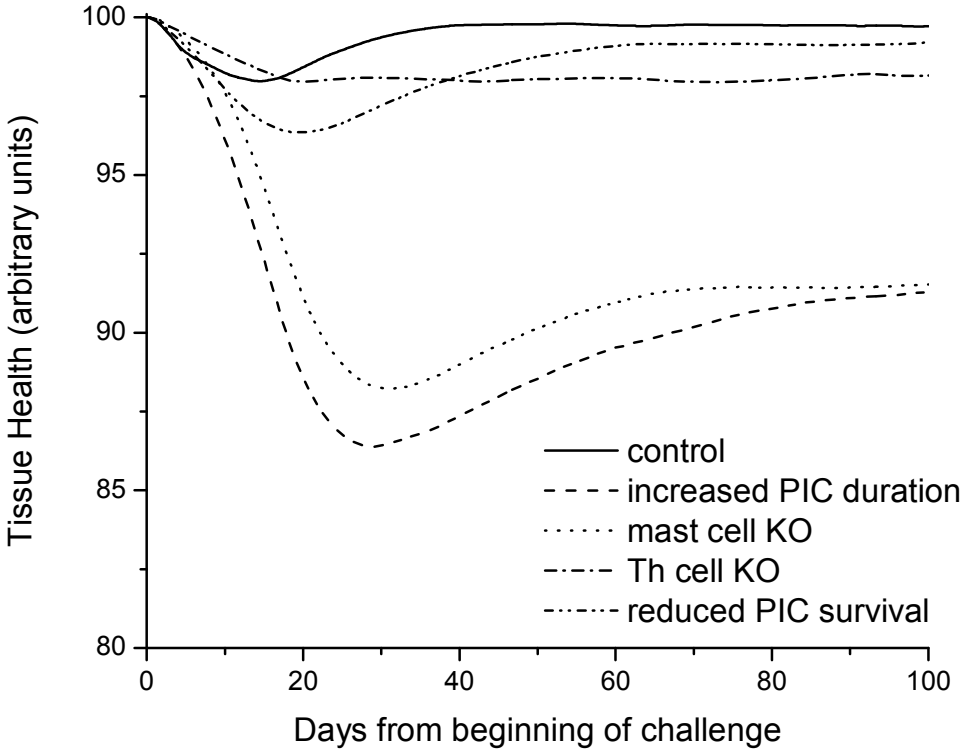

Figure 39: Effects of therapy on the exaggerated twitch caused by a 5-fold increase in the duration of activation of pro-inflammatory cells (PIC). Interventions included knocking out mast cells (mast), knocking out T-helper cells (Th), and halving the probability of survival of the pro-inflammatory cells at each time step (survival)

4.4. Discussion

One of the benefits of utilizing agent-based modeling is that it allows us to simulate the spatiotemporal behavior of a complex system, such as a community of inflammatory cells, in order to discover emergent dynamic behavior that would be difficult to reveal in any other way. This was the motivation for our original study in which we presented the inflammatory twitch hypothesis [5], and which we continue in the present study by investigating the consequences of certain interventions on the twitch

profile. Of course, the validity of any of the conclusions we reach depends critically on the extent to which our model captures the important aspect of reality, and this is always open to question even if we can demonstrate that the behavior of the model resembles experimental data [7]. To the extent that the model does capture reality, however, our present study reveals some interesting and not always expected behavior that may suggest approaches to the treatment of chronic inflammatory diseases such as allergic asthma.

Our major goal in this study was to see if we could manipulate the model so as to cause the twitch to become increased in magnitude and/or extended in scale. The latter effect, in particular, would presumably then constitute a model of chronic inflammation, a condition that is still poorly understood and frequently difficult to treat. We found that many of the interventions we tried had relatively little effect on the inflammatory twitch. In fact, most individual interventions, such as cell knockout, impaired migration, altered lifespan, or impaired activity of a single cell type, still resulted in twitches with cycles of damage and repair that in many cases were little different from the control. This finding supports our notion that the inflammatory twitch is a general mechanism used by the body to control the host response; such a control mechanism would need to have some degree of resilience to system defects in order to be robust. On the other hand, direct manipulation of the pro-inflammatory cells in the model had a very large effect on the twitch, suggesting that this is where we might focus our attention in terms of devising therapies. Even so, it is instructive to consider the biological significance of all our simulated interventions, regardless of their effect size.

Figure 34 shows the effects of knocking out cells involved in the initiation of the inflammatory response. We show the standard errors at the maximal point of the initial inflammatory response on each curve to show there is significant difference between the unaltered twitch (our control) and the interventions. Both the mast cells and antigen-presenting cells release chemical signals that initiate the inflammatory response, while T-helper cells amplify these signals to draw pro-inflammatory cells (the only cell type in the model that directly damages tissue) to the site of injury. Knocking out T-helper cells in our model can be thought of as simulating the effect of corticosteroid administration [10], and leads to a substantial decrease in twitch amplitude relative to the control twitch. By contrast, knocking out mast cells has a relative smaller effect on the twitch, which is in keeping with the observed benefits of sodium cromoglycate administration relative to steroid [11-12] and the fact that mast cells are relatively sparse in the lung [13]. Knocking out antigen-presenting cells has an effect similar to that of T-helper cells, which may be related to the fact that there are relatively more antigen-presenting cells that mast cells in the model as observed in the lung [8, 13]. Nevertheless, the overall shape and time course of the inflammatory twitch remains similar in each knock out, which is perhaps not something we might have guessed *a priori*.

Also somewhat surprising is the finding that reducing the mobility of cells involved in the resolution of inflammation by a factor of two only leads to subtle changes in the inflammatory twitch (Fig. 35). Slowing the anti-inflammatory cells directly responsible for repairing lung tissue marginally attenuates the response, while slowing the T-regulatory cells shifts the twitch to a slightly earlier peak. In both cases, however,

there is little change relative to the control twitch, which suggests that the rate of resolution of inflammation is not limited by the speed with which the reparative cellular machinery is able to move to a site of inflammation. Another possibility for the rate-limiting factor in the resolution phase is the degree of anti-inflammatory activity that takes place at the site of injury once the reparative machinery has arrived. We tested this by making substantial reductions in both the amount of chemical signals secreted by T-regulatory cells and the amount of repair performed at each time step by anti-inflammatory cells. Again, and somewhat to our surprise, we found relatively minimal effects in both cases (Fig. 36). The inflammatory twitch in our model thus exhibits a degree of resilience to changes in the system that produces it, which could be viewed as of benefit to the organism given the importance of maintaining a viable host response.

We eventually found an intervention that does have a significant effect on the inflammatory twitch, namely an increase in the duration over which antigen-presenting cells remain activated after encountering particles. Our model maintains these cells in the active state (i.e. releasing signals) until they encounter a critical number of particles, at which point they become quiescent for a period of roughly six months [5, 8-9]. When the critical number of particles for the antigen-presenting cells is increased 4-fold, we find that the twitch is nearly doubled both in amplitude and duration (Fig. 37). On the other hand, applying the same intervention to mast cells has relatively little effect on the twitch amplitude, perhaps because of the sparseness of this cell type in the model. Interestingly, doubling the number of mast cells has a minimal effect on the twitch (Fig. 37). Also interestingly, halving the duration over which both antigen-presenting cells and mast cells

remain quiescent also has little effect on the twitch amplitude but it leads to a second dip in tissue health before the end of the simulation period (Fig. 37). We suspect that this represents a reduction in the refractory period of the twitch due to the earlier re-activation of the mast cells (the other simulations also exhibit secondary dips, but these occur after the periods of time shown in the figures). In any case, these findings thus suggest that deactivating antigen-presenting cells (which we assume to be chiefly comprised of basophils and dendritic cells) might be an effective therapeutic approach for chronic inflammatory disease, but we are not aware of any therapies that operate via this mechanism.

By far the largest effect on the inflammatory twitch, however, was achieved in our model by manipulating the cells that actually create tissue damage: the pro-inflammatory cells (assumed to represent chiefly neutrophils and eosinophils). Increasing their lifespan following activation by a factor of 5 led to an enormous increase in the amplitude of the inflammatory twitch, eventually returning to a baseline health value that was far less than that observed in the unaltered twitch (Fig. 38). This finding is consistent with the well-documented existence of abnormally long-lived neutrophils and eosinophils in chronic allergic inflammatory diseases such as asthma [14-16]. The effect received a further substantial boost if both anti-inflammatory cells and mast cells were able to encounter a 4-fold increase in the number of particles before becoming desensitized. By contrast, simply increasing the survival of the antigen-presenting cells had little effect (Fig. 38).

The results shown in Figure 38 suggest that impaired apoptosis of neutrophils and eosinophils might be a key pathogenic mechanism in chronic inflammatory disease. An obvious question, then, is what therapies might cause the resulting exaggerated inflammatory twitch to revert back to normal. To investigate this question we applied a number of interventions to the model in which a 5-fold increase had been applied to the duration of activation of pro-inflammatory cells (i.e. using the PIC curve in Fig. 38 as the starting point). We found that removing the mast cells from the model had only a slight ameliorating effect on the exaggerated inflammatory twitch, but that knocking out the T-helper cells brought the twitch almost back to its control configuration (Fig. 39), which fits with the relatively greater efficacy of corticosteroids compared to cromolyn in reversing allergic inflammation. Most intriguing, however, was the finding that decreasing the survival of pro-inflammatory cells had an effect that was comparable in magnitude to that of T-helper cell elimination, and in fact caused the twitch to resolve back closer to the fully healthy state (Fig. 39). These results suggest that therapies aimed at increasing apoptosis in neutrophils and/or eosinophils might be efficacious in treating chronic allergic asthma [14-17].

As fascinating as these results might be, however, we must bear in mind that they are all based on a computational model that is itself the embodiment of a large number of simplifying assumptions made in the interests of computational and conceptual tractability as we have discussed previously [5]. For example, we assume that the alveolar tissue environment is currently homogenous and isotropic, whereas in fact the

various alveoli of the lung can be quite heterogeneous with physical and chemical anisotropies that may constrain the directions of cell movement [18-19].

A related assumption is that cytokines and other chemical signals diffuse at the same linear rate through the environment at each time step. Yet in reality, different chemical signals diffuse through the environment at different rates [20], and may diffuse in non-linear fashion [21-22]. Our model also ignores any functional differences between the various cell types involved in the onset of inflammation, including neutrophils and eosinophils, by lumping them all into a single pro-inflammatory cell type. Similar coarse-graining is applied to the various cells involved in the resolution of inflammation. The rationale behind these various assumptions is that we have captured the most important features of the cellular system involved in the inflammatory response, but this always remains open to question and underlies our conclusions.

Finally, we should point out that while the singular advantage of agent-based modeling relates to the ease with which the spatiotemporal dynamics of a complex system can be investigated, we have taken limited advantage of the spatial aspect in the present study. Figure 33 shows the configuration of the model during the peak of the inflammatory response under control conditions. The patchy appearance of the alveolar tissue damage (indicated by the darkened regions) reflects both the stochastic nature of the simulation as well as the fact that cytokine concentrations are not uniform and cells move according to directed diffusion from their source in the vasculature, yet we only consider on a global tissue health parameter that integrates this spatially distributed

damage. However, this model can be easily extended to include spatially heterogeneous properties throughout the alveolar region when the inclusion of this kind of detail becomes necessary. The present model thus represents a first foray into the computational modeling of the allergic inflammatory response in the lung.

In summary, we have presented a computational model of the allergic inflammatory response as an *in silico* laboratory for testing hypotheses about the nature of the allergic inflammatory response, focusing in particular on the factors that might cause the response to become pathologically accentuated and/or prolonged. Our model predicts what we term the inflammatory twitch as an emergent behavior arising from the spatiotemporal interactions between the major cell types involved, and shows that this inflammatory twitch is rather robust to a number of individual system defects. Nevertheless, the model also shows that the twitch can be significantly accentuated and prolonged by factors that increase the activity and lifetime of pro-inflammatory cells, and that interventions simulating the effects of cromolyn and corticosteroid administration can be effective in returning the twitch toward a more normal configuration. Perhaps most interestingly, our model also suggests that therapies directed at increasing the rate of apoptosis of inflammatory cells, such as activated neutrophils and eosinophils, could be particularly efficacious in treating chronic inflammatory airway disease.

4.5. Acknowledgements

This work was supported by NIH grants P30 GM103532, T32 HL076122 and F31 EB018215.

4.6. References

[1] DeKorte CJ. Current and emerging therapies for the management of chronic inflammation in asthma. Am J Health Syst Pharm. 2003 Oct 1;60(19):1949-59; quiz 60-1.

[2] Hale LP, Kant EP, Greer PK, Foster WM. Iron supplementation decreases severity of allergic inflammation in murine lung. PLoS One. 2012;7(9):e45667.

[3] Stanley D, Tunnicliffe W. Management of life-threatening asthma in adults. Continuing Education in Anaesthesia, Critical Care & Pain. 2008 June 1, 2008;8(3):95-9.

[4] Soto-Ramirez N, Ziyab AH, Karmaus W, Zhang H, Kurukulaaratchy RJ, Ewart S, et al. Epidemiologic methods of assessing asthma and wheezing episodes in longitudinal studies: measures of change and stability. J Epidemiol. 2013;23(6):399-410.

[5] Pothen JJ, Poynter ME, Bates JH. The inflammatory twitch as a general strategy for controlling the host response. J Immunol. 2013 Apr 1;190(7):3510-6.

[6] Brown BN, Price IM, Toapanta FR, DeAlmeida DR, Wiley CA, Ross TM, et al. An agent-based model of inflammation and fibrosis following particulate exposure in the lung. Math Biosci. 2011 Jun;231(2):186-96.

[7] Tanaka H, Masuda T, Tokuoka S, Takahashi Y, Komai M, Nagao K, et al. Time course study on the development of allergen-induced airway remodeling in mice: the

effect of allergen avoidance on established airway remodeling. Inflamm Res. 2002 Jun;51(6):307-16.

[8] Louis R, Schleich F, Barnes PJ. Corticosteroids: still at the frontline in asthma treatment? Clin Chest Med. 2012 Sep;33(3):531-41.

[9] Robison RG, Kumar R. Chapter 10: Pediatric asthma: principles and treatment. Allergy Asthma Proc. 2012 May-Jun;33 Suppl 1:S32-5.

[10] Church MK, Hiroi J. Inhibition of IgE-dependent histamine release from human dispersed lung mast cells by anti-allergic drugs and salbutamol. British journal of pharmacology. 1987 Feb;90(2):421-9.

[11] Fuchs B, Sjoberg L, Moller Westerberg C, Ekoff M, Swedin L, Dahlen SE, et al. Mast cell engraftment of the peripheral lung enhances airway hyperresponsiveness in a mouse asthma model. Am J Physiol Lung Cell Mol Physiol. 2012 Dec 15;303(12):L1027-36.

[12] van Rijt LS, Lambrecht BN. Dendritic cells in asthma: a function beyond sensitization. Clinical and experimental allergy : journal of the British Society for Allergy and Clinical Immunology. 2005 Sep;35(9):1125-34.

[13] Akdis CA. Therapies for allergic inflammation: refining strategies to induce tolerance. Nature medicine. 2012 May;18(5):736-49.

[14] Ilmarinen P, Kankaanranta H. Eosinophil apoptosis as a therapeutic target in allergic asthma. Basic Clin Pharmacol Toxicol. 2013 Jan;114(1):109-17.

[15] Oh J, Malter JS. Pin1-FADD interactions regulate Fas-mediated apoptosis in activated eosinophils. J Immunol. 2013 May 15;190(10):4937-45.

[16] Sun Z, Dragon S, Becker A, Gounni AS. Leptin inhibits neutrophil apoptosis in children via ERK/NF-kappaB-dependent pathways. PLoS One. 2013;8(1):e55249.

[17] Reddy AT, Lakshmi SP, Dornadula S, Pinni S, Rampa DR, Reddy RC. The nitrated fatty acid 10-nitro-oleate attenuates allergic airway disease. J Immunol. 2013 Sep 1;191(5):2053-63.

[18] Tamang DL, Pirzai W, Priebe GP, Traficante DC, Pier GB, Falck JR, et al. Hepoxilin A(3) facilitates neutrophilic breach of lipoxygenase-expressing airway epithelial barriers. J Immunol. 2012 Nov 15;189(10):4960-9.

[19] Salmon H, Franciszkiewicz K, Damotte D, Dieu-Nosjean MC, Validire P, Trautmann A, et al. Matrix architecture defines the preferential localization and migration of T cells into the stroma of human lung tumors. The Journal of clinical investigation. 2012 Mar 1;122(3):899-910.

[20] van Zyl JM, Derendinger B, Seifart HI, Van der Bijl P. Comparative diffusion of drugs through bronchial tissue. Int J Pharm. 2008 Jun 5;357(1-2):32-6.

[21] Hastings RH, Folkesson HG, Matthay MA. Mechanisms of alveolar protein clearance in the intact lung. Am J Physiol Lung Cell Mol Physiol. 2004 Apr;286(4):L679-89.

[22] Serrao KL, Fortenberry JD, Owens ML, Harris FL, Brown LA. Neutrophils induce apoptosis of lung epithelial cells via release of soluble Fas ligand. Am J Physiol Lung Cell Mol Physiol. 2001 Feb;280(2):L298-305.

CHAPTER 5: DISSECTING THE TWITCH

5.1. Introduction

The inflammatory response to a noxious stimulus is crucial for survival, and is initiated by a cascade of events beginning with the recognition of the stimulus by sentinel cells. Equally important for health, however, is the resolution of the inflammatory response when it is no longer needed. Indeed, failure of the inflammatory response to resolve may underlie a variety of chronic diseases. This raises the fundamental question of how the duration of the inflammatory response is controlled. In particular, it is difficult to imagine the existence of some agent in the body with the capacity to decide when inflammation is no longer necessary, so how is the inflammatory response turned off?

As a possible response to this question, we recently postulated that inflammation is subject to the same control strategy as skeletal muscle, namely through the repetitive invocation of self-limiting unitary events that, in the case of muscle, are known as twitches [1]. We hypothesized that the inflammatory equivalent, which we term the inflammatory twitch, continues to be invoked so long as the allergic stimulus is present. This allows an ongoing inflammatory response stream to be maintained while it is needed, but ensures that the response will automatically dissipate when the stimulus disappears. Of course, a skeletal muscle twitch lasts in the order of 100 ms while an inflammatory response would have to last for much longer, but the two systems may still have strong formal similarities in control structure despite their huge differences in timescale.

We previously used an agent-based computational model in a proof-of-concept study to show that a twitch-like event can, in principle, arise with respect to allergic inflammation in the lung [1]. We then used the model to perform a series of *in silico* experiments that explored how the inflammatory twitch could potentially fail to resolve [2], the notion being that such failure might explain the chronic inflammation characteristic of allergic asthma. Nevertheless, experimental data in support of the inflammatory twitch hypothesis remain somewhat sparse. In particular, while there is some evidence that the normal allergic inflammatory response is indeed self-limited [3-4], there has yet to be a comprehensive test of another key prediction of the hypothesis, namely that the response should be accompanied by a refractory period during which it cannot be reinitiated by continued antigen stimulation. Accordingly, the goal of the present study was to perform a detailed examination of the time-course of the components of the allergic inflammatory response in the lung and to determine if any of these components exhibit periods of refractoriness. We performed this investigation in ovalbumin-sensitized mice that were challenged with aerosolized ovalbumin for varying durations and then re-challenged after varying rest periods.

5.2. Experimental Design

Our studies conformed to the National Research Council Guide for the Care and Use of Laboratory Animals and were approved by the University of Vermont's Institutional Animal Care and Use Committee (IACUC).

5.2.1. Antigen Sensitization and Protocol

Experimental group	Days of challenge starting on Day 1	Recall challenge on Day 31
Saline-3	○○○	○
OVA-3	●●●	●
OVA-14	●●●●●●●●●●●●●	●
OVA-21	●●●●●●●●●●●●●●●●●●●●	●
OVA-31	●●●●●●●●●●●●●●●●●●●●●●●●●●●●●	●
Saline-31	○○○○○○○○○○○○○○○○○○○○○○○○○○○○○	○

Figure 40: Experimental design. All groups of mice were given IP injections of OVA and alum on day -14 and Day -7 relative to the beginning of the challenge period. All groups were given a single recall challenge on Day 31. Open circles represent challenge with saline. Closed circles represent challenge with 1% OVA

We studied 104 female BALB/cJ mice at 7-8 weeks of age (Jackson Laboratories) separated into five groups: Saline-3 (16 mice), Saline-31 (8 mice), OVA-3 (24 mice), OVA-31 (8 mice), OVA-14 (24 mice) and OVA-21 (24 mice). Numbers after Saline or OVA correspond to the number of consecutive days for which the mice were challenged. The experimental protocol is outlined in Figure 40. All mice were initially sensitized with intraperitoneal (IP) injections of 0.1 mL containing 20 μg ovalbumin (OVA) in phosphate-buffered saline suspended in 2 mg of alum (ThermoFisher Scientific) on Day -20 and Day -6. The different animal groups were then subjected to different regimens of daily OVA challenge, each regimen beginning on Day 1 as indicated in Figure 40. A daily challenge consisted of placing the animals in a closed chamber for 30 minutes within which they were exposed to aerosols of either 1% OVA in phosphate-buffered saline or to phosphate-buffered saline.

The Saline-3 and OVA-3 groups were challenged for the shortest duration of 3 consecutive days. Mice in Saline-3 were exposed to nebulized saline and then divided into two subgroups each containing 6-8 mice. One subgroup was studied (see below) one day after the 3 challenges (i.e. on Day 4). The other subgroup was maintained without further challenge for another 28 days, subjected to a saline recall exposure on day 31, and then studied a day later. Mice in OVA-3 were treated identically to the Saline-3 animals except that they were exposed to nebulized OVA instead of saline.

The Saline-31 and OVA-31 groups were challenged for the longest duration of 31 days. Mice in the Saline-31 group underwent daily exposure to nebulized saline (Day 1 to Day 31) and were studied a day later (i.e. on Day 32). Mice in OVA-31 were treated identically to Saline-31 animals except that they were exposed to OVA instead of saline.

The OVA-14 and OVA-21 groups were challenged with OVA for the intermediate durations of 14 and 21 days, respectively. Mice in OVA-14 were divided into two subgroups. One subgroup was studied one day after the final challenge (i.e. on Day 15). The other subgroup was maintained without challenge until Day 31 at which point they received a recall challenge with OVA and then were studied a day later (i.e. on Day 32). Mice in OVA-21 were treated similarly except that their initial sequence of daily challenges with OVA ended on Day 21.

5.2.2. Study Procedures

Lung Physiology: Mice were anesthetized with an intraperitoneal injection of sodium pentobarbital (90 mg/kg), tracheostomized, and cannulized. They were then attached to a computer-controlled mechanical ventilator (Flexivent, Scireq, Montreal, Quebec, Canada), paralyzed with an IP injection of pancuronium bromide (0.8 mg/kg), and administered regular ventilation at 200 breaths/min against a positive-end-expiratory pressure (PEEP) of 3 cmH_2O while EKG was monitored to ensure depth of anesthesia. The forced oscillation technique was used to measure respiratory impedance (Z_{rs}) over the frequency range from 1 to 20.5 Hz using a 2 s broadband perturbation in volume applied by the Flexivent exactly as we have done in a number of prior studies [5-7]. Each measurement of Z_{rs} was fit to the constant-phase model [6, 8]. We used two of the best-fit parameter values of the constant-phase model as our outcomes variables: 1) the Newtonian resistance (R_n) of the lung, which accurately estimates airway resistance [9] and 2) lung stiffness (H), which is essentially equivalent to lung elastance [6]. Two baseline values of R_n and H were obtained in this way. We then exposed each animal to an aerosol of saline, delivered for 10 s via the inspiratory line of the Flexivent, and then determined R_n and H every 10 s for 3 minutes for a total of 18 measurements of each parameter. This sequence was then repeated replacing the saline aerosol with aerosolized methacholine at a concentration of 12.5 mg/ml. Airway responsiveness to saline and to methacholine was determined from the averages of the 18 measurements of R_n and H made following each challenge.

Broncho-alveolar lavage: Following the end of the AHR protocol, bronchoalveolar lavage fluid (BALF) was gathered by lavaging the lungs with 1 mL of

saline. This lavage fluid was centrifuged at 600 *g* at 10ºC for 10 minutes and the resulting cell pellet was re-suspended in saline. Half of this sample underwent cell counting using an Advia 120 Hematology System (Bayer Healthcare, Tarrytown, NY) from which total cell numbers were counted. The other half of the sample was used to make cytospins that were stained and from which differential cell types were identified.

Cytokine Analysis: Following the gathering of BALF, left lobes of the mouse lungs were dissected and ground to a fine powder using a liquid nitrogen-chilled mortar and pestle, and subsequently resuspended and vortexed in 400 µL of saline. The suspensions were transferred into separate QiaShredder spin columns (Qiagen) and centrifuged at 11,000 rpm at 10ºC for 10 minutes. Flow-throughs were then transferred to clean microcentrifuge tubes, while avoiding the pellet on the bottom, and were stored at -80ºC until analysis. Following thawing on ice, total protein concentrations were assessed using a Bio-Rad (Bradford) assay, with relative cytokine concentrations assessed using a custom R&D Systems mouse cytokine panel and a Luminex instrument, according to manufacturer's instructions.

Statistics: Inter-group comparisons were made using paired t-tests or ANOVA, with post-hoc Bonferroni corrections for multiple comparisons as appropriate. Statistical significance was taken as $p < 0.05$.

5.3. Results

5.3.1. Twitch Time Course

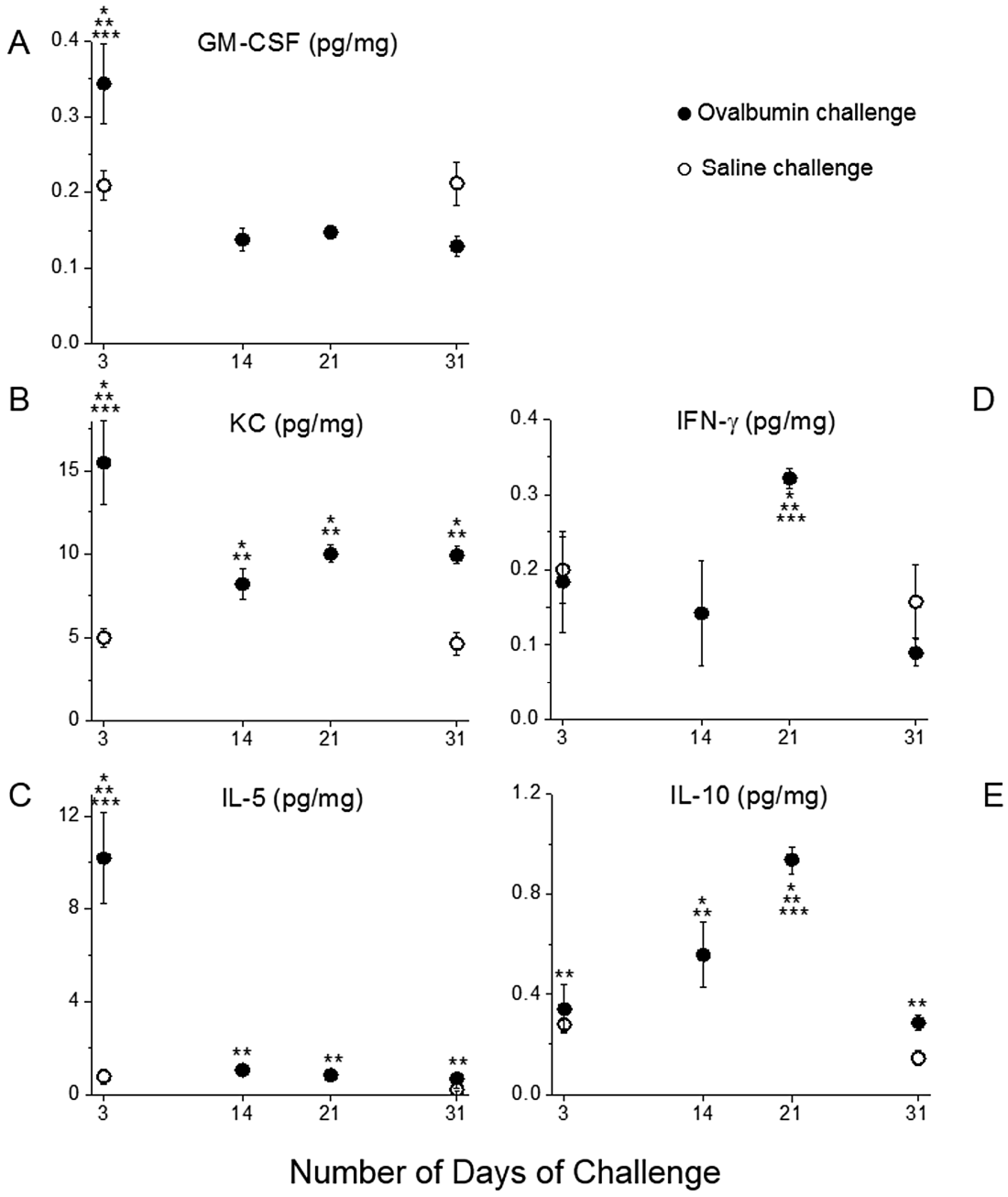

Figure 41: Closed circles show concentrations of cytokines measured in the left lobes of lungs of mice, characterized 24 hours following the last day of daily antigen challenge, and on day 31 immediately preceding and following recall challenge with OVA: A) GM-CSF, B) KC, C) IL-5, D) IFN-γ, and E) IL-10. Open circles show corresponding control measurements made in control mouse lungs 24 hours after 3 days of saline and a recall challenge with saline on day 31. All points are reported as means ± standard errors. * indicates a value statistically higher than Control 1, ** indicates a value statistically higher than Control 2, and * indicates a value statistically higher than the other three values in OVA-challenged animals**

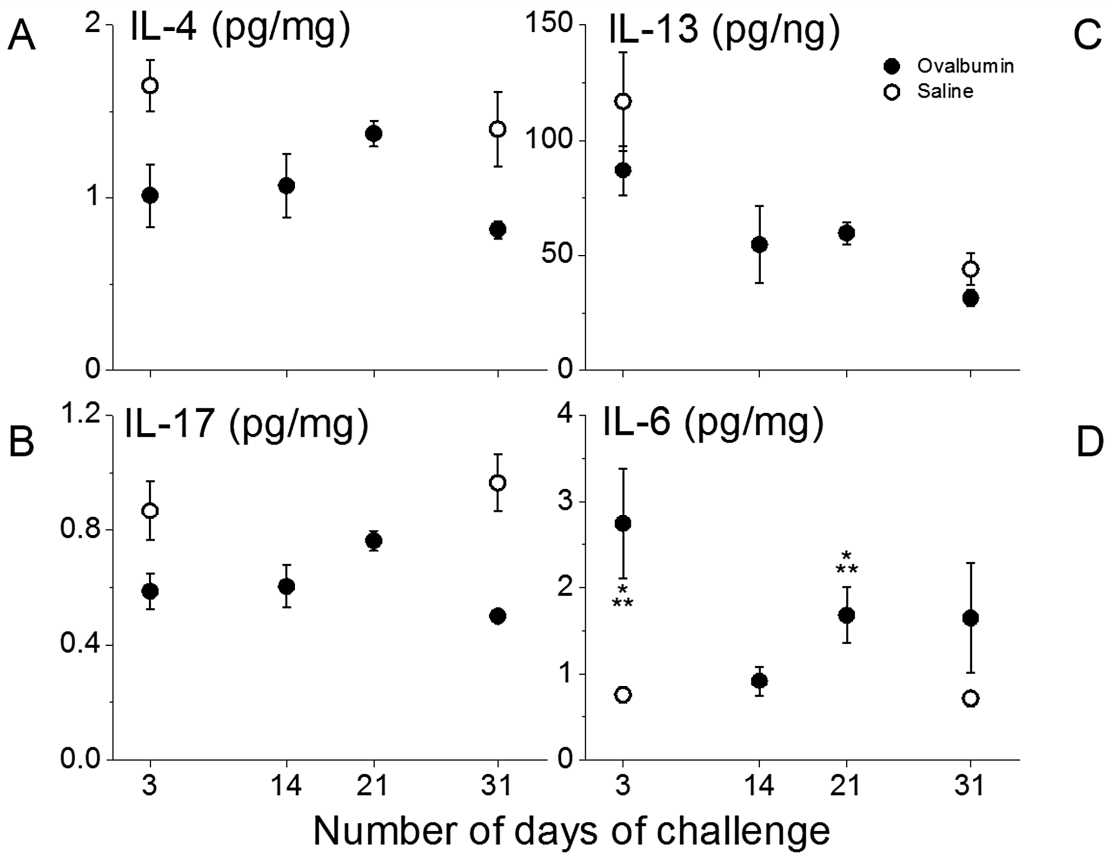

Figure 42: Closed circles show concentrations of cytokines measured in the left lobes of mouse lungs 24 hours following the final daily OVA challenge, and on day 31 immediately following recall challenge: A) IL-4, B) IL-17, C) IL-3, and D) IL-6. Open circles show corresponding control measurements made 24 hours after Day 3 of saline challenge (Control 1: left-hand point) and one day after saline recall challenge (Control 2: right-hand point). Points represent mean ± standard error. * indicates statistically higher than Control 1. ** indicates statistically higher than Control 2

Figure 41 shows that the temporal patterns of the lung cytokines over the 31 day study period could be separated into two groups. GM-CSF, KC and IL-5 levels in the OVA-challenged animals peaked transiently at Day 3 where they were significantly different from control (Figs. 41A-C). Afterwards, GM-CSF and IL-5 levels fell below at least one of the groups challenged with saline (control). KC levels also dropped after Day 3 but remained higher than both control measurements, and by Day 31 IL-5 was at a statistically significant but physiologically meaningless difference from baseline. In contrast, IFNγ and IL-10 levels in the challenged animals peaked transiently at Day 21

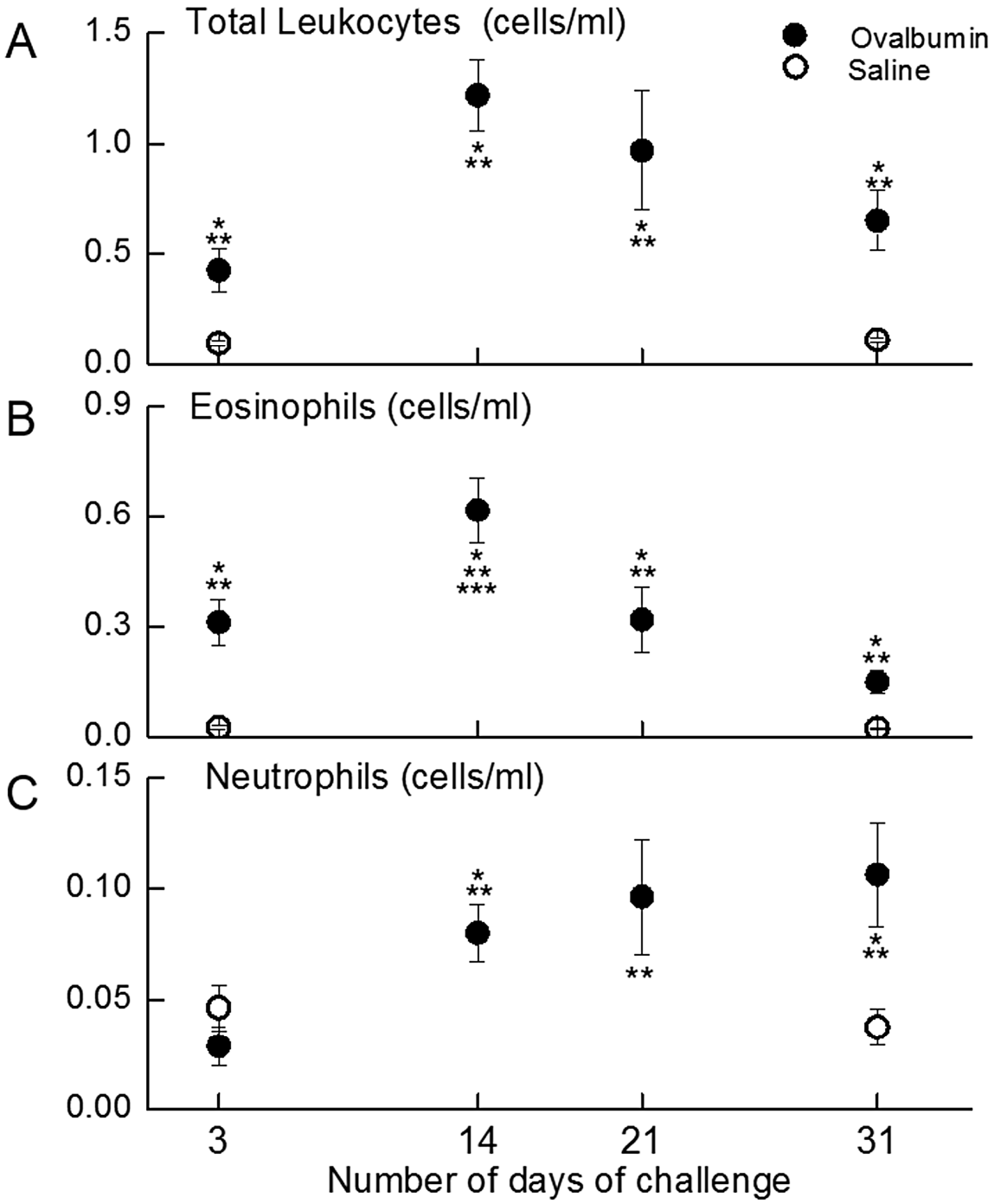

Figure 43: Closed circles show various cell types measured in BALF from mouse lungs 24 hours after 3, 14, 21 and 31 days of daily OVA challenge: A) total leukocytes, B) eosinophils, and C) neutrophils. Open circles show corresponding control measurements made 24 hours after 3 days (Control 1: left-hand point) and 31 days (Control 2: right-hand point) of saline challenge. Points represent mean ± standard error. * indicates statistically higher than Control 1. ** indicates statistically higher than Control 2

but were statistically indistinguishable from control at Day 3 and Day 31 (Figs. 41D and E). IL-4, IL-13 and IL-17 did not rise significantly above control in response to OVA (Figs. 42A-C), while IL-6 levels fell to control levels at Day 14 before rising again at Day 21 and Day 31 (Fig. 42D).

BALF total leukocytes and eosinophils for the OVA-treated mice were significantly higher than control mice at all time points measured from Day 3 to Day 31, both peaking at Day 14 (Figs. 43A and B). In contrast, neutrophil levels at Day 3 were not significantly different between OVA-treated and control animals but rose thereafter in the treated group to become significantly different from at least one control out to Day 31 (Fig. 43C).

The lung mechanics parameters *Rn* and *H* in response to Mch were significantly elevated in the OVA-treated mice compared to controls at all measured time points from days 3 to 31. *Rn* in the treated animals peaked at day 21 (Fig. 44A) while *H* peaked at day 14 (Fig. 44B).

5.3.2. Refractory Period

The existence of a refractory period in allergic inflammation is indicated by the need to wait for a certain duration of time following cessation of OVA challenge before inflammation can be re-instigated by a recall challenge. Figures 44A-C show that that GM-CSF, KC and IL-5 all exhibited significant increases in their levels with wait periods

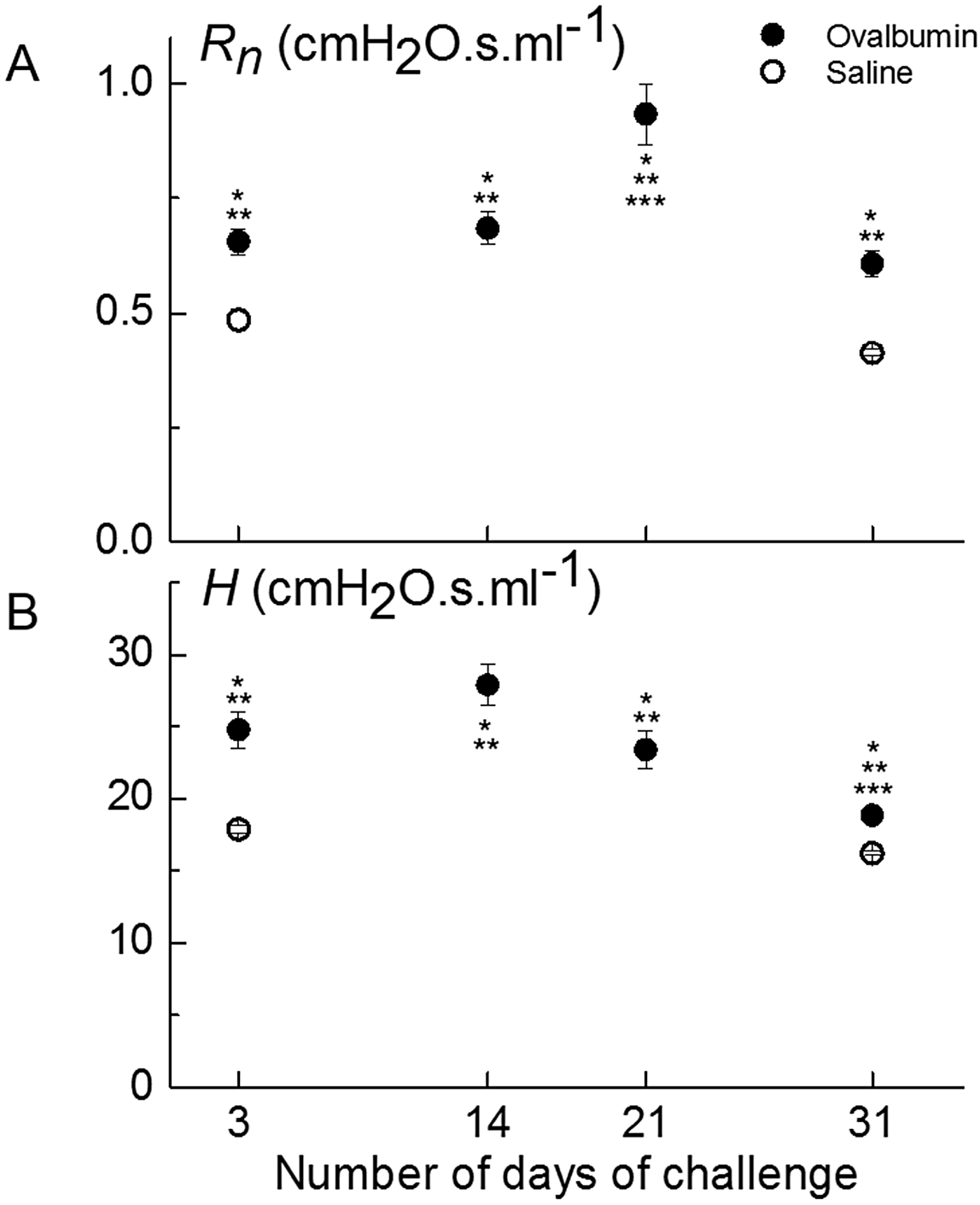

Figure 44: Closed circles show lung mechanics parameters measured in mice measured 24 hours after 3, 14, 21 and 31 days of daily OVA challenge: A) R_n, and B) H. Open circles show corresponding control measurements made 24 hours after 3 days (Control 1: left-hand point) and 31 days (Control 2: right-hand point) of saline challenge. Points represent mean ± standard error. * indicates statistically greater than Control 1. ** indicates statistically greater than Control 2. * indicates statistically distinct from the other three measurements in the OVA-challenged animals**

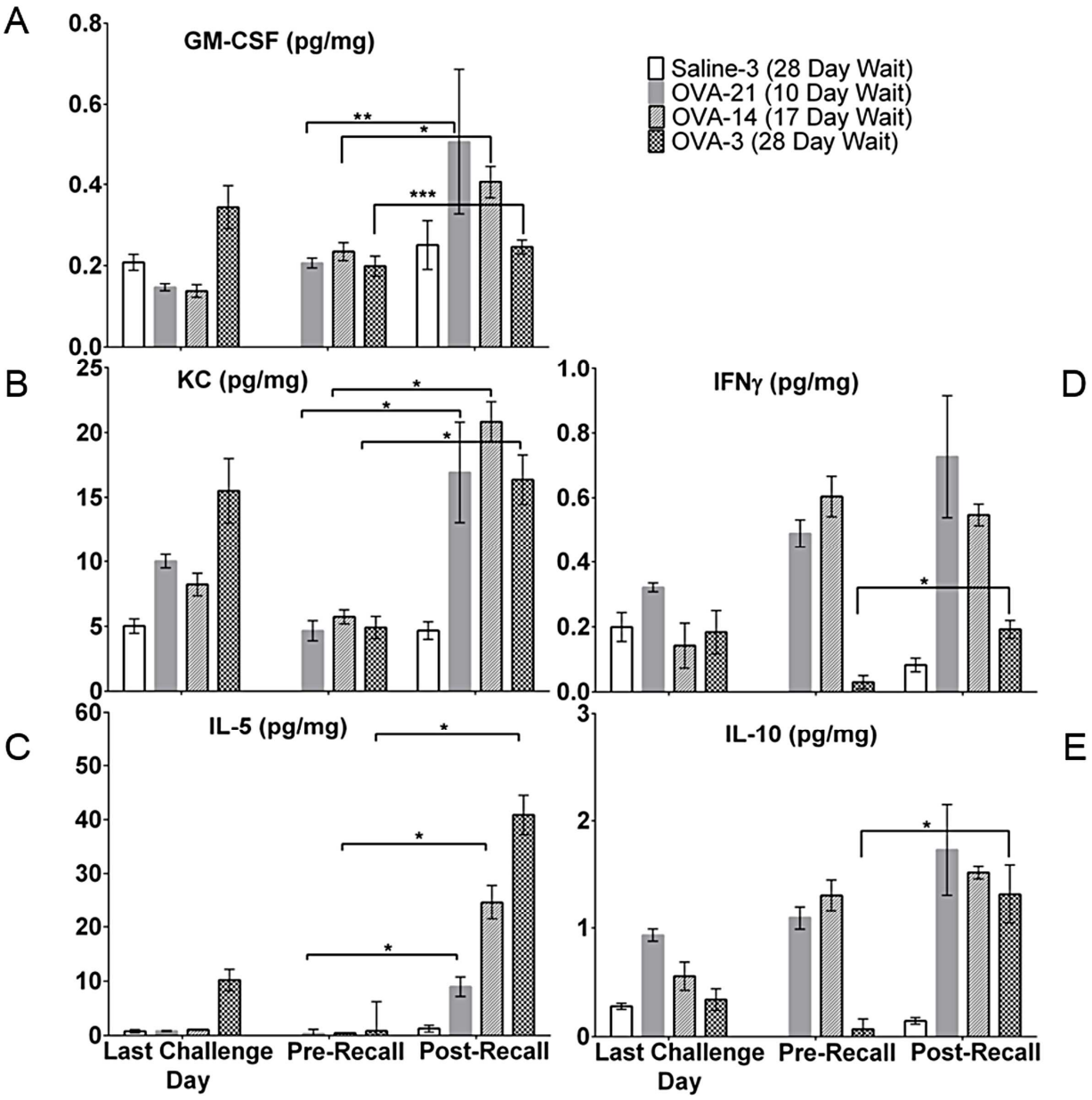

Figure 45: Concentrations of cytokines in the left lobes of lungs of mice measured 24 hours following 3, 14 and 21 days of OVA challenge, and both immediately preceding and following recall challenge: A) GM-CSF, B) KC, C) IL-5, D) IFN-γ, and E) IL-10. Control measurements were made 24 hours after 3 days of saline challenge and after a recall challenge with saline on day 31. Points represent mean ± standard error. * indicates significant increase following the recall challenge. ** and * indicate significant increases following removal of an outlier from the post-recall group and pre-recall groups, respectively**

of 10, 17 and 28 days after the end of the initial period of challenge, although the biological significance of the increase in GM-CSF at 28 days appears minimal. These findings suggest that the refractory period for these cytokines is no longer than 10 days. In contrast, IFNγ and IL-10 only increased significantly following a wait period of 28 days (Figs. 45D and E). Interestingly, for GM-CSF, IFNγ and IL-10 the gain in cytokine levels decreased as the wait period increased, whereas for IL-5 the gain increased with the wait period duration.

Variability also occurred with respect to the cellularity of the BALF. The number of total leukocytes and neutrophils were only increased by a recall challenge when it was given 28 days after the end of the initial challenge sequence, but not when the wait time was 10 or 17 days (Figs. 46A and C), indicating that their refractory periods are greater than 17 days. In contrast, eosinophils showed no significant increase in response to recall challenges at any of the three wait periods (Fig. 46B), indicating that the eosinophil refractory period is more than 28 days in length.

Variable refractory periods were also observed for the parameters of lung mechanics. Waiting 17 days before initiating recall challenge resulted in a statistically significant increase in *Rn* although it was not until 28 days that this increase was biologically significant (Fig. 47A). In contrast, *H* did not increase significantly with recall challenge after any of the wait times investigated (Fig. 47B). These findings thus suggest that the refractory period for lung hyperresponsiveness in terms of tissue

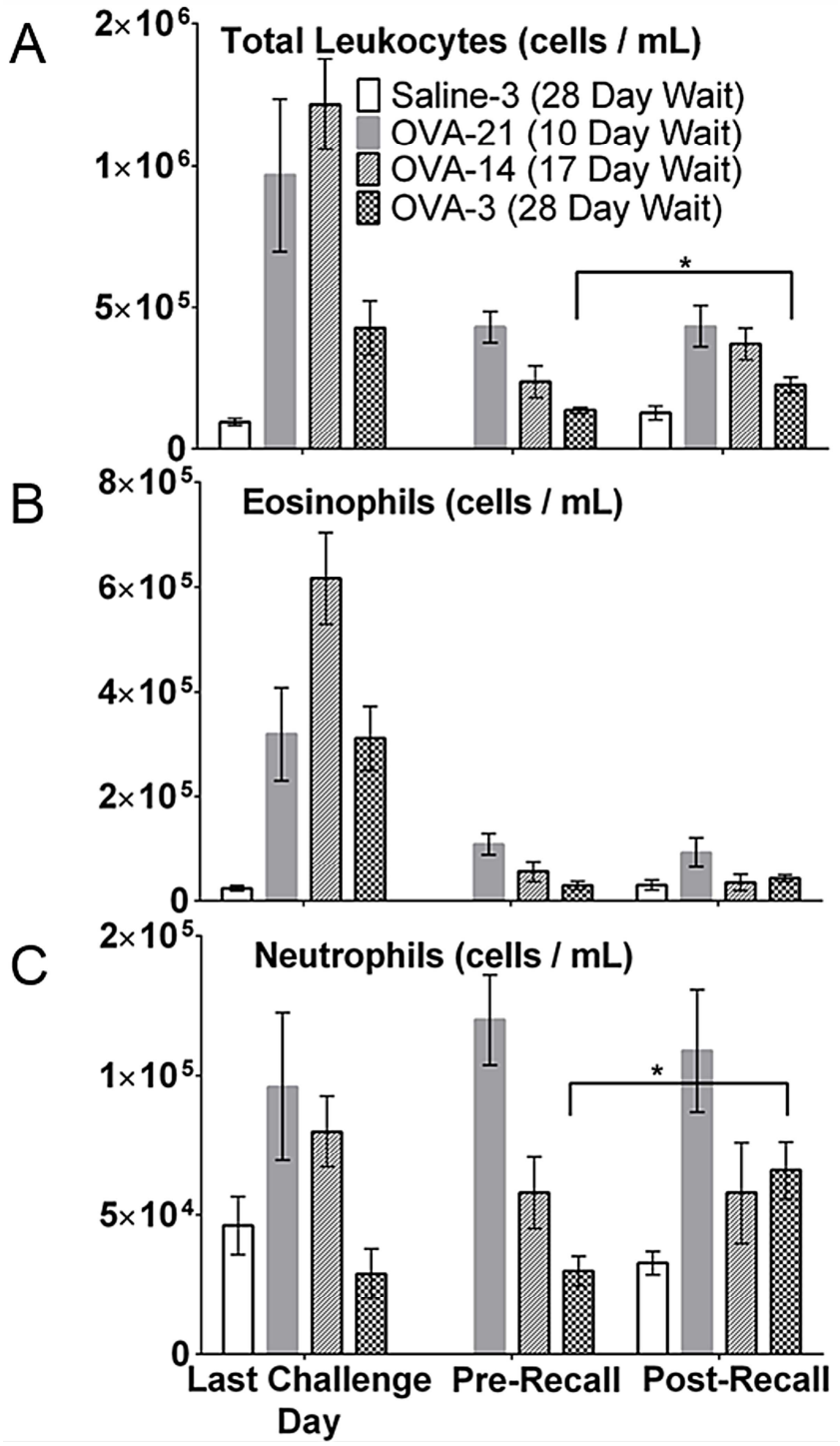

Figure 46: Numbers of cells measured in BALF from mouse lungs 24 hours following 3, 14 and 21 days of OVA challenge, and both immediately preceding and following recall challenge: A) total leukocytes, B) eosinophils, and C) neutrophils. Control measurements were made 24 hours after 3 days of saline challenge and after a recall challenge with saline on day 31. Points represent mean ± standard error. * indicates significant increase following the recall challenge

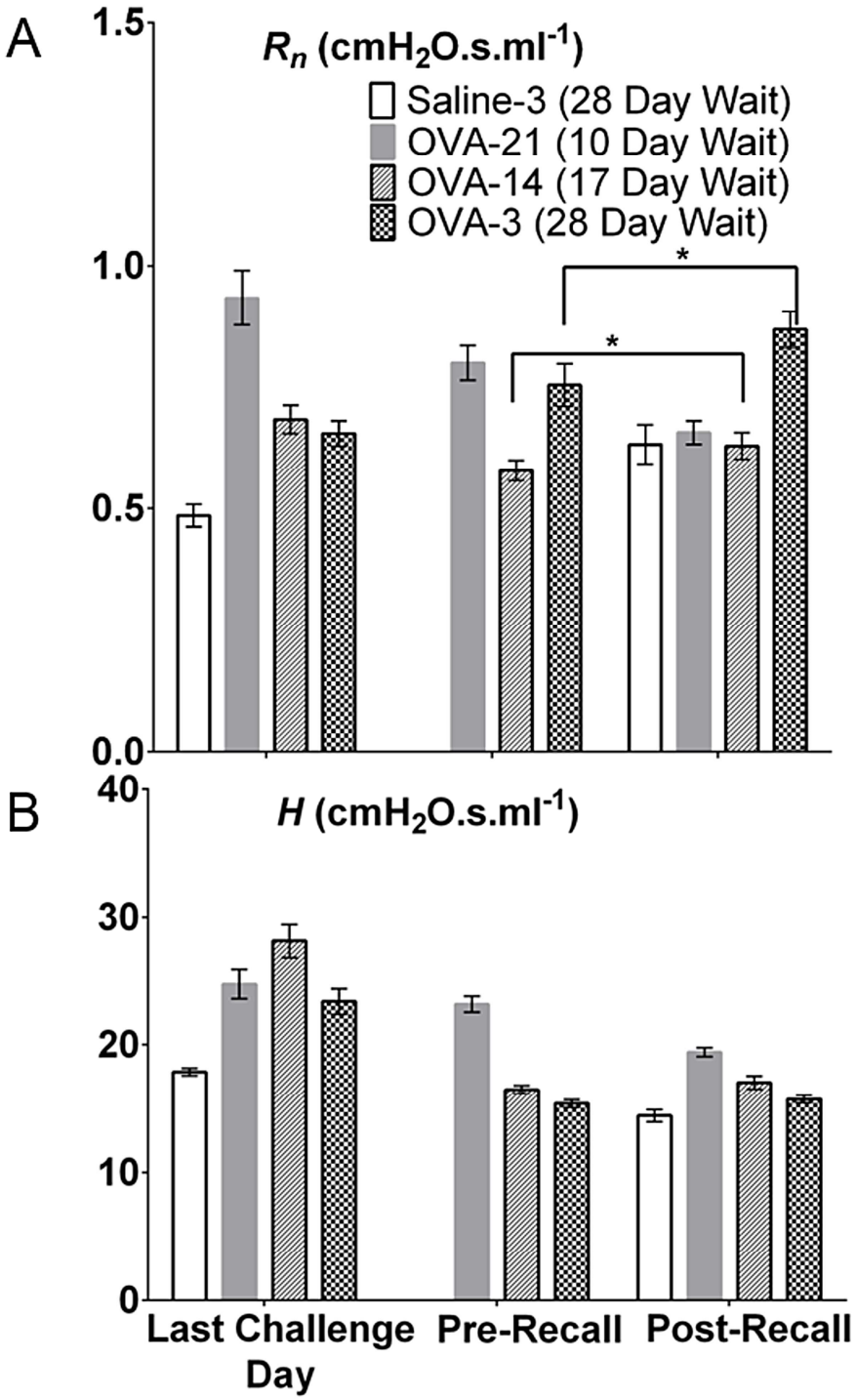

Figure 47: Measurements of lung mechanics parameters in mice 24 hours following 3, 14, and 21 days of OVA challenge, and both immediately preceding and following recall challenge: A) R_n, and B) H. Control measurements were made 24 hours after 3 days of saline challenge and after a recall challenge with saline on day 31. Points represent mean ± standard error. * indicates significant increase following the recall challenge

elastance is longer than 28 days while in terms of airway resistance it is less than or equal to 17 days.

5.4. Discussion

The findings of the present study show that each of the components involved in the allergic inflammatory response is part of a team that together produces a self-limited dynamic inflammatory response. The individual cell types (Fig. 43) and their cytokine products (Figs. 41 and 42) exhibit varying dynamics over the course of a month from the beginning of continual antigen challenge, but collectively they are responsible for the dynamics of the physiologic phenotype evident in Fig. 44. Our results go further than simply dissecting the components of the transient response to antigen, however, by demonstrating clear evidence of a refractory period in the dynamic phenotype (Fig. 47) as well as in some of its components (Figs. 45 and 46). A refractory period is key to any form of self-limited response because re-initiation of the response must be precluded for at least some period of time to allow it to be forced to resolve back to baseline. Evidence for the existence of such a refractory period in the allergic inflammatory response is seen in previous studies that showed both that continual stimulation with antigen for 30 days eventually leads to non-responsiveness [10] and that re-stimulation with antigen after a rest period elicits another vigorous response [4]. In fact, the dissipation of an allergic response in the face of continued antigen challenge is well-known to the immunology community as the phenomenon of local inhalational tolerance [11]. The inflammatory twitch hypothesis provides a teleological basis for the phenomenon of tolerance by showing how it potentially solves the thorny control problem presented by the need to

automatically turn off a response that would be harmful if it persisted beyond when it is needed, but for which there is no obvious "off switch".

We note that while there are clear signs of twitch-like behavior in our data, this does not apply to every relevant player in the allergic inflammatory response. An exception is the response pattern exhibited by neutrophils, which showed no signs of resolving to baseline (Fig. 43C). Also, total cell numbers (Fig. 43A), *Rn* (Fig. 44A), and KC (Fig. 41B) all peaked in their responses but remained at elevated plateaus out to Day 31, and some of the cytokines did not differ in their time courses relative to control (Fig. 42). There are several possible ways to interpret these findings. One is that those quantities that did not return baseline eventually would have if we had continued the experiment for long enough, which would mean that the inflammatory twitch lasts longer than the one month period over which we investigated it. Another possibility is that there are aspects of the response to continual antigen stimulation that are maintained indefinitely, and which would thus not conform to the twitch hypothesis. Indeed, such persistence is what one would expect of anything related to immune memory, so while those aspects of the allergic inflammatory response that need to be transient might be controlled in a twitch-like fashion, there are other aspects that need to remain active for the health of the organism. Also, it is possible that some components of the inflammatory response are capable of summation in the same way that force can summate in skeletal muscle. Thus, the refractory period in the allergic inflammatory twitch might be defined by events that resolve more quickly than the physiological phenotype shown in Fig. 43, such as the group of early cytokines that appear to have a refractory period of 10 days or

less (Fig. 40A-C), which would potentially allow the methacholine responsiveness phenotype to summate.

Putting these results together generates an overall picture of the allergic inflammatory response. While the complete response may take more than 31 days to manifest fully, within the 31 day window that we examined in the present study there are a number of distinct events that wax and wane over different time scales. First, there is an initial transient phase of early cytokines that peaks at Day 3 followed by responses in eosinophils and lung tissue stiffness that peaks at Day 14. Then there is a leukocyte peak between Day 14 and Day 21 that is followed by both the later cytokines and airway resistance, both peaking at Day 21. Drawing on our analogy with the skeletal muscle twitch, these various events are similar to the components of the muscle twitch that include the early action potential followed soon after by calcium influx and then later by force development. In other words, the muscle twitch and inflammatory twitch are both composed of a sequence of events in which the early events trigger the later events until there is eventual resolution back to baseline. It should be noted, however, that this may paint a somewhat oversimplified picture of the inflammatory twitch because its various cell and cytokine components do not function in isolation but rather operate as part of networks. The time-course of a particular component may thus reflect its changing environment as much as, or even more than, its own intrinsic dynamics.

An interesting question raised by our results is why some cytokines peak at Day 3 (GM-CSF, KC and IL-5 in Figs. 41A-C) while others peak at Day 21 (IL-10 and IFNγ in

Figs. 41D and E). IFNγ and IL-10 are known to be associated with Th1 and T-regulatory cells, respectively [12-14], while IL-5 is associated with Th2 cells [15]. GM-CSF and KC are also known to be associated with the activation of dendritic cells and the recruitment of neutrophils [16-17], cells also involved in the early phase of the allergic response. One possibility, therefore, is that the cytokine picture in Fig. 40 indicates a switch from an early Th2-mediated inflammatory phase to a later Th1-mediated resolution phase that involves T-regulatory cells. This is consistent with other studies showing that in mice allergic to *Aspergillus fumigatus*, interventions that target the Th2-mediated phase of the response result in decreased levels of not just IL-5, but also IFNγ, IL-4, IL-13 and lymphocytes (specifically $CD4^+$ T-cells) [18]. Interestingly, this also reduced airways hyperresponsiveness, although others have shown in mice allergic to OVA that Th1 cytokines do not induce airway hyperresponsiveness [19].

The inflammatory twitch hypothesis raises the possibility that pathologic alterations in some of the molecular and/or cellular events involved in the allergic inflammatory twitch could transform it into a non-resolving event. Such a transformation might correspond to the chronic inflammation characteristic of allergic asthma. We investigated this possibility theoretically in a previous study by manipulating our computational model in ways corresponding to plausible biological abnormalities [2]. Many of these manipulations, such as altering the amounts of chemical signals released by cells, knocking out certain cell types, and changing the speed of movement of cells within the tissue environment, did relatively little to change inflammatory twitch dynamics. However, increasing the life span (i.e. delaying apoptosis) of pro-

inflammatory cells in the model had a powerful effect on extending the magnitude and duration of simulated inflammation [2]. Interestingly, inflammatory cells have been documented to have longer lifespans in individuals with airway disease [20-23]. The results of the present study suggest that this might apply particularly to eosinophils (Fig. 42).

Finally, we must view the findings of our study within the context of its limitations. Perhaps most significant is the limitation placed by our study design on our ability to resolve the various features expected of a twitch-like response. We chose a design aimed at obtaining as much information as possible about the inflammatory twitch from a limited number of animals, but this gave far from complete coverage of all the possibilities. For example, we are not able to distinguish between the inflammatory effects due to length of antigen challenge from those of a rest period prior to recall challenge because challenge duration and rest duration varied oppositely in our study design (Figure 41). We also employed only a single day of recall challenge, allowing us to study only the most rapid response features inflammatory twitch that may differ from those of a more extended recall challenge. Fully characterizing the inflammatory twitch in all its aspects would require that our experiments be repeated over a significantly longer time scale than one month, and that many more configurations of challenge and rest be examined. This would have required a large number of additional mice, and we studied 104 mice over a total time of a month and a half as it was. Questions about the dynamics of the allergic inflammatory twitch thus remain. Nevertheless, we were able in

the present study to add significantly to our understanding of these dynamics, and to place this understanding within the framework of the inflammatory twitch hypothesis.

In conclusion, we have provided experimental evidence consistent with our allergic inflammatory twitch hypothesis. Specifically, we have demonstrated transient behavior in many of the cells and cytokines involved in the response as well as its phenotypic manifestation in terms of lung function. These findings support the notion that the allergic inflammatory twitch in normal mice lasts in the order of one month. We have also demonstrated clear evidence of refractory periods in many of these components of the response, some as short as only a few days. These findings corroborate the notion that control of the host response employs frequency modulation in the same way that control is exerted over muscle force, neural signaling, and indeed a host of other biological processes that are initiated by single instigating events. The inflammatory twitch hypothesis thus provides a general mechanism to explain how inflammation is controlled in a normal healthy individual, and also suggests how it might become aberrant in individuals who develop chronic inflammatory diseases such as allergic asthma.

5.5 Acknowledgements

This work was supported by NIH grants R01 HL103405, P30 GM103532, T32 HL076122, R21 AI112804, University of Vermont IGP, and F31 EB-018215. Special thanks to Nirav Dapharty and Minara Aliyeva for their assistance with the mice

experiments and data analysis, as well as Jennifer Ather and Laura Hoyt for their help with the cytokine analysis.

5.6. References

1. Pothen, J. J., M. E. Poynter and J. H. Bates. The inflammatory twitch as a general strategy for controlling the host response." J Immunol 190: 3510-3516. 2013.
2. Pothen, J. J., M. E. Poynter and J. H. Bates. A computational model of unresolved allergic inflammation in chronic asthma. Am J Physiol Lung Cell Mol Physiol 308: L384-390. 2015.
3. Tanaka, H., T. Masuda, S. Tokuoka, Y. Takahashi, M. Komai, K. Nagao and H. Nagai. "Time course study on the development of allergen-induced airway remodeling in mice: the effect of allergen avoidance on established airway remodeling." Inflamm Res 51(6): 307-316. 2002.
4. Riesenfeld EP, A. G., Bates JHT, Poynter ME, Wu M, Aimi S and LK Lundblad. "The Temporal Evolution of Airways Hyperresponsiveness and Inflammation." Allergy & Therapy S1. 2012.
5. Bates JH, Wagers SS, Norton RJ, Rinaldi LM, and Irvin CG. Exaggerated airway narrowing in mice treated with intratracheal cationic protein. *J Appl Physiol (1985)* 100: 500-506, 2006.
6. Wagers S, Lundblad LK, Ekman M, Irvin CG, and Bates JH. The allergic mouse model of asthma: normal smooth muscle in an abnormal lung? *J Appl Physiol (1985)* 96: 2019-2027, 2004.

7. Wagers SS, Haverkamp HC, Bates JH, Norton RJ, Thompson-Figueroa JA, Sullivan MJ, and Irvin CG. Intrinsic and antigen-induced airway hyperresponsiveness are the result of diverse physiological mechanisms. *J Appl Physiol (1985)* 102: 221-230, 2007.
8. Hantos Z, Daroczy B, Suki B, Nagy S, and Fredberg JJ. Input impedance and peripheral inhomogeneity of dog lungs. *J Appl Physiol (1985)* 72: 168-178, 1992.
9. Tomioka S, Bates JH, and Irvin CG. Airway and tissue mechanics in a murine model of asthma: alveolar capsule vs. forced oscillations. *J Appl Physiol (1985)* 93: 263-270, 2002.
10. Cojocaru, A., C. G. Irvin, H. C. Haverkamp and J. H. Bates. "Computational assessment of airway wall stiffness in vivo in allergically inflamed mouse models of asthma." J Appl Physiol 104(6): 1601-1610. 2008.
11. Kabbur, P. M., W. F. t. Carson, L. Guernsey, E. R. Secor, Jr., R. S. Thrall and C. M. Schramm. "Interleukin-10 does not mediate inhalational tolerance in a chronic model of ovalbumin-induced allergic airway disease." Cell Immunol 239: 67-74. 2006.
12. Holgate, S. “Mediator and Cytokine Mechanisms in Asthma.” Thorax 48.2 (1993): 103–109. Print.
13. Maynard CL and CT Weaver. “Diversity in the Contribution of IL-10 to T-Cell-Mediated Immune Regulation.” Immunological reviews 226 (2008): 219–233. PMC. Web. 18 Sept. 2015.

14. Ng, T. H. Sky et al. “Regulation of Adaptive Immunity; The Role of Interleukin-10.” Frontiers in Immunology 4 (2013): 129. PMC. Web. 18 Sept. 2015.
15. Doherty, TA, and DH Broide. “Group 2 Innate Lymphoid Cells: New Players in Human Allergic Diseases.” Journal of investigational allergology & clinical immunology 25.1 (2015): 1–11. Print.
16. Gajewska, B. U., R. E. Wiley and M. Jordana. "GM-CSF and dendritic cells in allergic airway inflammation: basic mechanisms and prospects for therapeutic intervention." Curr Drug Targets Inflamm Allergy 2(4): 279-292. 2003.
17. McKinley, L., J. Kim, G. L. Bolgos, J. Siddiqui and D. G. Remick. "CXC chemokines modulate IgE secretion and pulmonary inflammation in a model of allergic asthma." Cytokine 32(3-4): 178-185. 2005.
18. Paveglio SA, Allard J, Foster Hodgkins SR, et al. “Airway Epithelial Indoleamine 2,3-Dioxygenase Inhibits CD4+ T Cells during Aspergillus Fumigatus Antigen Exposure.” American Journal of Respiratory Cell and Molecular Biology 44.1 (2011): 11–23. PMC. Web. 21 Sept. 2015.
19. Nakada EM, Shan J, Kinyanjui MW, Fixman ED. “Adjuvant-Dependent Regulation of Interleukin-17 Expressing Γδ T Cells and Inhibition of Th2 Responses in Allergic Airways Disease.” Respiratory Research 15.1 (2014): 90. PMC. Web. 18 Sept. 2015.
20. Ilmarinen, P. and H. Kankaanranta. "Eosinophil apoptosis as a therapeutic target in allergic asthma." Basic Clin Pharmacol Toxicol 114: 109-117. 2014.

21. Oh, J. and J. S. Malter. "Pin1-FADD interactions regulate Fas-mediated apoptosis in activated eosinophils." J Immunol 190: 4937-4945. 2013.

22. Reddy, A. T., S. P. Lakshmi, S. Dornadula, S. Pinni, D. R. Rampa and R. C. Reddy. "The nitrated fatty acid 10-nitro-oleate attenuates allergic airway disease." J Immunol 191: 2053-2063. 2013.

23. Sun, Z., S. Dragon, A. Becker and A. S. Gounni. "Leptin inhibits neutrophil apoptosis in children via ERK/NF-kappaB-dependent pathways." PLoS One 8: e55249. 2013.

CHAPTER 6: INFERRING STEM CELL BEHAVIOR

6.1. Introduction

One of the hopes of stem cell research is being able to grow entire organs *ex vivo* for use in clinical transplantation and as model systems for study. An approach that may hold promise for the engineering of complex organs is the use of decellularized scaffolds devoid of cells and antigenic material that are then seeded with autologous stem cells in the hope that a fully functional organ will eventually develop [1, 2]. In the case of the lung, as with many organs, this promise remains far from realized [3, 4]. Indeed, stem cell research has thus far been essentially empirical, leading some to refer to these investigations as "modern alchemy" [1]. One possible reason for the current state of affairs is an almost complete lack of predictive modeling tools with which to guide the direction of investigation.

The ability to predict the course of tissue regeneration must rely on a knowledge of the rules governing how relevant cell types behave in the various situations they will encounter during the regeneration process. These rules indicate how each cell influences, and is influenced by, its neighboring cells and the surrounding microenvironment in which it finds itself [5, 6]. Armed with such rules one could, in principle, simulate the process of tissue regeneration to identify promising scenarios before trying them experimentally, thereby greatly increasing the efficiency of the search for effective regeneration strategies. The computational approach known as agent-based modeling [7, 8, 9, 10] seems perfectly suited to this endeavor. However, such modeling relies on

knowledge of the rules of cell behavior, about which we currently know little. On the other hand, agent-based modeling might also be of assistance in determining these rules through comparison of model predictions to experimental data.

Although sophisticated agent-based models have been applied to a variety of cellular systems, including the growth and maintenance of skin [11] the use of mesenchymal stem cells (MSCs) to generate bone [12], these models have yet to be applied to the study of stem cells in the lung. Accordingly, toward this end, we investigated the engraftment patterns of two different cell types relevant to the regeneration of lung tissue following their seeding onto decellularized lung scaffolds. Simultaneously, we employed an agent-based computational model to simulate engraftment patterns based on simple sets of behavioral rules governing how cells move, when they divide, and when they die. By determining which rules more closely recapitulated experimental observations we are able to infer those that plausibly might differentially regulate the behavior of the two cell types.

6.2. Methods

6.2.1. Computational Model

We created a computational model to study two Hypotheses, termed Hypotheses 1 and 2, respectively, regarding the behavior of stem cells on these decellularized scaffolds. Both hypotheses are motivated by experimental observations regarding two representative cell types investigated for seeding decellularized lung scaffolds: C10 epithelial cells, an immortalized mouse type 2 alveolar epithelial cell line, and bone

marrow-derived MSCs [13, 14]. From previous experiments we know that C10s tend to mostly be present at the tissue periphery at later time points [13]. Given the nature of cells to move via chemotaxis, this suggests that there is some substrate incorporated into the scaffold with a concentration that is highest at the borders of the tissue slice and decreases progressively toward the center. The identity of this substrate is currently unknown, but possibilities include oxygen or extracellular matrix components such as fibronectin and laminin that may be distributed preferentially toward the periphery of the alveolar tissue [15].

We used NetLogo 4.1.3 freeware [9, 10] to design a 3-dimensional agent-based model of a decellularized scaffold environment seeded with cells that can attach to and proliferate over it. The environment of the model represents an initially decellularized lung scaffold, and is composed of a set of contiguous cuboidal patches, each characterized by local variables that define its properties. The cells applied to the model scaffold are represented by discrete agents capable of moving around from patch to patch according to stochastic rules that define the likelihood of their rates and directions of movement.

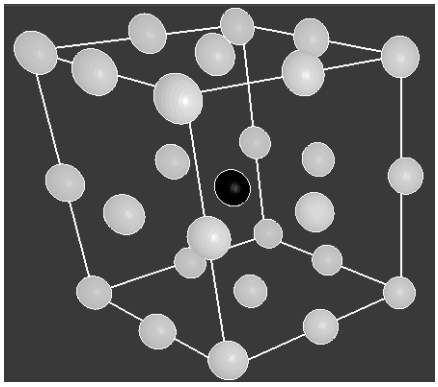

Figure 48: Diagram illustrating the location of a cell's neighbors. The cell (black ball) is at the center of the cube, and the 26 white balls illustrate the location of its neighbors in 3-D space

At every time point, only one cell can exist on each patch, meaning a motile cell cannot move into the same location as an already engrafted cell. However, additional rules allow the cells to interact with neighboring agents and the patches that they come into contact with. Each cell has up to 26 neighbors as illustrated in Figure 48. These interactions may involve any putative biological effect such as the alteration of the environment by the secretion of chemical signals, or a direct effect of one cell on another. In particular, we assume engrafted cells increase the substrate concentration of the patch they are on by an arbitrary value of 1. If the cell dies, then the patch substrate concentration is decreased by 1.

We represent the environment of the lung scaffold as 32 x 32 x 32 individual cubic patches, with the environmental border representing the edges of the scaffold. (The environment size and the spacing between the patches are constraints set by the NetLogo software.) Each patch has a local variable whose value represents the numerical concentration of a bioactive substrate that influences cell behavior (see below) such that the substrate concentration has a value $c = \frac{20\sqrt{x^2 + y^2}}{21.2}$ for any set of (x, y, z) coordinates, as the x, y and z axes range from -16 to 16 (in arbitrary distance units). While this formula is arbitrary, it creates an environment where in any x-y plane, the lowest substrate concentration ($c = 0$) is at the center ($x = 0$, $y = 0$) while the highest concentration is at the borders, thereby creating a substrate gradient and thus an impetus for cell movement and exploration of the environment. The cells are motile, and so move in 3 dimensions from one patch to another at each time step.

The scaffold was seeded at $t = 0$ with 30,000 randomly placed identical agents (cells) because this gave a seeding density that was visually reminiscent of the experimental situation. Experimentally we observe that most cells seem to engraft following initial seeding, at least for a while, so the cells in the model were each given a 95% chance of engrafting with the remaining cells being eliminated. The model was then run for 80 time steps using two different behavioral rules sets corresponding to computational Hypotheses 1 and 2. Each cell executes its set of commands once within

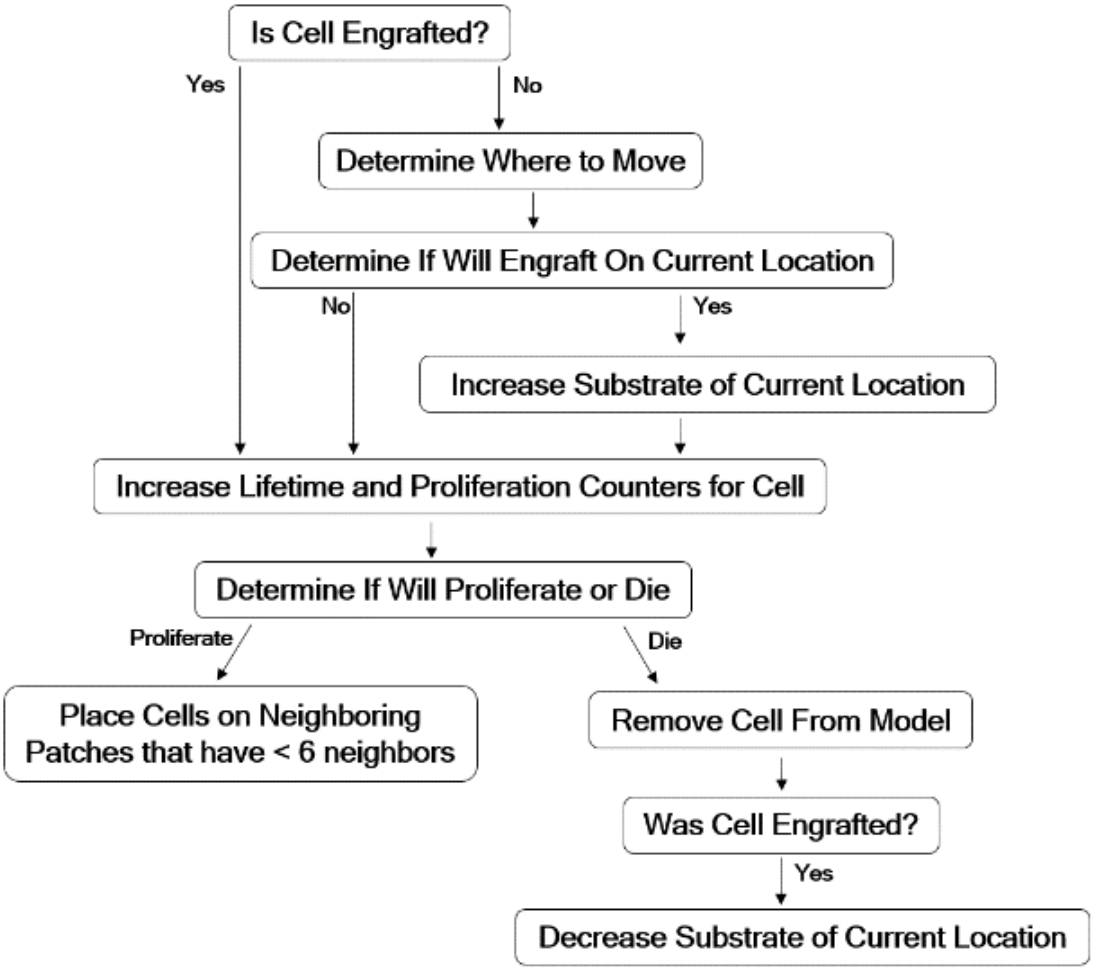

Figure 49: Schematic of the algorithm used with specific rule sets at each time point to implement Hypothesis 1 and Hypothesis 2 in the model

each time step, allowing it to potentially move to a neighboring patch, engraft to a patch, and/or undergo one round of proliferation. We ran the model for a total of 80 time steps because most of the cells in the model under both hypotheses had died by this time point, which matches what we observed experimentally (see below).

We show a schematic for the general behavior of the models in Figure 49. The specifics of the model using the rule set for Hypothesis 1 are as follows:

1. First, the motile cells determine where to move across all three axes. While each cell has 26 neighbors surrounding it (Fig 48) and there are numerous ways of modeling how it could move and the number of neighboring patches it could consider moving to, cell movement in NetLogo is modeled as a forward vector oriented randomly in some direction relative to the *x*, *y* and *z* axes, thus enabling the cells to explore their 3D environment by moving and considering neighbors in a 2-D fashion along the direction of the forward vector. The angle of the vector is randomly changed at each time step, changing the cell's orientation to the x, y and z axes, unless the cell senses a high substrate signal in one of the three patches ahead of its current direction (directly ahead, ahead to the left and ahead to the right), in which case the cell has a higher chance of moving toward the patch with the strongest signal. (Because of the angle orientation, these three patches may be above or below the cell's current location.) To simulate this in our model, the numerical variables representing concentrations of substrate, *c*, on these three patches are each multiplied by a random number, x_i, uniformly distributed on the interval [0, 1], that represents the likelihoods of moving in each of the directions. If

$S = (x_1 c_{ahead-and-straight} + x_2 c_{ahead-and-left} + x_3 c_{ahead-and-right}) > 1$, the cell moves towards the patch with the strongest signal, meaning that all cell movement in the model is probabilistic. If $S < 1$, the cell moves randomly to an adjacent patch. (The concentration of substrate on the current patch is c_{patch}.) The rules governing cell movement are based on previous models regarding cellular movement throughout the lung in the presence and absence of chemical stimuli [9, 10].

2. All motile cells then determine whether they will attach to the patch they are currently on. A random real number, N, uniformly distributed on the arbitrary interval [0, 100] is computed. If $N > N_{crit}$, where $N_{crit} = 5$, the cell is replaced by an immobile engrafted cell. Each engrafted cell has two parameters: T_{life}, the lifespan of the cell, and T_{prol}, the amount of time that must pass before the cell can proliferate into neighboring patches. Upon initially engrafting, T_{life} is chosen randomly on the uniformly distributed interval of [0, 36] time steps, and T_{prol} is set on the uniform interval [33, 87]. (This enables some cells to undergo apoptosis before having the opportunity to proliferate, and to have an increased likelihood of proliferating if the patch environment enables them to proliferate in a shorter amount of time.)
3. The lifetime counter, N_{life}, for the cell is incremented by 1. If $N_{life} = T_{life}$ the cell is eliminated from the model, representing cellular apoptosis.
4. The proliferation time counter, N_{prol}, for the cell is incremented by 1. If $N_{prol} = T_{prol}$ the cell places a copy of itself onto a single randomly selected neighbor that has at most 6 neighbors itself. (The number of neighbors is arbitrarily chosen, but is based on observations from our experimental images that cells that survive over time are

surrounded by a small number of cellular neighbors. This suggests that cells require some moderate degree of cell-cell interaction to thrive.) For each new cell, T_{life} is chosen randomly on the interval [0, 18] time steps, and T_{prol} is set to (33 - c_{patch}/ $c_{envfactor}$) + n, where $c_{envfactor}$ = 1.9 and n is a random number uniformly distributed on the interval [0, 54].

5. As long as an engrafted cell remains alive, c_{patch} is increased by c_{amount}. This implies that the engrafted cell through its actions, either directly or indirectly, permanently increases the concentration of substrate on the patch by c_{amount}. If the cell dies, then it is no longer able to maintain the substrate concentration at this level, so c_{patch} is decreased by c_{amount}. In our model, c_{amount} is set to 1.

Under the rule set for Hypothesis 1, engrafted cells have an equal probability of surviving anywhere in the environment, but a higher likelihood of proliferating on patches with higher concentrations of substrate. The rule set for Hypothesis 2 is identical to Hypothesis 1, with the exceptions that T_{life} is distributed uniformly on the interval [0, 45] and T_{prol} is set on the uniform interval [41, 103], and that for each new cell created, T_{life} is set to (c_{patch} / $c_{envfactor}$) + n, where $c_{envfactor}$ = 1.9, n is a random number uniformly distributed on the interval [0, 45], and T_{prol} is chosen randomly on the uniformly distributed interval [41, 103] time steps. Under this hypothesis, cells live longer relative to the cells in Hypothesis 1, and engrafted cells have a higher likelihood of surviving on patches with higher concentrations of substrate.

6.2.2. Experimental Data

Cells were seeded onto lung scaffolds from mice as described in Bonenfant et al. and Wallis et al. [13, 14]. Briefly, the study utilized adult C57BL/6J mice that were maintained at UVM in accordance with institutional and American Association for Accreditation of Laboratory Animal Care standards and review. Following heart-lung bloc harvest, lungs were decellularized under sterile conditions by tracheal and vascular infusion and immersion in 0.1% Triton-X solution for 24 hours and 2% sodium deoxycholate for a further 24 hours. Between each incubation step, lungs were rinsed with 5X penicillin/streptomycin (P/S) in deionized water. On day three, lungs were incubated for one hour each in 1M NaCl and porcine pancreatic DNase solution. Lungs were then rinsed with 1x PBS in 1x P/S. The left lobe of decellularized scaffolds was then inoculated through the airway with either $1x10^6$ mesenchymal stem cells (MSCs) isolated from mouse bone marrow (Sca-1+, CD106+, CD29+ and CD11b-, CD11c-, CD34-, and CD45-, from Dr. Darwin Prockop, NCRR/NIH Center for Preparation and Distribution of Adult Stem Cells at Texas A and M University) [16], or $1x10^6$ C10 mouse lung epithelial cells (gift from Dr. Matthew Poynter, University of Vermont). Cells were suspended in 3% low melting point agarose (SeaPrep Agarose, Cambrex) for inoculation. The inoculated lungs were then allowed to gel at +4°C for 30 minutes and manually sliced to sections of approximately 1mm thickness. Slices were then incubated at 37°C in respective growth media in order to remove the agarose. mMSCs (P6-P8) and slices inoculated with mMSCs were cultured in Iscove's Modification of Dulbecco's Medium supplemented with 2 mM L-glutamine, 100 U/mL penicillin and 100 mg/mL streptomycin (Fisher), 10% fetal bovine serum (Atlanta Biologicals) and 10% horse

serum (Invitrogen). C10 cells and slices inoculated with C10 cells were cultured in DMEM medium supplemented with 2 mM glutamine, penicillin/streptomycin, and 10% FCS. Media was changed every other day and individual slices were incubated at 37°C at 5% CO_2 in low adherence 12 well tissue culture plates. Scaffolds were harvested at days 1, 3, 7, 14, 21 and 28 after inoculation and fixed in 4% paraformaldehyde. Slices were then embedded in paraffin and sliced to 5μm thick slices, deparaffinized, and stained with hematoxylin and eosin (H&E).

6.2.3. Image Analysis

Images were taken from the top, middle and bottom of each experimental lung slice using an Olympus fluorescent microscope at 10x magnification. At each time point we imaged three slices, for a total of nine experimental images per time point. In our computational analysis, we took 30 screenshots of 2D slices from the 3D computational model scaffold every 10 time steps. We defined our model as having a total time duration evenly divided into 80 time steps. The time scale in this model is arbitrarily defined, but we can nevertheless map the speed of movement of a model cell from patch to patch onto the actual speed of movement of real cells, as follows. A model tissue slice consists of 32 x 32 patches corresponding to an area of lung scaffold roughly 1,000 μm x 1,000 μm, so each model patch has dimensions roughly 30 μm x 30 μm. As 80 time steps in the model correspond to 28 days of real time, a cell moving from patch to patch at each time step has a velocity of 0.002 time step/min, corresponding to an actual velocity of about 0.06

μ/min. This is of the same order of magnitude as we estimate the velocity of movement of cells engrafted to lung scaffolds (unpublished observations).

We quantified the patterns of cellular adherence in the images from both the experimental lung scaffolds and the agent-based model using a custom designed image analysis tool written in Matlab (Mathworks, Natick, MA), identifies cell nuclei and divides the image into tiles centered on them by implementing the following algorithm.

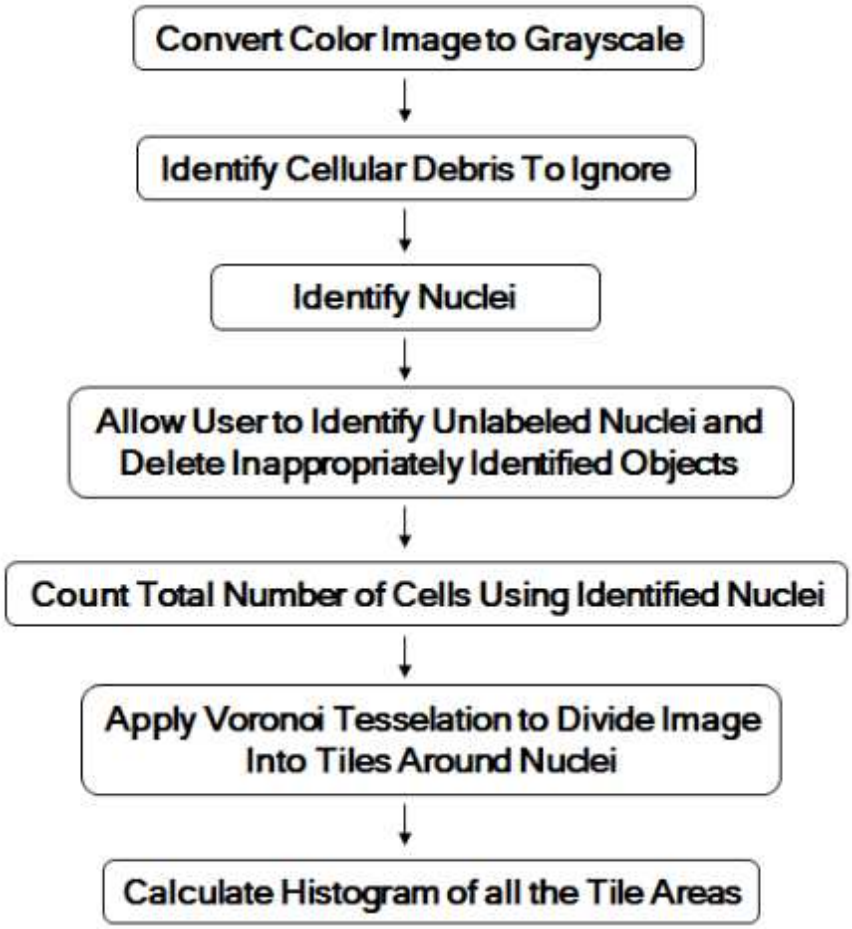

Figure 50: Illustration of the image analysis procedure used to define cell neighborhoods using Voronoi tessellation

(The Matlab code is available upon request from the authors.) A schematic of this algorithm is shown in Figure 50, and the details are as follows.

1. Convert the color image to grayscale.

2. Create a black and white version of the grayscale image using a pixel intensity threshold of 125 on an 8-bit scale from 0 (black) to 255 (white). Identify contiguous components of at least 300 pixels (considered to be a mixture of cellular clumps and debris) from the black and white image, which becomes the image's "mask" regions.

3. Convert the original grayscale image to a black and white image using a pixel intensity threshold value of 125. Outside the "mask" regions determined in Step 2, mark the centroids of all connected components of at most 20 pixels (likely to be cell nuclei).

4. Repeat Step 3, but with a pixel intensity threshold value of 85, and instead mark centroids within the "mask" regions.

5. Allow user to manually edit cell identification by including missed cells and deleting inappropriately included objects.

6. Count the total number of cells in the image by counting the number of cell nuclei.

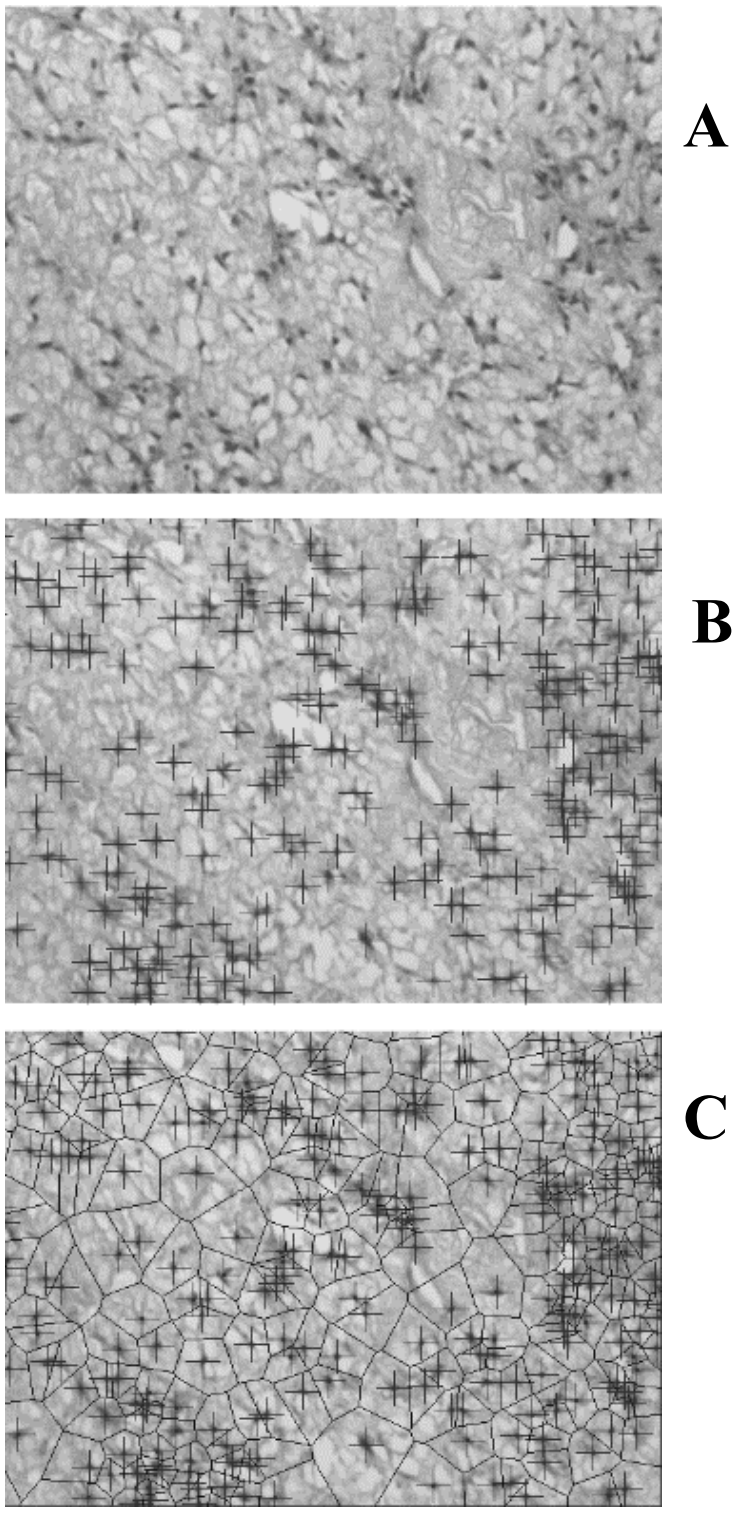

Figure 51: Experimental image (A), which is processed to mark all cells with crosses for counting (B) and then undergoes Voronoi tessellation to split the region into tiles centered around each cell (C)

7. Apply Voronoi tessellation [17, 18] such that each cell nucleus lies at the centroid of a polygon-shaped tile that defines the local neighborhood of that cell.

8. Calculate variance of the histogram of Voronoi tile areas.

Figure 51 shows an example of the image processing algorithm applied to an image of a slice from one of these experimental lung scaffolds, illustrating how the Voronoi tessellation defines the neighborhood of each cell. In particular, note that the areas of the

6.2.4. Statistical Analysis

The results of the cell culture experiments (C10 cells vs. MSCs) and the

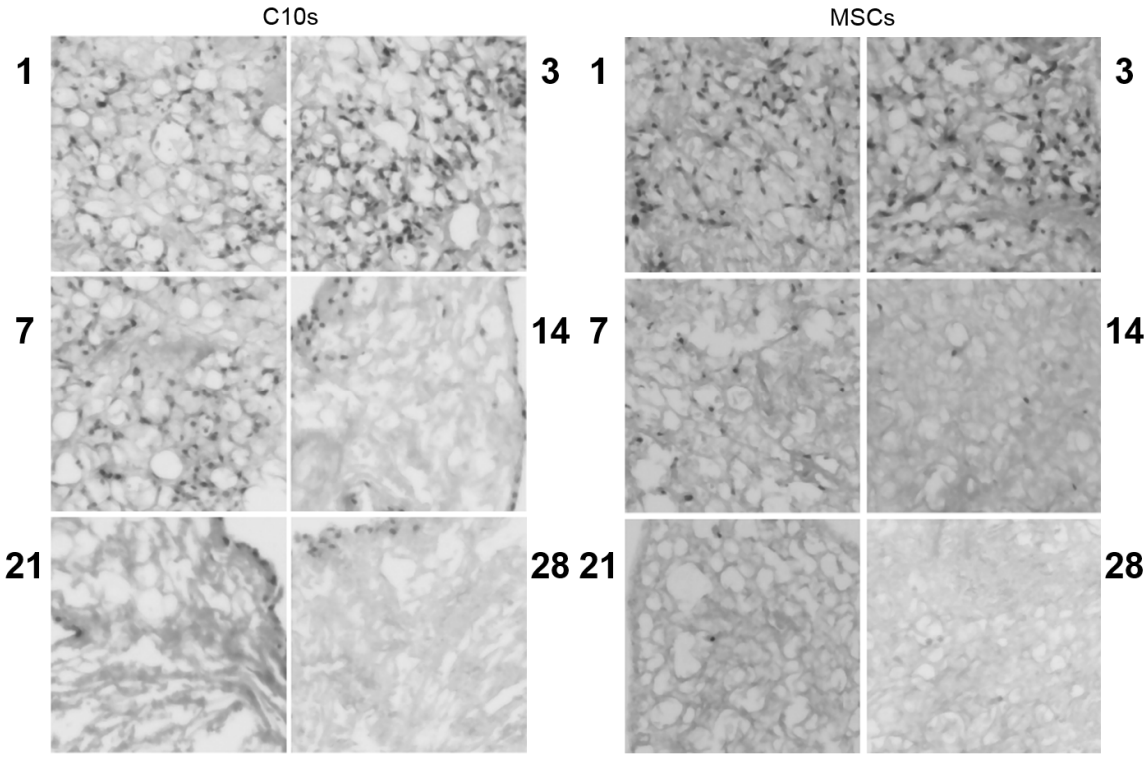

Figure 52: Experimental images of decellularized lung scaffolds at days 1, 3, 7, 14, 21 and 28, following seeding with C10 epithelial cells (left) and MSCs (right)

tiles around isolated cells are larger than those around cells which are clustered. computational modeling (Hypothesis 1 vs. Hypothesis 2) were compared by two-way ANOVA. Statistical significance was taken as $p < 0.05$. The sensitivity of model predictions to variations in model parameter values was assessed by one-way ANOVA.

6.3. Results

Sample images of the decellularized scaffolds at various time points following seeding with C10s or MSCs show evolving patterns of cellular engraftment and proliferation across these scaffolds, (Figure 52). We applied our image analysis tool to the 54 images (at 6 time points taken from 9 separate scaffold images) acquired over the 28 day time course with the two experimental cell types. Figure 53A shows the number of cells (mean ± SE) from the 9 scaffold images versus time after inoculation, where the results from each scaffold have been normalized to their respective values on Day 1. Both

C10 and MSC cell numbers eventually approach zero, but at different rates and were statistically significantly different ($p < 0.001$). Specifically, the MSC's have fallen off markedly by about day 7 whereas the C10 cells take about twice as long to reach correspondingly low numbers. It should be noted that both cell types eventually die out completely, meaning that attempts to engraft the scaffold with persistent cells (i.e. cells that survive and remain engrafted throughout the time course of the experiment) were ultimately unsuccessful. This speaks to the inherent difficulties of tissue regeneration in general, and the fact that in the case of the lung this field is still in its infancy.

Cell numbers and CVHV are expressed as percentages of their respective values at the initial time point. At the first time point the MSC cell number was 343.33 ± 60.27 and CVHV was 2.93 ± 5.26 x 10^5, while the C10 cell number was 692.44 ± 111.82 and

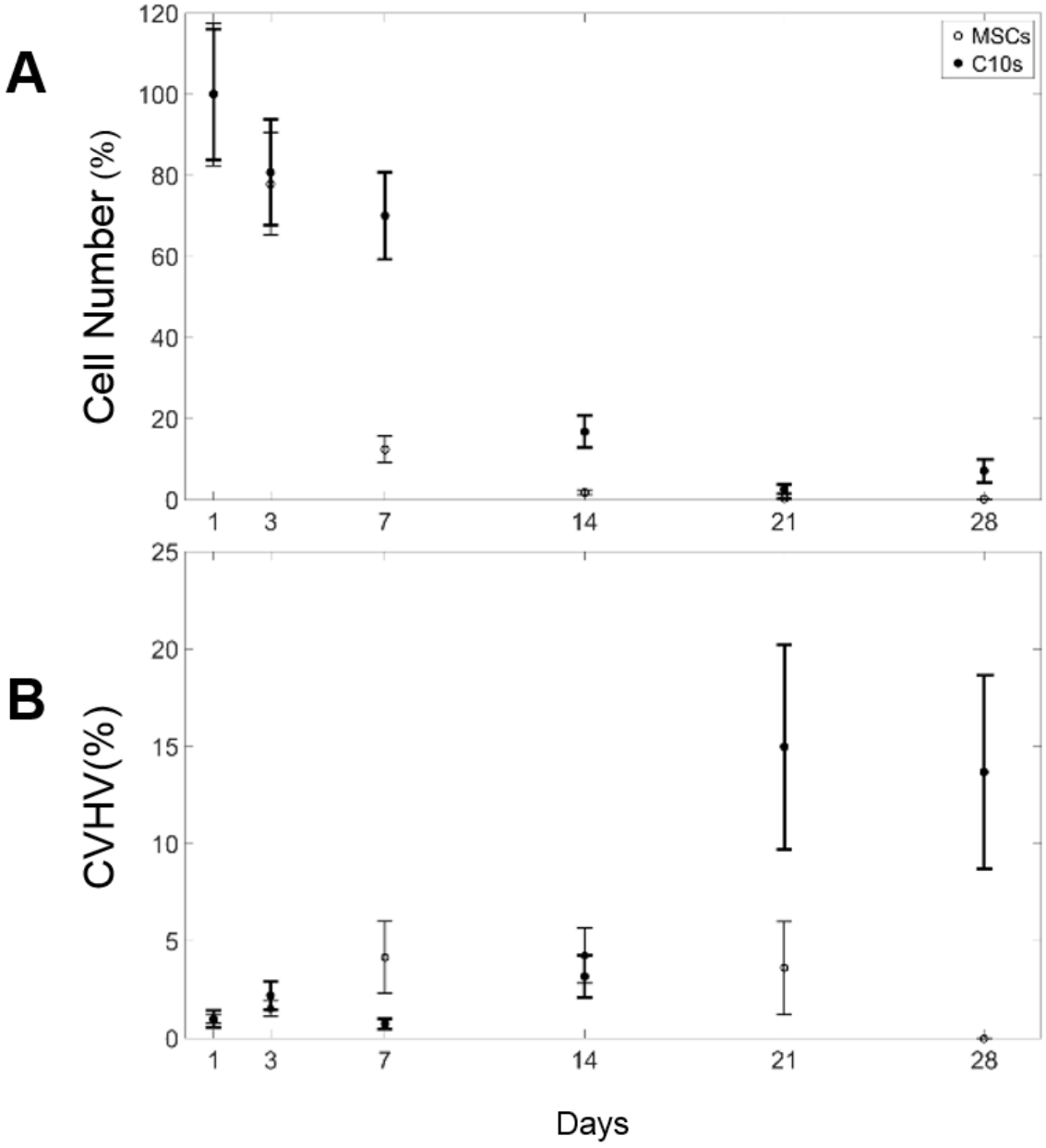

Figure 53: Experimental results (Mean ± SE) for (A) number of cells, and (B) CVHV for cells following the rules for MSCs (open circles) and C10 epithelial cells (closed circles) for all nine images gathered at days 1, 3, 7, 14, 21 and 28

CVHV was $2.07 \pm 8.84 \times 10^9$.

We also determined the variance of the histogram of the Voronoi tile areas at each time point. This variance gives a measure of the heterogeneity of cell clustering, but images with greater numbers of cells inherently have smaller variance values compared to images with fewer cells because more cells means a smaller mean area per cell. To control for this, we multiplied the histogram variance by the number of cells in the image

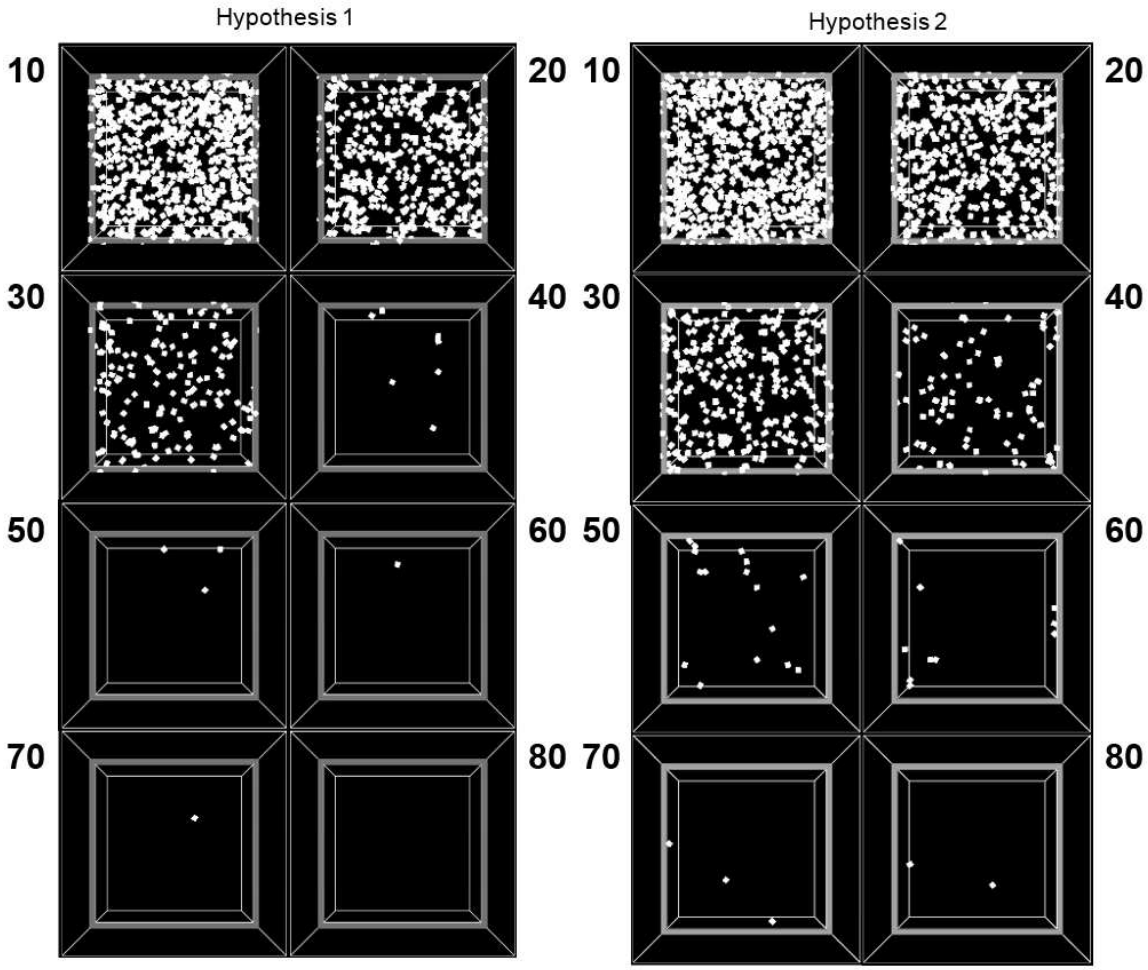

Figure 54: Representative screenshots of a computational model of a 3D lung scaffold at 10, 20, 30, 40, 50, 60, 70 and 80 time steps, following seeding with cells that behave according to (left) Hypothesis 1 (shorter-lived cells with preferential proliferation on areas of higher substrate) and (right) Hypothesis 2 (longer-lived cells with preferential survival on areas of higher substrate)

to derive what we term the Corrected Voronoi Histogram Variance (CVHV). Figure 53B shows that CVHV (mean ± SE, with the results from each scaffold normalized to their respective values on Day 1) versus time for the two cell types begins to diverge at about day 14, and is markedly different by the end of the experiment. The CVHV values for the two cell types were statistically significantly different ($p = 0.0064$).

We performed a corresponding procedure on images generated by the agent-based model, where 80 time steps in the model corresponds roughly to 30 days of experimental time as judged by the relative numbers of surviving cells at the these respective time points. Patterns of cellular proliferation and spreading throughout a simulated 2D slice of scaffold created by the agent-based model using the cellular rules specified by Hypotheses 1 and 2 are shown in Figure 54. Similar numbers of cells initially engraft to the scaffold in both cases, and as time progresses our image analysis tool enables us to quantify distinctions between the two hypotheses. While we observed a particularly rapid drop off for both models around 20 time points, we also observed a faster drop off of cell numbers in the model for Hypothesis 1 (increased proliferation on higher agent), as seen in Figure 55A, which shows mean ± SE cell number at each time point determined from 30 independent runs of the model with the results from each run normalized to its respective Day 1 value. The cell numbers were statistically significantly different for Hypothesis 1 vs. Hypothesis 2 ($p < 0.001$). Figure 55B shows the corresponding trends in CVHV at each time point. Under Hypothesis 1 (shorter lived cells with increased proliferation on higher local substrate concentration), this value initially rises until 40 time points, and then trends continually downward. Under Hypothesis 2 (longer lived

cells with increased survival on higher local substrate concentration), this value rises until 50 time points, and its values remain high relative to the initial CVHV values. The CVHV values under Hypothesis 1 vs. Hypothesis 2 were statistically significantly

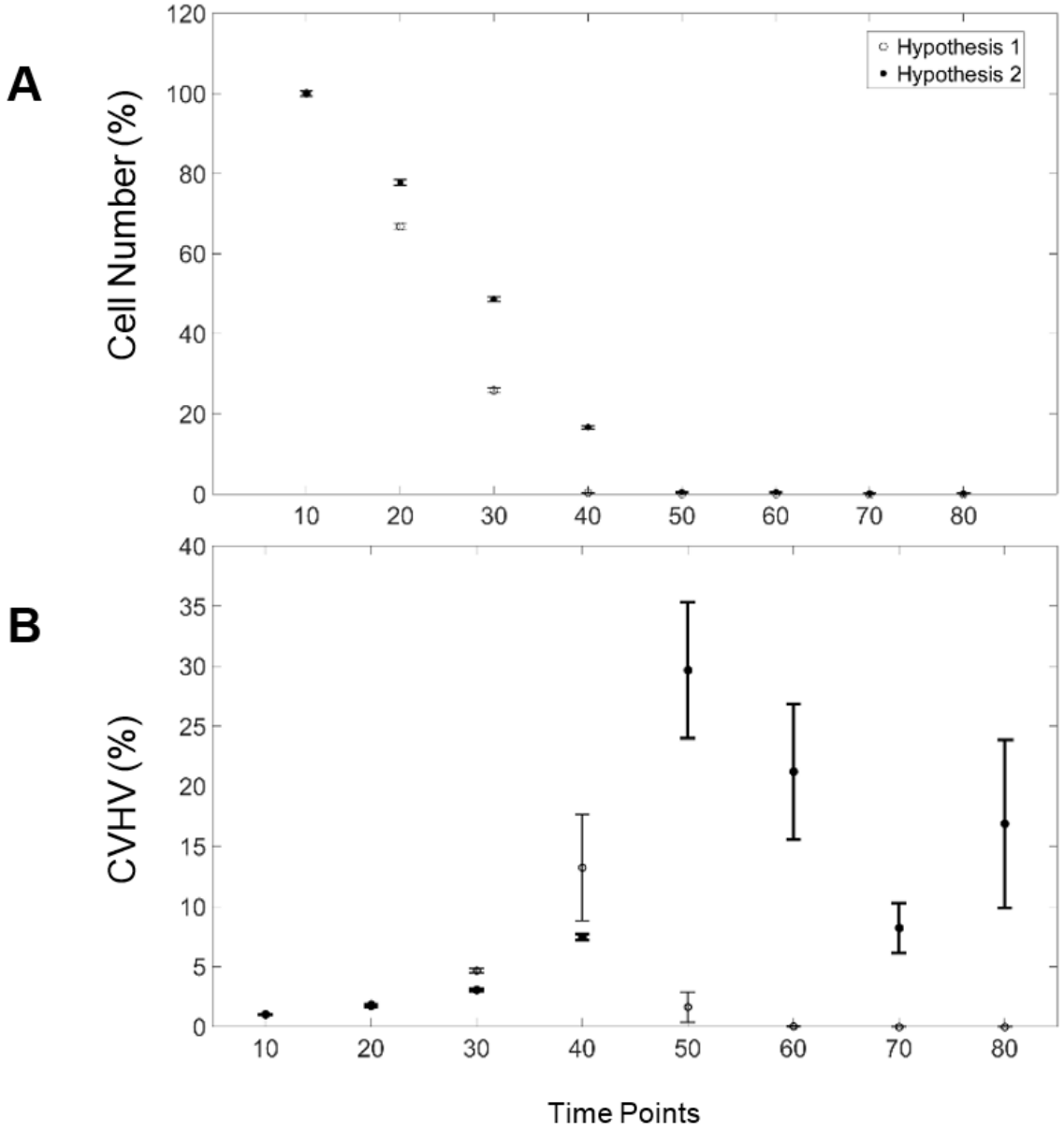

Figure 55: Computational model results (Mean ± SE) for (A) number of cells, and (B) CVHV for cells following the rules for Hypothesis 1 (open circles) and Hypothesis 2 (closed circles) for all 30 images of 2-D slices gathered from the 3D model at time points 10, 20, 30, 40, 50, 60, 70 and 80

different ($p < 0.001$). For both figures, as with the experimental cell numbers and corrected Voronoi centroids, we have normalized the values by the value observed at the first time point to focus in the trends.)

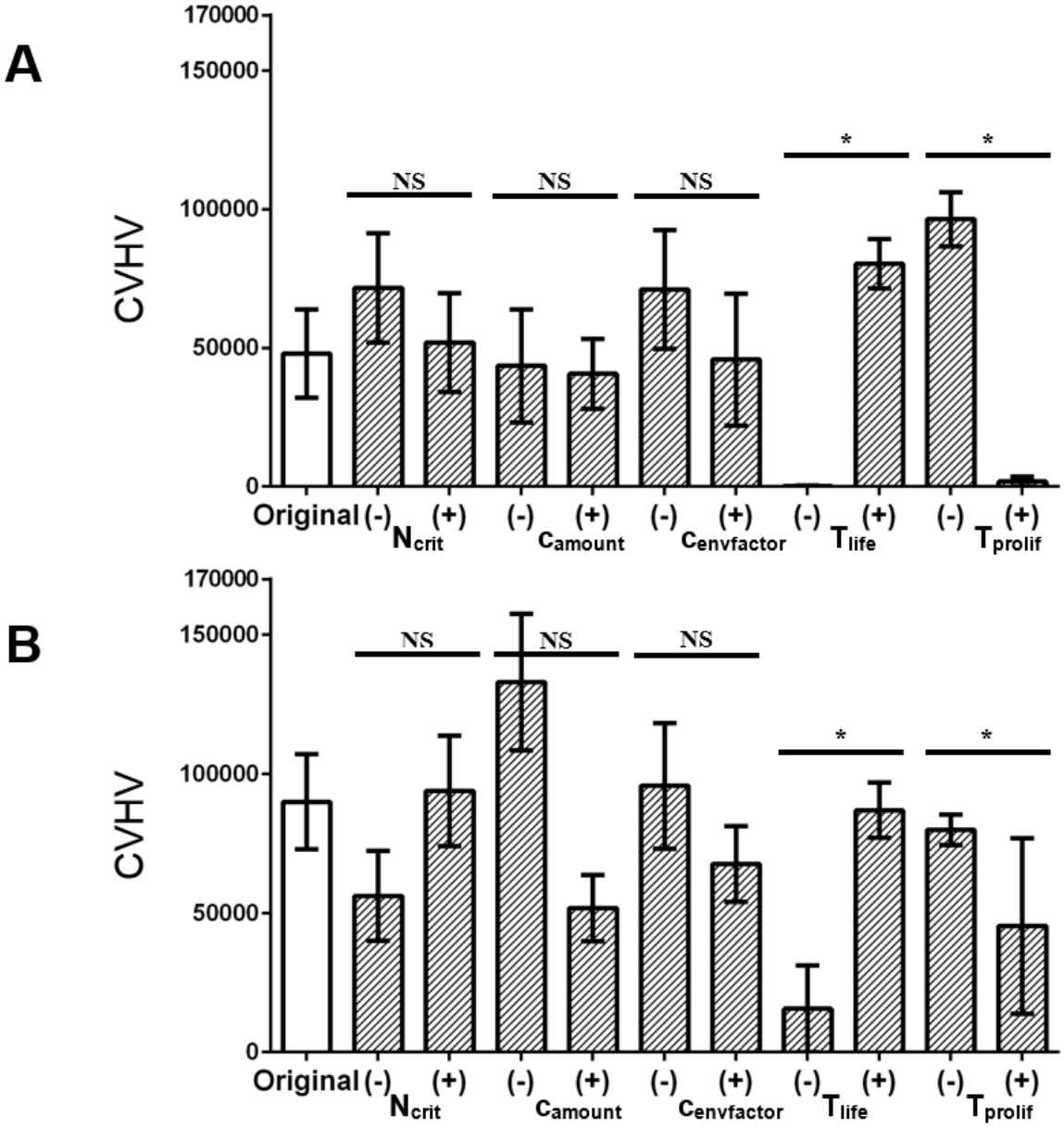

Figure 56: Sensitivity analysis of the model parameters expressed in terms of CVHV following (A) Hypothesis 1 measured at time point 40, and (B) Hypothesis 2 measured at time point 50

Cell numbers and CVHV are expressed as percentages of their respective values at the initial time point. At time point 10 under Hypothesis 1 there were 568.90 ± 4.24 engrafted cells with a CVHV value of $3.62 \pm 14 \times 10^3$, while for Hypothesis 2 there were 596.73 ± 4.76 engrafted cells with a CVHV value of $3.03 \pm 0.09 \times 10^3$. The sudden apparent increase in SE at time point 40 is due to the very low cell numbers at this point and beyond.

We show a sensitivity analysis in Figure 56 for the key parameters of the model under each of the two hypotheses, determined by increasing or decreasing each parameter in turn by 5 percent at the beginning of the simulation, and then measuring CVHV (see figure legend for details). We measure these values at time point 40 for Hypothesis 1 and time point 50 for Hypothesis 2, as these are time points at which we judged a dramatic drop in the number of engrafted cells in the original model as these are time points by which the initial cells must have engrafted and then proliferated or else have died, and thus variation to the model could theoretically have significant effects on its behavior. One-way ANOVA indicates that altering T_{life} and T_{prol} results in statistically significant changes to CVHV for the model under both Hypotheses, which is perhaps not surprisingly given that these are the two key parameters differentiating cellular behavior between the two Hypotheses. Altering the other parameters resulted in statistically insignificant changes to the CVHV value for either of the two Hypotheses.

The original CVHV value is shown at the far left. A, B, C, D and E show CVHV after increasing (+) and decreasing (-) the attachment probability (N_{crit}), the amount of collagen each cell adds to the environment (c_{amount}), the factor by which the cell lifetimes

or proliferation times are influenced by the environment ($c_{envfactor}$), the lifetime (T_{life}) and the proliferation time (T_{prol}), respectively, by 5%. NS indicates no significant change from control. * indicates statistically significant change from control.

6.4. Discussion

Stem cell research in the lung has gained considerable momentum recently with the advent of procedures for recellularizing decellularized lung scaffolds. Nevertheless, this research remains largely empirical with few predictive tools available to guide experimentation. As a start to filling this void we have developed a computational model for testing hypotheses about the rules that might govern cellular engraftment and proliferation on decellularized lung scaffolds. However, given the number and complexity of the cellular decisions that can potentially be made during this process, there is the potential for the number of plausible hypotheses to become so numerous that no one hypothesis can be supported by model predictions to the exclusion of all the others. Accordingly, in the present study we apply the model to a very simple experimental scenario about which the rules of cell behavior appear to be limited to local environmental factors, such as geometry and chemistry, determining the probabilities of engraftment, movement and death. Of course, this model is far from a completely accurate representation of the underlying physiology due to our current lack of knowledge about all the biological details, about which we are forced to make numerous assumptions. Once these assumptions are made we can calibrate the time scale of the model to actual time (e.g. the time scales of Fig 54 relative to Fig 52). Our intent here is

merely to capture what we believe to be the key aspects of real biological behavior in order to create a model that has useful predictive value in terms of the overall behavior of stem cell engraftment on lung scaffolds.

Both C10 cells and MSCs experience a progressive decline in cell numbers over the time course of the experiment (Fig 52A), so this observation alone does not suggest anything to distinguish the rules governing the behaviors of these two cells. Indeed, the almost complete disappearance of both cell types by the end of the 28 day suggests that the slice culture technique utilized in the present study may be insufficient to support appropriate long term recellularization, highlighting the need for continued investigation of alternative recellularization protocols and procedures. On the other hand, visual inspection of the way in which experimental cell distributions change suggested that there may be differences in the rules of behavior between the two cell types. These distributions suggest that the periphery of a slice of scaffold provides a different cellular environment compared to the scaffold center. We encode this environmental factor in the model by imposing a gradient in the concentration of a generic substrate that the cells are sensitive to, and thus that has the potential to cause the cells to make decisions that are influenced by their locations on the scaffold.

We codified differing tendencies in Hypothesis 1 versus Hypothesis 2, and then determined if the computational model would lead to qualitatively similar predictions based on the rules embodied in these hypotheses. The most straightforward manner in which to compare experiment to prediction is in terms of relative cell numbers. Although

having the same overall trends, the MSCs nevertheless decrease in number somewhat more precipitously than the C10s (Fig 52A). By including a greater tendency of cells to survive on regions of higher substrate concentration (Hypothesis 1) the model predicted similar differences in cell numbers (Fig 55A). These differences are difficult to appreciate simply from visual inspection of the model as time evolves (Fig 51), demonstrating that quantitative metrics are necessary in order to objectively test these hypotheses.

Cell numbers alone, however, give no information about the topographical details of the cell populations on the scaffold, yet these details appear to be critical to what distinguishes the two cell types. Accordingly, we devised an algorithm for calculating metrics related to cell topography. We wanted this algorithm to be robust, yet at the same time to be sensitive to the way in which the cells might be clumped together in groups versus being spread randomly over the scaffold. We felt that these requirements were best met by an algorithm that incorporates a spatially integrated measure of the local neighborhood surrounding each cell. Accordingly, we determined the centroid of the histogram of cell neighborhood areas, the CVHV (Figs 52B and 54B) because this uses all the information in the histogram to provide a quantity that is robust to noise. The cell neighborhoods themselves were determined using Voronoi tessellation, which produces a plan-filling set of tiles having centroid positions defined by each of the identified cells in the image, and thus provides an intuitively satisfactory way of defining each cell's territory. Nevertheless, the CVHV is still a relatively crude overall reflection of cellular spatial distribution. There are others we could potentially consider that contain more

information such as mean distance from some landmark, spatial frequency, or the distribution of distances between pairs of cells. Such metrics might be necessary to test hypotheses about cellular behavior that are more detailed than the two we consider in the present study.

The CVHV reveals a key distinction between the two experimental cell types. The CVHV values for C10s at later time points remain significantly higher relative to the initial CVHV values (Fig 52B). This same difference in CVHV was recapitulated in the model by Hypothesis 2 versus Hypothesis 1 (Fig 54B), supporting the notion that MSCs are more likely to proliferate on the regions of higher substrate concentration that are located toward the periphery of the scaffold as predicted by Hypothesis 1, while conversely the C10s are more inclined to survive on regions of higher substrate concentration as predicted by Hypothesis 2. These conclusions represent only the very beginning of an elucidation of the enormously complex set of rules governing how cells behave in a complex environment such as the decellularized lung scaffold. Nevertheless, they can now be considered notions that have stood up to the first level of scientific scrutiny, which provides direction for further mechanistic investigation. For example, we can now ask what the topographical substrate on the scaffold might be, the mechanisms by which C10s and MSCs respond to it, and potentially what might be manipulated on a scaffold to improve the success of recellularization.

Of course, these conclusions and the questions they generate are contingent upon the limitations of our computational model and of our experiments. Such limitations are

inevitably considerable given the biological complexities of an actual recellularization scenario, the current paucity of our knowledge about underlying mechanisms and biological parameters, and the need to make simplifications and approximations in the interests of computational tractability. For example, a decellularized scaffold is composed of a large number of extracellular and residual intracellular proteins and proteoglycans [13, 19], rather than a single functional substrate distributed as a linear gradient. Also, because sustained recellularization was ultimately unsuccessful in the experimental system employed in the present study, we consider here only the very initial events in the process, namely cellular attachment, movement and proliferation. Eventually the engrafted cells must differentiate if they are to successfully lead to a regenerated tissue, so our model will eventually have to incorporate these events into its rule set when suitable experimental data become available. It is also worth noting that there is still some degree of heterogeneity in the scaffold following decellularization. Studying cellular engraftment on homogeneously constructed artificial scaffolds might allow for more precise delineation of the rules of cellular behavior. On the other hand, the behavior itself might be fundamentally altered by an artificial environment so determining all the details of the rule sets required for a realistic agent-based model may eventually require a combination of both approaches. Our computational model thus represents a first step in the objective evaluation of sets of rules of cell governing the dynamic behavior of cells engrafted onto decellularized lung scaffolds. This complements other recent studies on the use of computational modeling to elucidate cellular behavior such as genetic

expression in individual stem cells [20, 21], the role of stem cells in tumor development and metastasis [22, 23], and embryogenesis in the pancreas [24].

In conclusion, we have developed an agent-based computational model of cell behavior following engraftment onto decellularized lung scaffold environments. The model suggests that MSCs tend to proliferate on areas of higher local concentrations of substrate when there is an increasing concentration gradient toward the periphery of the scaffold, but without affecting lifespan. In contrast, the model suggests that C10s proliferate uniformly everywhere, but are more likely to survive on areas of higher substrate concentration. It remains to be seen what the actual mechanisms are behind these behavioral rules, but they may suggest where to look.

6.5. Ethical Statement Regarding Animal Studies

All institutional and national guidelines for the care and use of laboratory animals were followed and approved by the appropriate institutional committees.

6.6 Acknowledgements

The authors thank Dino Sokocevic for his assistance in gathering experimental images. This work was supported by NIH grants R01 HL-124052, F31 EB-018215, RC4 HL-106625, R21 HL-087274 and R21 HL-094611.

6.7. References

1. Moran E. C., A. Dhal, D. Vyas, A. Lanas, S. Soker, and P. M. Baptista. Whole-organ bioengineering: current tales of modern alchemy. Transl. Res. 163: 259-267, 2014.

2. Badylak S. F., D. J. Weiss, A. Caplan, and P. Macchiarini. Engineered whole organs and complex tissues. Lancet. 379(9819):943-952, 2012.

3. Wagner D. E., R. W. Bonvillain, T. Jensen, E. D. Girard, B. A. Bunnell, C. M. Finck, A. M. Hoffman, and D. J. Weiss. Can stem cells be used to generate new lungs? Ex vivo lung bioengineering with decellularized whole lung scaffolds. Respirology. 18(6):895-911, 2013.

4. Calle E. A., M. Ghaedi, S. Sundaram, A. Sivarapatna, M. K. Tseng, and L. E. Niklason. Strategies for whole lung tissue engineering. IEEE Trans. Biomed. Eng. 61(5):1482-1496, 2014.

5. Caliari S. R. and B. A. Harley. Structural and biochemical modification of a collagen scaffold to selectively enhance MSC tenogenic, chondrogenic, and osteogenic differentiation. Adv. Healthc. Mater. 3: 1086-1096, 2014.

6. Kumar S., A. Das, and S. Sen. Extracellular matrix density promotes EMT by weakening cell-cell adhesions. Mol. Biosyst. 10: 838-850, 2014.

7. Chiacchio F., and M. Pennisi. Agent-based modeling of the immune system: NetLogo, a promising framework. Biomed. Res. Int. 2014: 907171, 2014.

8. Kaul H., and Y. Ventikos. Investigating biocomplexity through the agent-based paradigm. Brief. Bioinform. 16(1):137-152, 2015.

9. Brown B. N., I. M. Price, F. R. Toapanta, D. R. DeAlmeida, C. A. Wiley, T. M. Ross, T. D. Oury, and Y. Vodovotz. An agent-based model of inflammation and fibrosis following particulate exposure in the lung. Math. Biosci. 231: 186-196, 2011.

10. Pothen J. J., M. E. Poynter, and J. H. Bates. The inflammatory twitch as a general strategy for controlling the host response. J. Immunol. 190: 3510-3516, 2013.

11. Zhang, H., W. Hou, L. Henrot, S. Schnebert, M. Dumas, C. Heusele and J. Yang. "Modelling epidermis homoeostasis and psoriasis pathogenesis." J R Soc Interface 12(103), 2015.

12. Bayrak, E. S., H. Mehdizadeh, B. Akar, S. I. Somo, E. M. Brey and A. Cinar. Agent-based modeling of osteogenic differentiation of mesenchymal stem cells in porous biomaterials. Conf Proc IEEE Eng Med Biol Soc 2014: 2924-2927, 2014.

13. Bonenfant N. R., D. Sokocevic, D. E. Wagner, Z. D. Borg, M. J. Lathrop, Y. W. Lam, B. Deng, M. J. Desarno, T. Ashikaga, R. Loi, and D. J. Weiss. The effects of storage and sterilization on de-cellularized and re-cellularized whole lung. Biomaterials. 34(13):3231-3245, 2013,

14. Wallis J. M., Z. D. Borg, A. B. Daly, B. Deng, B. A. Ballif, G. B. Allen, D. M. Jaworski, and D. J. Weiss. Comparative assessment of detergent-based protocols for

mouse lung de-cellularization and re-cellularization tissue engineering - part C: Methods. 18(6):420-432, 2012.

15. Sokocevic, D., N. R. Bonenfant, D. E. Wagner, Z. D. Borg, M. J. Lathrop, Y. W. Lam, B. Deng, M. J. Desarno, T. Ashikaga, R. Loi, A. M. Hoffman and D. J. Weiss. The effect of age and emphysematous and fibrotic injury on the re-cellularization of de-cellularized lungs. Biomaterials 34(13): 3256-3269, 2013.

16. Sekiya I., B. L. Larson, J. R. Smith, R. Pochampally, J. G. Cui, and D. J. Prockop. Expansion of human adult stem cells from bone marrow stroma: conditions that maximize the yields of early progenitors and evaluate their quality. Stem Cells. 20(6):530-541, 2012.

17. Hodl I., J. Hodl, A. Worman, G. Singer, K. Besemer, and T. J. Battin. Voronoi tessellation captures very early clustering of single primary cells as induced by interactions in nascent biofilms. PLoS One. 6: e26368, 2011.

18. Prodanov D., N. Nagelkerke, and E. Marani. Spatial clustering analysis in neuroanatomy: applications of different approaches to motor nerve fiber distribution. J. Neurosci. Methods. 160: 93-108, 2007.

19. Gilpin S. E., J. P. Guyette, G. Gonzalez, X. Ren, J. M. Asara, D. J. Mathisen, J. P. Vacanti, and H. C. Ott. Perfusion decellularization of human and porcine lungs: bringing the matrix to clinical scale. J. Heart Lung Transplant. 33(3):298-308, 2014.

20. Przybilla, J., T. Rohlf, M. Loeffler, and J. Galle. Understanding epigenetic changes in aging stem cells--a computational model approach. Aging Cell. 13(2): 320-328, 2014.

21. Park, S. J., T. Umemoto, M. Saito-Adachi, Y. Shiratsuchi, M. Yamato, and K. Nakai. Computational promoter modeling identifies the modes of transcriptional regulation in hematopoietic stem cells. PLoS One. 9(4): e93853, 2014.

22. Norton, K. A. and A. S. Popel. An agent-based model of cancer stem cell initiated avascular tumour growth and metastasis: the effect of seeding frequency and location. J. R. Soc. Interface. 11(100): 20140640, 2014.

23. Jilkine, A. and R. N. Gutenkunst. Effect of dedifferentiation on time to mutation acquisition in stem cell-driven cancers. PLoS Comput. Biol. 10(3): e1003481, 2014.

24. Setty, Y. In-silico models of stem cell and developmental systems. Theor. Biol. Med. Model. 11:1, 2014.

CHAPTER 7: CONCLUSIONS AND FUTURE DIRECTIONS

In the studies presented in this thesis, agent-based modeling provided critical insight into the nature and behavior of the system. In all the instances mentioned below, the elucidated behavior could not have been easily predicted without the aid of computational simulation, and experimental exploration would have taken much time and effort.

For the twitch study, our model enabled us to take into account all of the allergic response's major cellular players and their most important behaviors with respect to each other and the environment, and showed that these interactions indeed result in twitch-like behavior—cycles of inflammation and subsequent repair that are dependent on the frequency of antigen stimulation. Furthermore, most attempts to change the nature of the response (such as knocking out key cell types, reducing the amount of chemical signals released and slowing key cell types) were unsuccessful, as they attenuated the magnitude of response but did not change the overall shape of the response. One exception of note was when the lifespan of activated pro-inflammatory cells (assumed to be chiefly composed of neutrophils and eosinophils) was extended, which resulted in a prolonged inflammatory response increased in magnitude that did not fully resolve to baseline. This increase in the inflammatory phase was further exacerbated when combined other alterations that on their own had not previously changed the response.

These observations fueled our subsequent experiments in mice to concretely test for implications of the twitch hypothesis to determine its experimental validity. We confirmed that continual antigen stimulation results in behavior consistent with the notion

of a twitch response with finite duration, as indicated by the trends in markers such as GM-CSF, total leukocytes and airway resistance. Furthermore, we found evidence of a refractory period, as seen in the recall responses in markers such as IL-5, total leukocytes and airway resistance. While not all of the markers demonstrate these two behaviors, within the 31 day window of the study we observe an early cytokine phase response that peaked at 3 days followed by an eosinophilic and lung tissue stiffness response that peaked at day 14. This was followed by a peak in leukocytes between days 14 and 21, followed by a late cytokine phase response and an airway resistance response that peaks at day 21.

For the stem cell study, we used agent-based modeling to create a simple experimental model of a decellularized lung scaffold environment to test how potential rules for stem cell behavior affect their seeding and engraftment patterns. We then matched these patterns against patterns in experimental scaffolds seeded with different types of progenitor cells, enabling us to generate hypotheses about the behavior for each progenitor cell type. Here we studied two cell types, C10 alveolar epithelial cells and mesenchymal stem cells (MSCs), that experience a similar drop in cell numbers following initial engraftment. By comparing them against engraftment patterns from our model's rule sets utilizing a parameter that provides information about the spatial distribution of these components, we were able to put forward the notion that C10s are more inclined to survive on regions of higher substrate, while MSCs are more likely to proliferate on regions of higher substrate.

Naturally, there are multiple means by which we could now extend these studies, but we focus on what the results indicate as intriguing avenues of exploration. For the twitch, our computational experiments in Chapter 4 indicate that the overall twitch behavior, including whether it is able to resolve to baseline, is determined by the behavior of what are assumed to be chiefly neutrophils and eosinophils. Though our current model provides insight into the generalized twitch response, it cannot provide insight into the precise dynamics of these individual components since they are lumped together into a single, pro-inflammatory cell type. Thus a natural next step would be to ungroup this lumped cell type into individual constituents, enabling us to individually account for both neutrophils and eosinophils and other potentially important cells such as the alveolar macrophage, which is proposed to have both pro-inflammatory and anti-inflammatory behavior. We could then test proposed rulesets for their behaviors to determine whether the dynamics mimic the trends indicated by experimental work in mice, including our own from Chapter 5.

This importance of pro-inflammatory cells also informed our direction for our proposed experiments. Within the 31 day window studied, we observed that by day 31 eosinophil levels had dropped but still remained elevated relative to baseline, while neutrophil levels remain elevated without evidence of a decline. To further understand the dynamics of these cellular responses *in vivo*, we could extend the study window to 60 days in order to observe whether both neutrophil and eosinophil levels eventually drop to baseline, or whether they remain elevated. These dynamics would provide further indication as to whether the twitch response behaves akin to skeletal muscle in allowing

individual twitch responses to summate, or whether it is akin to cardiac muscle where summation cannot occur. Extending the window would also enable us to test whether the eosinophil component has a refractory period longer than 28 days or whether it lacks refractory behavior altogether.

For the stem cell work, we have taken the first step in determining behavior for both C10s and MSCs by proposing potential behavior utilizing our agent-based model. A logical next step is thus to critically test these notions experimentally by determining how these cells behave in different environments. Of particular interest is the identity of the presumed substrate in our model, which we suggest is likely an extracellular matrix component or oxygen. To explore this further, we could place C10s and MSCs in artificial environments *in vitro*, such as a hydrogel with an ECM component such as fibrinogen or laminin, or gels with oxygen gas gradients across them. We could then observe the resulting behavior over time and compare it to a 2-D simulation of the models utilizing the proposed rule sets.

It is worth noting that these studies can be extended to address biomedical questions in other fields. For the stem cell work, this is perhaps most obvious in the potential to model other progenitor cell types and scaffold environments for other organs. For the twitch hypothesis, given its implications regarding the nature of chronic inflammatory conditions in general, we could extend it to study auto-immune diseases in other organ environments, where the defect involves the body becoming incorrectly primed to attack a component in the human body thereby resulting in continual antigen stimulation. Some of these diseases, such as multiple sclerosis in the central nervous

system and ulcerative colitis in the colon, have characteristic wax-and-wane behavior that may correlate to the cycles of damage and repair predicted by the twitch hypothesis.

Central to all of these studies is the agent-based modeling approach. By allowing us to take into account our understanding of the spatiotemporal dynamics of the biological systems involved, including cell-cell and cell-environment interactions, this form of computational modeling can help more rapidly determine the behavior of the lung (or any biological system) that might otherwise not be apparent. This enables us to vet multiple hypotheses prior to experimental work that is comparatively more costly in terms of time and resources in order to determine more promising avenues of research. Thus computational modeling, particularly agent-based modeling, has the potential to rapidly accelerate the rate at which we achieve important biomedical insights regarding organ structure and function and the underlying nature of pathophysiology of disease.

CHAPTER 8: BIBLIOGRAPHY

1. Abbas SMA. An agent-based model of the development of friendship links within Facebook. Computational and Mathematical Organization Theory 2013; 19.2: 232-252.

2. Ackerman E, Gatewood LC, Rosevear JW, Molnar GD. Concepts and Models of Biomathematics.Marcel Dekker; 1969. Blood glucose regulation and diabetes; pp. 131–56.

3. Ackerman E, Gatewood LC, Rosevear JW, Molnar GD. Model studies of blood glucose regulation. Bull Math Biophys. 1965;27:21–37.

4. Ackerman E, Rosevear JW, McGuckin WF. A mathematical model of the glucose tolerance test. Phys Med Biol. 1964;9:202–13.

5. Akdis CA. Therapies for allergic inflammation: refining strategies to induce tolerance. Nature medicine. 2012 May;18(5):736-49.

6. Alarcon T, Byrne HM, Maini PK. A cellular automaton model for tumour growth in inhomogeneous environment. J Theor Biol. 2003;225(2): 257–74.

7. Al-Husari M, Murdoch C, Webb SD. A cellular automaton model examining the effects of oxygen, hydrogen ions and lactate on early tumour growth. J Math Biol 2014; 69(4): 839-873.

8. Amini M, Wakolbinger T, Racer M, Nejad MG. Alternative supply chain production–sales policies for new product diffusion: An agent-based modeling and simulation approach. European Journal of Operational Research 2012; 216.2: 301-311.

9. An L. Modeling human decisions in coupled human and natural systems: review of agent-based models. Ecological Modelling 2012; 229: 25-36.

10. Anderson AR. A hybrid mathematical model of solid tumor invasion: the important of cell adhesion. Math Med Biol. 2005;22: 163–86.

11. Anderson AR, Weaver AM, Cummings PT, Quaranta V. Tumor morphology and phenotypic evolution driven by selective pressure from microenvironment. Cell. 2006;127(5): 905–15.

12. Arifin SM, Zhou Y, Davis GJ, Gentile JE, Madey GR, Collins FH. An agent-based model of the population dynamics of Anopheles gambiae. Malaria journal 2014; 13.1: 1-20.

13. Athale C, Mansury Y, Deisboeck TS. Simulating the impact of a molecular 'decision-process' on cellular phenotype and multicellular patterns in brain tumors. Journal of Theoretical Biology 2005; 233.4: 469-481.

14. Auricchio F, Conti M, Morganti S, Reali A. Simulation of transcatheter aortic valve implantation: a patient-specific finite element approach. Comput. Methods Biomech. Biomed. Eng. 2014; 17:1347–57.

15. Axelrod R. The dissemination of culture a model with local convergence and global polarization. Journal of Conflict Resolution 1997; 41.2: 203-226.

16. Badylak SF, Weiss DJ, Caplan A, Macchiarini P. Engineered whole organs and complex tissues. Lancet 2012; 379(9819):943-952.

17. Balhara J, Gounni AS. The alveolar macrophages in asthma: a double-edged sword. Mucosal Immunol 2012; 5: 605-609.

18. Bankhead A III, Heckendorn RB. Using evolvable genetic cellular automata to model breast cancer. Genet Program Evolvable Mach. 2007;8(4): 381–393.

19. Banks CM, Sokolowski JA. Modeling the Niger Delta Insurgency. The Social Science Journal 2010; 47.2: 271-293.

20. Barnes D, Chu D. Introduction to Modeling for Biosciences. London: Springer; c2010. Chapter 2: Agent-Based Modeling; p.15-77.

21. Barnes, PJ. Pathophysiology of allergic inflammation. Immunol Rev 2011; 242: 31-50.

22. Batchelor AM, Bartus K, Reynell C, Constantinou S, Halvey EJ, Held KF, Dostmann WR, Vernon J, Garthwaite J. Exquisite sensitivity to subsecond, picomolar nitric oxide transients conferred on cells by guanylyl cyclase-coupled receptors. Proc. Natl. Acad. Sci., 107 (2010), pp. 22060–22065.

23. Bates JH, Wagers SS, Norton RJ, Rinaldi LM, and Irvin CG. Exaggerated airway narrowing in mice treated with intratracheal cationic protein. J Appl Physiol 2006; 100: 500-506.

24. Bayrak, ES, Mehdizadeh H, Akar B, Somo SI, Brey EM, Cinar A. Agent-based modeling of osteogenic differentiation of mesenchymal stem cells in porous biomaterials. Conf Proc IEEE Eng Med Biol Soc 2014: 2924-2927.

25. Becher MA, Grimm V, Thorbek P, Horn J, Kennedy PJ, Osborne JL. BEEHAVE: a systems model of honeybee colony dynamics and foraging to explore multifactorial causes of colony failure. Journal of applied ecology 2014; 51.2: 470-482.

26. Beck A, Thubrikar M, Robicsek F. Stress analysis of the aortic valve with and without the sinuses of Valsalva. J. Heart Valve Dis. 2001; 10:1–11.

27. Becu N, Neef A, Schreinemachers P, Sangkapitux C. Participatory computer simulation to support collective decision-making: Potential and limits of stakeholder involvement. Land use policy 2008; 25.4: 498-509.

28. Beillas P, Papaioannou G, Tashman S, Yang KH. A new method to investigate in vivo knee behavior using a finite element model of the lower limb. Journal of Biomechanics. 2004;37(7):1019–1030.

29. Benenson I. Agent-based modeling: From individual residential choice to urban residential dynamics. Spatially Integrated Social Science 2004: 67-95.

30. Besier TF, Gold GE, Beaupré GS, Delp SL. A modeling framework to estimate patellofemoral joint cartilage stress in vivo. Medicine and Science in Sports and Exercise. 2005;37(11):1924–1930.

31. Besier TF, Gold GE, Delp SL, Fredericson M, Beaupré GS. The influence of femoral internal and external rotation on cartilage stresses within the patellofemoral joint. Journal of Orthopaedic Research.2008;26(12):1627–1635.

32. Billari FC Prskawetz A, Diaz BA, Fent T. The "Wedding-Ring": An agent-based marriage model based on social interaction. Demographic Research 2008; 17.3: 59-82.

33. Bohlmann, JD, Calantone RJ, Zhao M. The effects of market network heterogeneity on innovation diffusion: An agent-based modeling approach. Journal of Product Innovation Management 2010; 27.5: 741-760.

34. Bolie VW. Coefficients of normal blood glucose regulation. J Appl Physiol. 1961;16:783–8.

35. Bonenfant NR, Sokocevic D, Wagner DE, Borg ZD, Lathrop MJ, Lam YW, Deng B, Desarno MJ, Ashikaga T, Loi R, Weiss DJ. The effects of storage and sterilization on de-cellularized and re-cellularized whole lung. Biomaterials 2013; 34(13):3231-3245.

36. Brightman FA, Fell DA. Differential feedback regulation of the MAPK cascade underlies the quantitative differences in EGF and NGF signalling in PC12 cells. FEBS Lett. 2000;482:169–174.

37. Brown BN, Price IM, Toapanta FR, DeAlmeida DR, Wiley CA, Ross TM, Oury TD, Vodovotz Y. An agent-based model of inflammation and fibrosis following particulate exposure in the lung. Math Biosci. 2011 Jun;231(2):186-96.

38. Brown DG, Robinson DT. Effects of heterogeneity in residential preferences on an agent-based model of urban sprawl. Ecology and society 2006; 11.1: 46.

39. Brown DG, Page S, Riolo R, Zellner M, Rand W. Path dependence and the validation of agent-based spatial models of land use. International Journal of Geographical Information Science 2005; 19.2: 153-174.

40. Burke D, Dishowitz M, Sweetwyne M, Miedel E, Hankenson KD, Kelly DJ. The role of oxygen as a regulator of stem cell fate during fracture repair in TSP2-null mice. J Orthop Res 2013; 31(10): 1585-1596.

41. Cacciola G, Peters GW, Baaijens FP. A synthetic fiber-reinforced stentless heart valve. J. Biomech. 2000; 33:653–58.

42. Cacciola G, Peters GW, Schreurs PJ. A three-dimensional mechanical analysis of a stentless fibre reinforced aortic valve prosthesis. J. Biomech. 2000; 33:521–30.

43. Caliari SR, Harley BA. Structural and biochemical modification of a collagen scaffold to selectively enhance MSC tenogenic, chondrogenic, and osteogenic differentiation. Adv. Healthc. Mater 2014; 3: 1086-1096.

44. Calle EA, Ghaedi M, Sundaram S, Sivarapatna A, Tseng MK, Niklason LE. Strategies for whole lung tissue engineering. IEEE Trans. Biomed. Eng 2014; 61(5):1482-1496.

45. Campbell KC, Cooper WW Jr., Greenbaum DP, Wojcik LA. Modeling distributed human decision making in traffic flow management operations. Progress In Astronautics And Aeronautics 2001; 193: 227-238.

46. Campos D, Llebot JE, Méndez V. Limited resources and evolutionary learning may help to understand the mistimed reproduction in birds caused by climate change. Theoretical population biology 2008; 74.1: 16-21.

47. Capelli C, Bosi GM, Cerri E, Nordmeyer J, Odenwald T, Bonhoeffer P, Migliavacca F, Taylor AM, Schievano S. Patient-specific simulations of transcatheter aortic valve stent implantation. Med. Biol. Eng. Comput. 2012; 50:183–92.

48. Cataloglu A, Clark RE, Gould PL. Stress analysis of aortic valve leaflets with smoothed geometrical data. J. Biomech. 1977; 10:153–58.

49. Cataloglu A, Gould PL, Clark RE. Validation of a simplified mathematical model for the stress analysis of human aortic heart valves. J. Biomech. 1975; 8:347–48.

50. Cederman L. Endogenizing geopolitical boundaries with agent-based modeling. Proceedings of the National Academy of Sciences 2002; 99.suppl 3: 7296-7303.

51. Chand R, Haug E, Rim K. Stresses in the human knee joint. Journal of Biomechanics. 1976;9(6):417–422.

52. Chapa J, Bourgo RJ, Greene GL, Kulkarni S, An G. Examining the pathogenesis of breast cancer using a novel agent-based model of mammary ductal epithelium dynamics. PLoS One 2013; 8(5): e64091.

53. Chaturvedi AR, Dolk D, Chaturvedi R, Mulpuri M, Lengacher D, Mellema S, Poddar P, Foong C, Armstrong B. Understanding insurgency by using agent-based computational experimentation: Case study of Indonesia. Proceedings of the Agent 2005 Conference on Generative Social Processes, Models, and Mechanisms. 2005.

54. Chen J, Sprouffske K, Huang Q, Maley CC. Solving the puzzle of metastasis: the evolution of cell migration in neoplasms. PLoS One 2011; 6.4: e17933.

55. Chen, LL, Ulmer S, and Deisboeck TS. An agent-based model identifies MRI regions of probable tumor invasion in a patient with glioblastoma. Physics in medicine and biology 2009; 55.2: 329.

56. Chen WH, Toapanta FR, Shirey KA, Zhang L, Giannelou A, Page C, Frieman MB, Vogel SN, Cross AS. Potential role for alternatively activated macrophages in the secondary bacterial infection during recovery from influenza. Immunol Lett 2012; 141: 227-234.

57. Chen Y, Wang H, Zhang J, Chen K, Li Y. Simulation of avascular tumor growth by agent-based game model involving phenotype-phenotype interactions. Sci Rep 2015; 9:5:17992. Epub 2015 Dec 9.

58. Chiacchio F, Pennisi M. Agent-based modeling of the immune system: NetLogo, a promising framework. Biomed. Res. Int. 2014: 907171, 2014.

59. Cioffi-Revilla C, Luke S, Parker DC, Rogers D, Fitzhugh WW, Honeychurch W, Frohlich B, DePriest P, Amartuvshin C. Agent-based modeling simulation of social adaptation and long-term change in inner Asia. Advancing Social Simulation: The First World Congress. Springer Japan 2007.

60. Cioffi-Revilla C, Rouleau M. MASON RebeLand: An Agent-Based Model of Politics, Environment, and Insurgency. International Studies Review 2010; 12.1: 31-52.

61. Church MK, Hiroi J. Inhibition of IgE-dependent histamine release from human dispersed lung mast cells by anti-allergic drugs and salbutamol. British journal of pharmacology 1987 Feb;90(2):421-9.

62. Cojocaru A, Irvin CG, Haverkamp HC, Bates JH. Computational assessment of airway wall stiffness in vivo in allergically inflamed mouse models of asthma. J Appl Physiol 2008; 104(6): 1601-1610.

63. Collington, S. J., J. Hallgren, J. E. Pease, T. G. Jones, B. J. Rollins, J. Westwick, K. F. Austen, T. J. Williams, M. F. Gurish, and C. L. Weller. The role of the CCL2/CCR2 axis in mouse mast cell migration in vitro and in vivo. J Immunol 184: 6114-6123.

64. Conti C, Della Corte A, Votta E, Del Viscovo L, Bancone C, De Santo LS, Redaelli A. Biomechanical implications of the congenital bicuspid aortic valve: a finite element study of aortic root function from in vivo data. J. Thorac. Cardiovasc. Surg. 2010; 140:890-96.

65. Cruz J, Barahona P. An interval constraint approach to handle parametric ordinary differential equations for decision support, Online available from the World Wide Web: http://centria.di.fct.unl.pt/~pb/papers/cruz_ekdb99.pdf and http://centria.di.fct.unl.pt/~pb/papers/cruz_cp99.pdf.

66. Czaczkes TJ. How to not get stuck—Negative feedback due to crowding maintains flexibility in ant foraging. Journal of Theoretical Biology 2014; 360: 172-180.

67. d'Aquino P, August P, Balmann A, Berger T, Bousquet F, et al. Agent-based models of land-use and land-cover change. Proc. of an International Workshop. 2002.

68. Deadman P, Robinson D, Moran E. Colonist household decisionmaking and land-use change in the Amazon Rainforest: an agent-based simulation. Environment and Planning B: Planning and Design 2004; 31.5: 693-709.

69. DeKorte CJ. Current and emerging therapies for the management of chronic inflammation in asthma. Am J Health Syst Pharm. 2003 Oct 1;60(19):1949-59; quiz 60-1.

70. de Mul FF, Morales F, Smit AJ, Graaff R. A model for post-occlusive reactive hyperemia as measured with laser-Doppler perfusion monitoring. IEEE Trans Biomed Eng 2005; 52: 184–190.

71. Deshpande RS, Grayson WL, Spector AA. A Modeling Insight into Adipose-Derived Stem Cell Myogenesis. PLoS One 2015; 10(9): e0137918.

72. Devillers H, Lobry JR, Menu F. An agent-based model for predicting the prevalence of Trypanosoma cruzi I and II in their host and vector populations. Journal of Theoretical Biology 2008; 255.3: 307-315.

73. Dhaher YY, Kwon TH, Barry M. The effect of connective tissue material uncertainties on knee joint mechanics under isolated loading conditions. Journal of Biomechanics. 2010;43(16):3118–3125.

74. Dienz O, Rud JG, Eaton SM, Lanthier PA, Burg E, Drew A, Bunn J, Suratt BT, Haynes L, Rincon M. Essential role of IL-6 in protection against H1N1 influenza virus by promoting neutrophil survival in the lung. Mucosal Immunol 2012; 5: 258-266.

75. Dishion TJ. Stochastic Agent-Based Modeling of Influence and Selection in Adolescence: Current Status and Future Directions in Understanding the Dynamics of Peer Contagion. Journal of Research on Adolescence 2013; 23.3: 596-603.

76. Dixon DS. Preliminary results from an agent-based adaptation of friendship games. 86th Annual Conference of the Western Economics Association International. 2011.

77. Doherty, TA, Broide DH. Group 2 Innate Lymphoid Cells: New Players in Human Allergic Diseases. Journal of investigational allergology & clinical immunology 2015; 25.1: 1–11. Print.

78. Donahue TLH, Hull ML, Rashid MM, Jacobs CR. A finite element model of the human knee joint for the study of tibio-femoral contact. Journal of Biomechanical Engineering. 2002;124(3):273–280.

79. Du P, O'Grady G, Windsor JA, Cheng LK, Pullan AJ. A tissue framework for simulating the effects of gastric electrical stimulation and in vivo validation. IEEE Trans Biomed Eng. 2009;56:2755–2761.

80. Duca KA, Shapiro M, Delgado-Eckert E, Hadinoto V, Jarrah AS, Laubenbacher R, Lee K, Luzuriaga K, Polys NF, Thorley-Lawson DA. A virtual look at Epstein–Barr virus infection: biological interpretations. PLoS Pathog 2007; 3.10: e137.

81. Ekoff M, Nilsson G. Mast cell apoptosis and survival. Adv Exp Med Biol 2011; 716: 47-60.

82. Enderling H, Anderson ARA, Chaplain MAJ, Beheshti A, Hlatky L, Hahnfeldt P. Paradoxical dependencies of tumor dormancy and progression on basic cell kinetics. Cancer Res. 2009;69:8814–8821. doi: 10.1158/0008-5472.CAN-09-2115.

83. Engel C, Scholz M, Loeffler M. A computational model of human granulopoiesis to simulate the hematotoxic effects of multicycle polychemotherapy. Blood. 2004;104:2323–2331.

84. Epstein JM. Modeling civil violence: An agent-based computational approach. Proceedings of the National Academy of Sciences 2002; 99.suppl 3: 7243-7250.

85. Escobar E, Durgham R, Dammann O, Stopka TJ. Agent-based computational model of the prevalence of gonococcal infections after the implementation of HIV pre-exposure prophylaxis guidelines. Online Journal of Public Health Informatics 2015; 7.3.

86. Feuerstein GZ, Chavez J. Translational medicine for stroke drug discovery: the pharmaceutical industry perspective. Stroke 2009; 40(3 Suppl): S121-125.

87. Filatova OA, Miller PJO. An agent-based model of dialect evolution in killer whales. Journal of Theoretical Biology 2015; 373: 82-91.

88. Fioretti G. Agent-based simulation models in organization science. Organizational Research Methods 2013; 16.2: 227-242.

89. Flammiger A, Fiedler W, Bacher U, Bokemeyer C, Schneider M, Binder M. Critical imbalance of TNF-alpha and soluble TNF receptor 1 in a patient with macrophage activation syndrome: potential implications for diagnostics and treatment. Acta Haematol 2012; 128: 69-72.

90. Fontaine CM, Rounsevell MDA. An agent-based approach to model future residential pressure on a regional landscape. Landscape Ecology 2009; 24.9: 1237-1254.

91. Fox, BM, Moffitt RA, Wang MD. An agent-based stochastic tumor model for predicting mitotic arrest drug response. Engineering in Medicine and Biology Society, 2008. EMBS 2008. 30th Annual International Conference of the IEEE. IEEE, 2008.

92. Franz M, Schülke O, Ostner J. Rapid evolution of cooperation in group-living animals. BMC Evolutionary Biology 2013; 13.1: 235.

93. Franz M, van der Post D, Schülke O, Ostner J. The evolution of cooperative turn-taking in animal conflict. BMC Evolutionary Biology 2011; 11.1: 1.

94. Fuchs B, Sjoberg L, Moller Westerberg C, Ekoff M, Swedin L, Dahlen SE, et al. Mast cell engraftment of the peripheral lung enhances airway hyperresponsiveness in a mouse asthma model. Am J Physiol Lung Cell Mol Physiol. 2012 Dec 15;303(12):L1027-36.

95. Gajewska BU., Wiley RE, Jordana M. GM-CSF and dendritic cells in allergic airway inflammation: basic mechanisms and prospects for therapeutic intervention. Curr Drug Targets Inflamm Allergy 2003; 2(4): 279-292.

96. Galie P, Spilker RL.. A two-dimensional computational model of lymph transport across primary lymphatic valves. J Biomech Eng 2009; 131(11): 111004.

97. Galla T. Independence and interdependence in the nest-site choice by honeybee swarms: agent-based models, analytical approaches and pattern formation. Journal of Theoretical Biology 2010; 262.1: 186-196.

98. Gao J, Du P, O'Grady G, Archer R, Gibbons SJ, Farrugia G, Cheng LK. Cellular automaton model for simulating tissue-specific intestinal electrophysiological activity. Conf Proc IEEE Eng Med Biol Soc 2013: 5537-5540.

99. Garcia R. Uses of agent-based modeling in innovation/new product development research. Journal of Product Innovation Management 2005; 22.5: 380-398.

100. Garcia R, Jager W. From the Special Issue Editors: Agent-Based Modeling of Innovation Diffusion. Journal of Product Innovation Management 2011; 28.2: 148-151.

101. Garrison LA, Babcock DS. Alcohol consumption among college students: An agent-based computational simulation. Complexity 2009; 14.6: 35-44.

102. Gaston ME, desJardins M. Agent-organized networks for dynamic team formation. Proceedings of the fourth international joint conference on Autonomous agents and multiagent systems. ACM, 2005.

103. Geller A, Alam SJ. A Socio-Political and-Cultural Model of the War in Afghanistan. International Studies Review 2010; 12.1: 8-30.

104. Gevertz JL, Gillies GT, Torquato S. Simulating tumor growth in confined heterogeneous environments. Phys Biol. 2008;5: 036010.

105. Gevertz JL, Torquato S. Growing heterogeneous tumors in silico. Phys Rev E Stat Nonlin Soft Matter Phys. 2009;80: 051910.

106. Gevertz JL, Torquato S. Modeling the effects of vasculature evolution on early brain tumor growth. J Theor Biol 2006; 243(4): 517-531.

107. Giabbanelli P, Crutzen R. An agent-based social network model of binge drinking among Dutch adults. Journal of Artificial Societies and Social Simulation 2013; 16.2: 10.

108. Gilbert, N. Agent-Based Models. London: SAGE Publications; c2007. Chapter 1: The Idea of Agent-Based Modeling; p.1-20.

109. Gilpin SE, Guyette JP, Gonzalez G, Ren X, Asara JM, Mathisen DJ, Vacanti JP, Ott HC. Perfusion decellularization of human and porcine lungs: bringing the matrix to clinical scale. J. Heart Lung Transplant 2014; 33(3):298-308.

110. González PP, Cárdenas M, Gershenson C, Lagunez J. Advances in Systems Science: Measurement. Athens, Greece: Circuits and Control, WSES Press; 2001. Integration of computational techniques for the modelling of signal transduction; pp. 400–411.

111. Gotteland C, McFerrin BM, Zhao X, Gilot-Fromont E, Lélu M. Agricultural landscape and spatial distribution of Toxoplasma gondii in rural environment: an agent-based model. International journal of health geographics 2014; 13.1: 1.

112. Gotts NM, Polhill JG, Law ANR. Agent-based simulation in the study of social dilemmas. Artificial Intelligence Review 2003; 19.1: 3-92.

113. Gould PL, Cataloglu A. Stress analysis of the human aortic valve. Comput. Struct. 1973; 3:377–78, IN1–2, 379–84.

114. Grande-Allen K, Cochran R, Reinhall P, Kunzelman K. Finite-element analysis of aortic valvesparing: influence of graft shape and stiffness. IEEE Trans. Biomed. Eng. 2001; 48:647–59.

115. Grande KJ, Cochran RP, Reinhall PG, Kunzelman KS. Mechanisms of aortic valve incompetence: finite element modeling of aortic root dilatation. Ann. Thorac. Surg. 2000; 69:1851–5.

116. Grande-Allen KJ, Cochran RP, Reinhall PG, Kunzelman KS. Mechanisms of aortic valve incompetence: finite-element modeling of Marfan syndrome. J. Thorac. Cardiovasc. Surg. 2001; 122:946–54.

117. Groner ML, Cox R, Gettinby G, Revie CW. Use of agent-based modelling to predict benefits of cleaner fish in controlling sea lice, Lepeophtheirus salmonis, infestations on farmed Atlantic salmon, Salmo salar L. Journal of Fish Diseases 2013; 36.3: 195-208.

118. Grueter C, Schürch R, Czaczkes TJ, Taylor K, Durance T, Jones SM. Negative feedback enables fast and flexible collective decision-making in ants. PLoS One 2012; 7.9: e44501.

119. Günther M, Stummer C, Wakolbinger LM, Wildpaner M. An agent-based simulation approach for the new product diffusion of a novel biomass fuel. Agent-Based Modeling and Simulation. Palgrave Macmillan UK, 2014. 61-77.

120. Guzy MR, Smith CL, Bolte JP, Hulse DW, Gregory SV. Policy research using agent-based modeling to assess future impacts of urban expansion into farmlands and forests. Ecology and Society 2008; 13.1: 37.

121. Haczku A, Cao Y, Vass G, Kierstein S, Nath P, Atochina-Vasserman EN, Scanlon ST, Li L, Griswold DE, Chung KF, Poulain FR, Hawgood S, Beers MF, Crouch EC. IL-4 and IL-13 form a negative feedback circuit with surfactant protein-D in the allergic airway response. J Immunol 2006; 176: 3557-3565.

122. Hailegiorgis AB, Balan GC, Bassett JK, Gulden T, Kennedy WG. An agent based model of climate change and conflict among pastoralists in East Africa. Proceedings of the International Congress on Environmental Modeling and Software. 2010.

123. Hale LP, Kant EP, Greer PK, Foster WM. Iron supplementation decreases severity of allergic inflammation in murine lung. PLoS One. 2012;7(9):e45667.

124. Hantos Z, Daroczy B, Suki B, Nagy S, Fredberg JJ. Input impedance and peripheral inhomogeneity of dog lungs. J Appl Physiol 1992; 72: 168-178.

125. Hallett JM, Leitch AE, Riley NA, Duffin R, Haslett C, Rossi AG. Novel pharmacological strategies for driving inflammatory cell apoptosis and enhancing the resolution of inflammation. Trends Pharmacol Sci 2008; 29(5): 250-257.

126. Hammad H, Lambrecht BN. Dendritic cells and airway epithelial cells at the interface between innate and adaptive immune responses. Allergy 2011; 66: 579-587.

127. Hamill L, Gilbert N. A simple but more realistic agent-based model of a social network. Conf. European Social Simulation Assoc. 2008.

128. Hamill L, Gilbert N. Social circles: A simple structure for agent-based social network models. Journal of Artificial Societies and Social Simulation 2009; 12.2: 3.

129. Hao Z, Jin D, Zhang Y, Zhang J. A finite element 3D model of in vivo human knee joint based on MRI for the tibiofemoral joint contact analysis. Proceedings of the 1st international conference on Digital human modeling 2007; Beijing, China. pp. 616–622.

130. Hassan S, Salgado M, Pavon J. Friends forever: Social relationships with a fuzzy agent-based model. Hybrid Artificial Intelligence Systems. Springer Berlin Heidelberg 2008. 523-532.

131. Hastings RH, Folkesson HG, Matthay MA. Mechanisms of alveolar protein clearance in the intact lung. Am J Physiol Lung Cell Mol Physiol. 2004 Apr;286(4):L679-89.

132. Haut Donahue TL, Hull ML, Rashid MM, Jacobs CR. How the stiffness of meniscal attachments and meniscal material properties affect tibio-femoral contact pressure computed using a validated finite element model of the human knee joint. Journal of Biomechanics 2003;36(1):19–34.

133. Havas KA, Boone RB, Hill AE, Salman MD. A Brucellosis Disease Control Strategy for the Kakheti Region of the Country of Georgia: An Agent-Based Model. Zoonoses and Public Health 2014; 61.4: 260-270.

134. Heegaard J, Leyvraz PF, Curnier A, Rakotomananaa L, Huiskes R. The biomechanics of the human patella during passive knee flexion. Journal of Biomechanics. 1995;28(11):1265–1279.

135. Helbing, Dirk, ed. Social self-organization: Agent-based simulations and experiments to study emergent social behavior. Springer, 2012.

136. Heppenstall, AJ, Crooks AT, See LM, Batty M, eds. Agent-based models of geographical systems. Springer Science & Business Media; 2011.

137. Hodl I, Hodl J, Worman A, Singer G, Besemer K, Battin TJ. Voronoi tessellation captures very early clustering of single primary cells as induced by interactions in nascent biofilms. PLoS One 2011; 6: e26368.

138. Holgate, S. Mediator and Cytokine Mechanisms in Asthma. Thorax 1993; 48.2: 103–109. Print.

139. Hosseinali F, Alesheikh AA, Nourian F. Agent-based modeling of urban land-use development, case study: Simulating future scenarios of Qazvin city. Cities 2013; 31: 105-113.

140. Huang L, Huang Y, Wang Q, Xiao N, Yi D, Yu W, Qiu D. An agent-based model for control strategies of Echinococcus granulosus. Veterinary Parasitology 2011; 179.1: 84-91.

141. Hui C, Goldberg M, Magdon-Ismail M, Wallace WA. Simulating the diffusion of information: An agent-based modeling approach. International Journal of Agent Technologies and Systems 2010; 2.3: 31-46.

142. Ilmarinen P, Kankaanranta H. Eosinophil apoptosis as a therapeutic target in allergic asthma. Basic Clin Pharmacol Toxicol 2014; 114: 109-117.

143. Islam, SA, Luster AD. T cell homing to epithelial barriers in allergic disease. Nat Med 2012; 18: 705-715.

144. Jackson D, Holcombe M, Ratnieks F. Coupled computational simulation and empirical research into the foraging system of Pharaoh's ant (Monomorium pharaonis). Biosystems 2004; 76.1: 101-112.

145. Janssen-Heininger, YM, Poynter ME, Aesif SW, Pantano C, Ather JL, Reynaert NL, Ckless K, Anathy V, van der Velden J, Irvin CG, van der Vliet A. Nuclear factor kappaB, airway epithelium, and asthma: avenues for redox control. Proc Am Thorac Soc 2009; 6: 249-255.

146. Jermihov PN, Jia L, Sacks MS, Gorman RC, Gorman JH III, Chandran KB. Effect of geometry on the leaflet stresses in simulated models of congenital bicuspid aortic valves. Cardiovasc. Eng. Technol. 2011; 2:48–56.

147. Jiang B, Gimblett HR. An agent-based approach to environmental and urban systems within geographic information systems. Integrating Geographic Information Systems and Agent-based Modeling Techniques for Simulating Social and Ecological Processes 2002; 171-189.

148. Jilkine, A, Gutenkunst RN. Effect of dedifferentiation on time to mutation acquisition in stem cell-driven cancers. PLoS Comput. Biol. 2014; 10(3): e1003481.

149. Jjumba A, Dragićević S. High resolution urban land-use change modeling: Agent iCity approach. Applied Spatial Analysis and Policy 2012; 5.4: 291-315.

150. Johnson BR. Pattern formation on the combs of honeybees: increasing fitness by coupling self-organization with templates. Proceedings of the Royal Society of London B: Biological Sciences 2009; 276.1655: 255-261.

151. Johnson MD, McIntyre CC. Quantifying the neural elements activated and inhibited by globus pallidus deep brain stimulation J. Neurophysiol 2008; 100 2549–63.

152. Kabbur, PM, Carson WFT, Guernsey L, Secor ER Jr., Thrall RS, Schramm CM. Interleukin-10 does not mediate inhalational tolerance in a chronic model of ovalbumin-induced allergic airway disease. Cell Immunol 2006; 239: 67-74.

153. Kang HT, Lee HI, Hwang ES. Nicotinamide extends replicative lifespan of human cells. Aging Cell 2006; 5: 423-436.

154. Kansal AR, Torquato S, Chiocca EA, Deisboeck TS. Emergence of a subpopulation in a computational model of tumor growth. J Theor Biol. 2000;207(3): 431–41.

155. Kansal AR, Torquato S, Harsh GR IV, Chiocca EA, Deisboeck TS. Simulated brain tumor growth using a three-dimensional cellular automaton. J Theor Biol. 2000;203(4): 367–82.

156. Karsai I, Phillips MD. Regulation of task differentiation in wasp societies: A bottom-up model of the "common stomach". Journal of Theoretical Biology 2012; 294: 98-113.

157. Katayama S, Umetani N, Hisada T, Sugiura S. Bicuspid aortic valves undergo excessive strain during opening: a simulation study. J. Thorac. Cardiovasc. Surg. 2013; 145:1570–76.

158. Kaul H, Ventikos Y. Investigating biocomplexity through the agent-based paradigm. Brief. Bioinform. 2015; 16(1):137-152.

159. Keller JP, Desouza KC, Lin Y. Dismantling terrorist networks: Evaluating strategic options using agent-based modeling. Technological Forecasting and Social Change 2010; 77.7: 1014-1036.

160. Kennedy WG, Hailegiorgis AB, Rouleau M, Bassett JK, Coletti M, Balan BC, Gulden T. An agent-based model of conflict in East Africa and the effect of watering holes. Proceedings of the 19th Conference on Behavior Representation in Modeling and Simulation. 2010.

161. Kholodenko BN, Demin OV, Moehren G, Hoek JB. Quantification of short term signaling by the epidermal growth factor receptor. J. Biol. Chem. 1999;274:30169–30181.

162. Kiesling E, Günther M, Stummer C, Wakolbinger L. Agent-based simulation of innovation diffusion: a review. Central European Journal of Operations Research 2012; 20.2: 183-230.

163. Kim D, Batty M. Modeling Urban Growth: An Agent Based Microeconomic Approach to Urban Dynamics and Spatial Policy Simulation. Vol. 165. Working Paper Series, 2011.

164. Kitawaki T, Kadowaki N, Sugimoto N, Kambe N, Hori T, Miyachi Y, Nakahata T, Uchiyama T. IgE-activated mast cells in combination with pro-inflammatory factors induce Th2-promoting dendritic cells. International Immunology 2006; 18: 1789-1799.

165. Klatt J, Marsella S, Krämer NC. Negotiations in the context of AIDS prevention: an agent-based model using theory of mind. Intelligent virtual agents. Springer Berlin Heidelberg, 2011.

166. Kleinstreuer N, Dix D, Rountree M, Baker N, Sipes N, Reif D, Spencer R, Knudsen T. A computational model predicting disruption of blood vessel development. PLoS Comput Biol 2013; 9(4): e1002996.

167. Ko TH, Berry NM. Agent-based modeling with social networks for terrorist recruitment. AAAI. 2004.

168. Korobow A, Johnson C, Axtell R. An agent–based model of tax compliance with social networks. National Tax Journal 2007: 589-610.

169. Kowalska-Pyzalska A, Maciejowska K, Sznajd-Weron K, Weron R. Going Green: Agent-based modeling of the diffusion of dynamic electricity tariffs. No. HSC/13/05. Hugo Steinhaus Center, Wroclaw University of Technology, 2013.

170. Krepkin K, Costa J. Defining the role of cooperation in early tumor progression. Journal of Theoretical Biology 2011; 285.1: 36-45.

171. Krinner A, Roeder I, Loeffler M, Scholz M. Merging concepts - coupling an agent-based model of hematopoietic stem cells with an ODE model of granulopoiesis. BMC Syst Biol 2013; 7: 117.

172. Krucinski S, Vesely I, Dokainish MA, Campbell G. Numerical simulation of leaflet flexure in bioprosthetic valves mounted on rigid and expansile stents. J. Biomech. 1993; 26:929–43.

173. Kuandykov L, Sokolov M. Impact of social neighborhood on diffusion of innovation S-curve. Decision Support Systems 2010; 48.4: 531-535.

174. Kumar S, Das A, Sen S. Extracellular matrix density promotes EMT by weakening cell-cell adhesions. Mol. Biosyst. 2014; 10: 838-850.

175. Kuznar LA, Frederick W. Simulating the effect of nepotism on political risk taking and social unrest. Computational and Mathematical Organization Theory 2007; 13.1: 29-37.

176. Kuznar LA, Sedlmeyer R. Collective violence in Darfur: An agent-based model of pastoral nomad/sedentary peasant interaction. Human Complex Systems 2005; 1(4).

177. Labrosse MR, Boodhwani M, Sohmer B, Beller CJ. Modeling leaflet correction techniques in aortic valve repair: a finite element study. J. Biomech. 2011; 44:2292–98.

178. Laciana CE, Rovere SL. Ising-like agent-based technology diffusion model: Adoption patterns vs. seeding strategies. Physica A: Statistical Mechanics and its Applications 2011; 390.6: 1139-1149.

179. Lambrecht BN, Hammad H. The airway epithelium in asthma. Nat Med 2012; 18: 684-692.

180. Lammers WJEP, Al-Bloushi HM, Al-Eisaei SA, Al-Dhaheri FA, Stephen B, John R, Dhanasekaran S, Karam SM. Slow wave propagation and plasticity of interstitial cells of Cajal in the small intestine of diabetic rats. Exp Physiol. 2011;96:1039–1048.

181. Le QB, Seidl R, Scholz RW. Feedback loops and types of adaptation in the modelling of land-use decisions in an agent-based simulation. Environmental Modelling & Software 2012; 27: 83-96.

182. Lee BY, Bedford VL, Roberts MS, Carley KM. Virtual epidemic in a virtual city: simulating the spread of influenza in a US metropolitan area. Translational Research 2008; 151.6: 275-287.

183. Lemos C, Coelho H, Lopes RJ. Agent-based Modeling of Social Conflict, Civil Violence and Revolution: State-of-the-art-review and Further Prospects. EUMAS. 2013.

184. Ligmann-Zielinska A, Jankowski P. Exploring normative scenarios of land use development decisions with an agent-based simulation laboratory. Computers, Environment and Urban Systems 2010; 34.5: 409-423.

185. Ligmann-Zielinska A, Sun L. Applying time-dependent variance-based global sensitivity analysis to represent the dynamics of an agent-based model of land use change. International Journal of Geographical Information Science 2010; 24.12: 1829-1850.

186. Lim K, Deadman PJ, Moran E, Brondizio E, McCracken S. Agent-based simulations of household decision making and land use change near Altamira, Brazil. Integrating Geographic Information Systems and Agent-Based Modeling: Techniques for Simulating Social and Ecological Processes 2002: 277-310.

187. Lin S, DeVisser MH, Messina JP. An agent-based model to simulate tsetse fly distribution and control techniques: A case study in Nguruman, Kenya. Ecological Modelling 2015; 314: 80-89.

188. Lin Y, Abaid N. Modeling perspectives on echolocation strategies inspired by bats flying in groups. Journal of Theoretical Biology 2015; 387: 46-53.

189. Lotem A, Biran-Yoeli I. Evolution of learning and levels of selection: A lesson from avian parent–offspring communication. Theoretical Population Biology 2014; 91: 58-74.

190. Louis R, Schleich F, Barnes PJ. Corticosteroids: still at the frontline in asthma treatment? Clin Chest Med. 2012 Sep;33(3):531-41.

191. Lustick IS. Agent-based modelling of collective identity: testing constructivist theory. Journal of Artificial Societies and Social Simulation 2000; 3.1: 1.

192. Lustick I. PS-I: A user-friendly agent-based modeling platform for testing theories of political identity and political stability. Journal of Artificial Societies and Social Simulation 2002; 5.3.

193. Mach R, Schweitzer F. Modeling vortex swarming in daphnia. Bulletin of mathematical biology 2007; 69.2: 539-562.

194. Macklin P, Edgerton ME, Thompson AM, Cristini V. Patient-calibrated agent-based modelling of ductal carcinoma in situ (DCIS): from microscopic measurements to macroscopic predictions of clinical progression. Journal of Theoretical Biology 2012; 301: 122-140.

195. Madey G, Gao Y, Freeh V, Tynan R, Hoffman C. Agent-based modeling and simulation of collaborative social networks. AMCIS 2003 Proceedings: 237.

196. Manore CA, Hickmann KS, Hyman JM, Foppa IM, Davis JK, Wesson DM, Mores CN.. A network-patch methodology for adapting agent-based models for directly transmitted disease to mosquito-borne disease. Journal of Biological Dynamics 2015; 9.1: 52-72.

197. Manson SM. Agent-based modeling and genetic programming for modeling land change in the Southern Yucatan Peninsular Region of Mexico. Agriculture, Ecosystems & Environment 2005; 111.1: 47-62.

198. Manson SM, Evans T. Agent-based modeling of deforestation in southern Yucatán, Mexico, and reforestation in the Midwest United States. Proceedings of the National Academy of Sciences 2007; 104.52: 20678-20683.

199. Mansury Y, Deisboeck TS. The impact of "search precision" in an agent-based tumor model. Journal of Theoretical Biology 2003; 224.3: 325-337.

200. Mansury Y, Kimura M, Lobo J, Deisboeck TS. Emerging patterns in tumor systems: simulating the dynamics of multicellular clusters with an agent-based spatial agglomeration model. Journal of Theoretical Biology 2002; 219.3: 343-370.

201. Marsella SC, Pynadath DV, Read SJ. PsychSim: Agent-based modeling of social interactions and influence. Proceedings of the international conference on cognitive modeling. Vol. 36. 2004.

202. Martin C, Sun W. Simulation of long-term fatigue damage in bioprosthetic heart valves: effect of leaflet and stent elastic properties. Biomech. Model. Mechanobiol. 2013; doi: 10.1007/s10237-013-0532-x.

203. Martin KS, Blemker SS, Peirce SM. Agent-based computational model investigates muscle-specific responses to disuse-induced atrophy. Journal of Applied Physiology 2015; 118(10): 1299-1309.

204. Masoudi-Nejad A, Bidkhori G, Hosseini Ashtiani S, Najafi A, Bozorgmehr JH, Wang E. Cancer systems biology and modeling: Microscopic scale and multiscale approaches. Seminars in cancer biology. Vol. 30. Academic Press, 2015.

205. Masuda N, O'shea-Wheller TA, Doran C, Franks NR. Computational model of collective nest selection by ants with heterogeneous acceptance thresholds. Royal Society open science 2015; 2.6: 140533.

206. Maynard CL, Weaver CT. Diversity in the Contribution of IL-10 to T-Cell-Mediated Immune Regulation. Immunological Reviews 2008; 226: 219–233. PMC. Web. 18 Sept. 2015.

207. McCreesh N, Booth M. The effect of simulating different intermediate host snail species on the link between water temperature and schistosomiasis risk. PloS One 2014; 9.7: e87892.

208. McCreesh N, Nikulin G, Booth M. Predicting the effects of climate change on Schistosoma mansoni transmission in eastern Africa. Parasites & Vectors 2015; 8.1: 1-9.

209. McIntyre CC, Grill WM, Sherman DL, Thakor NV. Cellular effects of deep brain stimulation: model-based analysis of activation and inhibition J. Neurophysiol 2004; 91 1457–69.

210. McKinley L, Kim J, Bolgos GL, Siddiqui J, Remick DG. CXC chemokines modulate IgE secretion and pulmonary inflammation in a model of allergic asthma. Cytokine 2015; 32(3-4): 178-185.

211. Mesfar W, Shirazi-Adl A. Biomechanics of the knee joint in flexion under various quadriceps forces. Knee. 2005;12(6):424–434.

212. Millington J, Romero-Calcerrada R, Wainwright J, Perry G. An agent-based model of Mediterranean agricultural land-use/cover change for examining wildfire risk. Journal of Artificial Societies and Social Simulation 2008; 11.4: 4.

213. Minnicozzi M, Sawyer RT, Fenton MJ. Innate immunity in allergic disease. Immunol Rev 2011; 242: 106-127.

214. Miocinovic S, Parent M, Butson CR, Hahn PJ, Russo GS, Vitek JL, McIntyre CC. Computational analysis of subthalamic nucleus and lenticular fasciculus activation during therapeutic deep brain stimulation J. Neurophysiol 2006; 96 1569–80.

215. Moglo KE, Shirazi-Adl A. Cruciate coupling and screw-home mechanism in passive knee joint during extension-flexion. Journal of Biomechanics. 2005;38(5):1075–1083.

216. Mononen ME, Mikkola MT, Julkunen P, Ojala R, Nieminen MT, Jurvelin JS, Korhonen RK. Effect of superficial collagen patterns and fibrillation of femoral articular cartilage on knee joint mechanics-a 3D finite element analysis. Journal of Biomechanics 2012;45(3):579–587.

217. Mononen ME, Julkunen P, Töyräs J, Jurvelin JS, Kiviranta I, Korhonen RK. Alterations in structure and properties of collagen network of osteoarthritic and repaired cartilage modify knee joint stresses. Biomechanics and Modeling in Mechanobiology 2011;10(3):357–369.

218. Monteagudo A, Santos J. Treatment Analysis in a Cancer Stem Cell Context Using a Tumor Growth Model Based on Cellular Automata. PLoS One 2015; 10(7): e0132306.

219. Moran EC, Dhal A, Vyas D, Lanas A, Soker S, Baptista PM. Whole-organ bioengineering: current tales of modern alchemy. Transl. Res. 2014; 163: 259-267.

220. Morton CI, Hlatky L, Hahnfeldt P, Enderling H. Non-Stem Cancer Cell Kinetics Modulate Solid Tumor Progression. Theoretical Biology & Medical Modelling 2016; 8 (2011): 48.

221. de Mul FF, Morales F, Smit AJ, Graaff R. A model for post-occlusive reactive hyperemia as measured with laser-Doppler perfusion monitoring. IEEE Trans Biomed Eng 2005; 52: 184–190.

222. Muller G, Grébaut P, and Gouteux J. An agent-based model of sleeping sickness: simulation trials of a forest focus in southern Cameroon. Comptes Rendus Biologies 2004; 327.1: 1-11.

223. Nakada EM, Shan J, Kinyanjui MW, Fixman ED. Adjuvant-Dependent Regulation of Interleukin-17 Expressing Γδ T Cells and Inhibition of Th2 Responses in Allergic Airways Disease. Respiratory Research 2014; 15.1: 90. PMC. Web. 18 Sept. 2015.

224. Nakanishi, K. Basophils are potent antigen-presenting cells that selectively induce Th2 cells. Eur J Immunol 2010; 40: 1836-1842.

225. Namatame A, Morita H, Matsuyama K. Agent-based modeling for the study of diffusion dynamics. Proceedings of the 2009 Spring Simulation Multiconference. Society for Computer Simulation International, 2009.

226. Narang V, Wong SY, Leong SR, Harish B, Abastado JP, Gouaillard A. Selection of Mesenchymal-Like Metastatic Cells in Primary Tumors-An in silico Investigation. Front Immunol 2012; 3: 88.

227. Natarajan P, Singh A, McNamara JT, Secor ER Jr, Guernsey LA, Thrall RS, Schramm CM. Regulatory B cells from hilar lymph nodes of tolerant mice in a murine model of allergic airway disease are CD5(+), express TGF-beta, and co-localize with CD4(+)Foxp3(+) T cells. Mucosal Immunol 2012; 5(6):691-701.

228. Ng TL, Eheart JW, Cai X, Braden JB. An agent-based model of farmer decision-making and water quality impacts at the watershed scale under markets for carbon allowances and a second-generation biofuel crop. Water Resources Research 2011; 47.9.

229. Ng THS, Britton GJ, Hill EV, Verhagen J, Burton BR, Wraith DC. Regulation of Adaptive Immunity; The Role of Interleukin-10. Frontiers in Immunology 4 (2013): 129. PMC. Web. 18 Sept. 2015.

230. Nilsson F, Darley V. On complex adaptive systems and agent-based modelling for improving decision-making in manufacturing and logistics settings: Experiences from a packaging company. International Journal of Operations & Production Management 2006; 26.12: 1351-1373.

231. North MJ, Macal CM, St. Aubin J, Thimmapuram P, Bragen M, Hahn J, Karr J, Brigham N, Lacy ME, Hampton D Multiscale agent-based consumer market modeling. Complexity 2010; 15.5: 37-47.

232. Norton KA, Popel AS. An agent-based model of cancer stem cell initiated avascular tumour growth and metastasis: the effect of seeding frequency and location. J. R. Soc. Interface 2014; 11(100): 20140640.

233. Oh J, Malter JS. Pin1-FADD interactions regulate Fas-mediated apoptosis in activated eosinophils. J Immunol. 2013 May 15;190(10):4937-45.

234. O'Reilly A, Hankenson KD, Kelly DJ. A computational model to explore the role of angiogenic impairment on endochondral ossification during fracture healing. Biomech Model Mechanobiol. 2016.

235. Orr MG, Evans CR. Understanding long-term diffusion dynamics in the prevalence of adolescent sexual initiation: A first investigation using agent-based modeling. Research in Human Development 2011; 8.1: 48-66.

236. Padmanabha H, Correa F, Rubio C, Baeza A, Osorio S, Mendez J, Jones JH, Diuk-Wasser MA. Human Social Behavior and Demography Drive Patterns of Fine-Scale Dengue Transmission in Endemic Areas of Colombia. PloS One 2015; 10.12: e0144451.

237. Papaioannou G, Demetropoulos CK, King YH. Predicting the effects of knee focal articular surface injury with a patient-specific finite element model. Knee 2010;17(1):61–68.

238. Park, SJ, Umemoto T, Saito-Adachi M, Shiratsuchi Y, Yamato M, Nakai K. Computational promoter modeling identifies the modes of transcriptional regulation in hematopoietic stem cells. PLoS One 2014; 9(4): e93853.

239. Parker DC, Filatova T. A conceptual design for a bilateral agent-based land market with heterogeneous economic agents. Computers, Environment and Urban Systems 2008; 32.6: 454-463.

240. Parker DC, Manson SM, Janssen MA, Hoffmann MJ, Deadman P. Multi-agent systems for the simulation of land-use and land-cover change: a review. Annals of the association of American Geographers 2003; 93.2: 314-337.

241. Patel AA, Gawlinsky ET, Lemieux SK, Gatenby RA. Cellular automaton model of early tumour growth and invasion: the effects of native tissue vascularity and increased anaerobic tumour metabolism. J. Theor. Biol. 2001; 213: 315–331.

242. Paveglio SA, Allard J, Foster Hodgkins SR, et al. Airway Epithelial Indoleamine 2,3-Dioxygenase Inhibits CD4+ T Cells during Aspergillus Fumigatus Antigen Exposure. American Journal of Respiratory Cell and Molecular Biology 2011; 44.1: 11–23. PMC. Web. 21 Sept. 2015.

243. Peña E, Calvo B, Martínez MA, Doblaré M. A three-dimensional finite element analysis of the combined behavior of ligaments and menisci in the healthy human knee joint. Journal of Biomechanics.2006;39(9):1686–1701.

244. Peña E, Calvo B, Martínez MA, Doblaré M. Effect of the size and location of osteochondral defects in degenerative arthritis. A finite element simulation. Computers in Biology and Medicine 2007;37(3):376–387.

245. Peres R, Muller E, Mahajan V. Innovation diffusion and new product growth models: A critical review and research directions. International Journal of Research in Marketing 2010; 27.2: 91-106.

246. Perna A, Granovskiy B, Garnier S, Nicolis SC, Labédan M, Theraulaz G, Fourcassié V, Sumpter DJT. Individual rules for trail pattern formation in Argentine ants (Linepithema humile). PLoS Comput Biol 2012; 8.7: e1002592.

247. Poleszczuk J, Hahnfeldt P, Enderling H. Evolution and phenotypic selection of cancer stem cells. PLoS Comput Biol 2015; 11(3): e1004025.

248. Pollmächer J, Figge MT. Deciphering chemokine properties by a hybrid agent-based model of Aspergillus fumigatus infection in human alveoli. Frontiers in Microbiology 2015; 6:503.

249. Poore KD, Bauch CT. The impact of aggregating serogroups in dynamic models of Neisseria meningitidis transmission. BMC Infectious Diseases 2015; 15.1: 1.

250. Pothen JJ, Poynter ME, Bates JH. The inflammatory twitch as a general strategy for controlling the host response. J. Immunol 2013;190: 3510-3516.

251. Poynter, M. E., C. G. Irvin, and Y. M. Janssen-Heininger. Rapid activation of nuclear factor-kappaB in airway epithelium in a murine model of allergic airway inflammation. Am J Pathol 2002; 160: 1325-1334.

252. Precharattana M. Stochastic modeling for dynamics of HIV-1 infection using cellular automata. J Bioinform Comput Biol 2015: 1630001.

253. Prodanov D, Nagelkerke N, Marani E. Spatial clustering analysis in neuroanatomy: applications of different approaches to motor nerve fiber distribution. J. Neurosci. Methods 2007; 160: 93-108.

254. Przybilla, J, Rohlf T, Loeffler M, Galle J. Understanding epigenetic changes in aging stem cells--a computational model approach. Aging Cell 2014; 13(2): 320-328.

255. Qiao M, Wu D, Carey M, Zhou X, Zhang L. Multi-Scale Agent-Based Multiple Myeloma Cancer Modeling and the Related Study of the Balance between Osteoclasts and Osteoblasts. PloS One 10.12 (2015): e0143206.

256. Railsback S, Grimm V. Agent-Based and Individual-Based Modeling: A Practical Introduction. Princeton: Princeton University Press; c2011. Chapter 1: Models, Agent-Based Models, and the Modeling Cycle; p.3-13.

257. Ranga A, Bouchot O, Mongrain R, Ugolini P, Cartier R. Computational simulations of the aortic valve validated by imaging data: evaluation of valve-sparing techniques. Interact. Cardiovasc. Thorac. Surg. 2006; 5:373–78.

258. Rapaport O, Levi-Faur D, Miodownik D. The Puzzle of the Diffusion of Central-Bank Independence Reforms: Insights from an Agent-Based Simulation. Policy Studies Journal 2009; 37.4: 695-716.

259. Ravi B, Miodownik D, Nart J. REsCape: an agent-based framework for modeling resources, ethnicity, and conflict. The Journal of Artificial Societies and Social Simulation 2008; 11.27.

260. Reddy, AT, Lakshmi SP, Dornadula S, Pinni S, Rampa DR, Reddy RC. The nitrated fatty acid 10-nitro-oleate attenuates allergic airway disease. J Immunol 2013; 191: 2053-2063.

261. Reed, CE, Kita H. The role of protease activation of inflammation in allergic respiratory diseases. J Allergy Clin Immunol 2004; 114: 997-1008; quiz 1009.

262. Riesenfeld EP, A. G., Bates JHT, Poynter ME, Wu M, Aimi S and LK Lundblad. The Temporal Evolution of Airways Hyperresponsiveness and Inflammation. Allergy & Therapy 2012; S1.

263. Robbins MM, Robbins AM. Simulation of the population dynamics and social structure of the Virunga mountain gorillas. Am J Primatol 2004; 63(4): 201-223.

264. Robinson EJH, Ratnieks FLW, Holcombe M. An agent-based model to investigate the roles of attractive and repellent pheromones in ant decision making during foraging. Journal of Theoretical Biology 2008; 255.2: 250-258.

265. Robison RG, Kumar R. Chapter 10: Pediatric asthma: principles and treatment. Allergy Asthma Proc. 2012 May-Jun;33 Suppl 1:S32-5.

266. Roozmand O, Ghasem-Aghaee N, Hofstede GJ, Nematbakhsh MA, Baraani A, Verwaat T. Agent-based modeling of consumer decision making process based on power distance and personality. Knowledge-Based Systems 2011; 24.7: 1075-1095.

267. Rouleau M, Coletti M, Bassett JK, Hailegiorgis AB, Gulden T, Kennedy WG. Conflict in complex socio-natural systems: Using agent-based modeling to understand the behavioral roots of social unrest within the Mandera Triangle. Human Behavior-Computational Modeling and Interoperability Conference, 2009.

268. Sabzpoushan SH, Pourhasanzade F. A Cellular Automata-based Model for Simulating Restitution Property in a Single Heart Cell. J Med Signals Sens 2011; 1(1): 19-23.

269. Said LB, Bouron T, Drogoul A. Agent-based interaction analysis of consumer behavior. Proceedings of the first international joint conference on Autonomous agents and multiagent systems: part 1. ACM, 2002.

270. Salmon H, Franciszkiewicz K, Damotte D, Dieu-Nosjean MC, Validire P, Trautmann A, et al. Matrix architecture defines the preferential localization and

migration of T cells into the stroma of human lung tumors. The Journal of clinical investigation. 2012 Mar 1;122(3):899-910.

271. Sander B, Nizam A, Garrison LP Jr, Postma MJ, Halloran ME, Longini IM Jr. Economic evaluation of influenza pandemic mitigation strategies in the United States using a stochastic microsimulation transmission model. Value in Health 2009; 12.2: 226-233.

272. Santos J, Monteagudo A. Analysis of behaviour transitions in tumour growth using a cellular automaton simulation. IET Syst Biol 2015; 9(3): 75-87.

273. Sarpe V, Jacob C. Simulating the decentralized processes of the human immune system in a virtual anatomy model. BMC Bioinformatics 2013; 14 Suppl 6: S2.

274. Saul A, Smith T, Maire N. Stochastic simulation of endemic Salmonella enterica serovar Typhi: the importance of long lasting immunity and the carrier state. PloS One 2013; 8.9: e74097.

275. Schelling, TC. Dynamic models of segregation. The Journal of Mathematical Sociology 1971; 1(2): 143-186.

276. Schmitz JE, Kansal AR, Torquato S. A Cellular Automaton Model of Brain Tumor Treatment and Resistance. J Theor Med. 2002;4: 223–239.

277. Schoeberl B, Eichler-Jonsson C, Gilles ED, Muller G. Computational modeling of the dynamics of the MAP kinase cascade activated by surface and internalized EGF receptors. Nat. Biotechnol. 2002;20:370–375.

278. Scholl, HJ. Agent-based and system dynamics modeling: a call for cross study and joint research. System Sciences, 2001. Proceedings of the 34th Annual Hawaii International Conference on. IEEE, 2001.

279. Scholz M, Engel C, Loeffler M. Modelling human granulopoiesis under poly-chemotherapy with G-CSF support. J Math Biol. 2005;50:397–439. doi: 10.1007/s00285-004-0295-1.

280. Schramm ME, Trainor KJ, Shanker M, Hu MY. An agent-based diffusion model with consumer and brand agents. Decision Support Systems 2010; 50.1: 234-242.

281. Schreinemachers P, Berger T, Sirijinda A, Praneetvatakul S. The Diffusion of Greenhouse Agriculture in Northern Thailand: Combining Econometrics and Agent-Based Modeling. Canadian Journal of Agricultural Economics/Revue Canadienne d'agroeconomie 2009; 57.4: 513-536.

282. Sekiya I, Larson BL, Smith JR, Pochampally R, Cui JG, Prockop DJ. Expansion of human adult stem cells from bone marrow stroma: conditions that maximize the yields of early progenitors and evaluate their quality. Stem Cells 2012; 20(6):530-541.

283. Senior AM, Nakagawa S, Grimm V. The Evolutionary Consequences of Disrupted Male Mating Signals: An Agent-Based Modelling Exploration of Endocrine Disrupting Chemicals in the Guppy. PloS One 2014; 9.7: e103100.

284. Serrao KL, Fortenberry JD, Owens ML, Harris FL, Brown LA. Neutrophils induce apoptosis of lung epithelial cells via release of soluble Fas ligand. Am J Physiol Lung Cell Mol Physiol. 2001 Feb;280(2):L298-305.

285. Setty, Y. In-silico models of stem cell and developmental systems. Theor. Biol. Med. Model. 2014; 11:1.

286. Shiang K, Kandeel F. A Computational Model of the Human Glucose-Insulin Regulatory System. Journal of Biomedical Research 2016 Jan; 24.5 (2010): 347–364.

287. Shirazi R, Shirazi-Adl A. Computational biomechanics of articular cartilage of human knee joint: effect of osteochondral defects. Journal of Biomechanics 2009;42(15):2458–2465.

288. Shirazi R, Shirazi-Adl A, Hurtig M. Role of cartilage collagen fibrils networks in knee joint biomechanics under compression. Journal of Biomechanics. 2008;41(16):3340–3348.

289. Sibole SC, Erdemir A. Chondrocyte deformations as a function of tibiofemoral joint loading predicted by a generalized high-throughput pipeline of multi-scale simulations. PLoS One 2012;7(5)e37538.

290. Siettos CI, Anastassopoulou C, Russo L, Grigoras C, Mylonakis E.. Forecasting and control policy assessment for the Ebola virus disease (EVD) epidemic in Sierra Leone using small-world networked model simulations. BMJ Open 2016; 6.1: e008649.

291. Singer HM, Singer I, Herrmann HJ. Agent-based model for friendship in social networks. Physical Review E 2009; 80.2: 026113.

292. Simon, HU. Cell death in allergic diseases. Apoptosis 2009; 14: 439-446.

293. Smaldino P, Pickett C, Sherman J, Schank J. An agent-based model of social identity dynamics. Journal of Artificial Societies and Social Simulation 2012; 15.4: 7.

294. Sokocevic D, Bonenfant NR, Wagner DE, Borg ZD, Lathrop MJ, Lam YW, Deng B, Desarno MJ, Ashikaga T, Loi R, Hoffman AM, Weiss DJ. The effect of age and

emphysematous and fibrotic injury on the re-cellularization of de-cellularized lungs. Biomaterials 2013; 34(13): 3256-3269.

295. Solovyev A, Mi Q, Tzen YT, Brienza D, Vodovotz Y. Hybrid equation/agent-based model of ischemia-induced hyperemia and pressure ulcer formation predicts greater propensity to ulcerate in subjects with spinal cord injury. PLoS Comput Biol 2013; 9(5): e1003070.

296. Soncini M, Votta E, Zinicchino S, Burrone V, Mangini A, Lemma M, Antona C, Redaelli A. Aortic root performance after valve sparing procedure: a comparative finite element analysis. Med. Eng. Phys. 2009; 31:234–43.

297. Sopha BM, Klöckner CA, Hertwich EG. Adoption and diffusion of heating systems in Norway: coupling agent-based modeling with empirical research. Environmental Innovation and Societal Transitions 2013; 8: 42-61.

298. Soto-Ramirez N, Ziyab AH, Karmaus W, Zhang H, Kurukulaaratchy RJ, Ewart S, et al. Epidemiologic methods of assessing asthma and wheezing episodes in longitudinal studies: measures of change and stability. J Epidemiol. 2013;23(6):399-410.

299. Srbljinovic A, Penzar D, Rodik P, Kardov K. An agent-based model of ethnic mobilisation. Journal of Artificial Societies and Social Simulation 2013; 6.1: 1.

300. Stanley D, Tunnicliffe W. Management of life-threatening asthma in adults. Continuing Education in Anaesthesia, Critical Care & Pain. 2008 June 1, 2008;8(3):95-9.

301. Strömbom D, Mann RP, Wilson AM, Hailes S, Morton AJ, Sumpter DJ, King AJ. Solving the shepherding problem: heuristics for herding autonomous, interacting agents. Journal of The Royal Society Interface 2014; 11.100: 20140719.

302. Sueyoshi T, Tadiparthi GR. An agent-based decision support system for wholesale electricity market. Decision Support Systems 2008; 44.2: 425-446.

303. Sun W, Martin C, Pham T. Computational modeling of cardiac valve function and intervention. Annu Rev Biomed Eng 2014; 16: 53-76.

304. Sun, Z., S. Dragon, A. Becker and A. S. Gounni. Leptin inhibits neutrophil apoptosis in children via ERK/NF-kappaB-dependent pathways. PLoS One 2013; 8: e55249.

305. Tamang DL, Pirzai W, Priebe GP, Traficante DC, Pier GB, Falck JR, et al. Hepoxilin A(3) facilitates neutrophilic breach of lipoxygenase-expressing airway epithelial barriers. J Immunol. 2012 Nov 15;189(10):4960-9.

306. Tanaka, H, Masuda T, Tokuoka S, Takahashi Y, Komai M, Nagao K, Nagai H. Time course study on the development of allergen-induced airway remodeling in mice: the effect of allergen avoidance on established airway remodeling. Inflamm Res 2002; 51(6): 307-316.

307. Tang W, Bennett DA. Reprint of: Parallel agent-based modeling of spatial opinion diffusion accelerated using graphics processing units. Ecological Modelling 2012; 229: 108-118.

308. Teplitzky, B A, Connolly AT, Bajwa JA, Johnson MD. Computational modeling of an endovascular approach to deep brain stimulation. J Neural Eng 2014; 11(2): 026011.

309. Tomioka S, Bates JH, Irvin CG. Airway and tissue mechanics in a murine model of asthma: alveolar capsule vs. forced oscillations. J Appl Physiol 2002; 93: 263-270.

310. Totaro P, Morganti S, Ngo Yon C, Dore R, Conti M, Auricchio F, Vigano M. Computational finite element analyses to optimize graft sizing during aortic valve-sparing procedure. J. Heart Valve Dis. 2012; 21:141–47.

311. Twomey P, Cadman R. Agent-based modelling of customer behaviour in the telecoms and media markets. Emerald Insight 2002; 4.1: 56-63.

312. Vainstein V, Kirnasovsky OU, Kogan Y, Agur Z. Strategies for cancer stem cell elimination: Insights from mathematical modeling. Journal of Theoretical Biology. 2012;298:32–41.

313. Valbuena D, Verburg PH, Bregt AK, Ligtenberg A. An agent-based approach to model land-use change at a regional scale. Landscape Ecology 2008; 25.2: 185-199.

314. van Rijt LS, Lambrecht BN. Dendritic cells in asthma: a function beyond sensitization. Clinical and experimental allergy : journal of the British Society for Allergy and Clinical Immunology. 2005 Sep;35(9):1125-34.

315. Van Vo T, Hammer PE, Hoimes ML, Nadgir S, Fantini, S. Mathematical Model for the Hemodynamic Response to Venous Occlusion Measured With Near-Infrared Spectroscopy in the Human Forearm. Biomedical Engineering. IEEE Transactions 2007 April; 54 (4): pp.573-584.

316. van Zyl JM, Derendinger B, Seifart HI, Van der Bijl P. Comparative diffusion of drugs through bronchial tissue. Int J Pharm. 2008 Jun; 5;357(1-2):32-6.

317. Wagers SS, Haverkamp HC, Bates JH, Norton RJ, Thompson-Figueroa JA, Sullivan MJ, Irvin CG. Intrinsic and antigen-induced airway hyperresponsiveness are the result of diverse physiological mechanisms. J Appl Physiol 2007; 102: 221-230.

318. Wagers S, Lundblad LK, Ekman M, Irvin CG, Bates JH. The allergic mouse model of asthma: normal smooth muscle in an abnormal lung? J Appl Physiol 1985; 96: 2019-2027, 2004.

319. Wagner DE, Bonvillain RW, Jensen T, Girard ED, Bunnell BA, Finck CM, Hoffman AM, Weiss DJ. Can stem cells be used to generate new lungs? Ex vivo lung bioengineering with decellularized whole lung scaffolds. Respirology 2013; 18(6):895-911.

320. Wallis JM, Borg ZD, Daly AB, Deng B, Ballif BA, Allen GB, Jaworski DM, Weiss DJ. Comparative assessment of detergent-based protocols for mouse lung de-cellularization and re-cellularization tissue engineering - part C: Methods. 2012; 18(6):420-432.

321. Wang J, Zhang L, Jing C, Ye G, Wu H, Miao H, Wu Y, Zhou X. Multi-scale agent-based modeling on melanoma and its related angiogenesis analysis. Theor Biol Med Model 2013; 10: 41.

322. Wang Q, Sirois E, Sun W. Patient-specific modeling of biomechanical interaction in transcatheter aortic valve deployment. J. Biomech. 2012; 45:1965–71.

323. Wang Z, Birch CM, Sagotsky J, Deisboeck TS. Cross-scale, cross-pathway evaluation using an agent-based non-small cell lung cancer model. Bioinformatics 2009; 25.18: 2389-2396.

324. Wang Z, Butner JD, Kerketta R, Cristini V, Deisboeck TS. Simulating cancer growth with multiscale agent-based modeling. Seminars in cancer biology. Vol. 30. Academic Press, 2015.

325. Wang Z, Zhang L, Sagotsky J, Deisboeck TS. Simulating non-small cell lung cancer with a multiscale agent-based model. Theoretical Biology & Medical Modelling. 2007;4:50. doi:10.1186/1742-4682-4-50.

326. Weidmann, NB, Salehyan I. Violence and ethnic segregation: a computational model applied to Baghdad. International Studies Quarterly 2013; 57.1: 52-64.

327. Wichmann H, Loeffler M. Mathematical Modeling of Cell Proliferation: Stem Cell Regulation in Hemopoiesis. BocaRaton, Florida: CRC Press; 1985.

328. Wilson JT, van Loon R, Wang W, Zawieja DC, Moore JE Jr. Determining the combined effect of the lymphatic valve leaflets and sinus on resistance to forward flow. J Biomech 2015; 48(13): 3593-3599.

329. Wolterink, RG, Kleinjan A, van Nimwegen M, Bergen I, de Bruijn M, Levani Y, Hendriks RW. Pulmonary innate lymphoid cells are major producers of IL-5 and IL-13 in murine models of allergic asthma. Eur J Immunol 42: 1106-1116.

330. Wu H. A Case Study of Type 2 Diabetes Self-Management. BioMedical Engineering OnLine 2016 Jan; 4 (2005): 4.

331. Xie Y, Batty M, Zhao K. Simulating emergent urban form using agent-based modeling: Desakota in the Suzhou-Wuxian region in China. Annals of the Association of American Geographers 2007; 97.3: 477-495.

332. Young RC, Barendse P. Linking myometrial physiology to intrauterine pressure; how tissue-level contractions create uterine contractions of labor. PLoS Comput Biol 2014; 10(10): e1003850.

333. Zhang H, Zeng Y, Bian L, Yu X. Modelling urban expansion using a multi agent-based model in the city of Changsha. Journal of Geographical Sciences 2010; 20.4: 540-556.

334. Zhang, H., Hou W, Henrot L, Schnebert S, Dumas M, Heusele C, Yang J. Modelling epidermis homoeostasis and psoriasis pathogenesis. J R Soc Interface 2015; 12(103).

335. Zhang L, Athale CA, Deisboeck TS. Development of a three-dimensional multiscale agent-based tumor model: simulating gene-protein interaction profiles, cell phenotypes and multicellular patterns in brain cancer. Journal of Theoretical Biology 2007; 244.1: 96-107.

336. Zhang L, Chen LL, Deisboeck TS. Multi-scale, multi-resolution brain cancer modeling. Mathematics and Computers in Simulation 20098; 79.7: 2021-2035.

337. Zhang L, Jiang B, Wu Y, Strouthos C, Sun PZ, Su J, Zhou X. Developing a multiscale, multi-resolution agent-based brain tumor model by graphics processing units. Theoretical Biology and Medical Modelling 2011; 8.1: 46.

338. Zhang T, Gensler S, Garcia R. A Study of the Diffusion of Alternative Fuel Vehicles: An Agent-Based Modeling Approach. Journal of Product Innovation Management 2011; 28.2: 152-168.

339. Zhang T, Zhang D. Agent-based simulation of consumer purchase decision-making and the decoy effect. Journal of Business Research 2007; 60.8: 912-922.

340. Zhao CY, Greenstein JL, Winslow RL. Roles of phosphodiesterases in the regulation of the cardiac cyclic nucleotide cross-talk signaling network, Journal of Molecular and Cellular Cardiology, Volume 91, February 2016, Pages 215-227, ISSN 0022-2828.

341. Zhao K, Yen J, Ngamassi L, Maitland C, Tapia AH. Simulating inter-organizational collaboration network: a multi-relational and event-based approach. Simulation 2011: 0037549711421942.

342. Zhu J, Liang L, Jiao Y, Liu L. Enhanced invasion of metastatic cancer cells via extracellular matrix interface. PLoS One 2015; 10(2): e0118058.

343. Zhu L, Qualls WA, Marshall JM, Arheart KL, DeAngelis DL, McManus JW, Traore SF, Doumbia S, Schlein Y, Müller GC, Beier JC. A spatial individual-based model predicting a great impact of copious sugar sources and resting sites on survival of Anopheles gambiae and malaria parasite transmission. Malar J 2015; 14: 59.

344. Zou Y, Vladimir A, Fonoberov MF, Mezic I, Kevrekidis IG. Model reduction for agent-based social simulation: coarse-graining a civil violence model. Physical Review 2012; E 85.6: 066106.